Graduate School of Engineering and Science

Shibaura Institute of Technology

Thesis for the Degree of Doctor of Engineering

A Study on the Coding Techniques for Phase-Shift Pulse Brillouin Optical Time Domain Analysis (PSP-BOTDA) Fiber Optic Sensor

March 2014

Division	Functional Control Systems
Student ID	NB11106
Name	Mohd Saiful Dzulkefly Bin Zan
Supervisor	Prof. Dr. Tsuneo Horiguchi
Co-Supervisor	Prof. Dr. Norio Kashima

Contents

Abstract

Brillouin scattering-based fiber optic sensing systems have attracted much attention because they allow the measurement of strain/temperature with high accuracy and sensitivity. Among them, Brillouin optical time domain analysis (BOTDA) is of interest due to its capability to measure distributed strain/temperature with high spatial resolution over long distance range, which is beneficial for the application especially in the field of civil engineering for structural health monitoring of large structure such as buildings, dams, bridges etc. BOTDA technique is based on the stimulated Brillouin scattering (SBS) process, which involves the process of optical energy conversion between pulsed pump light (pump) and counter propagating probe light (probe) via acoustical phonon that acts as mediator. In the SBS process, the optical energy is transferred from the pump to probe when the probe frequency is set lower than the pump frequency; this process is called Stokes scattering process. Maximum interaction is obtained when the frequency difference between the two lights coincides with the Brillouin frequency shift (BFS) that is in a function of local temperature/strain. Moreover, by scanning the frequency difference between the two lights within the BFS vicinity, the Brillouin gain spectrum as a function of distance can be constructed.

Numerous researches have been conducted to improve the BOTDA sensing parameters such as spatial resolution, signal-to-noise ratio (SNR) etc. This is because, at the early stage of development, the best spatial resolution obtained was 1m, with the use of pump pulse of duration 10ns. Shortening the duration to less than 10ns, which is around the time constant of the acoustic wave amplitude τ_a for silica fiber could cause the Brillouin gain to decrease significantly and consequently broadens the bandwidth of the Brillouin gain spectrum. Both the gain decrease and the bandwidth broadening make it increasingly difficult to measure the BFS accurately.

However, the idea of using pre-pump pulse in a technique called pulse pre-pump BOTDA (PPP-BOTDA) has overcome the limitation in spatial resolution of the conventional BOTDA. PPP-BOTDA uses a weak pulse pre-pump with a long duration followed by an intense pulse with short duration. The acoustic wave excited by this pulse pre-pump provides Brillouin gain to the short pulse, resulting in a narrow spectral bandwidth and high spatial resolution measurement. Following to this success, several systems that are also based on pulse pre-pump technique have also been introduced, such as differential pulse-width pair BOTDA (DPP-BOTDA), optical differential parametric amplification BOTDA (ODPA-BOTDA) and phase-shift pulse BOTDA (PSP-BOTDA).

In order to improve the SNR, the idea of coding technique to modulate the pump light of BOTDA has been proposed. Basically, there are two types of coded pulses proposed in BOTDA; non-return-to-zero (NRZ) coded pulses and return-to-zero (RZ) coded pulses. Both types employ intensity modulation scheme to modulate the optical pulse. However, employing NRZ coded pulses has induced distortion in the measured Brillouin signal when the bit pulse duration is around or less than τ_a. This distortion is caused by varieties of additional gain of the preceding coded pulses. Consequently, return-to-zero (RZ) format has been introduced into the coded pulses of the high-spatial-resolution BOTDAs so that interactions between the preceding and succeeding bit pulses should not occur through the SBS process.

In this thesis, the employment of coding techniques in modulating the pump light of the BOTDA called coded phase-shift pulse BOTDA (PSP-BOTDA) is reported. In this work, the impact of pump light coding concept on the SNR and the spatial resolution of the Brillouin signals were studied. Actually, there are two types of conventional coded PSP-BOTDA that have already been proposed; they are coded discrete-PSP-BOTDA that uses RZ coded pulses and coded continuous-PSP-BOTDA that uses NRZ coded pulses. In contrast to the coded BOTDAs described previously,

the coded PSP-BOTDAs employ phase modulation scheme to modulate the optical pulse.

When employing the conventional coded discrete-PSP-BOTDA, theoretically, the SNR increases linearly with $\sqrt{L}$, where L is the code length. However, in the actual measurement, the use of AC-coupled amplifier for amplifying the coded electrical signal of high frequency rejects the DC and the low frequency component signals. As a result, the amplitude of the amplified signal exponentially decreases, especially when a very long pulse train is used. When light from laser diode (LD) is externally modulated with such a distorted electrical signal, the linear increase in the Brillouin signal with the code lengths cannot be obtained. As a result, the increment trend of the SNR with the code length becomes nonlinear as well. Therefore, in this thesis, the author proposes a new configuration of the coded electrical signal for the input of the AC-coupled amplifier to overcome the problems described above. The experimental results have shown that by using the proposed configuration, the SNR increases in much better accordance with $\sqrt{L}$ than the conventional pump configuration.

In the case of conventional coded continuous-PSP-BOTDA, it was previously found that the use of NRZ-formatted pulses employing Golay codes has successfully demonstrated sub-meter spatial resolution. The Brillouin signals obtained with the NRZ-coded pulses are also well decoded if the total duration of the coded pulses is around or less than τ_a. This is because the subtraction of Brillouin signal measured by a code and its inversion intrinsically cancels the Brillouin gain due to the interaction between each coded pulse and the probe, extracting only the Brillouin gain that is derived from the interaction of each coded pulse with the acoustic wave excited by the pre-pump pulse. However, since the acoustic wave decays significantly after τ_a, the decoded Brillouin signal is distorted, resulting in the degradation of the spatial resolution, especially when using Golay code of total duration longer than τ_a.

Therefore, in this thesis, instead of employing Golay codes, the author proposes to modulate the NRZ formatted pump light of the coded continuous-PSP-BOTDA with Walsh codes. It was found that the use of Walsh codes in the NRZ formatted pump induces little degradation in the spatial resolution, contrary to the previous results for Golay codes. This advantage of the Walsh code over the Golay code comes from the fact that decoding the Brillouin signals via Hadamard transform for Walsh codes is robust not only against variations in launched coded-pulse amplitudes but also against those in response signals. 20cm and 10cm of spatial resolutions were successfully attained for pulse durations of 2ns and 1ns cases, respectively. Apart from that, the maximum SNR improvement of 3dB was recorded for 8-bit Walsh code pulses having 1ns duration each, being consistent with analytical and numerical calculations.

In order to further improve the SNR, the author has also proposed in this thesis to simultaneously use RZ- and NRZ pulses to modulate the pump light for coded PSP-BOTDA. The coding systems employed in these proposed coding systems are Golay code and Walsh code. The use of the proposed combined codes offers higher SNR than that of the conventional coded PSP-BOTDA that uses only RZ- or NRZ coded pulses. Furthermore, after the decoding process, high spatial resolution corresponding to the coded pulse duration can still be attained. There are four types of coded PSP-BOTDAs that simultaneously use the RZ or NRZ pulse coding discussed in this dissertation; the dual Golay codes-PSP-BOTDA, the two types of combined Walsh and Golay codes-PSP-BOTDAs and dual Walsh codes PSP-BOTDA.

In the case of dual Golay codes-PSP-BOTDA, for NRZ pulses, it was found that the SNR improvement is limited by τ_a, which is 9ns for silica fibers. When using coded pulses of duration 1ns, the maximum code duration for NRZ pulses is 8ns (8 bits of Golay NRZ pulses). It was found that using longer NRZ pulses has caused distortion in the

Brillouin signal, leading to the degradation of the spatial resolution. On the other hand, for RZ pulses, the maximum code length that can be used is limited by the round trip time of light in fiber. Initial experiments for NRZ code length L_{cont}=4 (NRZ pulses), L_{disc}=8 (RZ pulses) have demonstrated about 7-dB enhancement in the optical signal-to-noise ratios when compared to the single pulse PSP-BOTDA. The same amount of enhancement was also achieved when L_{cont}=8, L_{disc}=4. Furthermore, the spatial resolution measurement of 10 cm was successfully demonstrated.

In the case of combined Walsh and Golay codes PSP-BOTDA, from the simulation and experimental results, it was confirmed that the assignment of Walsh codes to NRZ pulses has kept the spatial resolution high even when the code duration exceeds τ_a. Even though the Brillouin signal measured by the code sequences exponentially decays, the decoding process via Hadamard transform for Walsh coded NRZ pulses in the proposed system still produces more accurate decoded signals than that via Golay codes correlation calculations. From the rising edge length result obtained with the combined codes, the spatial resolution of 10cm was successfully demonstrated.

It was also found that the combination of Golay and Walsh codes has contributed higher optical SNIR than that of using only one kind of code in coded continuous- and coded discrete-PSP-BOTDAs. In the analysis, for both Golay and Walsh codes cases, the use of coded RZ pulses increases the optical SNIR by $\sqrt{L}$ (L: code length of Golay code or Walsh code). For NRZ pulses, however, the improvement became slow with increasing L and finally dropped from the maximum for long code length. This is due to the decrease of Brillouin signal induced by the acoustic wave decay. It was observed that the optical SNIR reached its maximum of 3dB when the total duration of the 8-bit coded NRZ pulses was 8ns, confirming that code duration of the NRZ pulses is limited by τ_a.

For dual Walsh codes PSP-BOTDA case, the robustness of Hadamard transform against the variations in the received signal amplitudes during the decoding process has contributed to the achievement of high spatial resolution measurement, even for total code duration $L_{cont}T_2$ (T_2: pulse duration) of longer than τ_a cases. In the simulations, the spatial resolutions of 20cm and 10cm has been confirmed with the use of T_2 = 2ns and 1ns, respectively. In terms of the optical SNIR, for dual Walsh codes case, the maximum optical SNIR of about 3dB was obtained when $L_{cont}T_2$ is set to around τ_a and $2\tau_a$. In the preliminary experiment, the impact of L_{disc} on the measured Brillouin signals was studied. Compared to the conventional PSP-BOTDA without coding, the total SNIR of about 5.4dB was obtained when L_{disc}=4 (L_{cont} fixed at 4 bits), which agrees well with the theoretical SNIR of 6dB.

Finally, from the numerical results obtained for the four types of combined codes system described above, measurement performance in terms of the measurement speed and the spatial resolution is analyzed and compared. It was found that the dual Golay codes PSP-BOTDA offers the fastest measurement speed to acquire the SNR for reducing BFS error to below 1MHz. In contrast, dual Walsh codes PSP-BOTDA provides the slowest measurement speed. On the other hand, the combination of Walsh (NRZ) and Golay (RZ) codes gives a good tradeoff between the measurement speed and spatial resolution. For the opposite combination of Walsh (RZ) and Golay (NRZ) codes, since the code duration for NRZ pulses is limited by τ_a, in order to achieve the required SNR, the code length for RZ pulses (code length for Walsh codes) has to be increased. However, it would cause significant increase in the measurement time. Therefore, it was concluded that there was little merit found in this combination.

In terms of the spatial resolution, dual Walsh codes PSP-BOTDA, however, provides the best measurement performance. As explained above, the robustness of Hadamard transform against the variation in the Brillouin signal amplitude has played an important role in realizing such a high spatial resolution measurement. The disadvantage of the dual Walsh codes PSP-BOTDA is that it takes longer time to accomplish the measurement because Walsh code uses as

many codewords as the amount of the code length. However, this disadvantage vanishes when once we measure the fiber of longer than 10km with 2cm spatial resolution and with the frequency accuracy of better than 1MHz. This is because in such a case signal averaging is required additionally, which results in the same measurement time it takes for both Walsh code and Golay code.

In conclusion, the combined code systems proposed in this thesis provide the method to have a balance of the tradeoff between the spatial resolution and the measurement time of the PSP-BOTDA in accordance to the measurement condition.

Chapter 1: Introduction

1.1 Research Introduction

Fiber optic communication technology is expanding at an explosive rate. The need for an optical communication in a nation is very high as the system has the potential to deliver better and more reliable services due to its technological advancement compared to other communication system. The advantage lies in its capability to transmit optical signal with low transmission losses of below 1dB/km and high speed data transfer rate [1]. Furthermore, fiber optic communication is an excellent choice for long haul communication, especially for undersea fiber optic network, thanks to its durability to withstand such an extreme environment.

Because of its prominent features against other communication systems, the evolution of the fiber optic communication technology has opened the way for other researches, including the research on fiber optic sensor. Studies have shown that the potential market for fiber optic sensor is increasing each year [2].

As such, in this thesis, the author has proposed and analyzed new techniques to measure distributed strain and temperature utilizing the existing distributed fiber optic sensor called Brillouin optical time domain analysis (BOTDA) for the purpose of improving the sensing efficiency. BOTDA is technique of measuring distributed strain and/or temperature along fiber optic cable by utilizing the occurrence of optical scattering in fiber called stimulated Brillouin scattering (SBS) [3]. BOTDA has found its applications especially in the civil engineering for structural health monitoring (SHM) for buildings, bridges, dams etc. This sensor can also be applied as a nerve system to detect crack on an airplane, intrusion detection in buildings, and even to detect leakage along petroleum/gas pipeline.

A BOTDA measurement system uses an intense pulsed light (pump) and a counter propagating continuous wave light (probe) of frequency value set at Stokes frequency injected into a fiber optic cable. When the frequency difference between the pump and the probe is tuned to the Brillouin frequency shift (BFS) of the fiber, the probe is amplified by the pump through the process of SBS. BOTDA measures the amplified probe waveform. The unique characteristic of the BFS is that it linearly increases with the increase in the strain or temperature of the fiber. Therefore, the BOTDA can measure local changes in the strain and temperature along the fiber.

At the early stage of development, the best spatial resolution obtained was 1m, with the use of pump pulse of duration 10ns [4]. This is because, shortening the duration to less than 10ns, which is around the time constant of the acoustic wave amplitude for silica fiber could cause the Brillouin gain to decrease significantly and consequently broadens the bandwidth of the Brillouin gain spectrum, resulting in the difficulty to measure BFS accurately. Therefore, it had been believed then that both the gain decrease and the spectral width broadening had precluded sub-meter spatial resolution measurements.

However, the spatial resolution problem in the BOTDA has been remarkably solved by a groundbreaking approach called Brillouin optical correlation domain analysis (BOCDA), which was proposed by Hotate and Hasegawa in 2000 [5]. BOCDA technique is slightly different from the BOTDA; instead of using time domain, it makes use of the optical correlation of pump and probe for the strain measurement. Since both pump and probe lights are in the form of continuous wave (cw), BOCDA is free from the spatial resolution limitation caused by the decay of the acoustic wave amplitude. As a result, the spatial resolution has been hugely improved up to 1.6mm [6]. However, BOCDA should keep a balance of the tradeoff between the spatial resolution and the distance range, requiring a further study on expanding the distance range.

Returning to back to the progress of BOTDA technology, a major breakthrough in the spatial resolution improvement was made from the experiments conducted by Bao et al. in 1999. In the experiment, it was found that the bandwidth of the Brillouin gain spectrum suddenly reduced when the pulse duration further decreased to the value smaller than the time constant of the acoustic wave [7]. This phenomenon was later explained by Lecoeuche et al. from numerical calculations that weak cw leakage from the electro-optic modulator had played a role of pre-pump [8]. This analysis had given researchers ideas to effectively use pre-pump pulse as a method to improve the spatial resolution; pulse pre-pump BOTDA (PPP-BOTDA) was proposed to improve the spatial resolution down to sub-meter range [9]. PPP-BOTDA uses a weak pulse pre-pump with a long duration followed by an intense pulse with short duration. The acoustic wave excited by this pulse pre-pump provides Brillouin gain to the short pulse. As a result, narrow spectral bandwidth and high spatial resolution measurement have been realized by this system.

Based on the same approach, in recent years, several other systems have also been introduced, such as differential pulse-width pair BOTDA (DPP-BOTDA), optical differential parametric amplification BOTDA (ODPA-BOTDA) and phase-shift pulse BOTDA (PSP-BOTDA). DPP-BOTDA uses two separate pump pulses with small width difference. The subtraction of the Brillouin signal in the electrical signal field produces the final measurement result. The width difference determines the spatial resolution [10]. ODPA-BOTDA practices the same approach, except that the pulses are generated at the Stokes and anti-Stokes frequencies and simultaneously injected into the fiber. This system allows simultaneous measurement of Brillouin gain and Brillouin loss. Thus, no subtraction is required at the post-processing stage because the signals due to the co-propagating pre-pump are cancelled out before reaching the photo detector [11]. PSP-BOTDA proposed by Horiguchi et al. uses two separate pump pulses having the same durations. One pump contains a preceding long pre-pump pulse (1^{st} pulse) and a succeeding short pulse (2^{nd} pulse); these pulses are in the same phase (no phase difference between the pulses). The other pump also contains a 1^{st} pulse and a 2^{nd} pulse; but the 2^{nd} pulse is in π-phase shift compared to the 1^{st} pulse [12]. Subtracting the two Brillouin signals obtained by each pump yields Brillouin signal whose intensity is approximately twice that of DPP-BOTDA. The spatial resolution is determined by the duration of the 2^{nd} pulse.

1.2 The Proposal on Pump Pulse Coding in the BOTDA

Coding techniques have been commonly used in optical time domain reflectometry (OTDR) that measures Rayleigh scattering in fibers for improving its performance [13, 14]. In general, the employment of coding technique in a measurement system can improve the signal-to-noise ratio (SNR) of the measured signal. The employment of pump light coding in PSP-BOTDA not only gives merit to the SNR improvement, but also gives benefit in faster measurement speed. To further discuss this benefit, let us consider an ideal system of conventional PSP-BOTDA without coding, measuring Brillouin signals over a 1000m length of fiber optic cable. In order to perform the measurements for 100 of frequencies (N_{freq} = 100) with 1000 times of averaging, the required total measurement time, $T_{measurement}$ for the conventional BOTDA can be described as

$$\begin{aligned} T_{measurement} &= RTT_{fiber} \times Averaging\ \ times \times N_{freq} \\ &= 10\mu s \times 1000 \times 100 \\ &= 1 sec \end{aligned} \tag{1.1}$$

where RTT_{fiber} is the round trip time of light in fiber. If we assume the same measurement conditions and 6dB of enhancement in optical SNR obtained with the coding, then the factor of the reduced measurement time F_T can be described as

$$F_T = \left(10^{(SNRenhancement/10)}\right)^2 = \left(10^{0.6}\right)^2 = 15.8 times \quad (1.2).$$

The analytical calculations above clearly give the merit of faster measurement speed that associated with the SNR improvement.

For the same purpose, coding techniques have been proposed in the BOTDA based fiber sensor [15-17]. It has been recognized, however, that the use of non-return-to-zero (NRZ)-formatted pulses in coded BOTDA has induced distortion in the measured Brillouin signal when the bit pulse duration is around or less than the time constant of the acoustic wave τ_a. This distortion is caused by varieties of additional gain of the preceding coded pulses. Consequently, return-to-zero (RZ) format has been introduced into the coded pulses of the high-spatial-resolution BOTDAs so that interactions between the preceding and succeeding bit pulses should not occur through the SBS process [15-17].

Despite the signal distortion problem described above, the proposal on the use of NRZ-formatted pulses employing Golay codes in the PSP-BOTDA called coded continuous-PSP-BOTDA has successfully demonstrated sub-meter spatial resolution, [18-19]. The Brillouin signals obtained with the NRZ-coded pulses are also well decoded if the total duration of the coded pulses is around or less than τ_a. This is because the subtraction process in the PSP-BOTDA intrinsically cancels the Brillouin gain due to the interaction between each coded pulse and the probe, extracting only the Brillouin gain that is derived from the interaction of each coded pulse with the acoustic wave excited by the pre-pump pulse. However, since the acoustic wave decays significantly after τ_a, the decoded Brillouin signal is distorted, resulting in the degradation of the spatial resolution, especially when using Golay code of total duration longer than τ_a.

To solve this problem, the author has proposed the employment of Walsh codes in the coded continuous-PSP-BOTDA. It was verified analytically, numerically and experimentally that Walsh codes can decode the Brillouin signals more accurately than the Golay codes do, without deteriorating the spatial resolution [20]. The robustness of the decoding process called Hadamard transform against the variations in the received Brillouin signal power has contributed to this success. It will be further discussed in details in Chapter 6 the advantages of employing Walsh codes over Golay codes in the coded continuous-PSP-BOTDA.

To further obtain higher SNR in the Brillouin signal, the author has proposed a technique of combining two codes in modulating the pump light of the coded PSP-BOTDA. This technique utilizes the simultaneous use of RZ- and NRZ pulses in modulating the pump light of the coded PSP-BOTDA [19, 21, 22]. Applying this technique can increase the total code length that can be used for the measurement. As a result, it is possible to obtain higher SNR than that of the previous coded continuous-PSP-BOTDA that uses only NRZ formatted pulses, the coded discrete-PSP-BOTDA that uses only RZ formatted pulses and obviously higher than that of other coded BOTDAs described in references [16] and [17]. Four types of code configurations are introduced in the combined codes PSP-BOTDA system; they are dual Golay codes-PSP-BOTDA, the two types of combined Walsh and Golay codes-PSP-BOTDAs and dual Walsh codes-PSP-BOTDA. Numerical simulations and experimental results are presented to show the advantages of employing four coding systems above in the PSP-BOTDA.

1.3 Thesis Structure

In general, Chapter 2 and Chapter 3 present the discussion on the background studies related to the BOTDA based sensing technique. In details, Chapter 2 explains the fundamental of the Brillouin scattering in fiber optic which covers

the theoretical formulation of spontaneous Brillouin scattering as well as stimulated Brillouin scattering (SBS). In Chapter 3, the literature review on the Brillouin based sensors are explained. Starting with the classic BOTDA technique, other techniques such as PPP-BOTDA, DPP-BOTDA, ODPA-BOTDA, PSP-BOTDA, coded PSP-BOTDA and BOCDA are also discussed in further details.

Chapter 4 ~ Chapter 11, which are the author's main contributions to this dissertation, discuss the proposed coding techniques in the PSP-BOTDA. In Chapter 4, a new concept of coding system for modulating the pump light of PSP-BOTDA techniques is described. The two basic coding systems employed in the PSP-BOTDA technique are Golay complementary pair (GCP) or also known as Golay codes and Walsh codes. To describe in brief, compared to the conventional PSP-BOTDA without coding, the employment of coding system has contributed to the achievement of higher SNR with high spatial resolution. The author has also proposed and discussed another new technique of combining two codes to modulate the pump light for further improving the signal-to-noise ratio (SNR). There are three combined code systems proposed in this chapter; the dual Golay codes, combined Walsh and Golay codes and dual Walsh codes. In Chapter 5, analysis on the employing GCP in the coded PSP-BOTDA called coded discrete-PSP-BOTDA is discussed. Coded discrete-PSP-BOTDA has been previously proposed to improve the SNR. However, in the experimental analysis, there were some problems in utilizing long code lengths due to the effects of the AC-coupled electrical amplifier used in the experiments. The author proposed a technique to overcome these problems. In Chapter 6, the author highlights the proposal for further improving the spatial resolution of the previously proposed coded continuous-PSP-BOTDA technique. In the previous studies, it was found that the spatial resolution of the coded continuous PSP-BOTDA employing Golay code has been degraded when the code length of duration longer than τ_a was used. The author has introduced a coding system called Walsh codes to overcome this problem. In Chapter 7, the simulation and experimental analysis on the employment of dual Golay codes in the PSP-BOTDA technique is discussed. Chapter 8 focusses on the proposal of combining Walsh and Golay codes in modulating the pump light of PSP-BOTDA. Chapter 9 discusses the dual Walsh codes proposal. The simulation results shown in Chapter 9 are also compared with that shown in Chapter 7 and further discussed for the purpose of comparing the sensing efficiency between the two techniques. Preliminary experiments were also conducted and the results are described in Chapter 9. In Chapter 10, the measurement performance of the BOTDA employing the proposed codes is numerically analyzed and presented. By referring to the actual measurement data reported in publications, the parameters used in the analytical calculations were determined. This study has highlighted the relationship between the SNR and the measurement time for longer fiber length (1km and 10km) with high spatial resolution (10cm and 2cm). The results obtained for the proposed coding systems are then analyzed and compared with that of conventional coded PSP-BOTDAs (coded discrete- and coded continuous-PSP-BOTDAs); this analysis has revealed that the proposed coding system can provide BOTDA with superior performance in the spatial resolution and measurement time than the conventional one. Finally, Chapter 11 gives the conclusions and the proposed future works of the research.

References

[1] G. P. Agrawal. "Fiber-optic Communication Systems 3rd Edition", Wiley Interscience Publication (2002).

[2] Matthew Peach, "Market for fiber optics sensors to hit $4bn by 2017", http://optics.org/news/4/6/17, 13th Jun. 2013.

[3] T. Horiguchi, M. Tateda, "BOTDA-nondestructive measurement of single-mode optical fiber attenuation characteristics using Brillouin interaction: theory", J. Lightwave Technol., vol. 6, no. 8, pp. 1170-1176, Aug. 1989.

[4] T. Horiguchi, T. Kurashima, and Y. Koyamada, "1 m spatial resolution measurement of distributed Brillouin frequency shift in single-mode fibers," in Tech. Dig. Symp. Opt. Fiber Meas., NIST Special Publication 864, Boulder, CO, pp. 73-76, Sept. 1994.

[5] K. Hotate and T. Hasegawa, "Measurement of Brillouin gain spectrum distribution along an optical fiber using a correlation-based technique –Proposal, experiment and simulation–," IEICE Trans. on Electron., vol. E83-C, no. 3, pp. 405-412, Mar. 2000.

[6] K. Y. Song, Z. He and K. Hotate, "Distributed strain measurement with millimeter-order spatial resolution based on Brillouin optical correlation domain analysis", Opt. Lett., vol. 31, no. 17, pp. 2526-2528, Sep. 2006.

[7] X. Bao and A. Brown, "Characterization of the Brillouin-loss spectrum of single-mode fibers by use of very short (<10-ns) pulses", Opt. Lett., vol. 24, no. 8, pp. 510-512, Apr. 1999.

[8] V. Lecoeuche, D. J. Webb, C. N. Pannell and D. A. Jackson, "Transient response in high-resolution Brillouin-based distributed sensing using probe pulses shorter than the acoustic relaxation time", Opt. Lett., vol. 25, no. 3, pp. 156-158, Feb. 2000.

[9] C. H. Li, K. Nishiguchi, M. Miyatake, A. Makita, M. Yokoyama, K. Kishida, T. Mizutani and N. Takeda, "PPP-BOTDA method to achieve 2cm spatial resolution in Brillouin distributed measuring technique", Technical Report of IEICE. OFT 108(32) (in Japanese), pp. 55-60, May 2008.

[10] W. Li, X. Bao, Y. Li and L. Chen, "Differential pulse-width pair BOTDA for high spatial resolution sensing", Opt. Exp., vol. 16, no. 26, pp. 21616-21625, Dec. 2008.

[11] Y. Li, X. Bao, Y. Dong and L. Chen, "A novel distributed Brillouin sensor based on optical differential parametric amplification", J. Lightw. Technol., vol. 28, no. 18, pp. 2621-2626, Sep. 2010.

[12] T. Horiguchi, R. Muroi, A. Iwasaka, K. Wakao and Y. Miyamoto, "Negative Brillouin gain and its application to distributed fiber sensing (presented poster style)", 33rd European Conference and Exhibition of Optical Communication (ECOC) 2007, P018, Sep. 2007; T. Horiguchi, R. Muroi, A. Iwasaka, K. Wakao and Y. Miyamoto, "BOTDA utilizing phase-shift pulse", IEICE Trans. Commun. (in Japanese), vol. J91-B, no. 2, pp. 207-216, Feb. 2008.

[13] M. D. Jones, "Using simplex codes to improve OTDR sensitivity", IEEE Photon. Tech. Lett., vol. 15, no. 7, pp. 822-824, Jul. 1993.

[14] D. Lee, H. Yoon, P. Kim, J. Park and N. Park, "Optimization of SNR improvement in the noncoherent OTDR based on simplex codes", J. Lightw. Technol., col. 24, no. 1, Jan. 2006.

[15] R. Muroi, T. Horiguchi, Y. Miyamoto, Y. Sato, A. Tachibana and A. Takakura, "PSP-BOTDA based on Golay code", IEICE Trans. Commun. (in Japanese), vol. J91-B, no. 11, pp. 1493-1501, November 2008.

[16] H. Liang, W. Li, N. Linze, L. Chen and X. Bao, "High-resolution DPP-BOTDA over 50 km LEAF using return-to-zero coded pulses", Opt. Lett., vol. 35, no. 10, pp. 1503-1505, May 2010.

[17] M. A. Soto, G. Bolognini and F. Di. Pasquale, "Analysis of pulse modulation format in coded BOTDA sensors", Opt. Exp., vol. 18, no. 14, pp. 14878-14892, Jul. 2010.

[18] D. Uchiyama, T. Horiguchi, H. Ando, Y. Okumoto, T. Sasaki and Y. Sawai, "Signal to noise improvement ratio for coded PSP-BOTDA", Technical report of IEICE. OFT 109 (377) (in Japanese), pp. 33-38, Jan. 2010.

[19] **M. S. D. B. Zan** and T. Horiguchi, "A dual Golay complementary pair of sequences for improving the performance of phase-shift pulse BOTDA fiber sensor" J. Lightw. Technol., vol. 30, no. 21, pp. 3338-3356, Nov. 2012.

[20] **M. S. D. B. Zan**, T. Tsumuraya and T. Horiguchi, "The use of Walsh code in modulating the pump light of high spatial resolution phase-shift-pulse Brillouin optical time domain analysis with non-return-to-zero pulses", J. Meas. Sci. Technol., vol. 24, no. 9 (094025), pp. 1-13, Jul. 2013.

[21] **M. S. D. B. Zan** and T. Horiguchi, "Analysis on the Employment of Combined Codes in Modulating the Pump Light of Phase Shift Pulse Brillouin Optical Time Domain Analysis (PSP-BOTDA)", Proc. of 51st Meeting on Lightwave Sensing Technol., LST51-17, pp. 115-120, Jun. 2013.

[22] **M. S. D. B. Zan**, K. Yokoyama and T. Horiguchi, "Combination of Walsh and Golay codes in modulating the pump light of phase-shift pulse BOTDA sensor", Proc. of the IEEE 4th Int. Conf. on Photonics (ICP 2013) 2013, Malaysia, No. 46 D2-AM2-A, Oct. 2013.

Chapter 2: Spontaneous and Stimulated Brillouin Scattering

2.1 Introduction to Chapter

Brillouin scattering is an optical scattering that occurs in a medium when light traveling through it interacts with optical density variations of the medium. The density variation is caused by the acoustic wave that also acts as pressure. The pressure then compresses the medium, causing the refractive index of the medium to change. In the case of fiber optic cable, the sound wave causes the change in the refractive index of the fiber core. As a result, this process causes the propagating light to scatter into the Brillouin scattered light. In other words, Brillouin scattering can be defined as the scattering of a photon from an acoustic phonon. Brillouin scattering phenomenon is subjected to the Doppler shift, because the sound wave also propagates along the fiber. Therefore, Brillouin scattering process causes the change in the frequency and energy of the scattered light. There are two components of scattered light induced by Brillouin scattering process. One is the scattered light with frequency shifted down to lower frequency known as Stokes component and the other one is the scattered light with frequency is shifted to higher frequency known as anti-Stokes component. In this thesis, the Stokes component is the main subject that will be explained in deep details.

Brillouin scattering can be detrimental in fiber optics communication system because it limits the performance of the signal transmission in terms of maximizing the input power. However, at the same time, the scattering is also useful for the applications such as the Brillouin fiber sensor, Brillouin fiber lasers and Brillouin fiber amplifiers [1-3]. Apart from that, the theory of slow light induced from the scattering phenomenon has led to the development of optical buffering in the future all-optical router communication systems [4].

Optical Brillouin scattering process falls in two categories, one is spontaneous Brillouin scattering and the other one is stimulated Brillouin scattering (SBS). In general, the spontaneous light scattering means the light is scattered under condition such that the optical properties of the medium are not modified by the incident light beam [5]. For spontaneous Brillouin scattering, the optical field of the incident light is usually so small that it does not modify the acoustic properties of the medium. In this case, the spontaneous Brillouin scattering originates from the scattering of the light from the acoustic wave that is thermally excited. On the contrary, the SBS usually appears when the optical field of the incident light used is sufficiently large, that it alters the density variation of the medium and causes the scattered light to become quite intense. The incident light and the scattered light can then beat together, giving rise in the acoustic wave through electrostriction process. Thus, under this condition, the scattered light and the acoustic wave mutually contribute to each other's growth [5].

In this chapter, spontaneous Brillouin scattering will be explained first which consists of both Stokes and anti-Stokes waves. In the next section, stimulated Brillouin scattering (SBS), which is the main fundamental process applied in this research, is also explained.

2.2 Nonlinear Wave Propagation

The theoretical formulation of the SBS process is considered from the propagation of light through a material and the response of the material system to the light interaction. This can be described from the Maxwell equations as listed below [5].

$$rot\,\tilde{\mathbf{H}} \equiv \nabla \times \tilde{\mathbf{H}} = \tilde{\mathbf{J}} + \frac{\partial \tilde{\mathbf{D}}}{\partial t} \tag{2.1}$$

$$rot\,\tilde{\mathbf{E}} \equiv \nabla \times \tilde{\mathbf{E}} = -\frac{\partial \tilde{\mathbf{B}}}{\partial t} \tag{2.2}$$

$$div\,\tilde{\mathbf{D}} \equiv \nabla \bullet \tilde{\mathbf{D}} = \tilde{\rho} \tag{2.3}$$

$$div\,\tilde{\mathbf{B}} \equiv \nabla \bullet \tilde{\mathbf{B}} = 0 \tag{2.4}$$

where $\tilde{E}$ is the electrical field vector of the optical light, $\tilde{\mathbf{H}}$ is the magnetic field vector , $\tilde{\mathbf{D}}$ is vector of the electric flux density, $\tilde{\mathbf{B}}$ is the vector of magnetic flux density, $\tilde{\mathbf{J}}$ is the vector of current density and $\tilde{\rho}$ is the charge density. The tilde sign (~) used in this chapter denotes the quantity that rapidly varies with time. To solve these equations, we first consider the regions of space that contains no free charges, so that

$$\tilde{\rho} = 0 \tag{2.5}$$

and contains no free current, so that

$$\tilde{\mathbf{J}} = 0 \tag{2.6}$$

We also assume that the material is nonmagnetic, so that

$$\tilde{\mathbf{B}} = \mu_0 \tilde{\mathbf{H}} \tag{2.7}$$

where μ_0 is the permeability of free space. However, we allow the material to be nonlinear in the sense that the fields $\tilde{\mathbf{D}}$ and $\tilde{\mathbf{E}}$ are related by

$$\tilde{\mathbf{D}} = \varepsilon_0 \tilde{\mathbf{E}} + \tilde{\mathbf{P}} \tag{2.8}$$

where ε_0 is the permittivity of free space and $\tilde{\mathbf{P}}$ is the dielectric polarization. By assigning Eqs. (2.5), (2.6) and (2.8) into Eq. (2.1), one may obtain

$$rot\,\tilde{\mathbf{H}} \equiv \nabla \times \tilde{\mathbf{H}} = \frac{\partial}{\partial t}\left(\varepsilon_0 \tilde{\mathbf{E}} + \tilde{\mathbf{P}}\right) \tag{2.9}$$

with $\tilde{\mathbf{P}}$ is expressed as

$$\tilde{\mathbf{P}} = \varepsilon_0 \chi \tilde{\mathbf{E}} + \tilde{\mathbf{P}}^{\mathbf{NL}} \tag{2.10}$$

where $\varepsilon_0 \chi \tilde{\mathbf{E}}$ denotes the linear polarization part and $\tilde{\mathbf{P}}^{\mathbf{NL}}$ the nonlinear polarization part. By using Eq. (2.10), we can then express Eq. (2.9) as

$$\begin{aligned} rot\,\tilde{\mathbf{H}} \equiv \nabla \times \tilde{\mathbf{H}} &= \frac{\partial}{\partial t}\left(\varepsilon_0 \tilde{\mathbf{E}} + \tilde{\mathbf{P}}\right) \\ &= \frac{\partial}{\partial t}\left(\varepsilon_0 \tilde{\mathbf{E}} + \varepsilon_0 \chi \tilde{\mathbf{E}} + \tilde{\mathbf{P}}^{\mathbf{NL}}\right) \\ &= \varepsilon \frac{\partial \tilde{\mathbf{E}}}{\partial t} + \frac{\partial \tilde{\mathbf{P}}^{\mathbf{NL}}}{\partial t} \end{aligned} \tag{2.11}$$

where

$$\varepsilon \equiv \varepsilon_0 (1 + \chi) = \varepsilon_0 \varepsilon_r \tag{2.12}$$

with ε_r is the material relative permittivity and χ is the electrical susceptibility. Next, the Eq. (2.7) is substituted into Eq. (2.2) to obtain

$$rot\,\tilde{\mathbf{E}} \equiv \nabla \times \tilde{\mathbf{E}} = -\frac{\partial \tilde{\mathbf{B}}}{\partial t} = -\mu_0 \frac{\partial \tilde{\mathbf{H}}}{\partial t} \tag{2.13}.$$

By assigning another rotation (∇) into Eq. (2.13), it then becomes

$$\nabla \times \nabla \times \tilde{\mathbf{E}} = -\mu_0 \frac{\partial}{\partial t}\left(\nabla \times \tilde{\mathbf{H}}\right) \tag{2.14}$$

Assigning Eqs. (2.11) and (2.12) into the right side of Eq. (2.14), one may get

$$\nabla \times \nabla \times \tilde{\mathbf{E}} = -\mu_0 \frac{\partial}{\partial t}\left(\varepsilon \frac{\partial \tilde{\mathbf{E}}}{\partial t} + \frac{\partial \tilde{\mathbf{P}}^{\mathbf{NL}}}{\partial t} \right)$$
$$= -\mu_0 \varepsilon \frac{\partial^2 \tilde{\mathbf{E}}}{\partial t^2} - \mu_0 \frac{\partial^2 \tilde{\mathbf{P}}^{\mathbf{NL}}}{\partial t^2} \tag{2.15}$$

By using the common relation of vector as expressed below,

$$\nabla \times (\nabla \times \tilde{\mathbf{E}}) = \nabla(\nabla \bullet \tilde{\mathbf{E}}) - \nabla^2 \tilde{\mathbf{E}} \tag{2.16}$$

the left-hand side of Eq. (2.16) is replaced with the right-hand side of the Eq. (2.15) and further organized to produce

$$\nabla(\nabla \bullet \tilde{\mathbf{E}}) - \nabla^2 \tilde{\mathbf{E}} = -\mu_0 \varepsilon \frac{\partial^2 \tilde{\mathbf{E}}}{\partial t^2} - \mu_0 \frac{\partial^2 \tilde{\mathbf{P}}^{\mathbf{NL}}}{\partial t^2} \tag{2.17}.$$

Assuming that the contribution of $\nabla \bullet \tilde{\mathbf{E}}$ is small and negligible, Eq. (2.17) then becomes

$$-\nabla^2 \tilde{\mathbf{E}} = -\mu_0 \varepsilon \frac{\partial^2 \tilde{\mathbf{E}}}{\partial t^2} - \mu_0 \frac{\partial^2 \tilde{\mathbf{P}}^{\mathbf{NL}}}{\partial t^2} \tag{2.18}$$

Using the relation $\mu_0 = 1/\varepsilon_0 c^2$ and the relation in Eq. (2.12), Eq. (2.18) then becomes

$$\nabla^2 \tilde{\mathbf{E}} - \frac{\varepsilon_r}{c^2} \frac{\partial^2 \tilde{\mathbf{E}}}{\partial t^2} = \frac{1}{\varepsilon_0 c^2} \frac{\partial^2 \tilde{\mathbf{P}}^{\mathbf{NL}}}{\partial t^2} \tag{2.19}$$

which notates the nonlinear wave propagation equation in media.

2.3 Spontaneous Light Scattering

2.3.1 Spontaneous Brillouin Scattering

In this section, the sound wave (pressure wave) equation involved in the optical scattering process that will be described next is related to the expression of Stokes scattering. The equation of motion for a sound wave given in terms of pressure wave $\Delta\tilde{p}$ can be described as

$$\frac{\partial^2 \Delta\tilde{p}}{\partial t^2} - \Gamma' \nabla^2 \frac{\partial \Delta\tilde{p}}{\partial t} - \upsilon^2 \nabla^2 \Delta\tilde{p} = 0 \tag{2.20}$$

where υ is the velocity of sound and Γ' is the damping parameter.

To study the nature of the acoustic wave equation in Eq. (2.20), we consider the propagation of the wave in an acoustic medium as

$$\Delta\tilde{p} = \Delta p\, e^{i(qz - \Omega t)} + c.c \tag{2.21}$$

where *c.c* is the complex conjugate. We introduce Eq. (2.21) in Eq. (2.20) and solve the equation step by step. We firstly expand the first term of Eq. (2.20)

$$\frac{\partial^2 \Delta\tilde{p}}{\partial t^2} = \frac{\partial^2}{\partial t^2} \Delta p e^{i(qz - \Omega t)} + c.c$$
$$= -\Omega^2 \Delta p e^{i(qz - \Omega t)} + c.c \tag{2.22}$$

Next we expand the second term of Eq. (2.20) as

$$\Gamma' \nabla^2 \frac{\partial \Delta\tilde{p}}{\partial t} = \Gamma' \frac{\partial^2}{\partial z^2} \frac{\partial \Delta\tilde{p}}{\partial t}$$
$$= iq^2 \Omega \Gamma' \Delta p e^{i(qz - \Omega t)} + c.c \tag{2.23}$$

Then we expand the third term of Eq. (2.20) as

$$\upsilon^2\nabla^2\Delta\tilde{p} = \upsilon^2\frac{\partial^2}{\partial z^2}\Delta p e^{i(qz-\Omega t)} + c.c$$
$$= -q^2\upsilon^2\Delta p e^{i(qz-\Omega t)} + c.c \tag{2.24}$$

We then substitute Eqs. (2.22), (2.23) and (2.24) into Eq. (2.20) and write the equation as follows

$$-\Omega^2\Delta p e^{i(qz-\Omega t)} - iq^2\Omega\Gamma'\Delta p e^{i(qz-\Omega t)} + q^2\upsilon^2\Delta p e^{i(qz-\Omega t)} = 0$$
$$-\Delta p e^{i(qz-\Omega t)}\left(\Omega^2 + iq^2\Omega\Gamma' - q^2\upsilon^2\right) = 0$$

$$\Omega^2 = q^2(\upsilon^2 - i\Omega\Gamma') \tag{2.25}.$$

We can then rewrite Eq. (2.25) as

$$q^2 = \frac{\Omega^2}{\upsilon^2 - i\Omega\Gamma'} = \frac{\Omega^2/\upsilon^2}{1-\frac{i\Omega\Gamma'}{\upsilon^2}} \approx \frac{\Omega^2}{\upsilon^2}\left(1+\frac{i\Omega\Gamma'}{\upsilon^2}\right) \tag{2.26}$$

which shows that

$$q \approx \frac{\Omega}{\upsilon} + \frac{i\Gamma}{2\upsilon} \tag{2.27}$$

where the phonon decay rate, Γ can be expressed as

$$\Gamma = \Gamma' q^2 \tag{2.28}.$$

The time constant of the acoustic wave amplitude, τ_a is defined as

$$\tau_a = \frac{2}{\Gamma} = \frac{2}{q^2\Gamma'} \tag{2.29},$$

which describes the time consumed by the amplitude of the acoustic wave to decay from 100% to 36.8% $(1/e)$.

Next process is to calculate the rate at which light is scattered out by the acoustic wave. We express the incident optical field that propagates in *z* direction as

$$\tilde{E}_0(z,t) = E_0 e^{i(\mathbf{k}\bullet\mathbf{r}-\omega t)} + c.c \tag{2.30}$$

The scattered field obeys the driven wave equation

$$\nabla^2\tilde{E} - \frac{n^2}{c^2}\frac{\partial^2\tilde{E}}{\partial t^2} = \frac{1}{\varepsilon_0 c^2}\frac{\partial^2\tilde{P}}{\partial t^2} \tag{2.31}$$

that is analogous to Eq. (2.17). The nonlinear polarization $\tilde{P}$ of the medium is described as

$$\tilde{P} = \varepsilon_0\left(\frac{\partial\varepsilon}{\partial\rho}\right)\Delta\tilde{\rho}\,\tilde{E}_0 \tag{2.32}$$

and the variation in the density, $\Delta\tilde{\rho}$ is given by

$$\Delta\tilde{\rho} = \left(\frac{\partial\rho}{\partial p}\right)_S\Delta\tilde{p} + \left(\frac{\partial\rho}{\partial S}\right)_p\Delta\tilde{S} \tag{2.33}$$

The first term of Eq. (2.33) describes the density fluctuations (acoustic wave) which leads to Brillouin scattering, while the second term of Eq. (2.33) describes the density fluctuations with the entropy $\Delta\tilde{S}$ (temperature fluctuations), which leads to Rayleigh-center scattering. Thus, by taking only the first contribution in Eq. (2.33) where $\Delta\tilde{p}$ denotes the incremental pressure, one can find that

$$\tilde{P}(\mathbf{r},t) = \varepsilon_0\left(\frac{\partial\varepsilon}{\partial\rho}\right)\left(\frac{\partial\rho}{\partial p}\right)_S\Delta\tilde{p}(\mathbf{r},t)\tilde{E}_0(z,t)$$

$$= \varepsilon_0 \gamma_e C_S \Delta\tilde{p}(\mathbf{r},t)\tilde{E}_0(z,t) \tag{2.34}$$

where C_S is called the adiabatic compressibility and γ_e is the electrostrictive constant, which is defined by

$$\gamma_e = \left(\rho \frac{\partial \varepsilon}{\partial \rho}\right)_{\rho=\rho_0} \tag{2.35}$$

We take a typical component of the thermally excited pressure disturbance within the interaction region to be given by

$$\Delta\tilde{p}(\mathbf{r},t) = \Delta p e^{i(\mathbf{q}\bullet\mathbf{r}-\Omega t)} + c.c \tag{2.36}$$

and solve the Eq. (2.31) by using Eq. (2.30) through Eq. (2.36) to produce

$$\begin{aligned}
&\nabla^2\tilde{\mathbf{E}} - \frac{n^2}{c^2}\frac{\partial^2\tilde{\mathbf{E}}}{\partial t^2} = \frac{1}{\varepsilon_0 c^2}\frac{\partial^2\tilde{P}}{\partial t^2} \\
&= \frac{\gamma_e C_S}{c^2}\frac{\partial^2}{\partial t^2}\left[\Delta\tilde{p}(\mathbf{r},t)\ \tilde{E}_0(z,t)\right] \\
&= \frac{\gamma_e C_S}{c^2}\frac{\partial^2}{\partial t^2}\left[\left(\Delta p e^{i(\mathbf{q}\bullet\mathbf{r}-\Omega t)} + \Delta p * e^{-i(\mathbf{q}\bullet\mathbf{r}-\Omega t)}\right)\left(E_0 e^{i(\mathbf{k}\bullet\mathbf{r}-\omega t)} + E_0 * e^{-i(\mathbf{k}\bullet\mathbf{r}-\omega t)}\right)\right] \\
&= \frac{\gamma_e C_S}{c^2}\frac{\partial^2}{\partial t^2}\left[\Delta p E_0 e^{i(\mathbf{k}+\mathbf{q})\bullet\mathbf{r}-i(\omega+\Omega)t} + \Delta p E_0 * e^{-i(\mathbf{k}-\mathbf{q})\bullet\mathbf{r}+i(\omega-\Omega)t} + \Delta p * E_0 e^{i(\mathbf{k}-\mathbf{q})\bullet\mathbf{r}-i(\omega-\Omega)t} + \Delta p * E_0 * e^{-i(\mathbf{k}+\mathbf{q})\bullet r+i(\omega+\Omega)t}\right] \\
&= \frac{\gamma_e C_S}{c^2}\left[(\omega+\Omega)^2 \Delta p E_0 e^{i(\mathbf{k}+\mathbf{q})\bullet\mathbf{r}-i(\omega+\Omega)t} - (\omega-\Omega)^2 \Delta p E_0 * e^{-i(\mathbf{k}-\mathbf{q})\bullet\mathbf{r}+i(\omega-\Omega)t}\right. \\
&\quad \left. + (\omega-\Omega)^2 \Delta p * E_0 e^{i(\mathbf{k}-\mathbf{q})\bullet\mathbf{r}-i(\omega-\Omega)t} - (\omega+\Omega)^2 \Delta p * E_0 * e^{-i(\mathbf{k}+\mathbf{q})\bullet\mathbf{r}+i(\omega+\Omega)t}\right] \\
&= -\frac{\gamma_e C_S}{c^2}\left[(\omega-\Omega)^2 \Delta p * E_0 e^{i(\mathbf{k}-\mathbf{q})\bullet\mathbf{r}-i(\omega-\Omega)t} + (\omega+\Omega)^2 \Delta p E_0 e^{i(\mathbf{k}+\mathbf{q})\bullet\mathbf{r}-i(\omega+\Omega)t} + c.c\right]
\end{aligned} \tag{2.37}$$

The first term of Eq. (2.37) leads to Stokes scattering, and the second term refers to anti-Stokes scattering; the angular frequency of both scattered lights is respectively downshifted and upshifted by the value of Ω.

2.3.2 Stokes Scattering

The illustration of the Brillouin scattering in a media for the case of Stokes scattering (first term of Eq. (2.37)) is shown in Fig. 2.1.

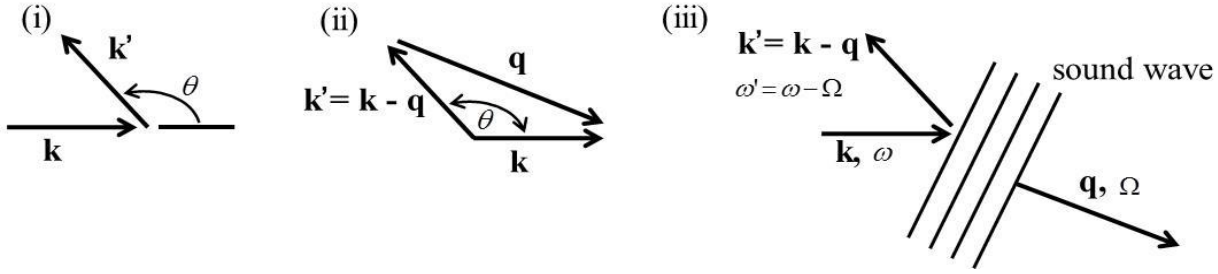

Fig. 2.1. Illustration of Brillouin scattering (Stokes scattering)

In Fig. 2.1, **k** is the wave vector of the incident optical field with its angular frequency of ω, **k'** and ω' is the wave vector and the angular frequency of the scattered light while **q** is the wave vector of the sound wave with its angular frequency of Ω. The scattered light comprises with wave vector and frequency can be expressed as

$$\mathbf{k'} = \mathbf{k} - \mathbf{q} \tag{2.38}$$

$$\omega' = \omega - \Omega \tag{2.39}$$

The angular frequency ω and the wave vector **k** of the incident light are related together according to

$$\omega = |\mathbf{k}|\left(\frac{c}{n}\right) \tag{2.40}$$

and the angular frequency Ω and wave vector **q** of the acoustic wave can be expressed as

$$\Omega = |\mathbf{q}|\upsilon \tag{2.41}$$

Therefore, one can change the form of Eq. (2.39) to become

$$\omega' = |\mathbf{k}'|\left(\frac{c}{n}\right) \tag{2.42}$$

In order to simultaneously satisfy the Eq. (2.38) through Eq. (2.42), the sound wave and its wave vector must have a particular value for any scattering direction. Fig. 2.1 (i) shows the relation of θ when the incident light is scattered at that particular angle. Figure 2.1 (ii) shows the vector relation between those two optical fields in (i) and Fig. 2.1 (iii) shows the relation of the wave vector of the sound wave disturbance that takes place when the incident field is scattered in a media. Take note that $|\mathbf{k}|$ is nearly equal to $|\mathbf{k}'|$ because Ω is much smaller than ω. From the diagram of Fig. 2.1 (ii), it shows that

$$|\mathbf{q}| = 2|\mathbf{k}|sin\left(\frac{\theta}{2}\right) \tag{2.43}$$

Therefore, Eq. (2.41) then becomes

$$\Omega = 2|\mathbf{k}|\upsilon sin\left(\frac{\theta}{2}\right) = 2n\omega\frac{\upsilon}{c}sin\left(\frac{\theta}{2}\right) \tag{2.44}$$

From Eq. (2.44), one easily finds that the Stokes shift Ω is equal to zero for forward scattering and becomes maximum for back scattering (i.e: θ = 180 degrees). Therefore, the Eq. (2.44) can be rewritten as

$$\Omega_{\max} = 2n\frac{\upsilon}{c}\omega \tag{2.45}$$

By taking the value of $n = 1.5, \upsilon = 5960\,ms^{-1}$, $\omega/2\pi = 1.9355\times10^{14}Hz$ for $\lambda = 1550nm$, one can calculate the value of $\Omega_{\max}/2\pi$ as

$$\frac{\Omega_{\max}}{2\pi} = 2n\frac{\upsilon}{c}f$$
$$= 2(1.5)\frac{5960}{3\times10^{8}}1.9355\times10^{14}$$
$$= 11.536GHz$$

2.3.3 Anti-Stokes Scattering

The illustration of the anti-Stokes scattering (second term of Eq. (2.37)) can be shown in Fig 2.2.

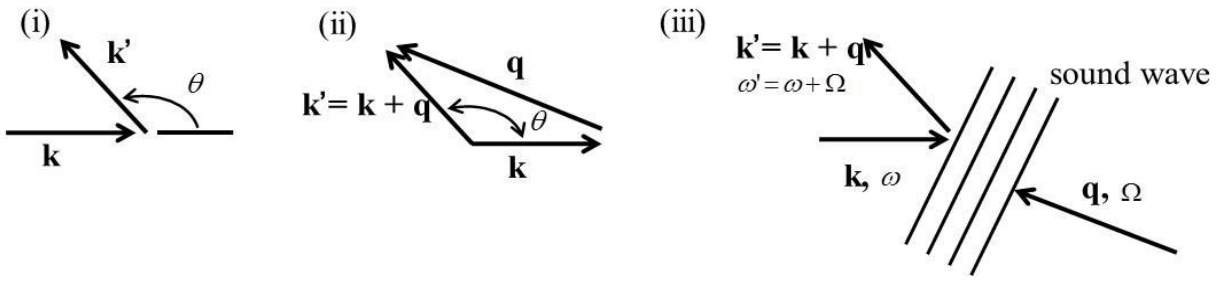

Fig. 2.2. Illustration of Brillouin scattering (anti-Stokes scattering)

The explanation on the anti-Stokes scattering resembles to that in the Stokes scattering in previous section. In Fig. 2.2 (i), it shows the relation of the wave vector of the scattered light when the incident light is scattered at the angle of θ. In Fig. 2.2 (ii), it shows the vector relations derived from (i) and Fig. 2.2 (iii) shows the involvement of sound wave when

the incident light is scattered in a media. From Fig. 2.2, the scattered light with its components of wave vector **k'** and angular frequency ω' can be expressed as

$$\mathbf{k'} = \mathbf{k} + \mathbf{q} \tag{2.46}$$

$$\omega' = \omega + \Omega \tag{2.47}$$

By using the same relations shown in Eq. (2.40) to Eq. (2.43), one can write the wave vector of the acoustic wave **q** as

$$|\mathbf{q}| = 2|\mathbf{k}|sin\left(\frac{\theta}{2}\right) \tag{2.48}$$

Therefore, the angular frequency Ω of the acoustic wave is given as

$$\Omega = 2|\mathbf{k}|\upsilon sin\left(\frac{\theta}{2}\right) = 2n\omega\frac{\upsilon}{c}sin\left(\frac{\theta}{2}\right) \tag{2.49}$$

From the above explanation and illustration in Fig. 2.2, the anti-Stokes scattering can be defined as the scattering of light from an oncoming sound wave. In contrast with the Stokes scattering, the anti-Stokes scattering shows that the frequency of the scattered light is shifted up since it is induced by the oncoming acoustic wave. The illustration of the Stokes and anti-Stokes scattering is shown in Fig. 2.3.

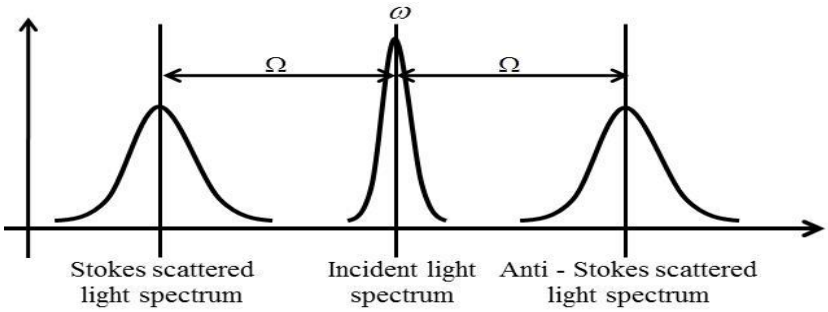

Fig. 2.3. The spectrum of Stokes and anti-Stokes waves

2.4 Stimulated Light Scattering

2.4.1 Stimulated Brillouin Scattering (SBS)

In the previous section of the spontaneous light scattering, we can see that the scattering of the light in a nonlinear medium is said to be spontaneous when the fluctuation of the dielectric constant are excited thermally. In this section, the physical and mathematical explanations of the stimulated light scattering especially involves in the stimulated Brillouin scattering (SBS) are explained.

2.4.2 The Physical Process of SBS

The schematic diagram of the SBS process can be depicted in Fig. 2.4.

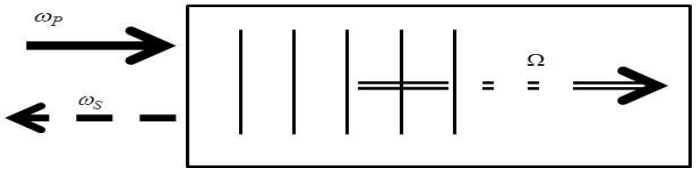

Fig. 2.4. The schematic diagram of the SBS process

The concept of SBS process can be visualized as an interaction between pump light (ω_p), Stokes light (ω_S) and acoustic wave (Ω) in a nonlinear medium. In Fig. 2.4, when an incident light is injected to the medium, an acoustic

wave is produced from the interaction between the incident light and the nonlinear medium, the sound wave which also acts as pressure wave modulates the refractive index of the medium and the variation of the refractive index causes the incident light to be scattered through Bragg diffraction. In the SBS case, the scattered light is usually in the backward direction to the incident light. The portion of the incident light scattered is downshifted in its frequency which implies the Doppler shift associates with the gratings that move at the acoustic velocity υ. The angular frequency of the scattered light is shifted downward in frequency to the Stokes frequency $\omega_S = \omega_P - \Omega$. By implying the energy conservation law, the Brillouin scattering process is said to be stimulated when [6]

(i) The beating of the pump light and the Stokes light increases the energy of acoustic wave ($\Omega = \omega_P - \omega_S$).

(ii) The beating between the pump light and the acoustic wave increases the energy of Stokes light ($\omega_S = \omega_P - \Omega$).

By properly setting the parameter to create SBS phenomena, the feedbacks resulted from the interaction explained in (i) and (ii) may lead to the exponential growth of the amplitude of the Stokes wave.

2.4.3 Formulation of the SBS Wave

Assume that the optical field of the pump light and the Stokes wave can be respectively represented as

$$\tilde{E}_p(z,t) = A_p(z,t)e^{i(k_p z-\omega_p t)} + c.c \tag{2.50}$$

$$\tilde{E}_S(z,t) = A_S(z,t)e^{i(-k_s z-\omega_S t)} + c.c \tag{2.51}.$$

The total field can be expressed as

$$\tilde{E}(z,t) = \tilde{E}_p(z,t) + \tilde{E}_S(z,t) \tag{2.52}$$

In a similar manner, the acoustic field can be described in terms of the material density distribution as

$$\tilde{\rho}(z,t) = \rho_0 + \left(\rho(z,t)e^{i(qz-\Omega t)} + c.c\right) \tag{2.53}$$

where $\Omega = \omega_p - \omega_S$, $q = 2k_p$, and ρ_0 is the mean density of the medium. The material density changes in the Brillouin medium is assumed to obey the acoustic wave equation (similar to the expression of Eq. (2.20))

$$\frac{\partial^2 \tilde{\rho}}{\partial t^2} - \Gamma'\nabla^2 \frac{\partial \tilde{\rho}}{\partial t} - \upsilon^2\nabla^2\tilde{\rho} = \nabla \bullet \mathbf{f} \tag{2.54}$$

where υ is the sound velocity and Γ' is a damping parameter. The right-hand side of Eq. (2.54) shows the divergence of the force per unit volume **f**, which can be expressed as

$$\mathbf{f} = \nabla p_{st}, \quad p_{st} = -\frac{1}{2}\varepsilon_0\gamma_e\left\langle \tilde{E}^2 \right\rangle \quad (p_{st}\text{: strictive pressure due to the presence of electric field}) \tag{2.55}$$

$$\begin{aligned}
\nabla \bullet \mathbf{f} &= -\frac{1}{2}\varepsilon_0\gamma_e 2\nabla^2\tilde{E}\tilde{E}^* \\
&= -\varepsilon_0\gamma_e\nabla^2\tilde{E}\tilde{E}^* \\
&= -\varepsilon_0\gamma_e\nabla^2(\tilde{E}_p + \tilde{E}_S)(\tilde{E}^*_p + \tilde{E}^*_S) \\
&= -\varepsilon_0\gamma_e\nabla^2\left[A_p A_p^* + A_p A^*_s e^{i(qz-\Omega t)} + A^*_p A_s e^{-i(qz-\Omega t)} + A_s A_s^*\right] \\
&= \varepsilon_0\gamma_e q^2\left(A_p A^*_s e^{i(qz-\Omega t)} + c.c\right)
\end{aligned} \tag{2.56}$$

We assume that the acoustic amplitude varies slowly in time and space so that we can introduce the slowly varying envelope approximation (SVEA) to simplify Eq. (2.54). Introducing Eq. (2.53) into the left part of Eq. (2.54)

$$\frac{\partial^2 \tilde{\rho}}{\partial t^2} - \Gamma' \nabla^2 \frac{\partial \tilde{\rho}}{\partial t} - \upsilon^2 \nabla^2 \tilde{\rho} =$$
$$\left(\frac{\partial^2 \rho}{\partial t^2} - 2i\Omega \frac{\partial \rho}{\partial t} - \Omega^2 \rho \right) e^{i(qz-\Omega t)} - \Gamma' \nabla^2 \left[\left(\frac{\partial \rho}{\partial t} - i\Omega \rho(z,t) \right) e^{i(qz-\Omega t)} \right] - \upsilon^2 \left(\frac{\partial^2 \rho}{\partial z^2} + 2iq \frac{\partial \rho}{\partial z} - q^2 \rho \right) e^{i(qz-\Omega t)} \tag{2.57}$$

Using SVEA to neglect the second derivatives of time and space, Eq. (2.57) is arranged to produce

$$\left(-2i\Omega \frac{\partial \rho}{\partial t} - \Omega^2 \rho - \Gamma' iq^2 \rho \Omega - \upsilon^2 2iq \frac{\partial \rho}{\partial z} + \upsilon^2 q^2 \rho \right) e^{i(qz-\Omega t)} = \left(-2i\Omega \frac{\partial \rho}{\partial t} + \left({\Omega_B}^2 - \Omega^2 - i\Omega \Gamma_B \right) \rho - \upsilon^2 2iq \frac{\partial \rho}{\partial z} \right) e^{i(qz-\Omega t)} \tag{2.58}$$

where

$$\Omega_B = q\upsilon \tag{2.59}$$

is the Brillouin frequency shift (in angular frequency) and the Brillouin gain bandwidth Γ_B (in angular frequency) is given as

$$\Gamma_B = q^2 \Gamma' \tag{2.60}$$

Since $\Gamma' = 2/\tau_a q^2$ (see Eq. 2.29), we assign this equation into Eq. (2.60) to obtain

$$\tau_a = \frac{1}{\pi \Delta \nu_B} \tag{2.61},$$

where $\Delta \nu_B$ is the Brillouin gain bandwidth given in ordinary frequency value.

By comparing the Eq (2.58) with that of Eq. (2.56), one may obtain

$$-2i\Omega \frac{\partial \rho}{\partial t} + \left({\Omega_B}^2 - \Omega^2 - i\Omega \Gamma_B \right) \rho - \upsilon^2 2iq \frac{\partial \rho}{\partial z} = \varepsilon_0 \gamma_e q^2 A_p {A_S}^* \tag{2.62}.$$

Equation (2.62) can be simplified by omitting the last term on its left-hand side. This term describes the propagation of phonons. Since the phonon propagation distance is typically small compared to the distance over which the source term on the right-hand side of Eq. (2.62) varies significantly, it is conventional to drop the term containing $\partial \rho / \partial z$ in describing SBS. If we drop the spatial derivative of Eq. (2.62) and assume steady state conditions ($\partial \rho / \partial t$ vanishes), we find that the acoustic amplitude is given by

$$\rho(z,t) = \varepsilon_0 \gamma_e q^2 \frac{A_p {A_S}^*}{{\Omega_B}^2 - \Omega^2 - i\Omega \Gamma_B} \tag{2.63}$$

The spatial evolution of the optical fields is described by the wave equation

$$\nabla^2 \tilde{E}_i - \frac{1}{(c/n)^2} \frac{\partial^2 \tilde{E}_i}{\partial t^2} = \frac{1}{\varepsilon_0 c^2} \frac{\partial^2 \tilde{P}_i}{\partial t^2}, \qquad \text{subscript } i = P \text{ (Pump), } S \text{ (Stokes)} \tag{2.64}$$

The total nonlinear polarization, which gives rise to the source term in this equation, is given by

$$\tilde{P}_i = \varepsilon_0 \Delta \varepsilon_r \tilde{E} = \varepsilon_0 \rho_0^{-1} \gamma_e \tilde{\rho} \tilde{E} \tag{2.65}$$

We next determine those parts of $\tilde{P}_i$ that can act as phase-match source terms for the pump and the Stokes field, which can be described as

$$\tilde{P}_P = p_p e^{i(k_p z - \omega_p t)} + c.c, \qquad \tilde{P}_S = p_s e^{i(-k_s z - \omega_s t)} + c.c, \tag{2.66}$$

where

$$p_p = \varepsilon_0 \rho_0^{-1} \gamma_e \rho A_S , \quad p_s = \varepsilon_0 \rho_0^{-1} \gamma_e \rho^* A_P \tag{2.67}$$

For the pump case, the Eq. (2.50) is introduced into the wave equation of Eq. (2.64) where the subscript *i* is replaced with *P* (pump), along with Eqs. (2.66) and (2.67). The time derivative of Eq. (2.50) is given

$$\frac{\partial \tilde{E}_P}{\partial t} = \left(\frac{\partial A_P}{\partial t} - i\omega_P A_P \right) e^{i(k_P z - \omega_P t)} + c.c \tag{2.68}.$$

The second time derivative is

$$\frac{\partial^2 \tilde{E}_P}{\partial t^2} = \left(\frac{\partial^2 A_P}{\partial t^2} - 2i\omega_P \frac{\partial A_P}{\partial t} - \omega^2{}_P A_P \right) e^{i(k_P z - \omega_P t)} + c.c \tag{2.69}$$

Next, we expand the space derivative of Eq. (2.50) to obtain

$$\frac{\partial \tilde{E}_P}{\partial z} = \left(\frac{\partial A_P}{\partial z} + ik_P A_P \right) e^{i(k_P z - \omega_P t)} + c.c \tag{2.70}$$

Similarly, we expand the second space derivative

$$\frac{\partial^2 \tilde{E}_P}{\partial z^2} = \left(\frac{\partial^2 A_P}{\partial z^2} + 2ik_P \frac{\partial A_P}{\partial z} - k^2{}_P A_P \right) e^{i(k_P z - \omega_P t)} + c.c \tag{2.71}$$

Next, the time derivative of the pump part of Eq. (2.66) is expanded to produce

$$\frac{\partial \tilde{P}_P}{\partial t} = \left(\frac{\partial P_P}{\partial t} - i\omega_P P_P \right) e^{i(k_P z - \omega_P t)} + c.c \tag{2.72}.$$

and its second time derivative can be expressed as

$$\frac{\partial^2 \tilde{P}_P}{\partial t^2} = \left(\frac{\partial^2 E_P}{\partial t^2} - 2i\omega_P \frac{\partial P_P}{\partial t} - \omega^2{}_P P_P \right) e^{i(k_P z - \omega_P t)} + c.c \tag{2.73}$$

Using the SVEA method, we omit the second derivative of Eq. (2.69) and Eq. (2.71). The second derivative of Eq. (2.73) is also omitted. Furthermore, the term $2i\omega_P \frac{\partial P_P}{\partial t}$ is also neglected since it is relatively small to the term $\omega_P^2 P_P$ in Eq. (2.73). Introducing Eqs. (2.69), (2.71) and (2.73) along with the expression of Eq. (2.67) into the wave equation of Eq. (2.64), one may obtain

$$\left[\left(2ik_P \frac{\partial A_P}{\partial z} - k_P^2 A_P \right) - \frac{1}{(c/n)^2} \left(-2i\omega_P \frac{\partial A_P}{\partial t} - \omega_P^2 A_P \right) \right] e^{i(k_P z - \omega_P t)} = -\left(\frac{1}{\rho_0 c^2} \omega_P^2 \gamma_e \rho A_S \right) e^{i(k_P z - \omega_P t)} \tag{2.74}$$

Organizing Eq. (2.74) and cancelling the term $k_P^2 A_P$ and $\omega_P^2 A_P$ since $k = \omega/c$, one may get

$$\frac{\partial A_P}{\partial z} + \frac{1}{(c/n)} \frac{\partial A_P}{\partial t} = \frac{i\omega_P \gamma_e}{2nc\rho_0} \rho A_S \tag{2.75}.$$

Equation (2.75) shows the wave equation of the SBS wave for the pump case. Performing the same method of calculation, the wave equation of the SBS wave for the Stokes case can be expressed as

$$-\frac{\partial A_S}{\partial z} + \frac{1}{(c/n)} \frac{\partial A_S}{\partial t} = \frac{i\omega_s \gamma_e}{2nc\rho_0} \rho^* A_P \tag{2.76}$$

In these equations, ρ is given by the solution to Eq. (2.62). Furthermore, we dropped the distinction between ω_P and ω_S by setting $\omega = \omega_P = \omega_S$. Considering a steady state condition, where the time derivative can be dropped and ρ is given by Eq. (2.63), the coupled-amplitude equations from Eqs. (2.75) and (2.76) then become

$$\frac{\partial A_P}{\partial z} = \frac{i\varepsilon_0 \omega q^2 \gamma^2{}_e}{2nc\rho_0} \frac{|A_S|^2 A_P}{\Omega_B{}^2 - \Omega^2 - i\Omega\Gamma_B} \tag{2.77}$$

$$\frac{\partial A_S}{\partial z} = -\frac{i\varepsilon_0 \omega q^2 \gamma^2{}_e}{2nc\rho_0} \frac{|A_P|^2 A_S}{\Omega_B{}^2 - \Omega^2 - i\Omega\Gamma_B} \tag{2.78}$$

Equations (2.77) and (2.78) indicate that SBS is a pure gain process, that the SBS process is automatically phase-matched. For this reason, it is possible to introduce coupled equations for the intensities of the two interacting optical waves. By defining the intensities as $I_i = 2n\varepsilon_0 cA_i A^*{}_i$ with $i = P$ or S, Eqs. (2.77) and (2.78) then become

$$\frac{\partial I_P}{\partial z} = -gI_P I_S \tag{2.79}$$

$$\frac{\partial I_S}{\partial z} = -gI_P I_S \tag{2.80}$$

In these equations, g is the SBS gain factor, which can be approximated as

$$g = g_0 \frac{(\Gamma_B / 2)^2}{(\Omega_B - \Omega)^2 + (\Gamma_B / 2)^2} \tag{2.81}$$

where g_0 is the line-center gain which can be given as

$$g_0 = \frac{\gamma_e^2 \omega^2}{n\upsilon c^3 \rho_0 \Gamma_B} \tag{2.82}$$

Take note that in the constant pump limit where I_P = constant, the solution for the Eq. (2.80) is given by

$$I_S(z) = I_S(L)e^{gIP(L-z)} \tag{2.83}$$

In this equation, a Stokes wave injected into the medium at $z = L$ experiences exponential growth as it propagates through the medium. Next, we find that the constant pump approximation corresponds to the case $I_S(z)$ = constant. Thus, the solution for the Eq. (2.79) can be expressed as

$$I_P(z) = I_P(0)e^{-gI_S z} \tag{2.84}$$

In contrast to that of the exponential growth of the Stokes wave shown in Eq. (2.83), Eq. (2.84) indicates that the pump intensity experiences attenuation due to the SBS process utilizing Stokes process.

References

[1] T. Horiguchi, T. Kurashima, M. Tateda, "A technique to measure distributed strain in optical fibers", Photonics Technol. Lett., vol. 2, no. 5, pp. 352-354, May 1990.

[2] K. O. Hills, B. S. Kawasaki and D. C. Johnson, "cw Brillouin laser", Appl. Phys. Lett., vol. 28, no. 10, pp. 608-609, May 1976.

[3] N. A. Olsson and J. P. van der Ziel, "Cancellation of fiber loss by semiconductor laser pumped Brillouin amplification at 1.5μm", Appl. Phys. Lett., vol. 48, no. 20, pp. 1329-1330, May 1986.

[4] Y. Okawachi, M. S. Bigelow, J. E. Sharping, Z. Zhu, A. Schweinsberg, D. J. Gauthier, R. W. Boyd, and A. L. Gaeta, "Tunable All-Optical Delays via Brillouin Slow Light in an Optical Fiber", Phys. Rev. Lett., 94, vol. 94, no. 15, pp. 153902-1-153902-4, Apr. 2005.

[5] R. W. Boyd, "Nonlinear Optics", 3rd Edition, Academic Press 2008.

[6] G. P. Agrawal, "Nonlinear Fiber Optics", 3rd Edition, Academic Press 2001.

Chapter 3: Literature Review on the Brillouin Scattering-based Sensing Techniques

3.1 Introduction to Chapter

Since the first demonstration of distributed BOTDA system [1], several techniques have been proposed to further improve the efficiency of the sensing system. In this chapter, some well-known techniques of measuring strain and temperature along fiber optic cable based on the conventional BOTDA are explained. They include the pulse pre-pump BOTDA (PPP-BOTDA), differential pulse-width pair BOTDA (DPP-BOTDA), optical differential parametric amplification BOTDA (ODPA -BOTDA) and phase-shift pulse BOTDA (PSP-BOTDA) to name a few.

Apart from the BOTDA, there is another technique of measuring the strain and temperature utilizing SBS called Brillouin optical correlation domain analysis (BOCDA). BOCDA however differs from the BOTDA technique in which that it is based on the optical correlation method. A brief explanation about this technique is also included.

3.2 Brillouin Optical Time Domain Analysis (BOTDA)

3.2.1 Principles of BOTDA

Brillouin optical time domain analysis (BOTDA) that utilizes the occurrence of SBS for distributed strain and temperature measurement was firstly proposed by Horiguchi et al. [1]. A simplified measurement system of the BOTDA is depicted in the Fig. 3.1.

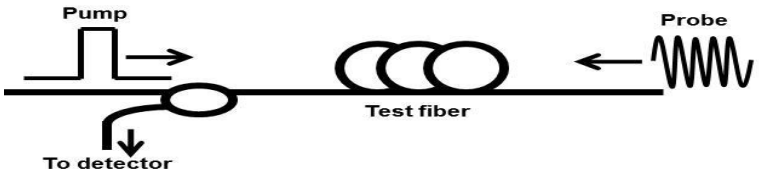

Fig. 3.1. A simplified BOTDA measurement setup.

In Fig. 3.1, pulsed light or also called pump is injected to one end of a fiber, while at the other end, a counter-propagating continuous wave light or also known as probe is injected. BOTDA utilizes the occurrence of SBS in fiber cables when pump light interacts with counter propagating probe light. The beating due to the frequency difference between the pump and the probe modulates the refractive index of fiber via electrostriction process, and then excites an acoustic wave that moves in the same direction as the pump. As a result, some of the pump light is backscattered into the SBS light. The frequency of the SBS light is down-shifted by the Stokes frequency; this frequency shift is called Brillouin frequency shift (BFS), which is described as

$$\nu_B = \frac{2n\upsilon}{\lambda_p} \tag{3.1},$$

where $\nu_B (=\Omega_B / 2\pi)$ is the BFS, υ is the acoustic velocity, n is the refractive index of the fiber, and λ_p is the pump wavelength. BFS is very unique that it linearly changes with the change in strain and temperature of the fiber. Therefore, BOTDA can measure distributed strain and temperature across the fiber by time-resolved measurement of the BFS. The peak Brillouin signal can be obtained when the frequency difference between the pump and the probe is equal to the BFS of the fiber; the energy transfers from pump to probe.

Furthermore, Brillouin gain spectrum along the fiber can be constructed by sweeping the frequency difference

between the pump and probe in the vicinity of the BFS of the fiber. The Brillouin gain bandwidth $\Delta\nu_B$ $(=\Gamma_B/2\pi)$ of the Brillouin gain spectrum can be expressed as a relation with the time constant of the acoustic wave amplitude by following expression:

$$\Delta\nu_B = \frac{1}{\pi\tau_a} \tag{3.2}$$

where τ_a is the time constant of the acoustic wave amplitude. As has been given in Chapter 2, τ_a is described as the time taken for the amplitude of the acoustic wave to decay from 100% to 36.8% $(1/e)$. Throughout the thesis, this term is used as a parameter to analyze the Brillouin signals obtained from the simulations and experiments.

As has been mentioned in Chapter 1, the best spatial resolution of the firstly demonstrated BOTDA was about 1m that corresponded to the pump pulse duration of 10ns. The spatial resolution, Δz can be described as

$$\Delta z = \frac{(c/n)T}{2} \tag{3.3}$$

where c is the light speed in vacuum, n is the refractive index of fiber, and T is the pulse duration. In order to improve the spatial resolution, one way is to reduce the pulse width of the optical pump. However, the pump pulse duration cannot be set shorter than τ_a, which is about 9ns for silica fibers, because the acoustic phonons excited by such a short pump pulse cannot generate the SBS efficiently. This will further cause the Brillouin gain to decrease and its gain bandwidth to spread. As a result, it becomes difficult to accurately determine the center frequency of the Brillouin gain spectrum.

3.2.2 Spatial Resolution

Spatial resolution is of important parameter in characterizing the efficiency of a fiber optic sensor. In the BOTDA system, the equation to determine its spatial resolution is as shown in Eq. (3.3). This equation shows on how one can calculate the spatial resolution theoretically. However, in the real measurement, the spatial resolution is analyzed by measuring the rising or falling time of the measured time domain Brillouin signals at the transition range between the test and reference fiber, as shown in Fig. 3.2. In Fig. 3.2, the spatial resolution is calculated by determining the rise or fall time that corresponds to the 10% or 90% of the average signal power. This rise or fall time is then converted into the length value which determines the spatial resolution. It should be noted here that the measured spatial resolution is smaller than that of the theoretical value calculated by using Eq. 3.3. This is because the evaluation method shown in Fig. 3.2 covers only 80% of the total rise/fall time. This method of evaluation is used throughout this thesis to analyze the spatial resolution of the decoded Brillouin signal.

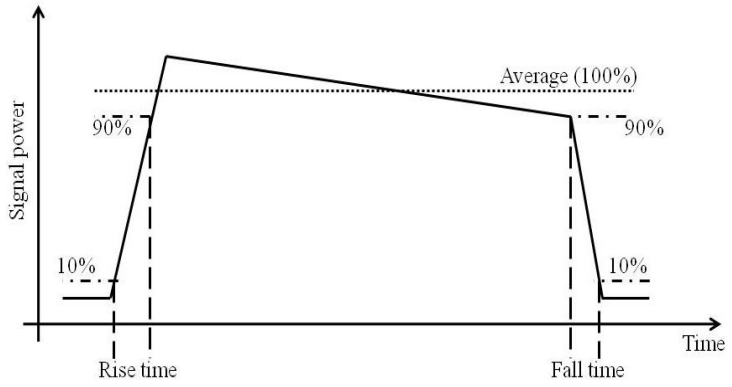

Fig. 3.2. Method of evaluating the spatial resolution.

3.3 Pulse Pre-Pump BOTDA (PPP-BOTDA)

As explained in Section 3.2, one way to improve the spatial resolution is by reducing the duration of the pump pulse. However, if the pump pulse duration is further decreased to shorter than 10ns, the Brillouin gain rapidly decreases and the spectral width of the Brillouin gain begins to increase from the natural linewidth of approximately 35 MHz. Therefore, it had been believed that both the gain decrease and the spectral width broadening had precluded sub-meter spatial resolution measurements. Breakthrough was made when it was found experimentally that the spectral width is suddenly reduced if the pulse duration decreases to further small values less than the time constant of the acoustic wave decay rate [2], and when it was subsequently clarified by numerical simulations that weak cw leakage of the pulse plays a role of pre-pump [3].

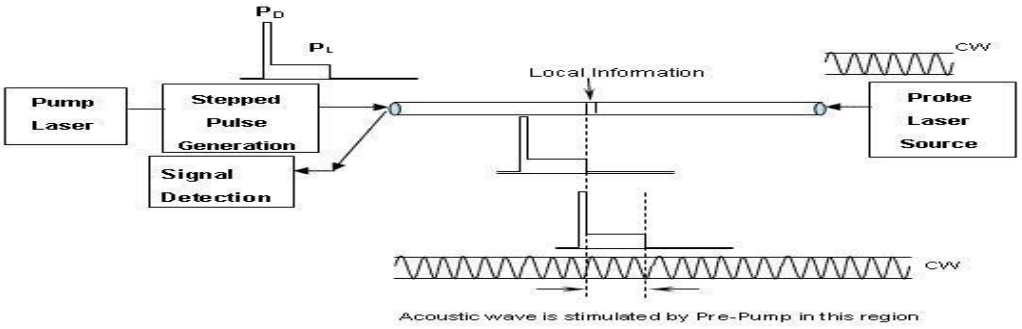

Fig. 3.3. PPP-BOTDA measurement setup (source from www.neubrex.com).

Based on the findings, an alternative approach called pulsed pre-pump BOTDA (PPP-BOTDA) has been reported, using weak pre-pump pulse with a long duration in front of the conventional intense pulse with a short duration [4]. The long pre-pump pulse excites acoustic waves that offer the succeeding short pulse the beneficial Brillouin gain, thus providing the advantages of a narrow spectral width and additional small gain at high spatial resolution. The measurement system of the PPP-BOTDA is depicted in Fig. 3.3. In Fig. 3.3, the shape of the pump pulse is modified to step function. In other words, the PPP-BOTDA utilizes a weak pre-pump of a few tens of nanoseconds (P_L) in duration and the following high peak-power pump of a short duration (P_D). The PPP-BOTDA makes the short pulse pump fall so steeply to suppress a trail of the Brillouin signal due to the presence of the transient phonons, achieving high spatial resolution. The trail has been unwanted response for the BOTDAs utilizing the light leakage from optical modulator [5].

3.4 Differential Pulse-width Pair BOTDA (DPP-BOTDA)

The differential pulse-width pair BOTDA (DPP-BOTDA) technique employs two pulsed pump lights having long durations with a small difference. After the Brillouin signals measured by these two pulses are detected and converted into the electrical signals by a photo detector, they are finally subtracted to produce the differential Brillouin signal. By performing the subtraction, the spatial resolution is improved by the pulse duration difference between the two pulsed pump lights. Figure 3.4 depicts the measurement setup of DPP-BOTDA technique [6].

In the DPP-BOTDA, the pulsed laser is tuned to the Stokes frequency while the cw is tuned to the pump frequency. In this measurement setup, the pulsed Stokes beam experiences Brillouin amplification at the expense of the cw pump; implying the energy conservation, this results in decrease in the cw pump power. By scanning the frequency difference between the two lasers, the changes in the cw pump power is measured to produce the Brillouin loss spectrum in the function of distance. Spatial resolution of 0.15m was reported by employing 20/19ns pulse pair over 1km of fiber length [6].

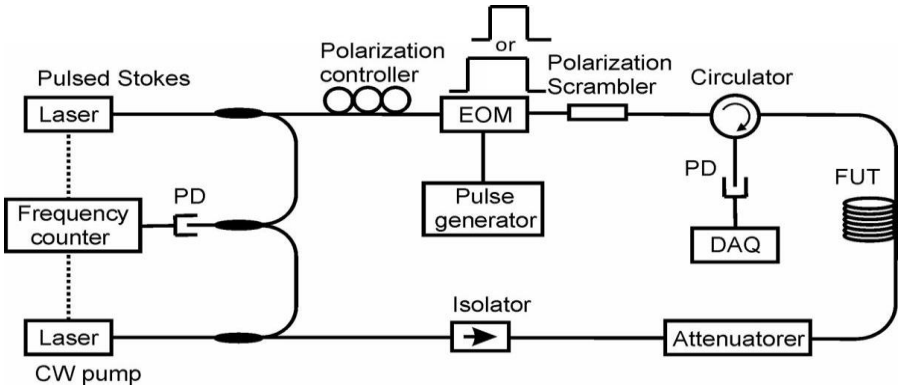

Fig. 3.4. DPP-BOTDA measurement setup [6].

3.5 Optical Differential Parametric Amplification BOTDA (ODPA-BOTDA)

Optical differential parametric amplification BOTDA (ODPA-BOTDA) resembles the DPP-BOTDA technique, except that the two pulsed lights are injected simultaneously into the fiber. The schematic diagram of the ODPA-BOTDA is shown in Fig. 3.5. Another interesting feature of the ODPA-BOTDA is that it employs the combination of the Stokes and anti-Stokes in the pulsed lights that allows the simultaneous generation of Brillouin gain and loss at the same position along the fiber cable [7]. At the overlapping region of the two pulses, the generation of Brillouin gain and loss cancels out each other on condition that the power of the two pulses is carefully balanced. Thus, compared to the DPP-BOTDA, the subtraction process of the two Brillouin signals is performed before the measured signals reached the photo detector.

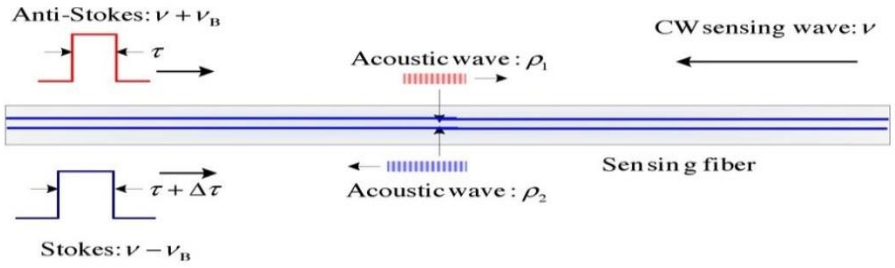

Fig. 3.5. Schematic diagram of the ODPA-BOTDA technique [7].

However, one needs to carefully set the peak power of the Stokes and anti-Stokes at the same level to obtain well balanced gain and loss interaction so that the Brillouin gain and Brillouin loss can be canceled completely. If the peak power of these lights is different, i.e. either Stokes or anti-Stokes dominates the process, it is impossible to obtain high spatial resolution with narrow Brillouin gain bandwidth measurements. Besides the power level, the timing between the two pulses should also be optimized at the same position so that no distortion is induced in the measured signal. In addition, according to [7], considering the issue arises from the different state of polarization in fiber, currently this technique restricts the use to the polarization maintained fiber (PMF).

3.6 Phase-Shift Pulse BOTDA (PSP-BOTDA)

In the phase-shift pulse BOTDA (PSP-BOTDA) technique, the pump is composed of two kinds of pulses; the 1st pulse of long duration, and the 2nd pulse of short duration [8]. As illustrated in Fig. 3.6, the following two pumps are used: 1) the 1st pulse followed by the 2nd pulse without phase shift and 2) the 1st pulse followed by the 2nd pulse with π shift in phase. The 2nd pulse width determines the spatial resolution. The 1st pulse is around or longer than the time

constant of the acoustic wave τ_a so that the acoustic wave grows to its full extent through the process of SBS. The 2nd pulse follows immediately after the 1st pulse in order to interact with the acoustic wave excited by the 1st pulse. The 2nd pulse is modulated with binary phase shift keying (BPSK).

First, pump 1) is injected to the fiber and the response is measured. Second, the measurement with pump 2) follows. In both measurements, a portion of the 2nd pulse is backscattered by the acoustic wave excited by the pre-pump; the 1st pulse. For pump 1), the 2nd pulse backscattered interferes with the probe constructively, increasing the Brillouin gain. Contrary to the case of pump 1), the 2nd pulse backscattered in the case of pump 2) interferes with the probe destructively, decreasing the Brillouin gain. The increase and the decrease in the gain have the same magnitude. Third, the response signal measured with pump 2) is subtracted from that obtained with pump 1). This process cancels the Brillouin amplified signals caused only by the 1st pulse and only by the 2nd pulse, leaving only the Brillouin amplified signal caused by a conjunction of the 2nd pulse and the acoustic wave excited by the 1st pulse. The differential Brillouin amplified signal of the PSP-BOTDA is much greater than the Brillouin amplified signal for the PPP-BOTDA explained above. This is because the pre-pump pulse and the 2nd pulse of the PSP-BOTDA have the same power while for the PPP-BOTDA the power of the pre-pump is about 10^{-3} of that of the 2nd pulse. Furthermore, subtracting the two Brillouin signals obtained by each pump yields a Brillouin signal whose intensity is approximately twice that of DPP-BOTDA.

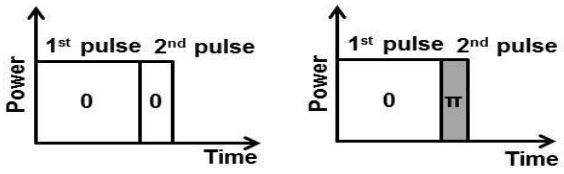

Fig. 3.6. Pump pulse configurations of PSP-BOTDA technique.

3.7 Coded PSP-BOTDA

3.7.1 Coded Discrete-PSP-BOTDA

Coded discrete-PSP-BOTDA was proposed as a technique to improve the signal-to-noise ratio (SNR) of the measured Brillouin signal [9]. In this technique, many kinds of codes such as Golay complementary pair (GCP) or also known as Golay codes can be employed to modulate the pump light of the PSP-BOTDA. GCP is a complementary sequence which is well-known for its property that the out-of-phase aperiodic autocorrelations coefficients of the codes sum to zero and the correlation in phase produces high amplitude [10].

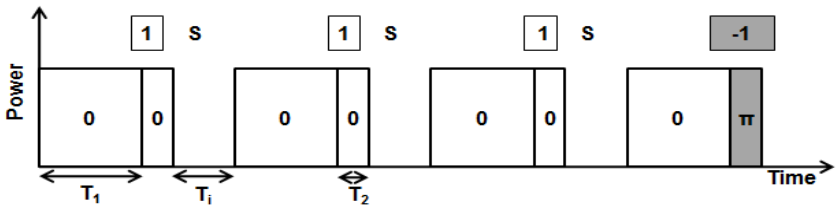

Fig. 3.7. Example of pump configuration of coded discrete-PSP-BOTDA in the case of 4 bits.

An example of pump light configuration for coded discrete-PSP-BOTDA is illustrated in Fig. 3.7, showing that return-to-zero (RZ) pulse formation is used to generate the pump light. In Fig. 3.7, a long pulse (1st pulse) of duration T_1 is used to excite the acoustic wave to generate the SBS wave. Next to it, much narrower pulse called the 2nd pulse is

appended. The 2nd pulse is phase-coded according to the bit-elements of the Golay code, and is used to measure the strain change along the fiber. The width of one element of a Golay code is T_2. The spatial resolution is determined by the duration of T_2. It can be seen from Fig. 3.7 that the bit-elements of a Golay code are appended separately to the 1st pulse, with the bit interval time T_i of each pulse group. The interval time must be set much longer than the time constant of the acoustic wave amplitude τ_a in order to avoid the Brillouin interaction among pulse groups. Thus, the available code length is limited by the amount of the round trip time (RTT) of light in the fiber. Previous numerical analysis has shown that the shortest T_i value that can be set in the coded-discrete-PSP-BOTDA was between 25~30ns [11].

3.7.2 Coded Continuous-PSP-BOTDA

Coded continuous-PSP-BOTDA is another technique introduced to improve the SNR of the Brillouin signal measured based on the PSP-BOTDA technique. The pump light configuration for the coded continuous-PSP-BOTDA is quite similar to that of coded discrete-PSP-BOTDA, except that the coded pulses are assigned as non-return-to-zero (NRZ) pulses [12]. An example of the pump light of coded continuous-PSP-BOTDA is depicted in Fig. 3.8.

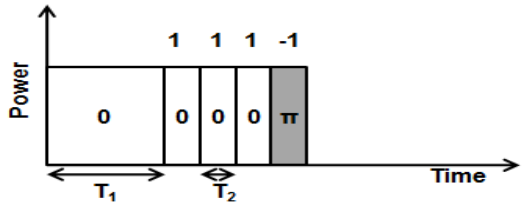

Fig. 3.8. Example of pump configuration of coded continuous-PSP-BOTDA in the case of 4 bits.

As can be seen in Fig. 3.8, the coded pulses are continuously appended together after a long 1st pulse. Similar to the conventional PSP-BOTDA and coded discrete-PSP-BOTDA techniques, the 1st pulse of width T_1 is used to grow the acoustic wave through the SBS process, while the 2nd pulses of width T_2 each, which are four pulses in the case of 4 bit code, are used to measure the strain and temperature changes. Assigning 1 and -1 bit-elements respectively to 0 and π shifts in phase, the four pulses are phase modulated with code series.

Previous studies have shown that the use of non-return-to-zero (NRZ) formatted pulses in coded BOTDA has induced distortion in the measured Brillouin signal when the bit pulse duration is around or less than τ_a. This distortion is caused by varieties of additional gain of the preceding coded pulses. Consequently, return-to-zero (RZ) format has been introduced into the coded pulses of the high-spatial-resolution BOTDAs so that interactions between the preceding and succeeding bit pulses should not occur through the SBS process [9, 13, 14].

Nevertheless, as already explained in Chapter 1, sub-meter spatial resolution has been successfully demonstrated by using the coded continuous-PSP-BOTDA employing Golay codes. The reason of this success is that the subtraction process in the PSP-BOTDA intrinsically cancels the Brillouin gain due to the interaction between each coded pulse and the probe [8]. Thus, this process partly removes the Brillouin gain variation among coded pulses. The PSP-BOTDA extracts only the Brillouin gain that is derived from the interaction of each coded pulse with the acoustic wave excited by the pre-pump pulse. However, since the acoustic wave decays significantly after the time constant of the acoustic wave τ_a, when the total duration of the coded pulses becomes more than τ_a, the waveform of the Brillouin signal decoded is distorted, resulting in the degradation of the spatial resolution. Thus, it was found that the total code duration available for coded-continuous PSP-BOTDA is limited by the time constant of the acoustic wave in fiber, which is around 9ns for silica fibers.

3.8 Brillouin Optical Correlation Domain Analysis (BOCDA)

Brillouin optical correlation domain analysis (BOCDA) is another technique of utilizing SBS to measure strain and temperature along fiber optic cable. Being different from the BOTDA technique that uses time domain analysis for the strain measurement, the BOCDA technique is based on optical correlation method. An example of the BOCDA measurement setup is shown in Fig. 3.9 [15]. In the BOCDA system, both pump and probe lights are modulated in frequency with a sinusoidal waveform, periodically generating correlation peak at a particular section along the fiber. SBS signal is observed when the frequency difference between the lightwaves coincides with the BFS of that particular section. The main feature of the BOCDA system is that it offers higher spatial resolution than the BOTDA technique up to millimeter order, which is described as

$$\Delta z = \frac{V_g \cdot \Delta \nu_B}{2\pi f_m \cdot \Delta f} \tag{3.4},$$

and

$$d_m = \frac{V_g}{2 f_m} \tag{3.5},$$

where V_g is the group velocity of light, f_m and Δf are respectively the modulation frequency and modulation amplitude of the light source and d_m is the measurement range. It can be seen from Eq. (3.4) that higher Δz can be obtained by increasing Δf rather than f_m, because of the trade-off between f_m and d_m according to Eq. (3.5) [16]. Although employing time-division pump-probe generation scheme can expand the measurement range, this will increase the measurement time with the increase in the number of time-division sections.

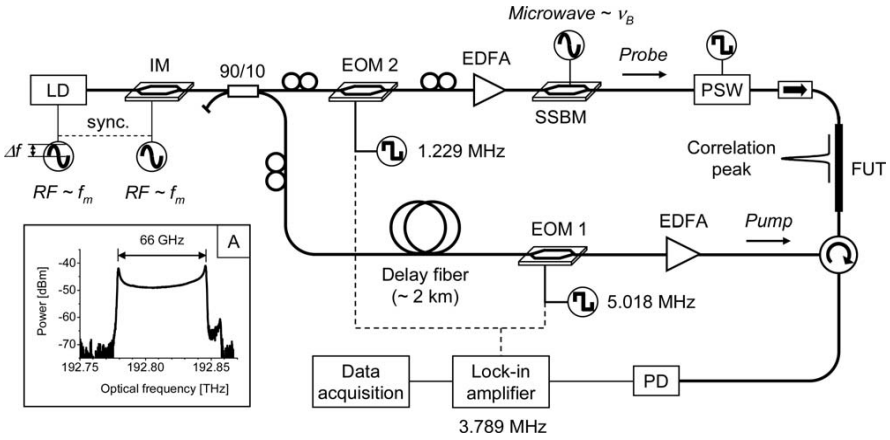

Fig. 3.9. Example of BOCDA measurement setup [15].

References

[1] T. Horiguchi, T. Kurashima, M. Tateda, "A technique to measure distributed strain in optical fibers", Photonics Technol. Lett., vol. 2, no. 5, pp. 352-354, May 1990.

[2] X. Bao and A. Brown, "Characterization of the Brillouin-loss spectrum of single-mode fibers by use of very short (<10-ns) pulses", Opt. Lett., vol. 24, no. 8, pp. 510-512, Apr. 1999.

[3] V. Lecoeuche, D. J. Webb, C. N. Pannell and D. A. Jackson, "Transient response in high-resolution Brillouin-based distributed sensing using probe pulses shorter than the acoustic relaxation time", Opt. Lett., vol. 25, no. 3, pp. 156-158, Feb. 2000.

[4] C. H. Li, K. Nishiguchi, M. Miyatake, A. Makita, M. Yokoyama, K. Kishida, T. Mizutani and N. Takeda, "PPP-BOTDA method to achieve 2cm spatial resolution in Brillouin distributed measuring technique", Technical Report of IEICE. OFT

108(32) (in Japanese), pp. 55-60, May 2008.

[5] S. Ashfar V., G. A. Ferrier, X. Bao and L. Chen, "Effect of the finite extinction ratio of an electro-optic modulator on the performance of distributed probe-pump Brillouin sensor system", Opt. Lett., vol. 28, no. 16, pp. 1418-1420, Aug. 2003.

[6] W. Li, X. Bao, Y. Li and L. Chen, "Differential pulse-width pair BOTDA for high spatial resolution sensing", Opt. Exp., vol. 16, no. 26, pp. 21616-21625, Dec. 2008.

[7] Y. Li, X. Bao, Y. Dong and L. Chen, "A novel distributed Brillouin sensor based on optical differential parametric amplification", J. Lightw. Technol., vol. 28, no. 18, pp. 2621-2626, Sep. 2010.

[8] T. Horiguchi, R. Muroi, A. Iwasaka, K. Wakao and Y. Miyamoto, "Negative Brillouin gain and its application to distributed fiber sensing (presented poster style)", 33rd European Conference and Exhibition of Optical Communication (ECOC) 2007, P018, Sep. 2007; T. Horiguchi, R. Muroi, A. Iwasaka, K. Wakao and Y. Miyamoto, "BOTDA utilizing phase-shift pulse", IEICE Trans. Commun. (in Japanese), vol. J91-B, no. 2, pp. 207-216, Feb. 2008.

[9] R. Muroi, T. Horiguchi, Y. Miyamoto, Y. Sato, A. Tachibana and A. Takakura, "PSP-BOTDA based on Golay code", IEICE Trans. Commun. (in Japanese), vol. J91-B, no. 11, pp. 1493-1501, November 2008.

[10] M. J. E. Golay, "Complementary series", IRE Trans. on Info. Theory, vol. IT-7, pp. 82-87, Apr. 1961.

[11] T. Sasaki, T. Horiguchi, **M. S. D. B. Zan** and D. Uchiyama, "Coded pulse interval dependence of the characteristic in discretely coded PSP-BOTDA", IEIE Trans. Commun. (Japanese edition), vol. J94-B, no. 11, pp. 1481-1489, Nov. 2011.

[12] D. Uchiyama, T. Horiguchi, H. Ando, Y. Okumoto, T. Sasaki and Y. Sawai, "Signal to noise improvement ratio for coded PSP-BOTDA", Technical report of IEICE. OFT 109 (377) (in Japanese), pp. 33-38, Jan. 2010.

[13] H. Liang, W. Li, N. Linze, L. Chen and X. Bao, "High-resolution DPP-BOTDA over 50 km LEAF using return-to-zero coded pulses", Opt. Lett., vol. 35, no. 10, pp. 1503-1505, May 2010.

[14] M. A. Soto, G. Bolognini and F. Di. Pasquale, "Analysis of pulse modulation format in coded BOTDA sensors", Opt. Exp., vol. 18, no. 14, pp. 14878-14892, Jul. 2010.

[15] K. Y. Song, Z. He and K. Hotate, "Distributed strain measurement with millimeter-order spatial resolution based on Brillouin optical correlation domain analysis", Opt. Lett., vol. 31, no. 17, pp. 2526-2528, Sep. 2006.

[16] Y. Mizuno, W. Zhou, Z. He and K. Hotate, "Proposal of Brillouin optical correlation-domain reflectometry (BOCDR)", Opt. Exp., vol. 16, no. 16, pp. 12148-12153, Aug. 2008.

Chapter 4: Coding Techniques

In later chapters, we will find in details the analysis on the employment of the proposed code systems in the PSP-BOTDA technique. Before we proceed to the analysis of the employment, it is important to understand the theoretical study of the proposed coding systems and the advantages, which is included in this chapter.

4.1 Introduction to Chapter

The coding system employed in modulating the pump light of PSP-BOTDA described in this thesis includes Golay complementary pair (GCP), that is also known as Golay codes and another one called Walsh codes. Improvement in the optical signal-to-noise ratio (SNR) of measured Brillouin signal is expected from this pump light coding concept. In this chapter, the fundamental concept that mainly covers the code generation algorithm and the decoding process of these two code systems is explained. In addition, the theoretical SNR contribution expected from the coding system is also described.

Moreover, in this chapter, the proposal of new concept of combining two codes called dual Golay codes, combined Walsh and Golay codes and dual Walsh codes are also explained. This new technique can further contributes to the achievement of higher SNR than that of using one kind of code system; the theoretical SNR is explained. The algorithm of combining the codes for the above mentioned coding systems are also given in details.

4.2 Golay Complementary Pair (GCP)

Golay complementary pair (GCP), which was firstly introduced in 1949 by Marcel J. E. Golay can be defined as [1]

Definition: *A pair of two of L-element sequences, A with elements (a_0, a_1, ... a_{L-1}) and B with elements (b_0, b_1, ..., b_{L-1}), is said to be complementary if the sum of the auto-correlations for the two sequences satisfies below equations.*

$$\Phi_{A,A}(k) + \Phi_{B,B}(k) = 2L\delta(k) \tag{4.1}$$

where

$$\Phi_{A,A}(k) = \sum_{m=0}^{L-k-1} a_{m+k} a_m \tag{4.2}$$

$$\Phi_{B,B}(k) = \sum_{m=0}^{L-k-1} b_{m+k} b_m \tag{4.3}$$

and

$$\delta(k) = \begin{cases} 1, & for\ k = 0 \\ 0, & otherwise \end{cases}.$$

In the equations above, L is the code length of Golay codes A and B, k is the bit shift during the auto-correlation calculation. The out-of-phase aperiodic auto-correlation coefficients sum to zero, while the summation gives a peak value of $2L$ for $k = 0$.

Let us consider a GCP, which consists of codes A and B. The codes can be generated, for example, through a method called recursion method, which can be expressed as follows.

$$\begin{pmatrix} A \\ B \end{pmatrix} \rightarrow \begin{pmatrix} A|B \\ A|\overline{B} \end{pmatrix} \tag{4.4}$$

In Eq. (4.4), '|' means concatenation, and overbar $\overline{\ }$ denotes bitwise inversion of the code. The expressions of A|B and $A|\overline{B}$ denote the new codes of A and B, respectively. An example of a GCP of 8 bits in length is given below;

$$\begin{pmatrix} A \\ B \end{pmatrix}_{L=8bit} = \begin{pmatrix} 111-111-11 \\ 111-1-1-11-1 \end{pmatrix} \tag{4.5}$$

which is generated from a pair of one bit code of A=1 and B=1 by using the recursion method three times. Fig. 4.1 shows a correlation function of a GCP of 8 bits. The special property of a GCP expressed by Eqs. (4.1) to (4.3) is clearly observed in Fig. 4.1, showing that the summation of the auto-correlation coefficients of Golay pair gives a peak value which corresponds to the value of $2L$ (in this case $2L$=16) and the aperiodic coefficients for both codes are cancelled to zero. The code gain of $2L$ and the zero side lobes are favorable for distributed sensing.

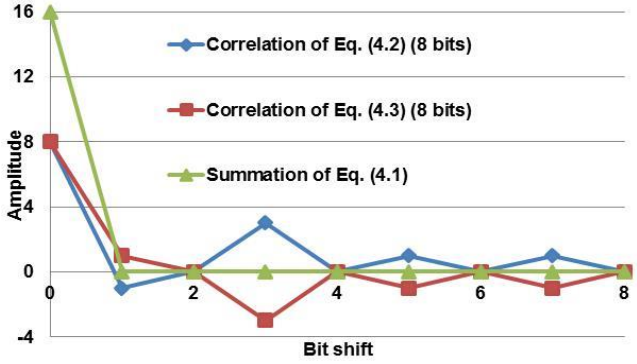

Fig. 4.1. Correlation functions for L=8.

4.2.1 The Employment of GCP in Coding the Pump Light of PSP-BOTDA

In the previous researches, the employment of GCP in the coded PSP-BOTDA is categorized into two systems. They are coded continuous-PSP-BOTDA [2] and coded discrete-PSP-BOTDA [3]. The examples of pump configurations for both systems in the case of 4 bits are depicted in Fig. 4.2 (a) and Fig. 4.2 (b), respectively.

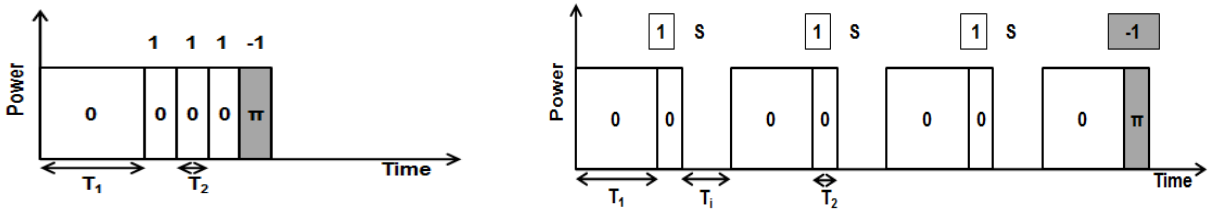

(a) (b)

Fig. 4.2. Coded PSP-BOTDA pump configurations in the case of 4 bits (a) Coded continuous-PSP-BOTDA (b) Coded discrete-PSP-BOTDA.

In Fig. 4.2 (a), the 1st pulse with width of T_1 is used to excite the acoustic wave to generate the SBS wave. Next to it, much narrower pulses called the 2nd pulses are appended. These pulses are phase-coded with a Golay code, and to measure the strain change. The width of one element of a GCP is T_2. In Fig. 4.2 (a), the bit-elements of a Golay code are continuously appended next to the 1st pulse. While in Fig. 4.2 (b), each element of the code is appended separately to the 1st pulse, with the bit interval time T_i of each pulse group.

For the coded continuous-PSP-BOTDA shown in Fig. 4.2 (a), the 1st pulse of width T_1 is used to grow the acoustic wave through the SBS process, while the 2nd pulses of width T_2 each, which are four pulses in the case of 4 bit code, are used to measure the strain and temperature changes. Assigning 1 and -1 bit-elements to 0 and π shifts in phase, the four pulses are phase modulated with code series of {1, 1, 1, -1}. As for the coded discrete-PSP-BOTDA shown in Fig. 4.2

(b), the 2nd pulse of width T_2 following the 1st pulse of width T_1 is assigned to one bit-element of the code. The four sets of the 1st and the 2nd pulses are generated and the 2nd pulses are phase-modulated with the code series of {1, 1, 1, -1}. The pulse sets are separated by T_i in time so that we can ignore the interactions between them through the process of the SBS. In both pump configurations T_2 determines the spatial resolution, as reported in [2] and [3].

4.2.2 Signal-to-Noise Improvement Ratio (SNIR)

The optical signal-to-noise improvement ratio (SNIR) for the coded PSP-BOTDA employing Golay codes can be described by comparing it with the conventional single pulse PSP-BOTDA in the measurement. For the convenience of the comparison, let us assume that the peak power and the total measurement time are equal for both measurement systems. Firstly, the SNR for the conventional PSP-BOTDA system using the 0-shift pump and π-shift is calculated. Since we consider the equal measurement time between the conventional PSP-BOTDA system and the coded PSP-BOTDA system, then the total number of measurements for both 0-shift and π-shift pumps for the conventional PSP-BOTDA becomes four. If we consider the number of the averaging for each measurement of pump is *N*, then the optical SNR for the conventional single pulse PSP-BOTDA system can be expressed as follows [2]

$$SNR^{single\,pulse PSP-BOTDA} = \sqrt{4N}\,\frac{h_k}{\sigma_\upsilon} \tag{4.6}$$

where h_k is the response signal of probe that experiences the Brillouin amplification and σ_υ is the quantized noise power during the A-D conversion.

Next, the SNR of the coded PSP-BOTDA is given. In the coded PSP-BOTDA system, the number of pumps used in the measurement is four, including the pumps for inverted Golay codes. Thus, the SNR for this case can be shown as

$$SNR^{coded PSP-BOTDA} = \sqrt{4NL}\,\frac{h_k}{\sigma_\upsilon} \tag{4.7}$$

where *L* is the code length of the Golay code. The SNIR of the coded PSP-BOTDA system can be expressed by dividing the Eq. (4.7) with Eq. (4.6) as

$$SNIR^{coded PSP-BOTDA} = \frac{SNR^{coded PSP-BOTDA}}{SNR^{single\,pulse PSP-BOTDA}} = \sqrt{L} \tag{4.8}$$

In the conventional BOTDA that employs intensity modulation for producing the coded pulses, the SNIR of the measurement system is $\sqrt{L/2}$ [4]. Therefore, with the employment of GCP in the coded PSP-BOTDA, the SNIR improves is two times higher than that of the conventional BOTDA.

4.3 Walsh Codes

4.3.1 Encoding and Decoding with Walsh Codes

Walsh codes are generated from a square Hadamard matrix (**H** matrix) consisting of bipolar elements (+1s and -1s). Each row of Hadamard matrix describes a Walsh code. Hadamard matrices have been widely used in OTDR [5] and spectrometry [6] applications. The expression of generating a Hadamard matrix for 2^k matrix order can be expressed as follows

$$\mathbf{H}_{2^k} = \begin{pmatrix} H_{2^{k-1}} & H_{2^{k-1}} \\ H_{2^{k-1}} & -H_{2^{k-1}} \end{pmatrix} = \mathbf{H}_2 \otimes \mathbf{H}_{2^{k-1}}$$
$$for\ k = 1, \tag{4.9}$$
$$\mathbf{H}_2 = \begin{pmatrix} 1 & 1 \\ 1 & -1 \end{pmatrix}$$

for $2 \le k \in N$, where $\otimes$ denotes Kronecker product. For instance, if k=2, the **H** matrix of order 4 that can be generated is

$$\mathbf{H}_4 = \begin{pmatrix} 1 & 1 & 1 & 1 \\ 1 & -1 & 1 & -1 \\ 1 & 1 & -1 & -1 \\ 1 & -1 & -1 & 1 \end{pmatrix} \quad (4.10).$$

From Eq. (4.10), one can immediately understand that the matrix elements are orthogonal; the order of the elements of the transposed matrix $\mathbf{H}^{\mathrm{T}}$ is exactly the same with the original one. Furthermore, the sequence of the elements also remains in the same order after matrix inversion $\mathbf{H}^{-1}$. The decoding process using Hadamard matrix is called Hadamard transform. In the spectrometry application, the Hadamard transform is processed in the space domain while for BOTDA, the decoding is processed in the time domain. Nevertheless, the process of decoding the measured Brillouin signals can be performed in the similar manner applied in the spectrometry.

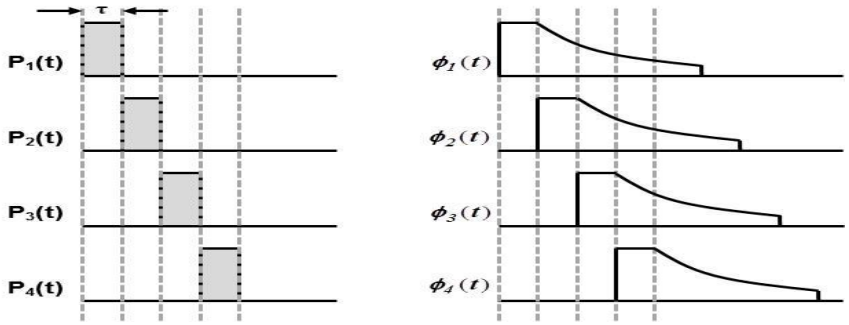

Fig. 4.3. Illustration of the single pulse input and its response in time domain.

We use the generated matrix in Eq. (4.10) as an example of performing Hadamard transform. Let us define the duration of each coded pulse as τ. Figure 4.3 illustrates the input of single pulse and its response in time domain. The single pulse corresponding to each code element in every row can be expressed as $P_1(t), P_2(t), P_3(t)$ and $P_4(t)$. When these pulse sequences are launched into the fiber, the trace signal $\eta(t)$ for each row can then be described as

$$\begin{aligned} &P_1(t)+P_2(t)+P_3(t)+P_4(t) \rightarrow \eta_1(t) = \phi_1(t)+\phi_2(t)+\phi_3(t)+\phi_4(t)+e_1(t) \\ &P_1(t)-P_2(t)+P_3(t)-P_4(t) \rightarrow \eta_2(t) = \phi_1(t)-\phi_2(t)+\phi_3(t)-\phi_4(t)+e_2(t) \\ &P_1(t)+P_2(t)-P_3(t)-P_4(t) \rightarrow \eta_3(t) = \phi_1(t)+\phi_2(t)-\phi_3(t)-\phi_4(t)+e_3(t) \\ &P_1(t)-P_2(t)-P_3(t)+P_4(t) \rightarrow \eta_1(t) = \phi_1(t)-\phi_2(t)-\phi_3(t)+\phi_4(t)+e_4(t) \end{aligned} \quad (4.11)$$

so that

$$\begin{pmatrix} \eta_1(t) \\ \eta_2(t) \\ \eta_3(t) \\ \eta_4(t) \end{pmatrix} = \mathbf{H}_4 \begin{pmatrix} \phi_1(t) \\ \phi_2(t) \\ \phi_3(t) \\ \phi_4(t) \end{pmatrix} + \begin{pmatrix} e_1(t) \\ e_2(t) \\ e_3(t) \\ e_4(t) \end{pmatrix} \quad (4.12)$$

where $\phi_1(t) \sim \phi_4(t)$ are the response signals for each launched $P_1(t) \sim P_4(t)$ pulses and $e_1(t) \sim e_4(t)$ the uncorrelated zero-mean noise. It should be noted here that the time delay between $\phi_i(t)$ and $\phi_{i+1}(t)$ is τ, which corresponds to the pulse duration.

We then perform Hadamard transform to calculate the estimate signal traces as $\hat{\phi}_1(t) \sim \hat{\phi}_4(t)$, which can be expressed as

$$\begin{pmatrix}\hat{\phi}_1(t)\\ \hat{\phi}_2(t)\\ \hat{\phi}_3(t)\\ \hat{\phi}_4(t)\end{pmatrix}=\mathbf{H}_4^{-1}\begin{pmatrix}\eta_1(t)\\ \eta_2(t)\\ \eta_3(t)\\ \eta_4(t)\end{pmatrix}=\begin{pmatrix}\phi_1(t)\\ \phi_2(t)\\ \phi_3(t)\\ \phi_4(t)\end{pmatrix}+\frac{1}{4}\mathbf{H}_4\begin{pmatrix}e_1(t)\\ e_2(t)\\ e_3(t)\\ e_4(t)\end{pmatrix} \tag{4.13}$$

$$\begin{aligned}\hat{\phi}_1(t)&=\phi_1(t)+\frac{e_1(t)+e_2(t)+e_3(t)+e_4(t)}{4}\\ \hat{\phi}_2(t)&=\phi_2(t)+\frac{e_1(t)-e_2(t)+e_3(t)-e_4(t)}{4}\\ \hat{\phi}_3(t)&=\phi_3(t)+\frac{e_1(t)+e_2(t)-e_3(t)-e_4(t)}{4}\\ \hat{\phi}_4(t)&=\phi_4(t)+\frac{e_1(t)-e_2(t)-e_3(t)+e_4(t)}{4}\end{aligned} \tag{4.14}$$

Next, the estimate traces in Eq. (4.14) are time-shifted with the factor τ and then averaged to produce

$$\begin{aligned}\hat{\phi}(t)&=\frac{\hat{\phi}_1(t)+\hat{\phi}_2(t+\tau)+\hat{\phi}_3(t+2\tau)+\hat{\phi}_4(t+3\tau)}{4}\\ &=\hat{\phi}_1(t)+\frac{e_1(t)+e_2(t)+e_3(t)+e_4(t)}{16}+\frac{e_1(t+\tau)-e_2(t+\tau)+e_3(t+\tau)-e_4(t+\tau)}{16}\\ &\quad+\frac{e_1(t+2\tau)+e_2(t+2\tau)-e_3(t+2\tau)-e_4(t+2\tau)}{16}\\ &\quad+\frac{e_1(t+3\tau)-e_2(t+3\tau)-e_3(t+3\tau)+e_4(t+3\tau)}{16}\end{aligned} \tag{4.15}$$

Note that the calculations in Eq. (4.15) are obtained based on the following relations:

$$\begin{aligned}&P_2(t)=P_1(t-\tau),\ \phi_2(t)=\phi_1(t-\tau)\\ &P_3(t)=P_1(t-2\tau),\ \phi_3(t)=\phi_1(t-2\tau)\,.\\ &P_4(t)=P_1(t-3\tau),\ \phi_4(t)=\phi_1(t-3\tau)\end{aligned}$$

Therefore, in the case of code length L=4, the electrical noise power $\varepsilon^{L=4}$ can be calculated as

$$\varepsilon^{L=4}=E\left[\left\{\hat{\phi}(t)-\phi_1(t)\right\}^2\right]=\frac{16\sigma^2}{16\times16}=\frac{1}{16}\sigma^2 \tag{4.16}$$

Equation (4.16) is calculated based on these assumptions [8]:

$$E\{e_i(t)\}=0, E\{e_i^2(t)\}=\sigma^2, E\{e_i(t)e_j(t)\}=0, (i\neq j) \tag{4.17}$$

4.3.2 Signal-to-Noise Improvement Ratio (SNIR)

From Eq. (4.16), when code length of 4 is used, the noise power is reduced by the factor of 16. From this, we can compare the enhancement in the SNR obtained in Eq. (4.16) over the single pulse PSP-BOTDA measured under the equal measurement times. Then, the noise power of 4-times averaging for single pulse PSP-BOTDA can be easily expressed as

$$\varepsilon^{single\ pulse}=\frac{\sigma^2}{4} \tag{4.18}$$

Therefore, the theoretical SNIR for code length L=4 can be expressed as

$$SNIR^{L=4} = \frac{\sqrt{\frac{\sigma^2}{4}}}{\sqrt{\frac{\sigma^2}{16}}} = \sqrt{4} = 2 \tag{4.19}$$

If we analyze the SNIR with arbitrary code length *L*, we can generalize the SNIR employing any code length of Hadamard codes as

$$SNIR^{L} = \sqrt{L} \tag{4.20}$$

which agrees with that reported by Sloane et al. [6].

4.3.3 Example of Matrix Calculations Involved in Hadamard Transform

In this section, we describe the matrix calculations involved in the Hadamard transform in the case of 4-bit Walsh codes. Firstly, based on Eq. 4.9, the generated 4-bit Walsh codes are as follows.

$$\mathbf{H}_4 = \begin{pmatrix} 1 & 1 & 1 & 1 \\ 1 & -1 & 1 & -1 \\ 1 & 1 & -1 & -1 \\ 1 & -1 & -1 & 1 \end{pmatrix}.$$

Next, we calculate the inverse matrix of $\mathbf{H}_4$, which can be shown as

$$\mathbf{H}_4^{-1} = \frac{1}{4}\begin{pmatrix} 1 & 1 & 1 & 1 \\ 1 & -1 & 1 & -1 \\ 1 & 1 & -1 & -1 \\ 1 & -1 & -1 & 1 \end{pmatrix}.$$

Then, the matrix calculation between $\mathbf{H}_4^{-1}$ and $\mathbf{H}_4$ is performed as follows

$$\begin{aligned} \mathbf{H}_4^{-1} \times \mathbf{H}_4 &= \frac{1}{4}\begin{pmatrix} 1 & 1 & 1 & 1 \\ 1 & -1 & 1 & -1 \\ 1 & 1 & -1 & -1 \\ 1 & -1 & -1 & 1 \end{pmatrix} \times \begin{pmatrix} 1 & 1 & 1 & 1 \\ 1 & -1 & 1 & -1 \\ 1 & 1 & -1 & -1 \\ 1 & -1 & -1 & 1 \end{pmatrix}, \\ &= \frac{1}{4}\begin{pmatrix} 4 & 0 & 0 & 0 \\ 0 & 4 & 0 & 0 \\ 0 & 0 & 4 & 0 \\ 0 & 0 & 0 & 4 \end{pmatrix} \end{aligned}$$

which produce the identity matrix of $\mathbf{H}_4$. Therefore, we can clearly observe from the above matrix calculation that the processed Walsh code produced 1s at main diagonal and 0s at other part, i.e., no side-lobes. The peak amplitude obtained from 2nd to 4th column in the above result is then shifted so that their peak amplitude is aligned to the peak amplitude of the 1st column, and finally averaged.

4.3.4 Robustness of Hadamard Transform Against the Amplitude Variation

In Section 4.3.3, the example of Hadamard transform calculation was performed with assuming that the amplitude of the coded pulses is uniform. However, in the view point of especially coded PSP-BOTDA employing NRZ pulses, the amplitude of the measured Brillouin signal exponentially decreases due to the decrease of the acoustic wave used for generating SBS (see Chapter 6). To clearly show the impact of such response signals decoding on the quality of the decoded signal, in this section the author provides the illustration and explanation on decoding the response signal with

decreased amplitudes via Hadamard transform. Under the same condition, the author also provides the signal decoded via auto-correlations for Golay codes for comparison purpose.

We begin with the Hadamard transform process of a 4x4 Hadamard matrix. The launched pulses according to the codes and their response signals are illustrated in Fig. 4.4. In Fig. 4.4, the amplitude of the launched pulses is same for all Walsh codes (W1~W4). On the other hand, we assume that there is a decrease in the response signals (R1~R4) measured by each codeword. Then, the matrix calculation between $\mathbf{H}_4^{-1}$ and the response signals $\mathbf{R}_4$ can be shown as follows

$$\mathbf{H}_4^{-1}\times\mathbf{R}_4=\frac{1}{4}\begin{pmatrix}1&1&1&1\\1&-1&1&-1\\1&1&-1&-1\\1&-1&-1&1\end{pmatrix}\times\begin{pmatrix}R_1&R_2&R_3&R_4\\R_1&-R_2&R_3&-R_4\\R_1&R_2&-R_3&-R_4\\R_1&-R_2&-R_3&R_4\end{pmatrix}.$$

$$=\frac{1}{4}\begin{pmatrix}4R_1&0&0&0\\0&4R_2&0&0\\0&0&4R_3&0\\0&0&0&4R_4\end{pmatrix}$$

Since the Hadamard transform uses orthogonal matrix in the calculations, it can be seen from the above result that peak amplitudes are produced at main diagonal while 0s at other parts. After that, the signals from 2nd to 4th columns are shifted so that their peak signals are aligned with the signal in the 1st column and finally averaged. Thus, we can clearly see that the decoded signal produces no side-lobe even when the amplitude of the received signals is not uniform. The key factor that contributes to such an undistorted decoded signal is the direction of the inner product calculation. One can see from Fig. 4.4 that we perform the inner product calculation between the row vector of the inverse Hadamard matrix and the column vector of the matrix produced from the response signals; the amplitude of the column vector is uniform.

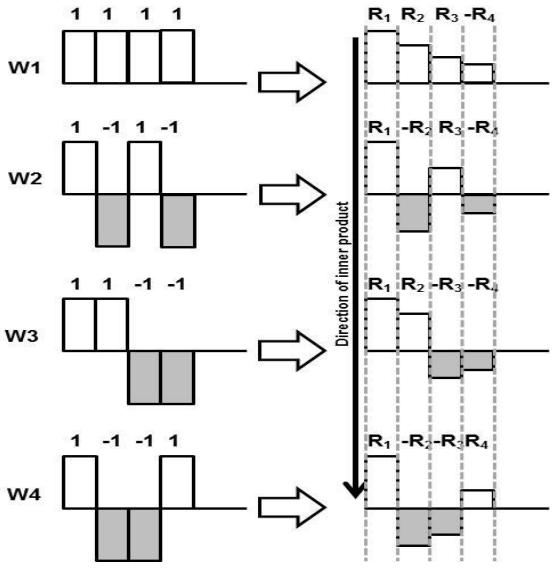

Fig. 4.4. Illustration of 4-bit Walsh codes and their response signals

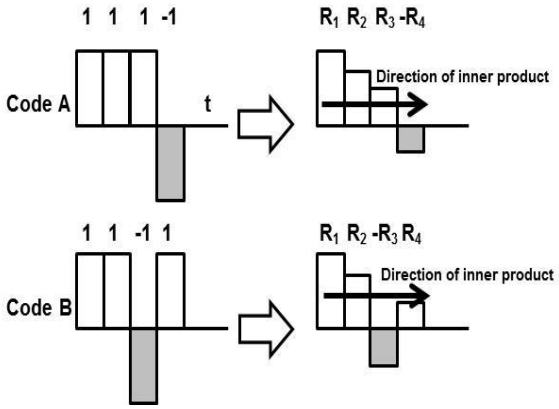

Fig. 4.5. Illustration of 4-bit Golay codes and their response signals.

Next, we perform the auto-correlation calculations for response signals measured by 4-bit Golay codes, being shown in Fig. 4.5. The auto-correlations for the response signal measured by codes A (1, 1, 1, -1) and B (1, 1, -1, 1) based on Eqs. (4.2) and (4.3) can be shown as

$$\begin{aligned}(\Phi_{ResA,A}) &\equiv (\Phi_{ResA,A}(0), \Phi_{ResA,A}(1), \Phi_{ResA,A}(2), \Phi_{ResA,A}(3)) \\ &= (R_1 + R_2 + R_3 + R_4,\ R_2 + R_3 - R_4,\ R_3 - R_4,\ -R_4) \\ (\Phi_{ResB,B}) &\equiv (\Phi_{ResB,B}(0), \Phi_{ResB,B}(1), \Phi_{ResB,B}(2), \Phi_{ResB,B}(3)) \\ &= (R_1 + R_2 + R_3 + R_4,\ R_2 - R_3 + R_4,\ -R_3 + R_4,\ R_4)\end{aligned}.$$

We then sum the above auto-correlations to obtain

$$(\Phi_{Res\,A,A}) + (\Phi_{Res\,B,B}) = (2(R_1 + R_2 + R_3 + R_4),\ 2(R_2 - R_4),\ 0,\ 0).$$

From the above calculation result, we can clearly see that the summation of auto-correlations produces a side-lobe of amplitude $2(R_2 - R_4)$. Since the inner product between the Golay codes A and B with their response signal is in the direction of the decreasing amplitude (as shown in Fig. 4.5), the summation after the auto-correlations has resulted in the side-lobe generation. Thus, it is important to note that in the case of Golay codes, uniform amplitude of signal is necessary in order to obtain a decoded signal with zero side-lobes.

Finally, it should be noted that the examples shown above are made for decoding the response signals from a single localized point. However, the above analysis is also applicable for the signals from a number of distributed points across the fiber because both Hadamard transform and auto-correlations are based on linear transformations.

4.4 Dual Golay Codes

In this section, the author presents the new concept of combining two GCPs to generate new code system called dual Golay codes. It will be shown later that the correlation result of the combined codes still holds the special property of the conventional GCP, that the out-of-phase aperiodic autocorrelation coefficients of the codes sum to zero, but with higher amplitude at the in-phase correlation.

4.4.1 Generating the Dual Golay Codes from Two GCPs

The dual Golay codes are generated by combining one GCP with another pair [7]. Let us consider two GCPs; the first pair of codes A and B and the second pair of codes C and D. These pairs and their elements can be expressed by

$$\begin{aligned}A &= (a_0, a_1, a_2, \ldots, a_{M-1}) \\ B &= (b_0, b_1, b_2, \ldots, b_{M-1})\end{aligned} \tag{4.21}$$

$$\begin{aligned}C &= (c_0, c_1, c_2, \ldots, c_{N-1}) \\ D &= (d_0, d_1, d_2, \ldots, d_{N-1})\end{aligned} \tag{4.22}$$

where *M* is the code length for codes A and B and *N* is the code length for codes C and D. The process of combining the two pairs is called *nesting*; the elements in A and B is multiplied by each element of C and D to generate the dual Golay codes, which can be explicitly expressed as

$$(A * C)_{MN} = (Ac_0, Ac_1, Ac_2, \ldots\ldots, Ac_{N-1}) \tag{4.23a}$$

$$(B * C)_{MN} = (Bc_0, Bc_1, Bc_2, \ldots\ldots, Bc_{N-1}) \tag{4.23b}$$

$$(A * D)_{MN} = (Ad_0, Ad_1, Ad_2, \ldots\ldots, Ad_{N-1}) \tag{4.24a}$$

$$(B * D)_{MN} = (Bd_0, Bd_1, Bd_2, \ldots\ldots, Bd_{N-1}) \tag{4.24b}$$

where * refers to the operator of the nesting process, and

$$\begin{aligned}(Ac_i) &= (a_0, a_1, a_2, \ldots\ldots, a_{M-1}) \quad for\ c_i = 1 \\ (Ac_i) &= (\bar{a}_0, \bar{a}_1, \bar{a}_2, \ldots\ldots, \bar{a}_{M-1}) \quad for\ c_i = -1\end{aligned} \tag{4.25}$$

and so on. From Eqs. (4.23) and (4.24), the combination of the two pairs results in four sequences of the dual Golay codes of length *MN*.

In the dual Golay code PSP-BOTDA system, we distinguish the two GCPs with different names for convenience; one pair is the 'continuous pulse codes' and the other pair is the 'discrete pulse codes'. One may immediately realize that these names correspond to the configuration in Figs. 4.2(a) and 4.2(b), respectively. This is because the pump light of the dual Golay code PSP-BOTDA is generated by combining the pump light of coded continuous-PSP-BOTDA with that of the coded discrete-PSP-BOTDA. Note that Figs. 4.2(a) and 4.2(b) include the long 1st pulse with a pulse width T_1 which is used to excite acoustic wave, as explained before. Since this section explains the methods to generate the dual Golay codes, it is convenient to express the codes in terms of bit value and also to exclude the 1st pulse. We assume the codes A and B in Eq. (4.21) as the continuous pulse codes, A^{cont} and B^{cont} and codes C and D in Eq. (4.22) as the discrete pulse codes, C^{disc} and D^{disc}. Since each pulse coded with C^{disc} or D^{disc} is generated separately as shown in Fig. 4.2(b), the dual Golay codes used in the PSP-BOTDA system should include zero elements. Then, modifying the right-hand sides of Eqs. (4.23) and (4.24), we obtain four sequences as follows;

$$(AC) = \left(A^{cont} * C^{disc}\right)_{(L_{cont}+L_{int})L_{disc}} = \left(A^{cont}c_0^{disc}, S, A^{cont}c_1^{disc}, S, \ldots\ldots, S, A^{cont}c_{L_{disc}-1}^{disc}, S\right) \tag{4.26a}$$

$$(BC) = \left(B^{cont} * C^{disc}\right)_{(L_{cont}+L_{int})L_{disc}} = \left(B^{cont}c_0^{disc}, S, B^{cont}c_1^{disc}, S, \ldots\ldots, S, B^{cont}c_{L_{disc}-1}^{disc}, S\right) \tag{4.26b}$$

$$(AD) = \left(A^{cont} * D^{disc}\right)_{(L_{cont}+L_{int})L_{disc}} = \left(A^{cont}d_0^{disc}, S, A^{cont}d_1^{disc}, S, \ldots\ldots, S, A^{cont}d_{L_{disc}-1}^{disc}, S\right) \tag{4.27a}$$

$$(BD) = \left(B^{cont} * D^{disc}\right)_{(L_{cont}+L_{int})L_{disc}} = \left(B^{cont}d_0^{disc}, S, B^{cont}d_1^{disc}, S, \ldots\ldots, S, B^{cont}d_{L_{disc}-1}^{disc}, S\right) \tag{4.27b}$$

Here, *S* denotes a sequence of the zero elements of length L_{int} that is the interval between the discretely configured coded pulses. Take note that the superscript refers to the type of the code. We call a set of these four sequences dual Golay codes. The four sequences have the same length, L_{dual} that is given by

$$L_{dual} = (L_{cont} + L_{int})L_{disc} \tag{4.28}$$

where L_{cont} is the code length of the continuous pulse codes and L_{disc} is the code length of the discrete pulse codes.

Let us make an example to generate the (AC) code by using Eq. (4.26a). Codes A^{cont} and C^{disc} are assumed to be the same 4 bit codes as follows;

$$A^{cont} = (111-1) \tag{4.29}$$

$$C^{disc} = (111-1) \tag{4.30}$$

The bit number L_{int} can be chosen as being any non-negative integers as long as the bit interference can be neglected. Here we assume L_{int} = 3 bits for simplification and the signal amplitude is zero in the interval. Then the (AC) code becomes

$$(AC) = (111-1000111-1000111-1000-1-1-11000) \tag{4.31}$$

and the total code length of (AC), L_{dual} equals to 28 bits according to Eq. (4.28). The form of the signal coded in the time domain is shown in Fig. 4.6 as a function of a bit. Since the 4th bit of the C^{disc} is -1, the elements of the 4th A^{cont} are inverted, as shown in Fig. 4.6.

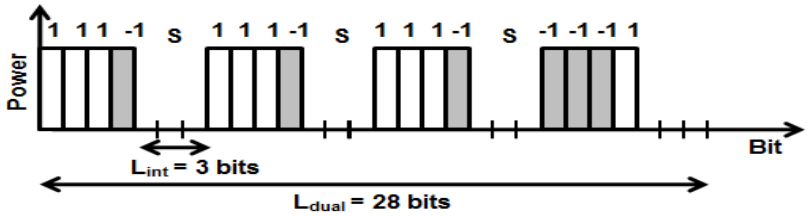

Fig. 4.6. An example of pulses modulated with (AC) code of the dual Golay codes. The 1st pulses are omitted.

4.4.2 Dual Golay Codes Correlation (Mutual Correlation)

The process of correlating the dual Golay codes is called *mutual correlation* [7]. For the dual Golay codes PSP-BOTDA system, the process decodes the measured data. The procedure of the mutual correlations is divided into two;

(i) Correlations with the pair of continuous pulse codes (A^{cont} and B^{cont}) and

(ii) Correlations with the pair of discrete pulse codes (C^{disc} and D^{disc}).

The correlations of (i) are expressed by Eqs. (4.32) - (4.35).

$$ {}_1\Phi_{(AC),A^{cont}}(k) = \sum_{m=0}^{L_{cont}-1} (ac)_{m+k}\, a_m^{cont} \tag{4.32} $$

$$ {}_1\Phi_{(BC),B^{cont}}(k) = \sum_{m=0}^{L_{cont}-1} (bc)_{m+k}\, b_m^{cont} \tag{4.33} $$

$$ {}_1\Phi_{(AD),A^{cont}}(k) = \sum_{m=0}^{L_{cont}-1} (ad)_{m+k}\, a_m^{cont} \tag{4.34} $$

$$ {}_1\Phi_{(BD),B^{cont}}(k) = \sum_{m=0}^{L_{cont}-1} (bd)_{m+k}\, b_m^{cont} \tag{4.35} $$

for $0 \le k \le L_{dual} - 1$, where k refers to the bit shift during the mutual correlation process and the subscript on the left side of Φ refers to the interval of sampling the dual Golay codes data for the correlation. It is assumed that the elements $(ac)_{m+k}$, $(bc)_{m+k}$, $(ad)_{m+k}$ and $(bd)_{m+k}$ of codes (AC), (BC), (AD) and (BD) are zeros for $m + k \ge L_{dual}$. As an example, Fig. 4.7 illustrates the way to calculate the correlation by using Eq. (4.32) when $L_{cont} = L_{disc} = 4$. The variable T in Fig. 4.7 denotes the time slot of the discrete pulse code element, and is given by

$$ T = L_{cont} + L_{int} \tag{4.36} $$

The correlations of (ii) are expressed as

$$ {}_T\Phi_{(AC),C^{disc}}(k) = \sum_{m=0}^{L_{disc}-1} (ac)_{(mT+k)}\, c_m^{disc} \tag{4.37} $$

$$ {}_T\Phi_{(AD),D^{disc}}(k) = \sum_{m=0}^{L_{disc}-1} (ad)_{(mT+k)}\, d_m^{disc} \tag{4.38} $$

$$ {}_T\Phi_{(BC),C^{disc}}(k) = \sum_{m=0}^{L_{disc}-1} (bc)_{(mT+k)}\, c_m^{disc} \tag{4.39} $$

$$ {}_T\Phi_{(BD),D^{disc}}(k) = \sum_{m=0}^{L_{disc}-1} (bd)_{(mT+k)}\, d_m^{disc} \tag{4.40} $$

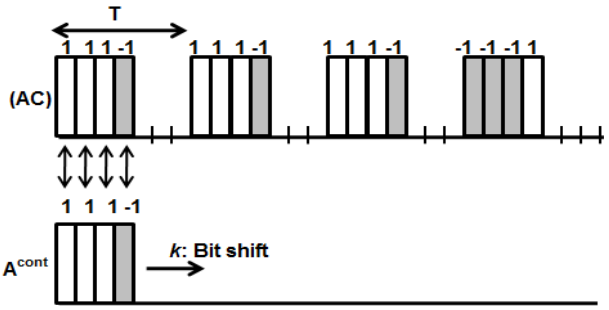

Fig. 4.7. Mutual correlation between (AC) and A^{cont} codes for $L_{cont}=L_{disc}=4$.

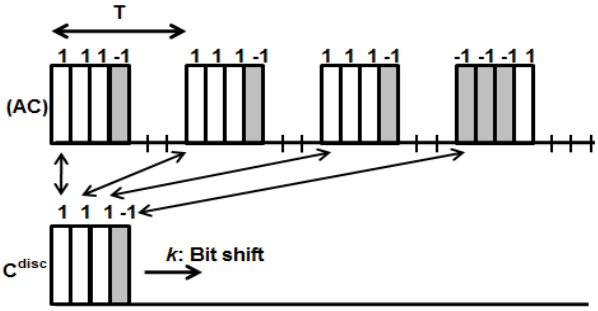

Fig. 4.8. Mutual correlation between (AC) and C^{disc} codes for $L_{cont}=L_{disc}=4$.

for $0 \le k \le L_{dual}-1$. The variable T on the left side of Φ indicates that the dual Golay codes data sampled with the interval T are correlated with the discrete pulse code. The elements $(ac)_{mT+k}$, $(ad)_{mT+k}$, $(bc)_{mT+k}$, and $(bd)_{mT+k}$ of codes (AC), (AD), (BC) and (BD) are assumed to be zeros for $mT+k \ge L_{dual}$. An example is shown in Fig. 4.8, where the way to calculate the correlation given by Eq. (4.37) is depicted, when $L_{cont} = L_{disc} = 4$.

There are two methods to perform the mutual correlations by using both the calculations of (i) based on Eqs. (4.32) to (4.35) and those of (ii) based on Eqs. (4.37) to (4.40). The first method processes (i) and (ii) in this order, while the second method calculates them in reverse order, which will be discussed in the next sections.

A. First Method to Perform Dual Golay Codes Mutual Correlation (Method I)

In this method, codes (AC) and (BC) form one pair and codes (AD) and (BD) the other pair. First, (AC) and (BC) codes are mutually correlated with A^{cont} and B^{cont} by using Eqs. (4.32) and (4.33), respectively. Summing both correlated codes and using Eqs. (4.1) to (4.3) give the following equation.

$$\begin{aligned}({}_1\Phi_{(AC),A^{cont}}(k)) + ({}_1\Phi_{(BC),B^{cont}}(k)) &= \left(\sum_{m=0}^{L_{cont}-1}(ac)_{m+k}\, a_m^{cont}\right) + \left(\sum_{m=0}^{L_{cont}-1}(bc)_{m+k}\, b_m^{cont}\right) \\ &= 2L_{cont}\, c_{\left\lfloor \frac{k}{T} \right\rfloor}^{disc}\, \delta\left(k - T\left\lfloor \frac{k}{T} \right\rfloor\right)\end{aligned} \tag{4.41}$$

where $\lfloor\ \rfloor$ notates the floor function and $\lfloor x \rfloor$ means the largest integer not greater than x. If we define the data generated from Eq. (4.41) as $(\tilde{C}^{disc})$, it can be expressed as

$$\left(\tilde{C}^{disc}\right) = 2L_{cont}\left(c_0^{disc}\,\delta(0), c_{\left\lfloor \frac{1}{T} \right\rfloor}^{disc}\,\delta\left(1 - T\left\lfloor \frac{1}{T} \right\rfloor\right), c_{\left\lfloor \frac{2}{T} \right\rfloor}^{disc}\,\delta\left(2 - T\left\lfloor \frac{2}{T} \right\rfloor\right), \ldots, c_{\left\lfloor \frac{L_{dual}-1}{T} \right\rfloor}^{disc}\,\delta\left(L_{dual}-1-T\left\lfloor \frac{L_{dual}-1}{T} \right\rfloor\right)\right) \tag{4.42}$$

Second, (AD) code is mutually correlated with A^{cont} by using Eq. (4.34) and (BD) code is mutually correlated with B^{cont} code using Eq. (4.35). Just as with the derivation of Eq. (4.41), summing both correlated codes above yields the following;

$$\begin{aligned}({}_1\Phi_{(AD),A^{cont}}(k)) + ({}_1\Phi_{(BD),B^{cont}}(k)) &= \left(\sum_{m=0}^{L_{cont}-1}(ad)_{m+k}\, a_m^{cont}\right) + \left(\sum_{m=0}^{L_{cont}-1}(bd)_{m+k}\, b_m^{cont}\right) \\ &= 2L_{cont}\, d_{\left\lfloor \frac{k}{T} \right\rfloor}^{disc}\, \delta\left(k - T\left\lfloor \frac{k}{T} \right\rfloor\right)\end{aligned} \tag{4.43}$$

The data generated from Eq. (4.43) is defined as $(\tilde{D}^{disc})$ whose expression can be similar to Eq. (4.42).

The third process is to mutually correlate the data $(\tilde{C}^{disc})$ with C^{disc} code by using Eq. (4.37) with modification: Replacing (AC) in Eq. (4.37) with the calculated data $(\tilde{C}^{disc})$, we mutually correlate the $(\tilde{C}^{disc})$ with C^{disc}. In a similar manner, we mutually correlate $(\tilde{D}^{disc})$ with the D^{disc} code by using Eq. (4.38). Summing these correlations results in the final correlation of the dual Golay codes;

$$\begin{aligned}({}_T\Phi_{(\tilde{C}^{disc}),C^{disc}}(k))+({}_T\Phi_{(\tilde{D}^{disc}),D^{disc}}(k)) &= \left(2L_{cont}\sum_{m=0}^{L_{disc}-1}(\tilde{c})^{disc}_{(mT+k)}\,c_m^{disc}\right)+\left(2L_{cont}\sum_{m=0}^{L_{disc}-1}(\tilde{d})^{disc}_{(mT+k)}\,d_m^{disc}\right) \\ &= 4L_{cont}L_{disc}\,\delta(k)\end{aligned} \tag{4.44}$$

Equation (4.44) shows that the peak value at zero-shift of the correlated code corresponds to $4L_{cont}L_{disc}$ and that the side lobes are canceled exactly.

B. <u>Second Method to Perform Dual Golay Codes Mutual Correlation (Method II)</u>

The second method is analogous to the first method except that for the second method, the mutual correlation starts with the correlation with the discrete pulse codes. First, using Eq. (4.37), the (AC) code is sampled at the interval *T*. The sampled data is mutually correlated with C^{disc} by using Eq. (4.37). Similarly, the (AD) code is sampled at the interval *T* and is mutually correlated with the D^{disc} code by using Eq. (4.38). The summation of these correlations is expressed as follows:

$$\begin{aligned}({}_T\Phi_{(AC),C^{disc}}(k))+({}_T\Phi_{(AD),D^{disc}}(k)) &= \left(\sum_{m=0}^{L_{disc}-1}(ac)_{(mT+k)}\,c_m^{disc}\right)+\left(\sum_{m=0}^{L_{disc}-1}(ad)_{(mT+k)}\,d_m^{disc}\right) \\ &= 2L_{disc}a_k^{cont}\,\delta\left(\left\lfloor\frac{k}{L_{cont}}\right\rfloor\right)\end{aligned} \tag{4.45}$$

Strictly speaking, a_k^{cont} with $k > L_{cont}-1$ has not been defined yet. However, hereafter we will use the expression of Eq. (4.45) for simplicity since δ in Eq. (4.45) equals to zero when $k > L_{cont}-1$. The data generated from Eq. (4.45) are denoted by $(\tilde{A}^{cont})$, and is given by

$$\left(\tilde{A}^{cont}\right)= 2L_{disc}\left(a_0^{cont},a_1^{cont},a_2^{cont},\ldots,a_{L_{cont-1}}^{cont},0,0\ldots\right) \tag{4.46}$$

Equations (4.45) and (4.46) show that the first $L_{cont\text{-}1}$ elements of $(\tilde{A}^{cont})$ agree with the A^{cont} elements multiplied with $2L_{disc}$, and the rest of $(\tilde{A}^{cont})$ elements are zeros.

Second, in a similar manner, (BC) and (BD) codes are mutually correlated with the C^{disc} and D^{disc} codes by using Eqs. (4.39), and (4.40), respectively. The summation of the correlations is as follows:

$$\begin{aligned}({}_T\Phi_{(BC),C^{disc}}(k))+({}_T\Phi_{(BD),D^{disc}}(k)) &= \left(\sum_{m=0}^{L_{disc}-1}(bc)_{(mT+k)}\,c_m^{disc}\right)+\left(\sum_{m=0}^{L_{disc}-1}(bd)_{(mT+k)}\,d_m^{disc}\right) \\ &= 2L_{disc}b_k^{cont}\,\delta\left(\left\lfloor\frac{k}{L_{cont}}\right\rfloor\right)\end{aligned} \tag{4.47}$$

We define the data generated from Eq. (4.47) as $(\tilde{B}^{cont})$ whose expression can be similar to Eq. (4.46).

Third, the data $(\tilde{A}^{cont})$ and $(\tilde{B}^{cont})$ are mutually correlated with A^{cont} and B^{cont}, respectively. The summation of these correlations yields the total correlation of the dual Golay codes:

$$\begin{aligned}({}_1\Phi_{(\tilde{A}^{cont}),A^{cont}}(k))+({}_1\Phi_{(\tilde{B}^{cont}),B^{cont}}(k)) &= \left(2L_{disc}\sum_{m=0}^{L_{cont}-1}(\tilde{a})^{cont}_{(m+k)}\,a_m^{cont}\right)+\left(2L_{disc}\sum_{m=0}^{L_{cont}-1}(\tilde{b})^{cont}_{(m+k)}\,b_m^{cont}\right) \\ &= 4L_{cont}L_{disc}\,\delta(k)\end{aligned} \tag{4.48}$$

It is not surprising that the final result of Eq. (4.48) agrees with that of Eq. (4.44) since the correlations are linear systems and the calculation order is exchangeable. From Eqs. (4.44) and (4.48), we can clearly see that the magnitude of correlation coefficient code for k = 0 is 4 times the product of the code length of the continuous and discrete pulse codes, and that the side lobes are canceled exactly.

4.4.3 Examples of Mutual Correlations

In this section, examples for both correlation methods (methods I and II) are explained for a clearer view on the mutual correlation equations provided. Consider a pair of the continuous pulse codes A^{cont} and B^{cont} of the code length L_{cont} = 4, and a pair of the discrete pulse codes C^{disc} and D^{disc} of the code length L_{disc} = 2, with the bit interval L_{int} = 3. The generated GCPs based on Eq. (4.4) and the generated dual Golay codes based on Eqs. (4.26) and (4.27) are as follows:

$$A^{cont} = (111-1) \tag{4.49}$$

$$B^{cont} = (11-11) \tag{4.50}$$

$$C^{disc} = (11) \tag{4.51}$$

$$D^{disc} = (1-1) \tag{4.52}$$

$$(AC) = (111-1000111-1000) \tag{4.53}$$

$$(BC) = (11-1100011-11000) \tag{4.54}$$

$$(AD) = (111-1000-1-1-11000) \tag{4.55}$$

$$(BD) = (11-11000-1-11-1000) \tag{4.56}$$

Then the total code length of the dual Golay codes L_{dual} based on Eq. (4.28) is 14 bits and the time-slot of the discrete pulse code T based on Eq. (4.36) is 7 bits.

A. Example of Method I

The mutual correlations between (AC) and A^{cont} of Eq. (4.32), and between (BC) and B^{cont} of Eq. (4.33), and their summation of Eq. (4.41) are illustrated in Fig. 4.9. In Fig. 4.9, the summed data $\left(\tilde{C}^{disc}\right)$ of Eq. (4.41) have two peaks of 8 (=2L_{cont}) in amplitude for k=0 and 7 (=T), and have zeros for other k values. The pattern of the peaks is the same with C^{disc}, except that the peaks are separated by the value of T=7. The mutual correlations between (AD) and A^{cont} of Eq. (4.34), and between (BD) and B^{cont} of Eq. (4.35), and their summation are shown in Fig. 4.10, showing that the summation based on Eq. (4.43) produces $\left(\tilde{D}^{disc}\right)$ with amplitude of 2L_{cont} = 8 and the pattern is the same with D^{disc}, as is the case explained above.

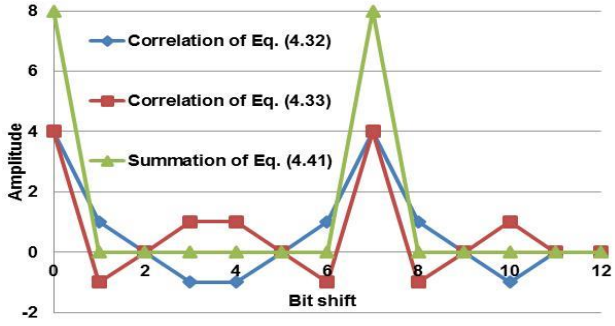

Fig. 4.9. Mutual correlation functions for (AC) of Eq. (4.32), (BC) of Eq. (4.33) and their sum of Eq. (4.41).

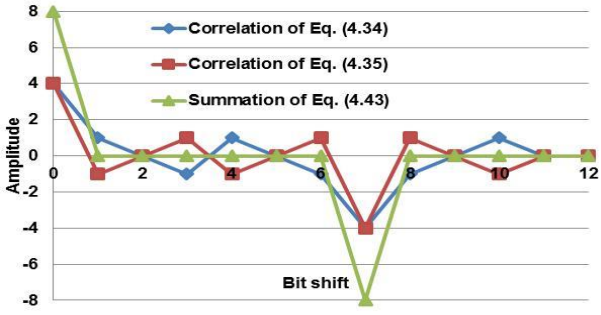

Fig. 4.10. Mutual correlation functions for (AD) of Eq. (4.34), (BD) of Eq. (4.35) and their sum of Eq. (4.43).

In the next process, the data $(\tilde{C}^{disc})$ shown in Fig. 4.9 and the data $(\tilde{D}^{disc})$ shown in Fig. 4.10 are mutually correlated with C^{disc} and D^{disc}, respectively. The mutual correlation functions and their summation of Eq. (4.44) are shown in Fig. 4.11. From Fig. 4.11, we can see that the amplitude of the summation of Eq. (4.44) at k = 0 equals to 32, which corresponds to $4L_{cont}L_{disc}$ = 32. Furthermore, the summation process produces no side lobes for other k values.

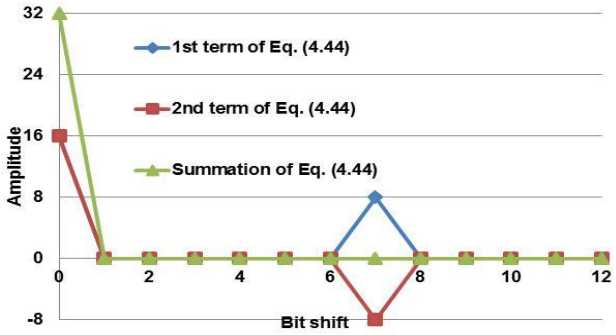

Fig. 4.11. Mutual correlation functions for ${}_{T}\boldsymbol{\Phi}_{\tilde{C}^{disc}C^{disc}}$, ${}_{T}\boldsymbol{\Phi}_{\tilde{D}^{disc}D^{disc}}$, and their sum of Eq. (4.44) based on method I.

B. Example of Method II

Using the same codes listed in Eqs. (4.49) to (4.56), an example based on Method II is explained. The mutual correlations between (AC) and C^{disc} of Eq. (4.37), and between (AD) and D^{disc} of Eq. (4.38), and their summation of Eq. (4.45) are illustrated in Fig. 4.12. In Fig. 4.12, the summed data $(\tilde{A}^{cont})$ produce the peak amplitudes of $2L_{disc}$=4 and -4. The data pattern is the same with the A^{cont}. Next, in a similar manner, the mutual correlations between (BC) and C^{disc} of Eq. (4.39), and (BD) and D^{disc} of Eq. (4.40), and their summation of Eq. (4.47) are calculated. The results are depicted in Fig. 4.13. The summed data have the peaks of 4 and -4 in amplitudes and the data pattern is the same with B^{cont}.

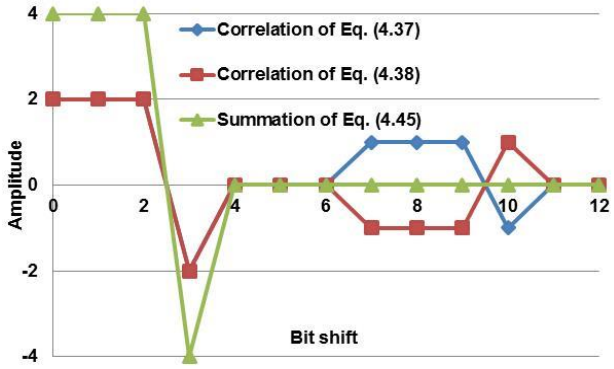

Fig. 4.12. Mutual correlation functions for (AC) of Eq. (4.37), (AD) of Eq. (4.38) and their sum of Eq. (4.45).

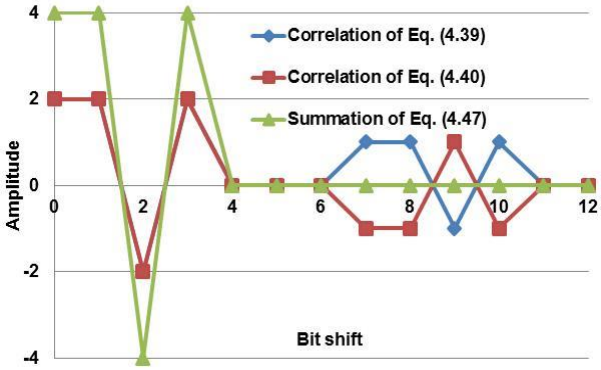

Fig. 4.13. Mutual correlation functions for (BC) of Eq. (4.39), (BD) of Eq. (4.40) and their sum of Eq. (4.47).

Finally, the mutual correlations between $(\tilde{A}^{cont})$ and A^{cont}, and between $(\tilde{B}^{cont})$and B^{cont}, and their summation are calculated by using Eq. (4.48), being depicted in Fig. 4.14. The summed data agree with that obtained by using Method I, as explained before. Therefore, we can confirm that both methods I and II can be applied to perform the correlation calculations of the dual Golay codes and further to be employed in the dual Golay codes PSP-BOTDA sensing system.

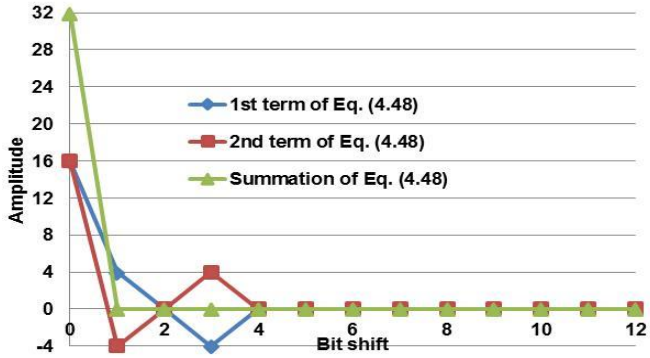

Fig. 4.14. Mutual correlation functions ${}_1\boldsymbol{\Phi}_{\tilde{A}^{cont},A^{cont}}$, ${}_1\boldsymbol{\Phi}_{\tilde{B}^{cont},B^{cont}}$, and their sum of Eq. (4.48) based on method II.

4.4.4 Signal-to-Noise Improvement Ratio (SNIR)

In the dual Golay codes PSP-BOTDA system, eight pumps are used for the measurement, which include the use of pump light modulated with the inverted dual Golay codes. The response signal of the dual Golay codes PSP-BOTDA system after the mutual correlation is defined as

$$Crr^{dualGolaycodesPSP-BOTDA} = 8NL_{cont}L_{disc}\,h_k \tag{4.57}$$

Analogous to the SNR calculations for the GCP of Eq. (4.7), we can define the SNR of the dual Golay codes as

$$\begin{aligned} SNR^{dualGolaycodesPSP-BOTDA} &= \frac{8NL_{cont}L_{disc}\,h_k}{\sqrt{8NL_{cont}L_{disc}}\sigma_\upsilon} \\ &= \sqrt{8NL_{cont}L_{disc}}\,\frac{h_k}{\sigma_\upsilon} \end{aligned} \tag{4.58}$$

On the other hand, including the inverted codes, the coded discrete- or coded continuous-PSP-BOTDA system employing Golay codes uses four pumps each measurement. Thus, to make the measurement times to be equal with that of the dual Golay codes, the measurement for each code must be repeated twice. Based on these considerations, we can then describe the SNR for coded continuous- or coded discrete-PSP-BOTDA analogous to Eq. (4.7) as

$$SNR^{codedPSP-BOTDA} = \sqrt{8L_{contordisc}}\,\frac{h_k}{\sigma_\upsilon} \tag{4.59}$$

Thus, we can describe the SNIR of the dual Golay codes over the coded PSP-BOTDA (discrete or continuous) as

$$\begin{aligned} SNIR^{dualGolaycodesPSP-BOTDA} &= \frac{SNR^{dualGolaycodesPSP-BOTDA}}{SNR^{codedPSP-BOTDA}} \\ &= \frac{\sqrt{8NL_{cont}L_{disc}}\,\dfrac{h_k}{\sigma_\upsilon}}{\sqrt{8NL_{cont\,or\,disc}}\,\dfrac{h_k}{\sigma_\upsilon}} \\ &= \sqrt{L_{cont\,or\,disc}} \end{aligned} \tag{4.60}.$$

From Eq. (4.60), it is concluded that compared to the coded continuous- or coded discrete-PSP-BOTDA, the theoretical SNIR for dual Golay codes PSP-BOTDA improves with $\sqrt{L_{cont\,or\,disc}}$.

Based on the explanations above, we can easily derive the theoretical SNIR of the dual Golay codes PSP-BOTDA compared to the conventional single pulse PSP-BOTDA measured under the same measurement times. In particular, the

measurement with 0-shift and π-shift pumps must each be repeated 4 times with N times averaging. Then, the SNR for the conventional PSP-BOTDA can be expressed as

$$SNR^{single\,pulse\,PSP-BOTDA} = \sqrt{8N}\,\frac{h_k}{\sigma_v} \tag{4.61}.$$

Ultimately, from Eqs. (4.58) and (4.61), we can express the SNIR for dual Golay codes against the conventional single pulse PSP-BOTDA as

$$\begin{aligned} SNIR^{dual\,Golay\,codes\,PSP-BOTDA} &= \frac{SNR^{dual\,Golay\,codes\,PSP-BOTDA}}{SNR^{single\,pulse\,PSP-BOTDA}} \\ &= \frac{\sqrt{8NL_{cont}L_{disc}}\,\frac{h_k}{\sigma_v}}{\sqrt{8N}\,\frac{h_k}{\sigma_v}} \\ &= \sqrt{L_{cont}L_{disc}} \end{aligned} \tag{4.62}$$

in which we can see that the SNIR improves largely with $\sqrt{L_{cont}L_{disc}}$.

4.5 Combined Walsh and Golay Codes

As described in Section 4.4, combining two GCPs to generate dual Golay codes is beneficial for achieving higher SNR measurement than using only one kind of code. It should be noted however, that this concept is not restricted only to the same two GCPs, but can also be applied to two different code systems. Therefore, in this section, the author proposes another new technique of combining two different codes; Golay codes and Walsh codes.

4.5.1 Generation of Combined Walsh and Golay Codes

Consider a Hadamard matrix of dimension $M \times M$ with the elements of

$$H_M = \begin{bmatrix} a_{11} & a_{12} & \cdots & a_{1M} \\ a_{21} & a_{22} & \cdots & a_{2M} \\ \vdots & & & \vdots \\ a_{M1} & a_{M2} & \cdots & a_{MM} \end{bmatrix} \tag{4.63}$$

and a GCP of a pair C and D with the elements of

$$\begin{aligned} C &= (c_0, c_1, c_2, \ldots, c_{K-1}) \\ D &= (d_0, d_1, d_2, \ldots, d_{K-1}) \end{aligned} \tag{4.64}$$

where M is the code length for Walsh codes and K is the code length for Golay codes. As explained in Section 4.3, every row of a Hadamard matrix defines the Walsh codes. Therefore, based on the elements of Eq. (4.63), one can define the Walsh codes as

$$\begin{aligned} W_1 &= (a_{11}, a_{12}, \ldots, a_{1M}) \\ W_2 &= (a_{21}, a_{22}, \ldots, a_{2M}) \\ &\vdots \qquad\qquad \vdots \\ W_M &= (a_{M1}, a_{M2}, \ldots, a_{MM}) \end{aligned} \tag{4.65}$$

Similar to the case of dual Golay codes, it is easy to express the process of combining the elements of the Walsh codes of Eq. (4.65) with the elements of Golay codes of Eq. (4.64) as

$$
\begin{aligned}
&(C*W_1)_{MK} = c_0(a_{11},a_{12},\ldots,a_{1M}), c_1(a_{11},a_{12},\ldots,a_{1M}), c_2(a_{11},a_{12},\ldots,a_{1M}),\ldots,c_{K-1}(a_{11},a_{12},\ldots,a_{1M})\\
&(C*W_2)_{MK} = c_0(a_{21},a_{22},\ldots,a_{2M}), c_1(a_{21},a_{22},\ldots,a_{2M}), c_2(a_{21},a_{22},\ldots,a_{2M}),\ldots,c_{K-1}(a_{21},a_{22},\ldots,a_{2M})\\
&\quad\vdots \qquad\qquad\qquad\qquad\qquad\qquad \vdots\\
&(C*W_M)_{MK} = c_0(a_{M1},a_{M2},\ldots,a_{MM}), c_1(a_{M1},a_{M2},\ldots,a_{MM}), c_2(a_{M1},a_{M2},\ldots,a_{MM}), c_{K-1}(a_{M1},a_{M2},\ldots,a_{MM})\\
&\textit{and}\\
&(D*W_1)_{MK} = d_0(a_{11},a_{12},\ldots,a_{1M}), d_1(a_{11},a_{12},\ldots,a_{1M}), d_2(a_{11},a_{12},\ldots,a_{1M}),\ldots,d_{K-1}(a_{11},a_{12},\ldots,a_{1M})\\
&(D*W_2)_{MK} = d_0(a_{21},a_{22},\ldots,a_{2M}), d_1(a_{21},a_{22},\ldots,a_{2M}), d_2(a_{21},a_{22},\ldots,a_{2M}),\ldots,d_{K-1}(a_{21},a_{22},\ldots,a_{2M})\\
&\quad\vdots \qquad\qquad\qquad\qquad\qquad\qquad \vdots\\
&(D*W_M)_{MK} = d_0(a_{M1},a_{M2},\ldots,a_{MM}), d_1(a_{M1},a_{M2},\ldots,a_{MM}), d_2(a_{M1},a_{M2},\ldots,a_{MM}), d_{K-1}(a_{M1},a_{M2},\ldots,a_{MM})
\end{aligned}
\tag{4.66}
$$

where MK is the code length generated from the combination of two codes. The process of combining the codes can be performed the other way around; that is, the elements of the Golay codes are put into each element of Walsh codes. However, in this section, only the combination of Eq. (4.66) will be used to explain the encoding and decoding methods of the combined codes.

Let us make an example of generating the combined Walsh and Golay codes based on Eq. (4.66). In this combination, we set the Golay codes as the discrete pulses while the Walsh codes the continuous pulses. We set the code length for Golay codes L_{disc}=4 bits and the code length for Walsh codes L_{cont}=2bits. Note that for the application in the coded PSP-BOTDA, we should also include the bit interval of length L_{int} which composed of zero amplitude intervals. We set L_{int}=3. The generated Walsh and Golay codes are

$$
\begin{aligned}
W_1 &= (11)\\
W_2 &= (1-1)
\end{aligned}
\tag{4.67}
$$

$$
\begin{aligned}
C &= (111-1)\\
D &= (11-11)
\end{aligned}
\tag{4.68}
$$

Next, multiplying the elements of Walsh codes with each element of Golay codes and further including L_{int}, the generated combined Walsh and Golay codes are expressed as

$$
\begin{aligned}
(C*W_1)_{(L_{cont}+Li_{nt})L_{disc}} &= (110001100011000-1-1000)\\
(C*W_2)_{(L_{cont}+Li_{nt})L_{disc}} &= (1-10001-10001-1000-11000)\\
(D*W_1)_{(L_{cont}+Li_{nt})L_{disc}} &= (1100011000-1-100011000)\\
(D*W_2)_{(L_{cont}+Li_{nt})L_{disc}} &= (1-10001-1000-110001-1000)
\end{aligned}
\tag{4.69}
$$

where in this case the total code length L_{dual} = (L_{cont}+L_{int})L_{disc} = 20 bits.

The process of decoding the combined codes involves the Hadamard transform calculations and the Golay autocorrelation calculations. The decoding process can be performed by firstly performing the Hadamard transform for Hadamard matrix and then the autocorrelations for Golay codes, or in the reverse order. However, one should carefully select the combination of the codes when decoding via either order. For the codes generated in Eq. (4.69), if one tries to perform the Hadamard transform first, the $(C*W_1)$ and $(C*W_2)$ codes should be selected for the first Hadamard transform; then the combination of $(D*W_1)$ and $(D*W_2)$ for the next Hadamard transform calculation. Then the results for obtained from these decoding processes are used for the autocorrelations with Golay code.

If one wishes to perform the autocorrelations first, the combination of $(C*W_1)$ and $(D*W_1)$ must be used for the first autocorrelations; then the combination of $(C*W_2)$ and $(D*W_2)$ for the next autocorrelations. Two correlation results obtained from these calculations are then used in the Hadamard transform calculation for the decoding process.

4.5.2 Signal-to-Noise Improvement Ratio (SNIR)

The code length for both Walsh and Golay codes is in the form of 2^n (n=0,1,…m). However, in the case of Walsh codes, the number of pumps is defined by the code length, while for any length of Golay codes, only two pumps are used. Suppose we have M number of pumps for Walsh codes, the total number of pumps used for the combined Walsh and Golay codes is $2M$. Furthermore, we should also include the number of pumps modulated with the inverted codes, which sums the total pumps to $4M$. Based on the above considerations, for N averaging times, we can express the SNR for the combined Walsh and Golay codes PSP-BOTDA as

$$SNR^{combined\,Walsh\,Golay\,PSP-BOTDA} = \sqrt{4MNL_{cont}L_{disc}}\,\frac{h_k}{\sigma_\upsilon} \tag{4.70}$$

The SNR for L-bit of Golay coded PSP-BOTDA (coded continuous- or coded discrete-PSP-BOTDA) is already described in Eq. (4.7). However, to equally compare the SNR for the combined Walsh and Golay codes PSP-BOTDA with the conventional Golay coded PSP-BOTDA, Eq. (4.7) must be modified. In details, including the pumps modulated with the inverted codes, measurement with each pump must be repeated M times. We can then express the SNR for coded continuous- or coded-discrete-PSP-BOTDA employing Golay codes as

$$SNR^{coded\,PSP-BOTDA} = \sqrt{4MNL_{cont\,or\,disc}}\,\frac{h_k}{\sigma_\upsilon} \tag{4.71}$$

Therefore, from Eqs. (4.70) and (4.71), we can explicitly show the SNIR for combined Walsh and Golay codes PSP-BOTDA against the coded continuous- or coded discrete-PSP-BOTDA as

$$\begin{aligned} SNIR^{combinedWalshGolayPSP-BOTDA} &= \frac{SNR^{combinedWalshGolayPSP-BOTDA}}{SNR^{codedPSP-BOTDA}} \\ &= \frac{\sqrt{4MNL_{cont}L_{disc}}\,\frac{h_k}{\sigma_\upsilon}}{\sqrt{4MNL_{cont\,or\,disc}}\,\frac{h_k}{\sigma_\upsilon}} \\ &= \sqrt{L_{cont\,or\,disc}} \end{aligned} \tag{4.72}.$$

Similar to the dual Golay codes PSP-BOTDA case, the SNIR for combined Walsh and Golay codes PSP-BOTDA improves with $\sqrt{L_{cont\,or\,disc}}$, but in this case $\sqrt{L_{cont\,or\,disc}}$ corresponds to Walsh codes. It should be noted here that considering the same measurement times, the SNIR for the combined Walsh and Golay codes PSP-BOTDA against the conventional coded continuous- or coded discrete-PSP-BOTDA employing Walsh codes shall give the same result as in Eq. (4.72) of $\sqrt{L_{cont\,or\,disc}}$. However, since the SNIR for this case is derived from the division of SNR for combined Walsh Golay codes over the SNR for conventional Walsh codes, $\sqrt{L_{cont\,or\,disc}}$ corresponds to Golay codes.

In a similar manner, we can describe the theoretical SNIR for the combined Walsh and Golay codes PSP-BOTDA over the conventional single pulse PSP-BOTDA measured under equal measurement times as follow

$$SNIR^{CombinedWalshGolayPSP-BOTDA} = \frac{SNR^{combinedWalshGolayPSP-BOTDA}}{SNR^{single pulsePSP-BOTDA}}$$
$$= \frac{\sqrt{4MNL_{cont}L_{disc}}\,\frac{h_k}{\sigma_\upsilon}}{\sqrt{4MN}\,\frac{h_k}{\sigma_\upsilon}} \tag{4.73}$$
$$= \sqrt{L_{cont}\,L_{disc}}$$

4.6 Dual Walsh Codes

Combining two sets of Walsh codes of code length L for modulating the pump light of the PSP-BOTDA is another new coding concept that is proposed in this thesis. We call this coding system dual Walsh codes. In this section, the algorithm for encoding and decoding the dual Walsh codes is described.

4.6.1 Generating the Dual Walsh Codes

Similar to the dual Golay codes, dual Walsh codes are the codes generated from the combination of a Hadamard matrix with another one. However, unlike the dual Golay codes whose number of code pattern is only four for any combination of code lengths, the number of the code patterns for the dual Walsh codes increases with the dimension of the combined two Hadamard matrices. For example, the combination of a 4×4 Hadamard matrix with a 2×2 Hadamard matrix will generate eight patterns of dual Walsh codes.

Suppose we have these 4×4 and 2×2 Hadamard matrices. Their bit elements can be respectively shown as

$$\begin{aligned} W_1 &= (1111)\\ W_2 &= (1-11-1)\\ W_3 &= (11-1-1)\\ W_4 &= (1-1-11) \end{aligned} \tag{4.74}$$

and

$$\begin{aligned} WW_1 &= (11)\\ WW_2 &= (1-1) \end{aligned} \tag{4.75}$$

We assign the 2×2 matrix as the discrete pulses and 4×4 the continuous pulses. Then we set the bit interval L_{int} of zero amplitudes to L_{int}=3 to be inserted between the discrete pulses. Thus, the total code length, L_{dual} = (L_{cont}+L_{int})L_{disc} =14 bits. By multiplying the continuous pulses with each of discrete pulses, one can obtain the generated dual Walsh codes as

$$\begin{aligned} (WW_1 * W_1)_{14} &= (11110001111000)\\ (WW_1 * W_2)_{14} &= (1-11-10001-11-1000)\\ (WW_1 * W_3)_{14} &= (11-1-100011-1-1000)\\ (WW_1 * W_4)_{14} &= (1-1-110001-1-11000)\\ (WW_2 * W_1)_{14} &= (1111000-1-1-1-1000)\\ (WW_2 * W_2)_{14} &= (1-11-1000-11-11000)\\ (WW_2 * W_3)_{14} &= (11-1-1000-1-111000)\\ (WW_2 * W_4)_{14} &= (1-1-11000-111-1000) \end{aligned} \tag{4.76}$$

Since the generation of the dual Walsh codes involves two Hadamard matrices, the decoding process requires the Hadamard transform to be calculated in two stages. In the above case, at the first stage, the codes $(WW_1 * W_1)$, $(WW_1 * W_2)$, $(WW_1 * W_3)$ and $(WW_1 * W_4)$ are used in one set and decoded with the 4×4 Hadamard matrix and

the $(WW_2 * W_1)$, $(WW_2 * W_2)$, $(WW_2 * W_3)$ and $(WW_2 * W_4)$ are combined in another set and decoded with the same 4×4 matrix. At the second stage, the two results produced from the first stage are then decoded with the 2×2 Hadamard matrix to produce the final decoded result.

4.6.2 Signal-to-Noise Improvement Ratio (SNIR)

As explained previously, the number of code patterns for Walsh codes is defined by the code length used. Suppose we have a $K \times K$ Hadamard matrix that is combined with an $M \times M$ Hadamard matrix. Then the number of dual Walsh codes generated from these matrices is *MK*. Including the measurement for pump modulated with the inverted codes for *N* averaging times, the SNR for the dual Walsh codes PSP-BOTDA can be described as follow

$$SNR^{dual\ Walsh\ codes\ PSP-BOTDA} = \sqrt{2MKNL_{cont}L_{disc}}\,\frac{h_k}{\sigma_\upsilon} \tag{4.77}$$

To derive the SNIR for the dual Walsh codes, we first derive the SNR for the conventional coded continuous- or coded discrete-PSP-BOTDA employing Walsh codes. Suppose we use an $M \times M$ Hadamard matrix for the measurement, including the pumps for inverted codes, the measurement for *N* averaging times must be repeated *K* times. We can show the SNR for L_{cont} or L_{disc} of the conventional coded PSP-BOTDA employing Walsh codes as

$$SNR^{coded\ PSP-BOTDA} = \sqrt{2MKNL_{cont\,or\,disc}}\,\frac{h_k}{\sigma_\upsilon} \tag{4.78}.$$

Thus, the SNIR for dual Walsh codes PSP-BOTDA over the conventional coded PSP-BOTDA is expressed as

$$SNIR^{dual\ Walsh\ codes\ PSP-BOTDA} = \sqrt{L_{cont\,or\,disc}} \tag{4.79}$$

Finally, we can explicitly express the SNIR for the dual Walsh codes against the conventional single pulse PSP-BOTDA measured under the same measurements times with that of dual Walsh codes case as

$$\begin{aligned} SNIR^{dual\ Walsh\ codes\ PSP-BOTDA} &= \frac{SNR^{dual\ Walsh\ codes\ PSP-BOTDA}}{SNR^{single\ pulse\ PSP-BOTDA}} \\ &= \frac{\sqrt{2MKNL_{cont}L_{disc}}\,\frac{h_k}{\sigma_\upsilon}}{\sqrt{2MKN}\,\frac{h_k}{\sigma_\upsilon}} \\ &= \sqrt{L_{cont}\,L_{disc}} \end{aligned} \tag{4.80}$$

Similar to the dual Golay codes and combined Walsh and Golay codes system, compared to the conventional single pulse PSP-BOTDA, the SNIR for the dual Walsh codes is proportional to $\sqrt{L_{cont}\,L_{disc}}$.

4.7 Conclusions of Chapter

In conclusion, the process of combining two codes in modulating the pump light of the PSP-BOTDA offers higher SNR compared to the previously proposed coded continuous- or coded discrete-PSP-BOTDAs. The numerical and experimental analysis will be further discussed in the later chapters to compare with the theoretical SNIR discussed in this chapter.

References

[1] M. J. E. Golay, "Complementary series", IRE Trans. on Info. Theory, vol. IT-7, pp. 82-87, Apr. 1961.

[2] D. Uchiyama, T. Horiguchi, H. Ando, Y. Okumoto, T. Sasaki and Y. Sawai, "Signal to noise improvement ratio for coded

PSP-BOTDA", Technical report of IEICE. OFT 109 (377) (in Japanese), pp. 33-38, Jan. 2010.

[3] R. Muroi, T. Horiguchi, Y. Miyamoto, Y. Sato, A. Tachibana and A. Takakura, "PSP-BOTDA based on Golay code", IEICE Trans. Commun. (in Japanese), vol. J91-B, no. 11, pp. 1493-1501, Nov. 2008.

[4] H. Liang, W. Li, N. Linze, L. Chen and X. Bao, "High-resolution DPP-BOTDA over 50 km LEAF using return-to-zero coded pulses", Opt. Lett., vol. 35, no. 10, pp. 1503-1505, May 2010.

[5] M. D. Jones, "Using simplex codes to improve OTDR sensitivity", IEEE Photon. Tech. Lett. Vol. 15, no. 7, pp. 822-824, Jul. 1993.

[6] N. J. A. Sloane, T. Fine, P. G. Phillips and M. Harwit, "Codes for multiplex spectrometry", App. Opt, vol. 8, no. 10, pp. 2103-2106, Oct. 1969.

[7] **M. S. D. B. Zan** and T. Horiguchi, "A dual Golay complementary pair of sequences for improving the performance of phase-shift pulse BOTDA fiber sensor", J. Lightw. Technol. vol. 30, no. 21, pp. 3338-3356, Nov. 2012.

[8] D. Lee, H. Yoon, P. Kim, J. Park and N. Park, "Optimization of SNR improvement in the noncoherent OTDR based on simplex codes", J. Lightw. Technol. vol. 24, no. 1, pp. 322-328, Jan. 2006.

Chapter 5: Analysis on the Electrical Signal Configuration for Modulating the Pump Light of Coded Discrete-PSP-BOTDA

5.1 Introduction to Chapter

The employment of Golay complementary sequences (Golay codes) in the PSP-BOTDA technique was firstly introduced by Muroi et al. [1]. The technique is called coded discrete-PSP-BOTDA. The benefit of using Golay complementary sequences is that the side-lobes of the autocorrelation functions of two Golay codes sum to zero and produce signal of amplitude 2*L* (*L*: code length) at the main lobe [2]. Theoretically, the improvement in the optical SNR of the coded discrete-PSP-BOTDA system increases in proportion to $\sqrt{L}$. This is because the coded BOTDA signal is proportional to *L* while the white noise accumulates in proportional to $\sqrt{L}$ through the correlation of the Golay complementary code.

Coded discrete-PSP-BOTDA employs return-to-zero (RZ) pulse coding technique in generating the coded pump light. As illustrated in Fig. 5.1, the pump light is composed of a pulse of long duration T_1, followed by a short pulse of duration T_2. The long pulse, which is called the 1st pulse, excites acoustic wave effectively, while the 2nd pulse, which is modulated according to Golay codes interacts with this acoustic wave to generate SBS wave which is then used for strain measurement. In order to avoid the Brillouin signal interaction between the preceding and the succeeding bit pulses groups, every pulse group must be separated by the time interval T_i of longer than the time constant of the acoustic wave τ_a. Thus, the available code length in the coded discrete-PSP-BOTDA is limited by the round trip time (RTT) of the light in fiber. It was found from the numerical calculations that the shortest value of T_i that can be set to obtain optimum SNIR without distorting the Brillouin signal is about 25~35ns [3].

However, if one employs a high speed and high output amplifier that is commonly used for optical communication system to drive an electro-optic modulator, the SNR becomes less than the expected value $\sqrt{L}$ for long code length. The reason lies in the use of an AC-coupled electrical amplifier used to amplify the Golay coded electrical signals. The AC-coupled amplifier rejects the DC and the low frequency component signals. As a result, the amplitude of the amplified signal exponentially decreases, especially when a very long pulse train is used. When light from a laser is modulated by an electro-optic modulator with such a distorted electrical signal and then used as the pump light of the sensor, the linear increase in the Brillouin signal with the code lengths cannot be obtained. As a result, the increment trend in the SNR with the code length becomes nonlinear as well. If we could use a DC-coupled electrical amplifier having high speed and high output, this problem would not occur. However, such sophisticated amplifiers are very expensive, raising the measurement system cost.

Thus, in this chapter, the author introduces a new configuration of the Golay coded electrical signal for the input of the AC-coupled amplifier to overcome the problems described above. It will be shown later in the experimental analysis that by using the proposed configuration, the SNR increases in much better accordance with square root of the code length ($\sqrt{L}$) than the conventional configuration of the electrical signal.

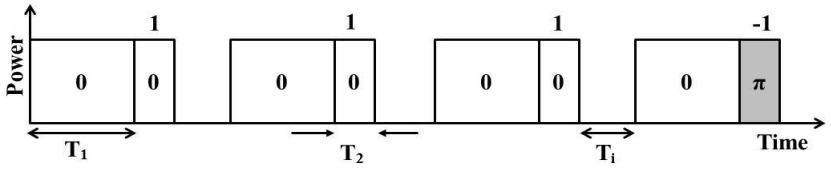

Fig. 5.1. Example of pump light of coded discrete-PSP-BOTDA system.

5.2 Coded Discrete-PSP-BOTDA

5.2.1 Lightwave Phase-Modulation with Golay Coded Electrical Signal

Figure 5.2(a) shows as an example one of a pair of the conventional 4-bit Golay coded electrical signal for PSP-BOTDA. A pulse group consists of a wide pulse of duration T_1 (1st pulse) and a narrow pulse of duration T_2 (2nd pulse). The 1st pulse is used to produce an optical pulse that grows acoustic wave through long interaction with the CW probe light. The 2nd pulse is formatted according to the Golay codes that contain bipolar elements (±1). Each pulse group is separated by an interval time T_i.

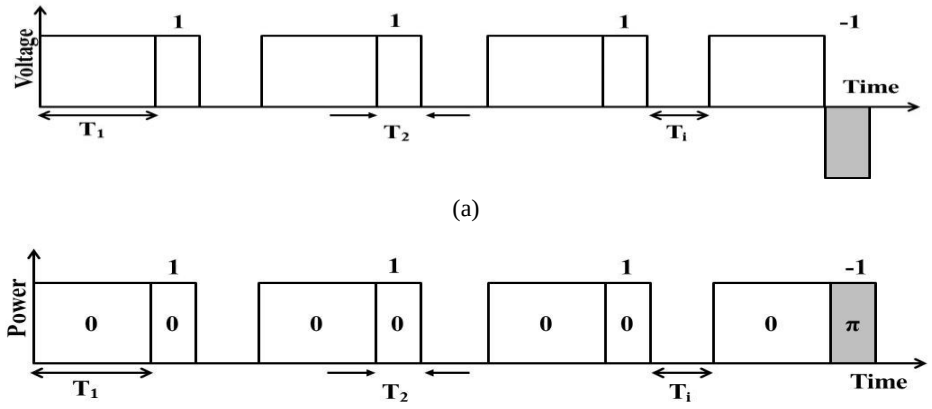

Fig. 5.2. Configurations of the conventional 4-bit Golay coded signal (a) Electrical signal, (b) Optical signal.

This electrical signal is then supplied to an electro-optic modulator to generate the pump light for coded discrete-PSP-BOTDA. The modulator modulates lightwave from a laser diode with the Golay coded electrical signal. Phase modulation scheme is employed to generate the pump light. Figure 5.2(b) shows the light that has been produced by the modulator with the electrical signal of Fig. 5.2(a). The 2nd electrical pulse of +1 code is transformed into an optical pulse that is in the same phase with the 1st optical pulse while the -1 code is transformed into the optical pulse of π-shift in phase compared to the 1st optical pulse. The 1st optical pulse is used to excite the acoustic wave for the purpose of SBS generation, while the 2nd optical pulse is used for the strain and temperature measurements with high spatial resolution, Δz given by

$$\Delta z = \frac{(c/n)T_2}{2} \tag{5.1}$$

where c is the light speed in vacuum and n is the fiber refractive index. Each pulse group is separated by T_i whose value is set longer than τ_a to avoid Brillouin interaction among the pulse groups.

5.2.2 Coded Discrete-PSP-BOTDA Measurement System

In the classic BOTDA system, the interaction of the single pulse pump, the probe light and the acoustic wave generates the SBS wave that is used for the strain and temperature measurement. However, in the coded discrete-PSP-BOTDA, since the pump light is composed of the 1st pulses and coded 2nd pulses, three kinds of SBS waves are generated during the measurement. They are; (i) SBS wave caused by the 1st pulse only, (ii) SBS wave caused by the 2nd pulse only and (iii) SBS wave caused by the interaction between the 2nd pulse and the acoustic wave generated by the 1st pulse.

The subtraction of the response signal obtained by using one of a pair of Golay coded pump light (e.g. 1,1,1,-1) from

that obtained by using its inversion (-1,-1,-1,1) cancels the SBS signals of i) and ii), leaving only the SBS signal of iii) that is doubled because of the different sign between the code and its inversion. The measurement is then continued by using the other of the pair of Golay coded pump light and its inversion. The response obtained with one code is subtracted from those measured with the inverted code. The doubled response signals thus obtained by the subtractions are decoded by performing the auto-correlation calculations with their respective code and then summed to produce the final measurement result.

5.3 Electrical Signal Configurations to Produce the Pump Light of Coded Discrete-PSP-BOTDA

5.3.1 Conventional Electrical Signal Configuration

The experimental setup for generating the electrical signal is illustrated in Fig. 5.3(a). An arbitrary waveform generator was used to generate the electrical signal that composed of the 1st pulse and the Golay coded pulses. This electrical was then amplified to about 4V (amplitude) by an AC-coupled electrical amplifier. Voltage of about 4V is required to efficiently drive an electro-optic modulator used in the experiments for generating the coded pump light. An example of the electrical signal amplified by an AC-coupled electrical amplifier for the coded discrete-PSP-BOTDA system is shown in Fig. 5.3(b). The code used was one of a pair of 32-bit Golay code sequence. In the experiment, the amplitude of all 1st pulses was set to positive value. It is clearly observed that the rejection of the low frequency and DC component signals caused a signal distortion and shift to the negative side.

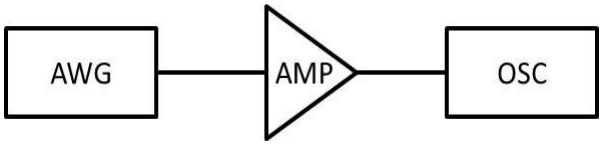

Fig. 5.3(a). Experimental setup for generating electrical signal.

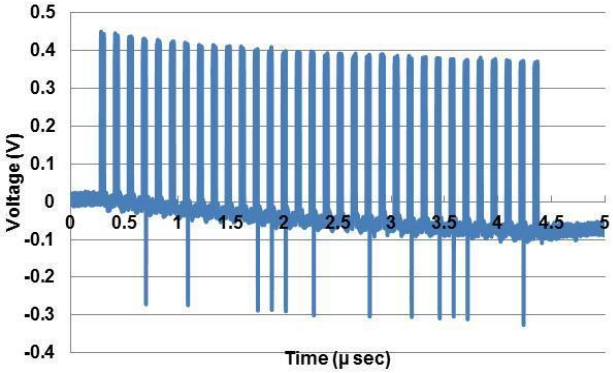

Fig. 5.3(b). Amplified electrical signal of the 32-bit coded discrete-PSP-BOTDA (conventional configuration).

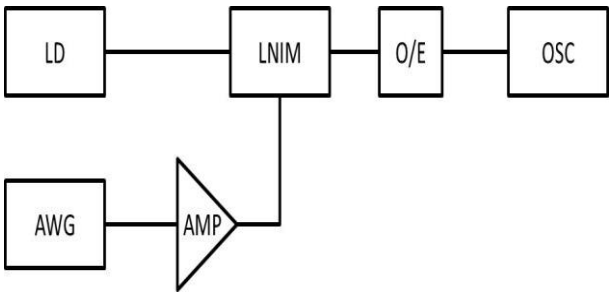

Fig. 5.4(a). Experimental setup for modulating the pump light with the Golay codes.

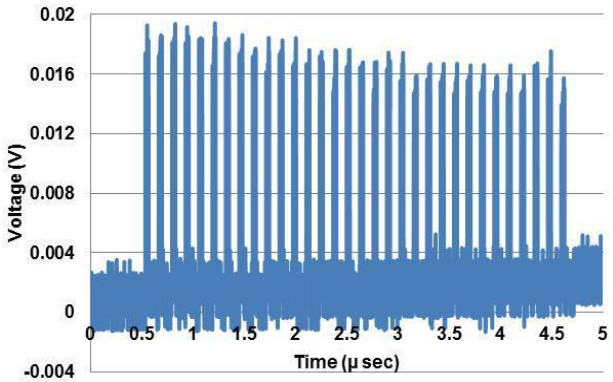

Fig. 5.4(b). Optical signal of the 32-bit coded discrete-PSP-BOTDA (Conventional configuration).

The amplified electrical signal was then used to modulate the light from laser diode by using an electro-optic modulator. The experimental setup is shown in Fig. 5.4(a). The optical signal modulated with the amplified electrical signal of Fig. 5.4(a) is shown in Fig. 5.4(b). This signal was then used as the pump light in the coded discrete-PSP-BOTDA. As a consequence of the distortion in the electrical signal, the optical power of the pump signal became uneven; it decreased almost exponentially, as can be observed in Fig. 5.4(b). Furthermore, due to the gradual shift of the electrical signal to negative side, the optical signal at the interval time T_i leaked through the electro-optic modulator. This leakage of the optical signal may become considerably high if it is amplified by an optical amplifier; resulting in the generation of unwanted Brillouin signals.

5.3.2 Proposed Electrical Signal Configuration

Since the use of AC-coupled amplifier affects the evenness of the signal amplitude, the author proposes a new electrical signal configuration. In contrast to the configuration in Fig. 5.3(b), in the proposed configuration, the amplitudes of the 1st pulses were set to positive and negative values alternately. By doing this, the positive and negative pulses become almost balanced; the increasing shift of the signal to the negative side can be prevented. An example of one of a pair of the proposed 4-bit Golay coded electrical signal is illustrated in Fig. 5.5.

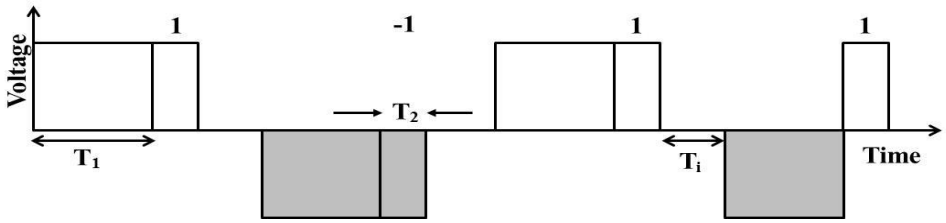

Fig. 5.5. Configuration of the proposed electrical signal for the coded discrete-PSP-BOTDA.

An example of the amplified electrical signal formatted with the proposed configuration is illustrated in Fig. 5.6(a). As explained above, the voltage of the 1st pulse is alternately set to positive and negative values. It can be observed that the amplitude of the signal is well balanced with little voltage offset, although there was a small difference in the amplification rate of the amplifier used between the positive and negative signals. The optical signal modulated with the signals of Fig. 5.6(a) is shown in Fig. 5.6(b). As expected, the amplitudes of each pulse group were almost uniform.

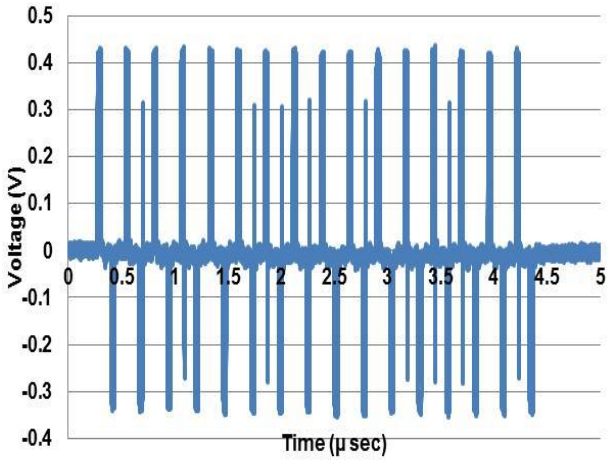

Fig. 5.6(a). Amplified electrical signal of the 32-bit coded discrete-PSP-BOTDA (Proposed configuration).

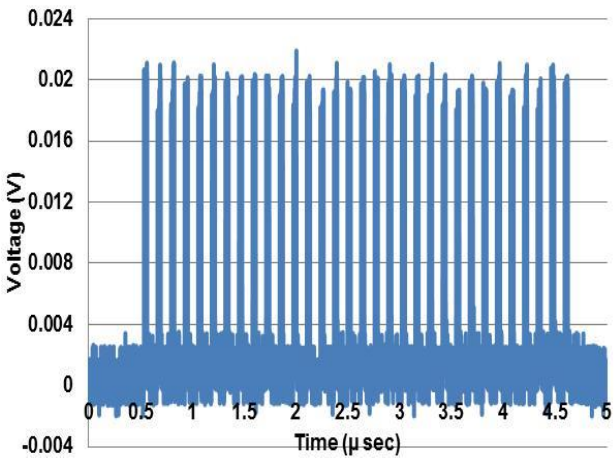

Fig. 5.6(b). Optical signal of the 32-bit coded discrete-PSP-BOTDA (Proposed configuration).

5.4 Experiments

5.4.1 Experimental Setup

The experimental setup is illustrated in Fig. 5.7(a). Light from an LD of 1550 nm in wavelength and 6mW in power was divided by a 1 x 2 optical coupler (50:50). One was used to generate the probe light and the other the pump light. To generate probe light, the light from LD was modulated by a single-side band modulator (SSBM) with a high frequency electrical signal from an RF oscillator (RF OSC). The RF OSC was set at 10.555GHz in frequency. Then, the bias voltages at the SSBM were adjusted so that carrier light can be suppressed and the probe light of frequency downshifted by the amount of 10.555GHz can be generated. The probe light was monitored by an optical spectrum analyzer (OSA). The probe light was amplified by an EDFA (EDFA 2) to 2mW.

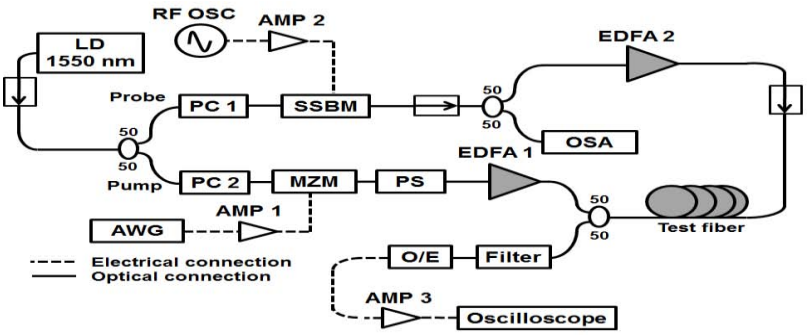

(a)

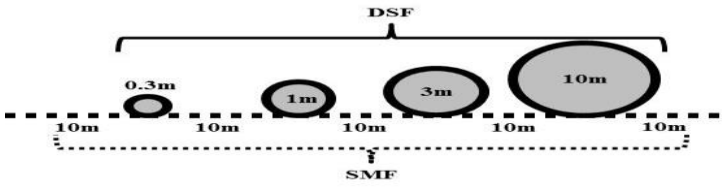

(b)

Fig 5.7(a). Experimental setup of the coded discrete-PSP-BOTDA, (b). The arrangement of the fiber used in the experiment.

As for producing the coded pump light, the light from LD was modulated by an electro-optics modulator, a Mach-Zehnder modulator (MZM) with the electrical signal that was supplied from an arbitrary waveform generator (AWG). The AWG generates the Golay coded electrical signal that consists of the 1st pulses and the 2nd pulses. This signal was then amplified by an AC-coupled electrical amplifier (AMP 1) before being input to the MZM. The amplifier used in the experiments was Picosecond Pulse Labs Model 5865 whose lower cut-off frequency was 30 kHz. The modulated light passed through a polarization scrambler that randomized the polarization state of the light to reduce the polarization induced noise in the BOTDA signal. Then the light was amplified by an EDFA (EDFA 1) to obtain pump light of 100mW in power. The measured Brillouin signal was converted into electrical signal and then digitized and averaged by a digital oscilloscope. This signal was processed by a computer for the decoding process.

The fiber arrangement used in the experiment is illustrated Fig. 5.7(b). Dispersion shift fibers (DSFs) of 0.3m, 1m, 3m and 10m in lengths were used as the test fibers, while single mode fibers (SMFs) of 10m in length were spliced between the test fibers and used as a reference. The BFS difference between the SMF and DSF cables was approximately 320MHz. The duration of T_1 was 30ns, T_2 1ns which corresponded to 10cm of spatial-resolution and the interval time, T_i 100ns. The Golay code lengths were set to 1, 2, 4, 8, 16 and 32bits. The experiments were conducted by using both conventional and proposed configurations for comparison.

5.4.2 Experimental Results

A. Using Conventional Electrical Signal Configuration

The measured Brillouin amplification signals for all code lengths in the case of conventional electrical signal configuration are illustrated in Fig. 5.8 [4]. It is observed that the Brillouin signal increases with respect to the code length, as indicated by the arrow shown in the figure. However, as expected, the signal does not increase linearly with the code length, especially in the case of 16 and 32 bits. The apparent decreasing pump waveform (e.g. Fig. 5.4(b)) for 16 and 32 bit codes might have generated uneven level in the Brillouin signal especially at 10m test section. It also might be due to the presence of a quite high optical power leakage during the interval time T_i since the leakage contributed to the generation of undesired SBS light.

We then performed the optical SNR analysis based on the measured data. The measured optical SNR for each code length was divided by the optical SNR for 1-bit code to find the relative SNR. The results for all code lengths are shown in Fig. 5.9. The theoretical optical SNR, which is approximated as $10log\sqrt{L}$ (dB) where L is the code length, is also included for comparison. One can clearly see that the optical SNR in dB increases almost linearly for code length up to 8 bits at all tests sections, while they start to deviate from the straight line and drop off for longer code lengths. The maximum relative SNR obtained for 32 bits case is 5.6dB (3m section), that is about 2dB lower than the theoretical value.

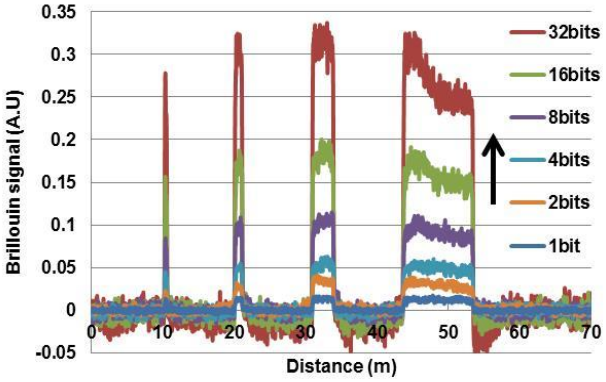

Fig. 5.8. Measured Brillouin signals of coded discrete-PSP-BOTDA for all code lengths (conventional configuration).

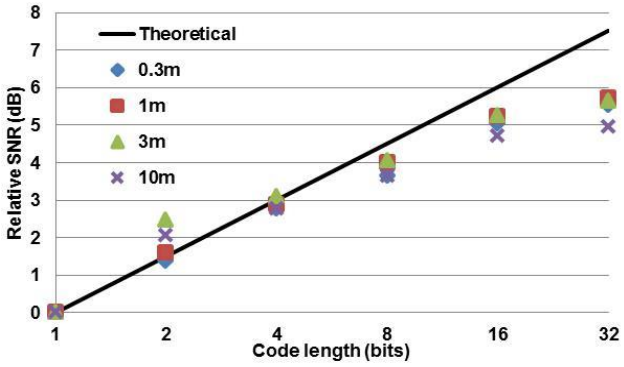

Fig. 5.9. Measured relative SNRs (conventional configuration).

B. Using Proposed Electrical Signal Configuration

The measured Brillouin signals for all code lengths in the case of proposed configuration are illustrated in Fig. 5.10 [4]. The arrow indicates the increase in the Brillouin signal with respect to the code length. Under the same measurement condition, in the case of 16 and 32 bits, the Brillouin signals measured with the proposed configuration are higher than that of the conventional configuration shown in Fig. 5.8. Furthermore, the Brillouin signal shown in Fig. 5.10 increases almost linearly with the code length. In addition, the level of the measured Brillouin signals is almost uniform for all code lengths, even at the long test sections.

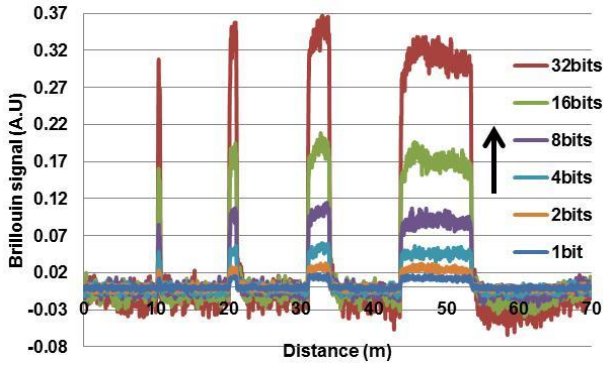

Fig. 5.10. Measured Brillouin signals of coded discrete-PSP-BOTDA for all code lengths (proposed configuration).

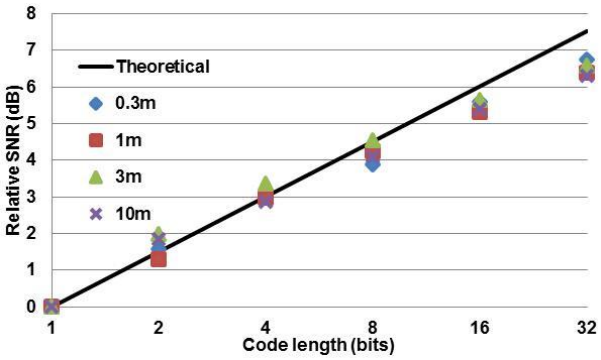

Fig. 5.11. Measured relative SNRs (proposed configuration).

We then examined the rising edges of the Brillouin signal to analyze the spatial resolution of the system. We measured the distance required for the Brillouin signal to rise from 10% to 90% of the average Brillouin power height. In the case of 32 bits, the spatial resolution obtained as in a way described above was 8 cm for 1m test section and 8.5cm for other test sections. The values were slightly shorter than the theoretical value of 10cm, because we used the 10% to 90% rising edges in our analysis. Therefore we conclude that the spatial resolution as high as 10cm has been achieved.

The results on the relative SNR are depicted in Fig. 5.11. In contrast to the results shown in Fig. 5.9, the relative SNRs in Fig. 5.11 show a linear increment with respect to the code length. The increase in the experimental SNR agrees with the theoretical one, although slight discrepancy is observed for 32 bits case. This might be due to the difference in the electrical amplification rate between the positive and negative voltages. From the result, the maximum relative SNR obtained at 3m test section is about 6.6dB, which is quite comparable to the theoretical value of 7.5dB.

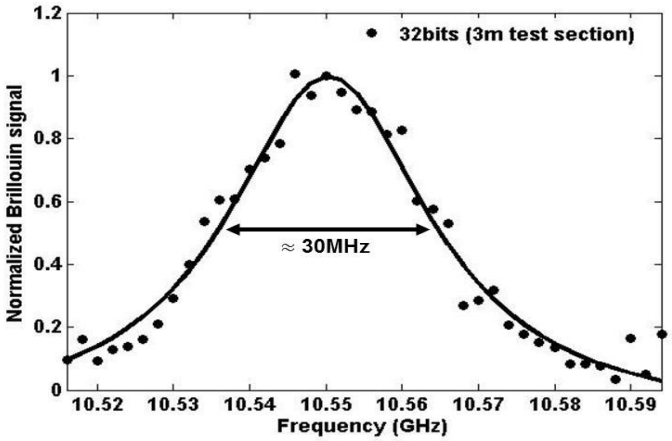

Fig. 5.12. Brillouin gain spectrum (BGS) for 32-bit code, measured at 3m test section (proposed configuration).

We further investigated the Brillouin gain spectrum (BGS) of the test fiber. Figure 5.12 illustrates the BGS measured at the 3m test section for 32 bit code. There is no distortion in the spectrum shape as can be seen in the figure. The spectrum width was measured at the full width at half maximum, being about 30MHz. Therefore, it is confirmed that the characteristics of the measured spectrum are very similar to the spectrum of steady state condition.

5.5 Conclusions of Chapter

Employing Golay complementary sequences in the coded discrete-PSP-BOTDA system can contribute to the improvement in the optical signal-to-noise ratio (SNR) with the code length. A uniform optical power of the coded pulses is required to realize such improvement in optical SNR. However, when an AC-coupled amplifier is used to amplify the coded electrical signals which are input to an electro-optic modulator, the waveform of the optical pulses modulated are distorted. This distortion degrades the correlation characteristic of the coded BOTDA signal. Experiments for bit duration T_2 of 1ns have shown that the relative SNR increases almost linearly for code length up to 8 bits; however in the case of 16 and 32 bits, the relative SNR decreases and deviates from its linear form.

To solve this problem, the author has introduced a new electrical signal configuration for the input signal of the AC-coupled electrical amplifier. The Golay coded electrical signal is modified by alternately setting the amplitude of the 1st pulse to positive and negative values. As a result, the amplitude of the amplified signal becomes almost uniform at all pulse groups and the shift of the mean voltage of the pulse signal is reduced. This new configuration of the coded electrical signals is used to generate the pump light in the coded discrete-PSP-BOTDA. The analysis of the measured relative signal-to-noise ratio (SNR) shows that the relative optical SNR in dB increases linearly with respect to the increase in the Golay code length as expected from the theory. A maximum optical SNR of 6.6dB in the case of 32-bit has been obtained, which is 1dB improvement compared to the conventional one. Finally, it is suggested that the new configuration is also applicable to other coded PSP-BOTDAs that simultaneously use both RZ- and NRZ- pulses. The analysis regarding this application will be further discussed in Chapter 8 and Chapter 9.

References

[1] R. Muroi, T. Horiguchi, Y. Miyamoto, Y. Sato, A. Tachibana and A. Takakura, “PSP-BOTDA based on Golay code”, IEICE Trans. Commun. (in Japanese), vol. J91-B, no. 11, pp. 1493-1501, Nov. 2008.

[2] M. J. E. Golay, “Complementary series”, IRE Trans. on Info. Theory, vol. IT-7, no. 2, pp. 82-87, Apr. 1961.

[3] T. Sasaki, T. Horiguchi, **M. S. D. B. Zan** and D. Uchiyama, “Coded pulse interval dependence of the characteristic in discretely coded PSP-BOTDA”, IEICE Trans. Commun. (in Japanese), vol. J94-B, no. 11, pp. 1481-1489, Nov. 2011.

[4] **M. S. D. B. Zan**, T. Horiguchi, "A new electrical signal configuration for modulating pump light of coded discrete-phase shift pulse-BOTDA," Proc. of the IEEE 3rd Int. Conf. on Photonics (ICP 2012), vol., no., pp.294,298, Oct. 2012.

Chapter 6: Analysis of Employing Walsh- and Golay Coded Non-Return-to-Zero (NRZ) Pulses in the Coded Continuous-PSP-BOTDA

6.1 Introduction to Chapter

The employment of Golay coded non-return-to-zero (NRZ) pulses in the coded continuous-PSP-BOTDA for the purpose of improving the spatial resolution and the SNR has been previously reported [1]. Using this system, sub-meter spatial resolution measurement was successfully demonstrated. The Brillouin signals obtained with the NRZ-coded pulses are also well decoded if the total duration of the coded pulses is around or less than the time constant of the acoustic wave τ_a. The reason for this success is that the subtraction process in the PSP-BOTDA intrinsically cancels the Brillouin gain due to the interaction between each coded pulse and the probe. Thus, this process partly removes the Brillouin gain variation among coded pulses. The PSP-BOTDA extracts only the Brillouin gain that is derived from the interaction of each coded pulse with the acoustic wave excited by the pre-pump pulse. However, since the acoustic wave decays significantly after τ_a, when the total duration of the coded pulses becomes more than τ_a, the waveform of the Brillouin signal decoded is distorted, resulting in the degradation of the spatial resolution; this should be addressed.

Therefore, in this chapter, the author proposes to modulate the NRZ-formatted pump light of the coded continuous-PSP-BOTDA with Walsh codes [2, 3]. The author also compares in this chapter the Brillouin signal obtained by employing Walsh codes with that using Golay codes. It was verified analytically, numerically and experimentally that Walsh codes can decode the Brillouin signals accurately without deteriorating the spatial resolution

6.2 Pump Light Configuration of Coded Continuous-PSP-BOTDA

The NRZ formatted coded continuous-PSP-BOTDA has two kinds of coded bit pulses which are respectively separated in phase from the pre-pump pulse by zero and π. In particular, the code elements of +1s correspond to zero-phase shift while -1s to π-phase shift. Through the process of the SBS, the two kinds of coded bit pulses provide the increase and decrease in the Stokes power (probe), respectively. Consequently, the PSP-BOTDA allows the easy use of Walsh codes, as well as the use of bipolar Golay codes. An example of the pump light modulated with a 4-bit Walsh code in the coded continuous-PSP-BOTDA is illustrated in Fig. 6.1.

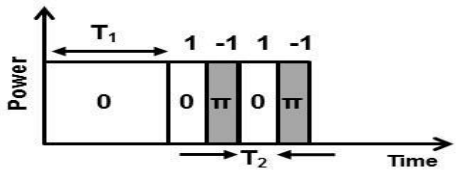

Fig. 6.1. A coded continuous-PSP-BOTDA pump light configuration employing a 4-bit Walsh code.

Conventionally, simplex codes have been also used in BOTDA having the spatial resolution of around or larger than one meter. However, if we shorten the width of coded NRZ pulses to less than 10ns to improve the spatial resolution of the conventional simplex coded BOTDA, the *k*-th Brillouin response signal due to the *k*-th bit pulse becomes affected by the preceding *k*-1 bit pulses. In contrast, the *k*-th Brillouin signal for coded PSP-BOTDA is determined solely by the *k*-th bit pulse, not affected by the preceding bit pulses [4]. This makes more accurate measurement possible by using the PSP-BOTDA with Walsh codes than the conventional intensity-modulation-based BOTDA with simplex codes. Another merit of employing Walsh codes in the PSP-BOTDA system is that it offers higher theoretical SNIR of $\sqrt{L}$ than the commonly used simplex codes, whose theoretical SNIR is $(L+1)/2\sqrt{L}$. The difference in the SNIR contribution

between Walsh coded PSP-BOTDA and simplex coded BOTDA largely lies in the type of modulation scheme employed for generating the coded pump pulses; Walsh coded PSP-BOTDA employs phase modulation scheme to generate the ±1 coded pump pulses, while simplex coded BOTDA system employs intensity modulation scheme to generate 1 and 0 coded pump pulses.

6.3 Analytical Calculations Involving Walsh Codes in the Coded Continuous-PSP-BOTDA

6.3.1 Encoding and Decoding with Walsh Codes

Walsh codes are generated from a square Hadamard matrix (**H** matrix) which consists of bipolar elements (+1s and -1s). Every row of Hadamard matrix of order *L* defines a Walsh function or Walsh code of length *L*. Hadamard matrices have been widely used in OTDR [5] and spectrometry [6] applications.

We define the single pulse that has duration T_2 and corresponds to each code element in every row of **H** matrix as $P_1(t), P_2(t), \cdots, P_L(t)$ where $P_{i+1}(t) = P_i(t - T_2)$. When these pulse sequences are encoded by using **H** matrix and launched into the fiber, the response signal $\eta(t)$ for each row can be described as

$$\begin{pmatrix} \eta_1(t) \\ \eta_2(t) \\ \cdots \\ \eta_L(t) \end{pmatrix} = \mathbf{H} \begin{pmatrix} \phi_1(t) \\ \phi_2(t) \\ \cdots \\ \phi_L(t) \end{pmatrix} + \begin{pmatrix} e_1(t) \\ e_2(t) \\ \cdots \\ e_L(t) \end{pmatrix}, \tag{6.1}$$

where $\phi_1(t), \cdots, \phi_L(t)$ are the response signals for each $P_1(t), \cdots, P_L(t)$ pulses and $e_1(t), \cdots, e_L(t)$ the uncorrelated zero-mean noise. We define the response signal $\phi_i(t)$ for BOTDA as the change in the probe light power due to Brillouin amplification with the pulse pump $P_i(t)$. It should be noted here that the time delay between $\phi_i(t)$ and $\phi_{i+1}(t)$ is T_2, which corresponds to the pulse duration. In the case of measurement with coded continuous-PSP-BOTDA, Eq. (6.1) should be modified to include response signal for the pulse pre-pump whose pulse width is T_1. However, since the subtraction process of the coded continuous-PSP-BOTDA removes the response signal for the pulse pre-pump, we start with Eq. (6.1) by regarding the $\eta_i(t)$ as $(\eta_{pi}(t) - \eta_{mi}(t))/2$, $\phi_i(t)$ as $(\phi_{pi}(t) - \phi_{mi}(t))/2$ and $e_i(t)$ as $(e_{pi}(t) - e_{mi}(t))/2$, where the quantities referenced with the subscripts *p* and *m* are obtained by using matrices **H** and **–H**, respectively.

We then perform the Hadamard transform to calculate the estimate signals traces $\hat{\phi}_1(t) \sim \hat{\phi}_L(t)$, which can be expressed as

$$\begin{pmatrix} \hat{\phi}_1(t) \\ \hat{\phi}_2(t) \\ \cdots \\ \hat{\phi}_L(t) \end{pmatrix} = \mathbf{H}^{-1} \begin{pmatrix} \eta_1(t) \\ \eta_2(t) \\ \cdots \\ \eta_L(t) \end{pmatrix} = \begin{pmatrix} \phi_1(t) \\ \phi_2(t) \\ \cdots \\ \phi_L(t) \end{pmatrix} + \mathbf{H}^{-1} \begin{pmatrix} e_1(t) \\ e_2(t) \\ \cdots \\ e_L(t) \end{pmatrix} = \begin{pmatrix} \phi_1(t) \\ \phi_2(t) \\ \cdots \\ \phi_L(t) \end{pmatrix} + \begin{pmatrix} \hat{e}_1(t) \\ \hat{e}_2(t) \\ \cdots \\ \hat{e}_L(t) \end{pmatrix}. \tag{6.2}$$

Next, the estimates in Eq. (6.2) are time-shifted with the factor T_2 and then averaged to produce

$$\hat{\phi}(t) = \phi(t) + \hat{e}(t), \tag{6.3}$$

where

$$\hat{\phi}(t) = \sum_{i=1}^{L} \hat{\phi}_i(t + (i-1)T_2)/L \ , \tag{6.4}$$

$$\phi(t) = \sum_{i=1}^{L} \phi_i(t + (i-1)T_2)/L \, , \tag{6.5}$$

and

$$\hat{e}(t) = \sum_{i=1}^{L} \hat{e}_i (t + (i-1)T_2) / L \,. \tag{6.6}$$

In contrast to the previous coded OTDR [5], time shifted $\phi_i(t + (i-1)T_2)$ $(i = 2,3,\cdots,L)$ in Eq. (6.5) for coded PSP-BOTDA is not generally identical to $\phi_1(t)$, as described below. However, as will be explained in next sections, $\hat{\phi}(t)$ decoded provides high spatial resolution measurements, improved SNR and Brillouin gain bandwidth as narrow as or even less than that for steady state measurements.

According to equation (A. 10) in [4], the increase in the probe power caused by the *k*-th bit pulse of coded PSP-BOTDA is given by,

$$p_k = \frac{1}{1+\Delta^2}\{\exp(-k\tau)[\cos(k\tau\Delta) - \Delta\sin(k\tau\Delta)] - \exp(-t_k)[\cos(t_k\Delta) - \Delta\sin(t_k\Delta)]\} \tag{6.7}$$

which has been derived by assuming pump depletion can be ignored. For simplicity, proportional constant in Eq. (6.7) is determined so that $p_k = 1$ for $\Delta = 0, \tau = 0$ and $t_k = \infty$. In addition, other parameters in Eq. (6.7) are normalized by time constant of acoustic wave $\tau_a = 1/\pi\Delta\nu_B$ where $\Delta\nu_B$ is FWHM of Brillouin gain spectrum: code bit pulse width $\tau = T_2/\tau_a$, delay $t_k = (T_1 + kT_2)/\tau_a$ with pulse pre-pump width T_1 and frequency detuning from Brillouin frequency shift $\Delta = (\omega_p - \omega_s - \omega_B)\cdot\tau_a$, where ω_p and ω_s are the frequencies of pump and Stokes wave, respectively, and ω_B is the Brillouin frequency shift (BFS).

Assuming that τ is very short, response $\phi_i(t)$ for the *i*-th bit pulse can be approximated as follows:

$$\phi_i(t) = p_i R(t - (i-1)T_2), \tag{6.8}$$

where $R(t)$ is an impulse response function given by

$$R(t) = \begin{cases} \exp(-\alpha V_g t/2) & 0 \le t \le 2L_f/V_g \\ 0 & otherwise \end{cases} \tag{6.9}$$

where α is an attenuation coefficient of a fiber, V_g group velocity of light in the fiber, and L_f fiber length. Substituting Eq. (6.8) into Eq. (6.5) allows us to rewrite Eq. (6.5) as

$$\phi(t) = R(t)\sum_{i=1}^{L} p_i / L \tag{6.10}.$$

6.3.2 Spatial Resolution and Improvement in SNR (SNIR)

As can be seen from Eq. (6.10), decoded average signal $\phi(t)$ decreases with increasing *L* since p_i and thus $\phi_i(t)$ are proportional to $\beta^i \equiv \exp(-i\tau) < 1$. We can also see from Eq. (6.10) that irrespective of code length *L*, decoded signal $\phi(t)$ is proportional to the impulse response $R(t)$ due to the single pulse; thus the signal decoded by Hadamard transform and the time-shift suffers from no signal waveform distortion due to the decoding; we can consequently attain high spatial resolution determined by the code bit pulse width T_2 even when using long codes. This feature is in contrast to that of the Golay codes decoding in which the acoustic wave decay invokes severe distortion in the decoded signal waveform when the total code pulse duration is longer than τ_a. The origin of this advantage of Walsh code over Golay code for the coded continuous-PSP-BOTDA is similar to that of simplex code over Golay code for conventional OTDR [5]. The only difference is that the non-uniformity among the responses $\phi_i(t)$ is mainly due to the acoustic wave decay for the former, and due to the variation of the intensity among the input single pulses $P_i(t)$ for the latter.

Now, let us consider optical signal-to-noise improvement ratio (SNIR) by the proposed coding. As expected, p_i of Eq. (6.7) takes its maximum when $\Delta = 0$. In addition, the second term in the right side of (6.7) can be usually

neglected since the factor $\exp(-t_k)$ decays significantly for long duration of the pulse pre-pump T_1. Then, decoded signal power of Eq. (6.10) for $\Delta = 0$ can be approximated as

$$\phi(t) \approx R(t)\sum_{i=1}^{L}\exp(-i\tau)/L = R(t)\sum_{i=1}^{L}\beta^i / L \tag{6.11}.$$

Noise power after the decoding process, which is derived from Eq. (6.6), can be given by [6], [7]

$$\varepsilon = E\left[\left\{\hat{\phi}(t)-\phi_1(t)\right\}^2\right] = E\left[\hat{e}(t)^2\right] = \frac{1}{L}\sigma^2, \tag{6.12}$$

where $\sigma^2 = E\left(\hat{e}_i(t)^2\right)$. Therefore, the optical SNIR for code length L can be obtained from Eqs. (6.11) and (6.12), being expressed as

$$SNIR = \left(\sum_{i=1}^{L}\beta^{i-1}/L\right)/\left(1/\sqrt{L}\right) = \sum_{i=1}^{L}\beta^{i-1}/\sqrt{L}\,. \tag{6.13}$$

It is interesting to note that if we assume the acoustic wave decay can be neglected, namely $\beta = 1$, Eq. (6.13) becomes $SNIR = \sqrt{L}$, which is usually given for Hadamard spectroscopy [6]. By inspecting Eq. (6.13) for $\beta < 1$, we can find that SNIR is optimized when the total duration of the coded pulses LT_2 is $\tau_a \sim 2\tau_a$ as shown in Fig. 6.2.

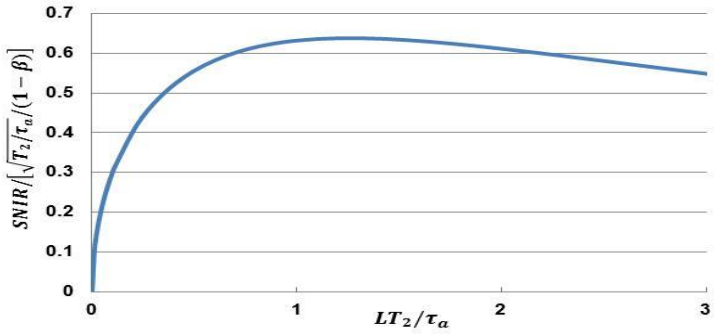

Fig. 6.2. SNIR as a function of the total coded pulse duration LT_2.

6.3.3 Brillouin Gain Spectrum (BGS)

Brillouin gain spectrum obtained by PSP-BOTDA with Walsh coded NRZ pulses is given by Eq. (6.10) with Eq. (6.7) that is in proportion to the average of $p_i(i = 1,2,\cdots L)$. Assuming a typical condition that $\tau = T_2/\tau_a = 0.1, T_1/\tau_a = 3$, Fig. 6.3 shows p_1, p_5, p_{10}, and p_{20} as a function of normalized frequency detuning Δ. Figure 6.3 also includes Brillouin gain spectrum in a steady state that is denoted by p_{st} and given by $1/(1+\Delta^2)$. We found from Fig. 6.3 that p_i s are similar in the profile of the Brillouin gain to the steady state gain p_{st}, and that the frequency at the peak of p_i is identical to that of p_{st}. The decrease in p_i at $\Delta = 0$ with increasing i is due to the decay of the acoustic wave excited by the pre-pump pulse as explained before. Oscillating behavior of p_i at large i with respect to Δ, which does not occur for p_{st}, is caused by rapid change in the phase difference between the acoustic wave excited by the pre-pump pulse and the probe cw light launched into the fiber. For the same reason, we can find even negative p_i in the side-lobes of the spectrum, where the probe light power decreases. We can also find that the phase difference offers Brillouin gain bandwidth that is slightly narrower than that of p_{st}.

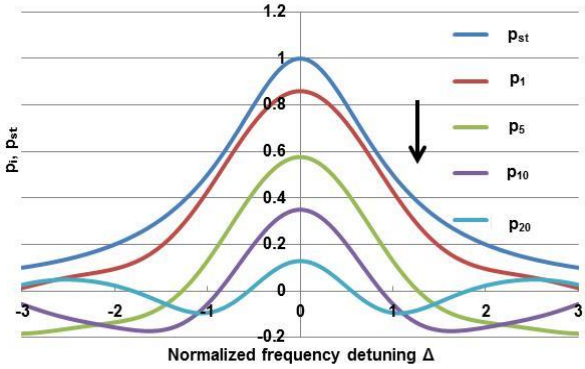

Fig. 6.3. Analytical calculations of BGS for steady state case (p_{st}) and some examples of spectra of p_i.

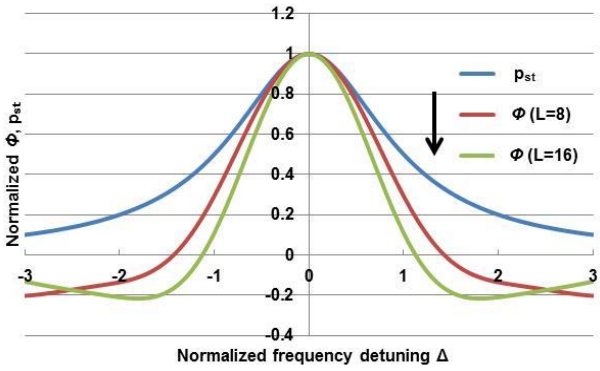

Fig. 6.4. Analytical calculations of BGS for steady state case (p_{st}), 8-bit and 16-bit Walsh coded PSP-BOTDA cases.

Figure 6.4 shows the Brillouin gain spectrum calculated from Eq. (6.10) for L=8 and 16 bits, assuming $\tau = T_2 / \tau_a = 0.1, T_1 / \tau_a = 3$. The spectrum is normalized to unity at $\Delta = 0$ for comparison. We found that both spectra are very similar to that of p_{st} and that the widths of the spectra are even narrower than that of p_{st}, confirming that we can accurately measure the distributed Brillouin frequency shift with Walsh coded PSP-BOTDA proposed.

6.4 Simulations

In this section we describe the simulations of employing Walsh codes in the coded continuous-PSP-BOTDA. We also include the simulation results of employing Golay codes in the same technique for the purpose of comparison.

6.4.1 Simulation Setup

The simulation setup of coded continuous-PSP-BOTDA is shown in Fig. 6.5. The pump light is composed of the 1st pulse with a long duration T_1 and coded 2nd pulses with short duration T_2 each. These 2nd pulses are phase modulated with Walsh codes or Golay codes. In particular, the +1s are modulated into zero shift pulses while -1s are modulated into π-shift pulses to produce the pump light of coded continuous-PSP-BOTDA. The modulated pump light is injected into one side of a fiber, while the cw probe light that is also called Stokes wave is injected from the other side.

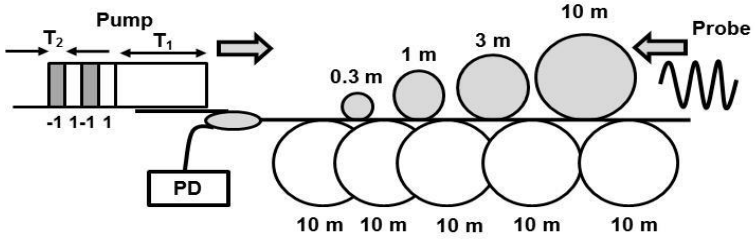

Fig. 6.5. Simulation setup of coded continuous-PSP-BOTDA.

As presented in Fig. 6.5, the test fiber is configured into four sections; 0.3m 1m, 3m and 10m in lengths. Reference fibers of 10m in length are spliced between these fiber sections. The BFS difference between the test and reference fibers was set to 300MHz. The Brillouin gain spectrum width $\Delta\nu_B$ was assumed to be 35MHz; then τ_a was 9ns. The probe light amplified through SBS process is detected by a photodiode (PD), resulting in the Brillouin signal. This numerical calculation was performed based on the interactions of three waves in the fiber cable, which can be modelled as [8]

$$\frac{\partial E_p}{\partial t}+\frac{\partial E_p}{\partial z}=-E_s E_a$$
$$\frac{\partial E_s}{\partial t}-\frac{\partial E_s}{\partial z}=E_p E_a^* \quad , \tag{6.14}$$
$$\frac{\partial E_a}{\partial t}+[1+i\Delta]E_a=E_p E_s^*$$

where E_p, E_s and E_a are the normalized pump, Stokes and acoustic field, respectively. Δ is the normalized frequency detuning expressed by $\Delta=\left[\left(\omega_p-\omega_S\right)-\omega_B\right]\cdot\tau_a$ where ω_p and ω_s are the frequencies of pump and Stokes wave, respectively, and ω_B is the Brillouin frequency shift (BFS).

In the case of Walsh codes, a set of *L*-waveforms of change in the Stokes wave power due to the Brillouin amplification was decoded through the Hadamard transform process, time-shifted and finally averaged to obtain the final result. We note here that the change in the Stokes wave power due to the Brillouin amplification is shortly called the Brillouin signal. This decoding process is similar to that for simplex codes. As for the Golay codes, only two patterns of the measured Brillouin signals corresponding to a pair of complementary sequences are decoded by auto-correlation calculations and then summed to produce the final result. It should be noted here that for both Walsh and Golay codes, actual measurement doubles the number of the Brillouin signals required since the codes whose sign of elements is inverted are also used for subtracting the Brillouin signal caused by the pre-pump by itself.

To efficiently excite the acoustic wave, we set the duration T_1 to 30ns. We first performed the simulations by setting the duration T_2 to 2ns for Walsh codes and then the calculations by setting the duration T_2 to 1ns for both Walsh and Golay codes. The pump power was set to 30mW for T_2 = 2ns case and 60mW for T_2 = 1ns case, while the probe power was set to 2mW for both cases.

6.4.2 Results and Discussions

A. Pump Light Coding with Walsh Codes for T_2=2ns [2] [3]

The lengths of the Walsh codes were set to 1, 2, 4, 8 and 16 bits. The coded pulse duration was fixed to 2ns, which theoretically translates into 20cm of spatial resolution. Figure 6.6 plots the calculated Brillouin signal for each Walsh code length when the frequency difference between the pump and the probe was tuned to the BFS of the four test fibers, which was assumed to be 300MHz lower in the BFS than the reference fibers. It was found from Fig. 6.6 that the transitions of the Brillouin signals in the test fibers are very sharp, even when total duration of the coded pulses is much longer than τ_a (for 8 and 16 bit codes). We also observed in Fig. 6.6 that as the code length increases, the average Brillouin signal processed decreases accordingly. This is due to the fact that the acoustic wave excited by the long pulse of the duration T_1 exponentially decays.

We then analyzed the optical SNIR in the four sections of the 0.3m, 1m, 3m and 10m in lengths, assuming random noise is added in each data sampling. The SNIRs were calculated as a function of code length L =1, 2, 4, 8, and 16 bits under the condition of the same measurement time, so that every codeword of length L was averaged 16/L times. The results are shown in Fig. 6.7, where we found the SNIRs rise in all sections up to about 1.7dB at code length of 4 bits. This code length corresponds to the code duration of 8ns. However, the SNIR declines for longer code lengths. This is because, as explained above, the interaction between coded pulse and the acoustic wave for SBS generation becomes weak in order of the code sequence. The analytical calculation of SNIR based on Eq. (6.13) is also included in Fig. 6.7. We can clearly see that the simulation results at the four fiber sections agree well with the analytical calculation result. It should be noted that the straight line in Fig. 6.7 represents the SNIR that is expected for the OTDRs based on the

Rayleigh scattering where no acoustic wave is involved. Therefore, the deviation of the data for the four sections from straight line represents the effect of the acoustic wave decay.

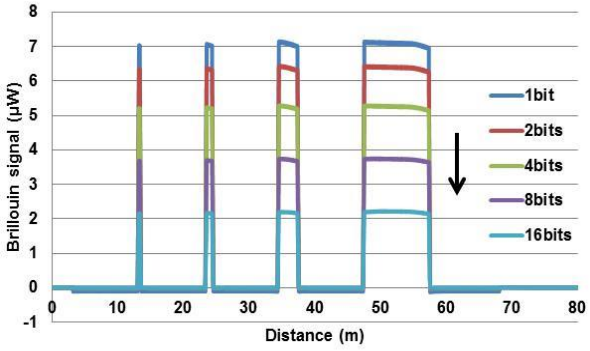

Fig. 6.6. Calculated Brillouin signals by employing 2ns of pulse width of Walsh codes.

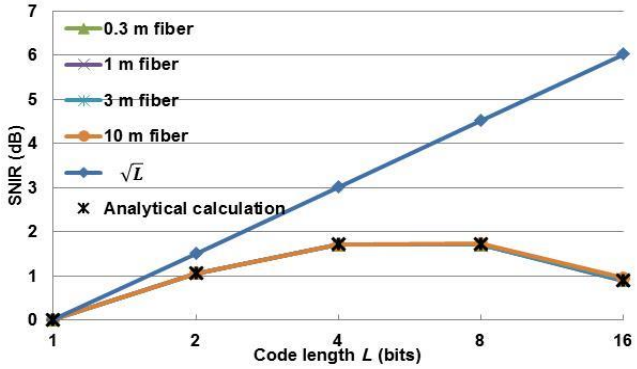

Fig. 6.7. Calculated optical signal-to-noise improvement ratio (SNIR).

B. Pump Light Coding with Walsh Codes and Golay Codes for T_2=1ns [3]

In this simulation, the duration T_2 was set to 1ns for both Walsh and Golay codes, which corresponds to 10cm of spatial resolution. The code lengths were set to 1, 2, 4, 8, 16 and 32 bits. The calculated Brillouin signals for all code lengths employing Walsh codes are shown in Fig. 6.8. Similar to the results shown in Fig. 6.6, we can see that the rising and falling edges at all test sections show sharp transitions. Henceforth, the transient regions where the Brillouin signal rises and falls are referred to as rising and falling edges, respectively.

However, in the case of Golay codes, as can be observed in Fig. 6.9, the appearance of side-lobes has caused the increase in the rising and falling edge lengths especially when code lengths of 16 and 32 bits were used. This is because strong Brillouin interaction was obtained only for the duration of code sequence less than τ_a. For code sequence beyond τ_a, the Brillouin interaction became weak and this consequently distorted the Brillouin signal after the correlation. Furthermore, in the case of 32-bit Golay codes, one can clearly observe the appearance of overshoots and undershoots around the splice points between the test and reference fibers, causing the signal distortions. The distortions were due to crosstalk noise that occurred through the process of calculating correlations. Negative crosstalk induces undershoots, while positive crosstalk produces overshoots of the Brillouin signals. These distortions give rise to misreading of measured Brillouin signals.

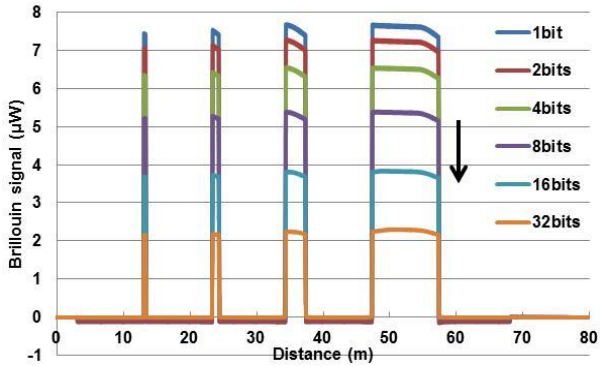

Fig. 6.8. Calculated Brillouin signals in the case of Walsh codes.

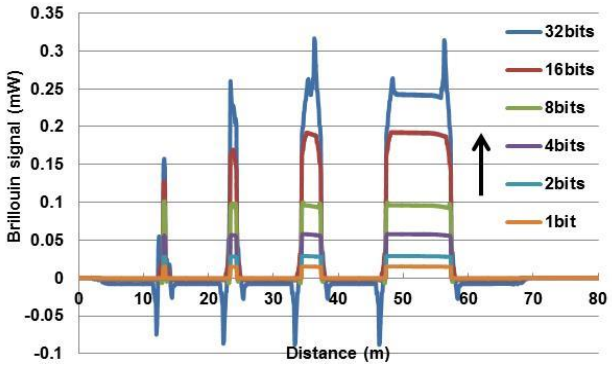

Fig. 6.9. Calculated Brillouin signals in the case of Golay codes.

On the other hand, in the case of Walsh codes, the encoding of the pump light and the decoding of the Brillouin signals via Hadamard transform produced no side-lobes, as can be seen in Fig. 6.8. It is known that for OTDR employing simplex codes, the variation in the launched pulse amplitude cause no side-lobes of the decoded signal [5]. We have noticed that the variation in the response to the code bit pulse does not generate side-lobes either, and that this is true for Walsh codes as well as for simplex codes. Therefore, compared to auto-correlation calculations for Golay codes, recovering the Brillouin signals using the Hadamard transform is robust against the variation in the received signal. This is especially true for coded continuous-PSP-BOTDA since its Brillouin signal decreases with the decrease in the acoustic wave amplitude and the decrease rate is the same among the *L*-responses to the *L*-sequences of the coded pump light.

Next, we focused on the rising edges of the Brillouin signals illustrated in Figs. 6.8 and 6.9; the rising time was evaluated by the time required for the Brillouin signal at the transition region to rise from 10% to 90% of the final value; then the rising time was transformed into a distance across the fiber, that we call the rising edge length. The rising edge lengths evaluated at 1m test section for both Walsh and Golay codes are shown in Fig. 6.10. In Fig. 6.10, for both codes, the rising edge length is around 8cm for code lengths up to 8 bits. Take note that this value is smaller than the theoretical spatial resolution (10cm), because the evaluation covers about 80% of the total rise time at the transition region. For Golay codes of 16 and 32 bits, as predicted, the rising edge lengths increase up to 50cm and 130cm, respectively. Therefore, from this analysis, we have confirmed that compared to Golay codes, coding the pump light with Walsh codes for Brillouin signal measurement offers more accurate signal recovery.

More analysis was performed to compare the optical SNIRs between the two types of codes. Figure 6.11 shows how the optical SNIR calculated at 0.3m test section changes with the code length. One can clearly observe that for both codes, the SNIR increases with code length up to 8 bits and then decreases for longer codes. The peak SNIR obtained for Walsh codes was 3dB while for Golay codes 3.6dB at *L*=8bits. This code length of 8 bits corresponds to the code sequence duration of 8ns, which is around τ_a=9ns. This result is consistent with that of Fig. 6.7 for Walsh codes of 2ns bit pulse where maximum SNIR is obtained at *L*=4bits. Therefore, the total code duration must be set around or less than τ_a to obtain the highest SNIR in either code system.

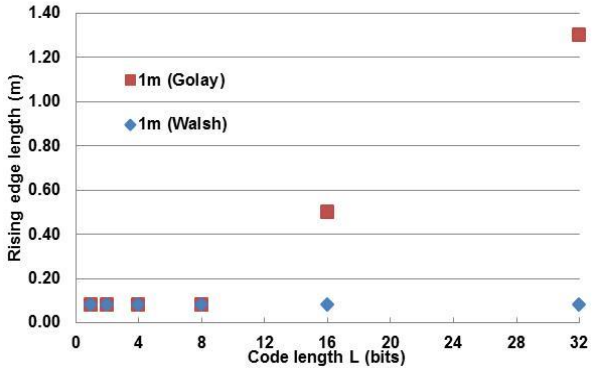

Fig. 6.10. Calculated rising edge length at the transition region between the reference fiber and the 1m test section.

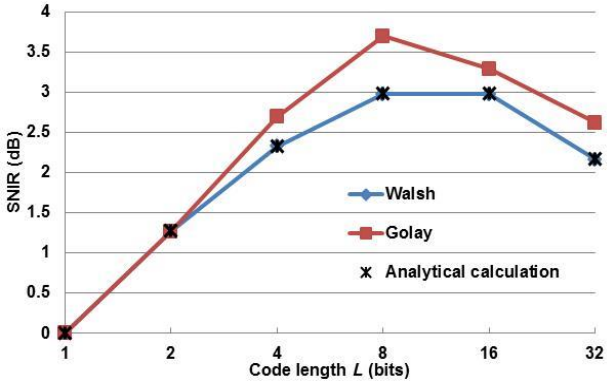

Fig. 6.11. Calculated optical SNIR at 0.3m test section for both Walsh and Golay codes.

Figure 6.11 also shows the SNIR obtained from analytical expression of Eq. (6.13) for the case of Walsh coding. We can easily show that Eq. (6.13) holds also for the case of PSP-BOTDA coded with Golay code if we assume no crosstalk may be brought about by correlation calculations of Golay code. Then, numerically simulated SNIRs for

Walsh and Golay codes should be identical to the analytical one. However, Fig. 6.11 shows that the numerically obtained SNIRs for Golay coding are slightly larger than the analytical ones. In addition, in other simulations for 1m, 3m and 10m sections, which were reported in [4], revealed that this discrepancy for Golay coding increases with increase in the section length. In contrast, the numerically obtained SNIRs for Walsh coding agree well with the analytical ones, as shown in Fig. 6.11. This discrepancy and agreement indicate that the crosstalk occurs for Golay coding, but not for Walsh coding, respectively. Therefore, Fig. 6.11 does not necessarily show the superiority of the Golay codes over the Walsh codes in terms of the SNIR. Rather, Fig. 6.11 indicates that compared to Golay codes, the employment of Walsh codes in coded continuous-PSP-BOTDA offer more reasonable SNIR results without crosstalk.

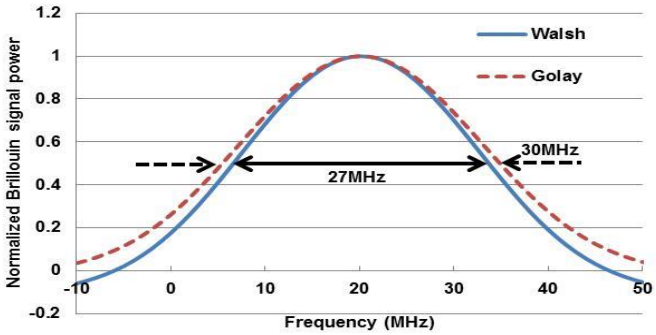

Fig. 6.12. Brillouin gain spectra (BGS) simulated at a distance of 50m (10m test section) for both 8-bit Walsh and Golay codes cases.

We then performed another simulation for the case of small BFS difference between the test and reference fibers. In this simulation, we assumed that the BFS of the test fiber was 20MHz larger than that of the reference fiber. The code length was set to 8 bits for both Walsh and Golay codes. The Brillouin gain spectra (BGS) simulated at a distance of 50m (10m test section) for both codes are depicted in Fig. 6.12. The Brillouin signal power was normalized for the purpose of comparing BGS obtained with two codes. One can see that there is little distortion in the spectrum shape for both Walsh and Golay codes. In addition, for Walsh codes case, the spectrum width was 27MHz, while for Golay codes case 30MHz. It is interesting to observe that both spectrum widths are narrower than the steady-state gain spectrum of 35MHz, indicating that the calculated BGSs for coded PSP-BOTDA are consistent with the analytical ones described in Section 6.3.3. It is also confirmed that the BGS peak was at frequency offset of 20MHz for both Walsh and Golay codes, indicating that the coded PSP-BOTDA proposed accurately measure the local small change in the BFS.

6.5 Experiments

In this section we discuss the experimental analysis of coded continuous-PSP-BOTDA system employing Walsh codes. We also show the experimental results obtained by employing Golay complementary sequences for comparison. We set the parameters of the experiments to be the same with the simulations.

6.5.1 Experimental Setup

The sensor configuration of coded continuous-PSP-BOTDA is depicted in Fig. 6.13. A laser diode of wavelength 1550nm and power of 6mW (8dBm) was used as a source and its output was injected to a 3dB fiber coupler. One arm propagates the light for generating the pump and the other one for the probe. To create an electrical signal that was composed of the long pulse (1st pulse) and the Walsh/Golay coded pulses (2nd pulses), an arbitrary waveform generator (AWG) was used. The rise time of the coded pulses was 0.5ns. This electrical signal was then amplified by an electrical amplifier and after that fed to a Mach-Zehnder modulator (MZM). The MZM was used to modulate the light with the

coded electrical signal. The DC bias voltage supplied to the MZM was carefully adjusted to a null point. Phase modulation scheme is introduced to modulate the coded 2nd pulses. In particular, as shown in Fig. 6.13, the MZM phase-modulated the light with +1 and -1 coded electrical signals into 0-shift and π-shift optical pulses, respectively. A polarization scrambler (PS) was used to continuously change the state of polarization of the input pump light in order to reduce the polarization induced noise. An EDFA (EDFA1) was placed after the MZM to amplify the pump power to 60mW for both 1st and 2nd pulses. This pump was then injected into an end of the test fiber. Soto et al. have previously reported the distortion in the amplified coded pump pulse due to the gain depletion of the EDFA when it is placed after the MZM [9]. To avoid such distortion, they have proposed the modification in the measurement setup by placing the EDFA before the MZM. However, in our experiment, the total pulse pump duration including the pre-pump was as short as 62ns at the most; then we observed little distortion in the amplified pump pulse signal even when the EDFA was situated after the MZM.

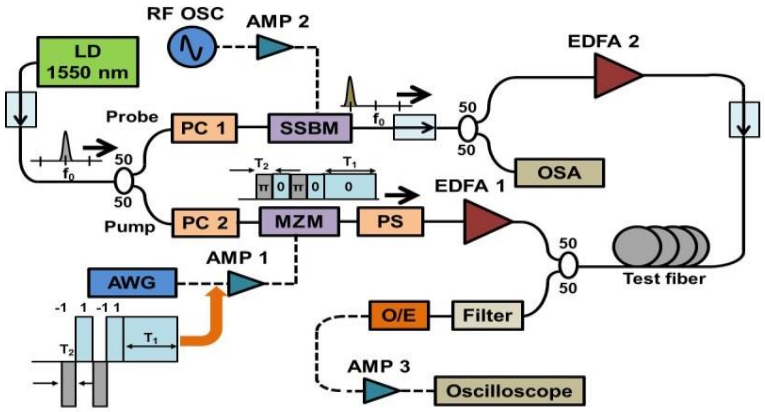

Fig. 6.13. Experimental setup of coded continuous-PSP-BOTDA.

To produce the Stokes frequency-shifted probe light, a single side-band modulator (SSBM) was used. Previous report has shown that the use of dual side-band modulator (DSBM) to simultaneously generate both Stokes and Anti-Stokes frequencies-shifted probe light has favourably improved the pump depletion and non-local effects in the measurement [10]. However, this technique requires a special optical band-pass filter of less than 10 GHz bandwidth and careful tuning of its center frequency so that one frequency component of the probe should be selected and directed to a detector. In our proof-of principle experiment, since the fiber tested was short and the pump power was 60 mw at most, the pump depletion could be ignored. So, in this experiment, we preferred to use SSBM for ease of measurement. The amount of the frequency shift of the probe light was controlled by the frequency of electrical signal supplied from an RF oscillator (RF OSC). The generated probe light was then split by a 3dB fiber coupler; one arm was connected to an optical spectrum analyser (OSA) for monitoring purpose and the other one was fed to an EDFA (EDFA2) for optical amplification. The probe power was amplified up to 2mW before being injected into the other end of the test fiber. The test fiber was made of dispersion shift fibers (DSF) with the length of 0.3m, 1m, 3m and 10m each. Standard single mode fiber (SMF) cables of 10m in length were spliced between the DSF cables as the references. The difference in BFS between the DSF and SMF cables is about 300MHz, which is equivalent to about 0.6% strain.

We placed an optical-bandpass filter (bandwidth~100GHz), being transparent to the Brillouin amplified signal, just before an O/E converter, and reduced the spontaneous noise emitted from the EDFA2. Then, the Brillouin amplified signal was converted into an electrical signal by an O/E converter, amplified by an electrical amplifier (AMP 3) before

being digitized and averaged by an oscilloscope. Finally, the recorded data was decoded by either Hadamard transform or auto-correlation calculation method, depending on the type of code used in the measurements.

6.5.2 Results and Discussions

A. Measurement with Walsh Codes for T_2=2ns

The measured Brillouin signals in the case of 2ns of pulse width are shown in Fig. 6.14. The results show the amplified Brillouin signals for 1, 2, 4 8 bits of code lengths [2]. As observed in Fig. 6.14, the Brillouin signal decreases as the code length increases. As explained before, this is due to the fact that the acoustic wave excited by the 1st pulse for the amplifying the Brillouin signal decays with time. However, it is interesting to observe that as the signal decreases with code length, the random noise decreases more rapidly. Furthermore, as expected, little deterioration at the transitions of the Brillouin signals in the test sections was seen even when the total duration of the coded pulses is longer than τ_a=9ns. By evaluating the 80% of the rising edge length at 3m test section, rising edge length of 16cm was obtained for all code lengths. Thus, we have successfully demonstrated 20cm spatial resolution measurement system, which corresponded to 2ns of pulse width.

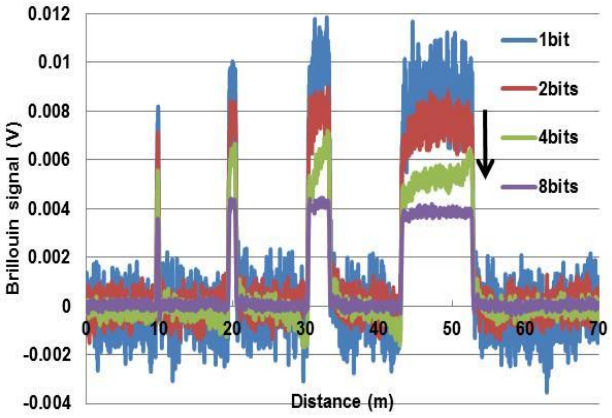

Fig. 6.14. Measured Brillouin signals in the case of Walsh codes for 2ns of pulse width.

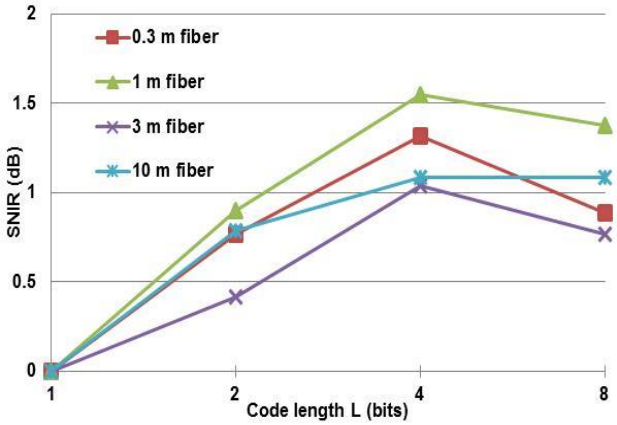

Fig. 6.15. Measured optical SNIR versus code length.

We then analyzed the optical signal-to-noise improvement ratio (SNIR) of the measured Brillouin signals at all test sections, being plotted in Fig. 6.15. The SNIRs were calculated by dividing the SNR measured for code length *L* by the SNR for 1-bit code length, and further by dividing it with $\sqrt{L}$. The second division was made so that the SNIRs were compared under the condition of the same measurement time. The absolute SNRs measured at 0.3m, 1m, 3m and 10m test section in the case of 1-bit Walsh code were 8.6dB, 10.2dB, 10.8dB and 10.1dB, respectively. Overall, the optical SNIR for each test section reached its peak when the code length is equal to 4 bits (8ns of total pulse duration). The peak SNIR measured at 1m test section was about 1.5dB, which is consistent with the simulation. As explained in the simulation section, the interaction between the coded pulses and the excited acoustic wave for SBS generation gets weak in order of the code sequence. Thus we can see that for longer code length, the improvement rate has declined.

To justify the above discussion, we examined the normalized amplification rate of the Brillouin signal versus time. The representative result of amplification rate measured at the 1m test section is shown in Fig. 6.16. Figure 6.16 plotted the peak intensity of the Brillouin signals $\hat{\phi}_1(t) \sim \hat{\phi}_8(t)$, corresponding to eight code sequences, which were Hadamard-transformed but not time-shifted yet. The theoretical acoustic decay rate based on Eq. (6.13) was also calculated, being plotted in the same figure. We can see that the experimental results of the Brillouin signal decay with

time are well in line with the theoretical acoustic wave decay with the time constant of τ_a =9ns. Furthermore, when the code duration got longer than time constant τ_a, the amplification rate decreased below a half of its maximum, which consequently led to the decrease of the SNIR for 8 bits code as illustrated in Fig. 6.15.

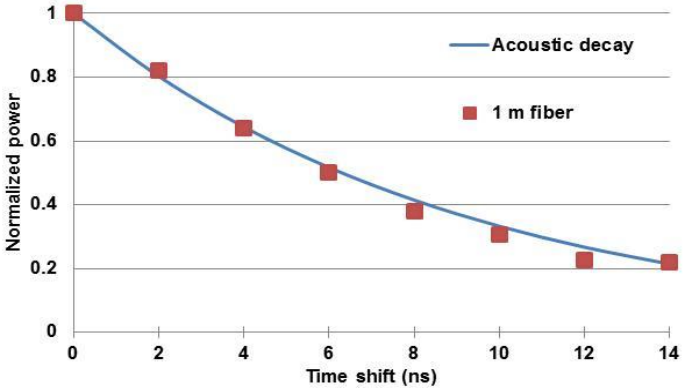

Fig. 6.16. Decrease in Brillouin signal versus time.

B. *Measurement with Walsh Codes and Golay Codes for T_2=1ns [3]*

We continued the experiments by employing Walsh codes and Golay codes for 1ns pulse duration. The code lengths for Walsh codes were set to 1, 2, 4, 8 and 16 bits while for Golay codes 1, 2, 4, 8, 16 and 32 bits [3].

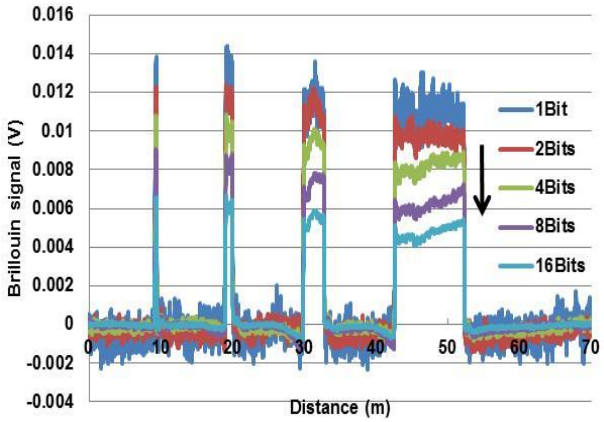

Fig. 6.17. Measured Brillouin signals by employing Walsh codes.

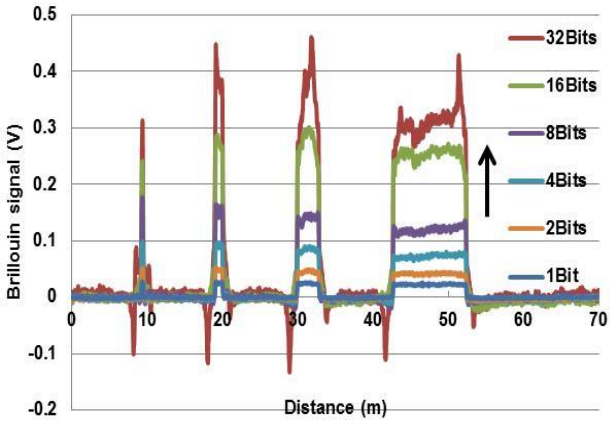

Fig. 6.18. Measured Brillouin signals by employing Golay codes.

Figures 6.17 and 6.18 illustrate the Brillouin signal measured when the pump and probe frequencies difference was tuned to the BFS of the DSFs, that was 10.555GHz. As observed in Fig. 6.17, for all Walsh code lengths, there is only small signal distortion at the rising and falling edges. On the contrary, in Fig. 6.18, the length of the rising and falling edges has increased significantly when code lengths of 16 and 32 bits were used. In addition, as discussed previously, the negative and positive crosstalk noises caused undershoots and overshoots around the splice points of the test and reference fibers.

In order to evaluate the spatial resolution, we calculated the rising edge lengths at 1m test section for both codes by using the method described in Section 6.4. The results are shown in Fig. 6.19. In the case of Walsh codes, the rising edge length ranges from 8cm to 8.5cm for code lengths of 1, 2, 4, 8 and 16bits. This slight discrepancy might be due to the limited rise time (0.5ns) of the coded pulses generated by the AWG. In general, we have successfully obtained 10cm

of spatial resolution by using 1ns of pulse duration for Walsh codes. In the case of Golay codes, the rising edge length varied from 8cm to 10cm for code lengths up to 8 bits. However, when the code lengths of 16 and 32 bits were used, the rising edge lengths have increased significantly up to 50cm and 122cm, respectively. Overall, we have confirmed that the experimental results for both Golay and Walsh codes are consistent with the simulations.

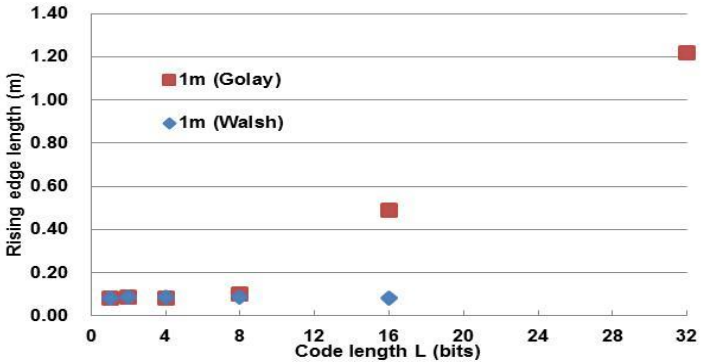

Fig. 6.19. Rising edge length of 1m test section for both Walsh and Golay codes.

Figures 6.20 and 6.21 show how the optical SNIRs at all test sections changed with the code length for Walsh codes and Golay codes, respectively. The SNIRs were evaluated based on the signals displayed in Figs. 6.17 and 6.18, and the divisions with $\sqrt{L}$ for Walsh coding and $\sqrt{2}$ for Golay coding were also performed so that the comparison of SNR was made under the condition of the same measurement time, as described in Sub-section A of Section 6.5.2. The factor 2 for the Golay coding came from the fact that the Golay coding uses a pair of sequences to complement correlations. The absolute SNRs obtained from 1-bit Walsh code measurement at all test sections were between 13dB and 13.3dB, while the SNRs from 1-bit Golay code measurement were between 12.9dB and 13.7dB. Obviously, these results agreed well each other. We can see in Fig. 6.20 that SNIR curves for Walsh codes at all fiber sections were almost the same and in good agreement with the calculations shown in Fig. 6.11; the SNIR reached its maximum when the code length equaled to 8 bits or 16 bits, whose total duration almost corresponded to τ_a =9ns or 2 τ_a =18ns, as predicted.

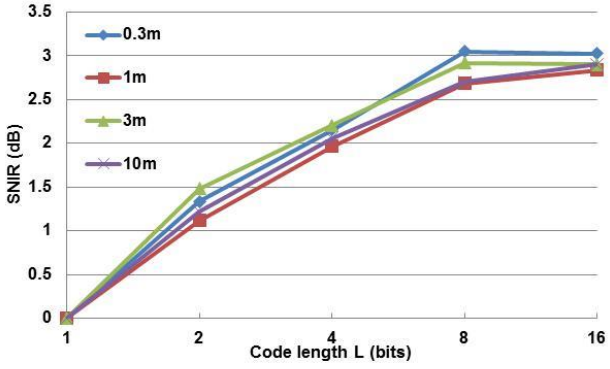

Fig. 6.20. Measured optical SNIR for Walsh codes.

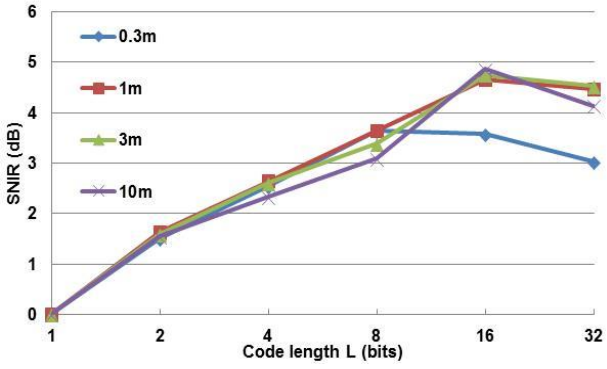

Fig. 6.21. Measured optical SNIR for Golay codes.

We also can see in Fig. 6.21 that the SNIR curve for Golay codes at 0.3m section was similar with that for Walsh codes and agreed well with the calculation. However, the SNIR for Golay codes at longer sections were slightly higher than that at the 0.3m section especially when L=16 and 32 bits. This is because, as explained before, crosstalk spuriously increased SNIR. The crosstalk also increased the rising edge length as shown in Fig. 6.19, and degraded the spatial resolution. Therefore, the spurious increase in SNIR for Golay codes with L=16 and 32 bits was meaningless; so

we found that the code length of the Golay code should be less than 8 bits; namely the total code duration should be around or less than τ_a=9ns. Therefore, the maximum SNIR of about 3dB can be achieved by using 8-bit Golay code as well as Walsh code. However, we note here that Walsh code has more tolerance of setting the total code pulse duration T_{total} than Golay code to achieve the best SNIR and to maintain the high spatial resolution simultaneously; the duration T_{total} for Walsh coding can be set to from τ_a to $2\tau_a$; however, the duration T_{total} for Golay coding should be in the vicinity of τ_a.

C. Brillouin Gain Spectrum and Brillouin Frequency Shift Measurement [3]

In this experiment, we compared the BGS obtained with 8-bit Walsh code and 1-bit Walsh code. The latter corresponds to the BGS measured with the conventional PSP-BOTDA system without the coding. In the experiment, the signals measured with the conventional PSP-BOTDA without coding were averaged 8 times as many as the signals measured with 8-bit Walsh code, so that the measurement time was the same, excluding the time for signal decoding overhead. The results are depicted in Figs. 6.22 and 6.23, respectively. Lorentzian fitting curves were also included in both Figs. 6.22 and 6.23, showing the BGSs measured at a distance of 32.3m (3m test section). In the case of Walsh code (Figs. 6.22), the measured Brillouin gain width was approximately 28MHz, which agreed well with the simulation result of Fig. 6.12. For the 1-bit Walsh code shown in Figs. 6.23, namely, for the PSP-BOTDA without coding, we observed that the Brillouin gain bandwidth was slightly broader than that measured with the 8-bit code. Note that both bandwidths of 28MHz and 31MHz were narrower than the steady state one which was evaluated at 35MHz by using the measured acoustic wave time constant of 9ns. These results were consistent with the analytical results shown in Figs. 6.3 and 6.4.

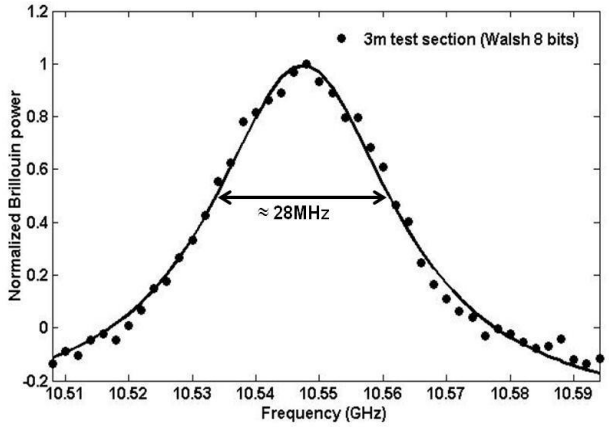

Fig. 6.22. Measured and Lorentzian fitted Brillouin gain spectrum (BGS) at a distance of 32.3m (3m test section), when using 8-bit Walsh code.

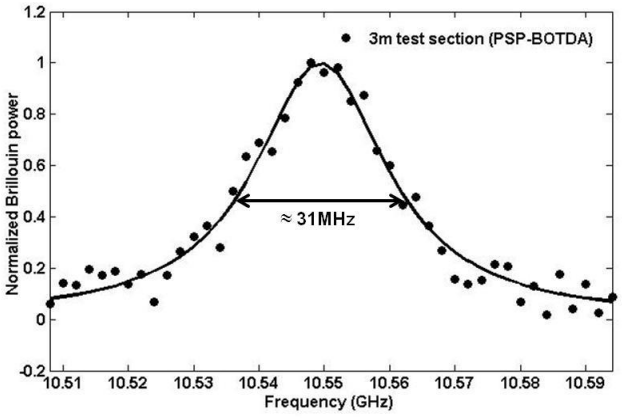

Fig. 6.23. Measured and Lorentzian fitted Brillouin gain spectrum (BGS) at a distance of 32.3m (3m test section), when using the conventional PSP-BOTDA.

Figure 6.24 shows the BFS distributions measured for 1-bit and 8-bit Walsh cases. The measurement with the 1-bit code is identical to that with the conventional PSP-BOTDA. Figure 6.24 revealed that both results agreed well with the BFS-distribution of the spliced SMFs and DSFs. The accuracy of the BFS for Walsh code is better than that for the conventional PSP-BOTDA. The BFS accuracy (standard deviation) measured at the 3m test section for conventional PSP-BOTDA was approximately 1.13MHz, which corresponds to 1.1°C of temperature resolution or $2.2\text{x}10^{-5}$ strain resolution. For 8-bit Walsh code case, we obtained an excellent frequency accuracy of about 0.62MHz, which translates into 0.6°C of temperature resolution or $1.2\text{x}10^{-5}$ strain resolution. Therefore, it is confirmed that the employment of

Walsh code has contributed to the improvement of the BFS measurement accuracy. Applying the same method of analyzing the spatial resolution explained in Section 6.4.2, as shown in the inset of Fig. 6.24, we have obtained the transient length of 8cm corresponding to 80% of the 10cm-spatial resolution at the transition region of the 3m test section, in good agreement with the theoretical prediction.

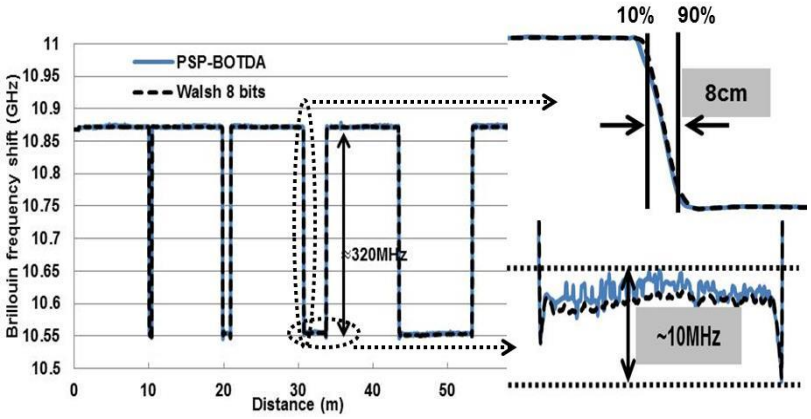

Fig. 6.24. Comparison in BFS distribution between measurement with 8-bit Walsh code and the conventional PSP-BOTDA.

D. Further Discussion on the Comparison Between Walsh Codes and Golay Codes [3]

The simulation and experimental results have indicated that the acoustic wave time constant (9ns for 35MHz Brillouin gain bandwidth) has limited the maximum total duration of the coded pulses that can be efficiently used for both Golay and Walsh codes. In terms of the SNIR evaluation, the maximum SNIR was obtained for both Walsh and Golay codes when their code duration was set to about τ_a. However, the use of Golay codes of duration longer than the acoustic wave time constant τ_a has caused poor spatial resolution, while for Walsh code, the spatial resolution remains as good as the theoretical one even when the total duration of the coded pulses is two times as long as the time constant τ_a.

It has already been explained in Sections 4.2 and 4.3 that the process of decoding the Golay codes via auto-correlations and Walsh codes via Hadamard transform produces no side-lobes at the decoded signal. In the case of Golay codes, however, it is important to note that these side-lobes do not appear after the correlation only if the amplitude is uniform for all coded pulses. In the coded continuous-PSP-BOTDA viewpoint, this means a uniform level of received Brillouin signal power is necessary to produce decoded Brillouin signal with good spatial resolution, which is however cannot be realized due to the exponential decay of acoustic wave amplitude with time. As a result, for Golay codes, the auto-correlations that involve inner product of Brillouin signals with the codewords in time direction cause distortion in the decoded signal. The distortion causes detrimental effects on the spatial resolution when the total coded pulse duration exceeds τ_a.

On the other hand, for Walsh codes, decoded signal with no side-lobes can still be obtained under the same condition. The reason for this robustness against the uneven amplitudes lies in Hadamard transform process. In the Hadamard transform, the matrix calculation involves the inner product of every row vector of inverse Hadamard matrix with the synchronized Brillouin signals which are represented by the matrix column vector. The power of the synchronized Brillouin signal measured by each Walsh code pattern is same, even when the Brillouin signals decay

with time due to the acoustic wave damping. Therefore, in contrast to Golay codes, despite the decrease in the received Brillouin signals, true signal without distortion can still be decoded with the use of Walsh codes.

In terms of SNIR, one might think that both Golay and Walsh codes approximately offer the same measurement performance, as long as the total coded pulse duration is set to τ_a in order to obtain the achievable highest SNIR. However, when we apply the coded BOTDA practically, we should take into account that fibers of a different kind or produced differently vary in the Brillouin gain bandwidth. For examples, optical fibers with different GeO_2-core concentration have the Brillouin gain bandwidth ranging from 31MHz to 55MHz at the pump wavelength of 1.32μm [11]. Therefore, if the real Brillouin gain bandwidth of the fiber used happens to be wider than the value calculated from the typical acoustic wave time constant τ_a , the total duration of the Golay coded pulses must be shorten, resulting in decrease in SNIR. Otherwise, the spatial resolution would be degraded. On the other hand, for Walsh code case, the spatial resolution will not be degraded even if the duration has exceeded the acoustic wave constant τ_a. Furthermore, the SNIR for Walsh code would be kept almost optimal even if the code duration becomes two times as long as τ_a. Therefore, we conclude that Walsh code is better solution to build a practical coded PSP-BOTDA system.

6.6 Conclusions of Chapter

Modulating the pump light of the conventional BOTDA with non-return-to-zero (NRZ) formatted code system to realize sub-meter spatial resolution measurement has induced distortion in the Brillouin signal due to the variety of Brillouin gain caused by the preceding coded pulses, when coded pulse duration is around or less than the time constant of the acoustic wave amplitude τ_a. However, we have shown that this problem can be overcome by introducing NRZ formatted coding system which includes Walsh codes and bipolar Golay codes in coded continuous-phase shift pulse-BOTDA (PSP-BOTDA). This is because in contrast to the conventional BOTDA that is based on the intensity modulation, PSP-BOTDA can remove the Brillouin gain variation due to the sequence of the coded pulses and utilizes the only Brillouin gain that is induced by pre-pump pulse.

Holistic analysis on the employment of Walsh codes in coding the pump light of coded continuous-PSP-BOTDA for attaining sub-meter spatial resolution and improving the signal-to-noise ratio has been presented. By comparing the processed Brillouin signals with that obtained by using Golay codes, we have found that the use of Walsh codes decodes the Brillouin signal without degrading the spatial resolution even when the total code pulse duration becomes two times as long as τ_a at least. We have also found that for the Golay coded PSP-BOTDA, in contrast, the use of the coded pulses whose total duration exceeds τ_a increasingly degrades the spatial resolution. This advantage of the Walsh code over the Golay code comes from the fact that the decoding the Brillouin signals via Hadamard transform is robust not only against variations in launched coded-pulse amplitudes but also against those in response signals. We have attained 20cm and 10cm of spatial resolution by using NRZ formatted code system having pulse durations of 2ns and 1ns, respectively.

In terms of the BGS, we have found from the simulation and experimental results that the BGS measured by using Walsh coded PSP-BOTDA has become narrower than the steady-state gain spectrum. This narrowing is favourable to measure the BFS accurately. Furthermore, it was also found that the use of Walsh codes has contributed to the achievement of higher BFS measurement accuracy than that of using conventional PSP-BOTDA technique.

We have also found that the experimental SNIR dependence on the code length for Walsh codes agrees well with that calculated by analytical and numerical methods. For both Walsh and Golay codes, the maximum SNIR can be achieved only for total code duration of around the time constant of the acoustic wave amplitude τ_a; so we have verified

by experiments that 8-bit Walsh and Golay codes having 1ns pulse each enable the optical signal-to-noise improvement ratio (SNIR) of about 3dB. Even though the maximum SNIR for Golay codes measured is slightly higher than that for Walsh codes, this difference is merely caused by the crosstalk to the intrinsic signal after the auto-correlation calculations for decoding the Golay codes. Furthermore, this crosstalk contribution varies for different fiber length. Therefore, from these findings we have confirmed that the employment of Walsh codes in the coded continuous-PSP-BOTDA offers a more intrinsic SNIR compared to that of Golay codes.

We have also confirmed that even when the total coded pulse duration becomes two times as long as τ_a at least, the spatial resolution of the Walsh coded PSP-BOTDA maintains high spatial resolution and almost the same SNIR with the maximum SNIR that is obtained when the total coded pulse duration is around τ_a .

Based on the findings described above, we conclude that the Walsh coded PSP-BOTDA offers better solution than the Golay coded PSP-BOTDA. This is because the former maintains high spatial resolution even if the acoustic wave time constant τ_a of fibers used, which is inversely proportional to the Brillouin gain bandwidth, varies and happens to be less than the total coded pulse duration designed. In contrast, for the latter, the spatial resolution is significantly degraded.

References

[1] Uchiyama, T. Horiguchi, H. Ando, Y. Okumoto, T. Sasaki and Y. Sawai, "Signal to noise improvement ratio for coded PSP-BOTDA", Technical report of IEICE. OFT 109 (377) (in Japanese), pp. 33-38, Jan. 2010.

[2] **M. S. D. B. Zan**, T. Tsumuraya and T. Horiguchi, "The use of Walsh functions in modulating pump light of high-spatial resolution BOTDA with NRZ pulses" 22nd International. Conf. on Optical Fiber Sensors (OFS-22) 2012, pp. 84219J-1 - 84219J-4, Oct. 2012.

[3] **M. S. D. B. Zan**, T. Tsumuraya and T. Horiguchi, "The use of Walsh code in modulating the pump light of high spatial resolution phase-shift-pulse Brillouin optical time domain analysis with non-return-to-zero pulses", J. Meas. Sci. Technol., vol. 24, no. 9 (094025), pp. 1-13, Jul. 2013.

[4] **M. S. D. B. Zan** and T. Horiguchi, "A dual Golay complementary pair of sequences for improving the performance of phase-shift pulse BOTDA fiber sensor" J. Lightw. Technol., vol. 30, no. 21, pp. 3338-3356, Nov. 2012.

[5] M. D. Jones, "Using simplex codes to improve OTDR sensitivity", IEEE Photon. Tech. Lett. Vol. 15, no. 7, pp. 822-824, Jul. 1993.

[6] N. J. A. Sloane, T. Fine, P. G. Phillips and M. Harwit, "Codes for multiplex spectrometry", App. Opt, vol. 8, no. 10, pp. 2103-2106, Oct. 1969.

[7] D. Lee, H. Yoon, P. Kim, J. Park and N. Park, "Optimization of SNR improvement in the noncoherent OTDR based on simplex codes", J. Lightw. Technol. vol. 24, no. 1, pp. 322-328, Jan. 2006.

[8] V. Lecoeuche, D. J. Webb, C. N. Pannell and D. A. Jackson, "Transient response in high-resolution Brillouin-based distributed sensing using probe pulses shorter than the acoustic relaxation time", Opt. Lett., vol. 25, no. 3, pp. 156-158, Feb. 2000.

[9] M. A. Soto, G. Bolognini, F. Di Pasquale and L. Thevenaz, "Long-range Brillouin optical time-domain analysis sensor employing pulse coding techniques", J. Meas. Sci. Technol. vol. 21. No. 9 (094024), pp. 1-7, Jul. 2010.

[10] A. Minardo, R. Bernini and L. Zeni, "A simple technique for reducing pump depletion in long-range distributed Brillouin fiber sensors ", IEEE Sens. J., vol. 9, no. 6, pp. 633-634, June 2009.

[11] M. Nikles, L. Thevenaz and P. A. Robert, "Brillouin gain spectrum characterization in single-mode optical fibers", J. Lightw. Technol., vol. 15, no. 10, pp. 1842-1851, Oct. 1997.

Chapter 7: The Employment of Dual Golay Codes in High Spatial Resolution PSP-BOTDA for Improving the Signal-to-Noise Ratio (SNR)

7.1 Introduction to Chapter

As discussed respectively in the previous Chapters 5 and 6, it was found that coded discrete-PSP-BOTDA employing Golay coded return-to-zero (RZ) pulses and coded continuous-PSP-BOTDA employing Golay coded or Walsh coded non-return-to-zero (NRZ) pulses contribute to the achievement of higher optical SNR compared to that of the conventional PSP-BOTDA with no pulse coding [1-6] with good correlation results. The simulation and experimental results reported have verified the merits of employing coding system in the PSP-BOTDA to measure strain with high optical SNR and high spatial resolution. Actually, it is possible to obtain even higher optical SNR with the use of combined codes in the coded PSP-BOTDA technique.

To address the matter above, in this chapter, the author proposes a new technique of combining two codes in modulating a pump light of PSP-BOTDA. In particular, the author introduces the simultaneous use of Golay coded RZ pulses and Golay coded NRZ pulses in a single pump light of PSP-BOTDA called dual Golay codes PSP-BOTDA. From the analysis, it was found that the combination of two Golay complementary pairs (GCPs) in a single pump pulse of coded PSP-BOTDA indeed offers higher optical SNR than that of the coded continuous- and coded discrete-PSP-BOTDAs [7]. Moreover, high spatial resolution measurement was also successfully demonstrated. In this chapter, the simulations on the dual Golay codes PSP-BOTDA were performed and the results are described. Experiments were also conducted and the results are discussed and compared with that obtained from the simulations.

7.2 Pump Light Configurations

As explained in Chapter 4, dual Golay codes are generated by combining two GCPs. The configuration of the pulse pump of the dual Golay codes PSP-BOTDA is based on the combination of the pump light of coded continuous-PSP-BOTDA and the pump light of coded discrete-PSP-BOTDA. The examples of the pump light for coded continuous-, coded discrete- and dual Golay codes PSP-BOTDAs are illustrated in Fig. 7.1(a), Fig. 7.1(b) and Fig. 7.1(c), respectively. The pump in Fig. 7.1(c) is configured by the following procedure; First, four coded pulses in Fig. 7.1(a) are multiplied with each code element of the 2^{nd} pulse each in Fig. 7.1(b). Therefore, the sign of bit-elements of the four pulses are inverted if the value of the bit-element shown in Fig. 7.1(b) is -1 while the four pulses are left as they are if the value of the bit-element in Fig. 7.1(b) is +1. Then the sixteen values of the bit-elements are obtained and depicted in Fig. 7.1(c). It should be noted that in this example the code length used for the dual Golay codes PSP-BOTDA is four times greater than that used for the previous coded PSP-BOTDAs.

T_1 is the width of the 1^{st} pulse, T_2 is the width of one element of the dual Golay code pulses, and T_i is the interval time between adjacent groups of pulses. The use of the pump based on the dual Golay codes in Fig. 7.1(c) makes a greater contribution to the increase in the optical SNR of the Brillouin signal than the previous pumps shown in Figs. 7.1(a) and 7.1(b). This is because a dual Golay code makes it possible to generate more coded pulses within the round trip time (RTT), and to increase the optical SNR with the number of the coded pulses.

The value of T_i is crucial for accurate and efficient measurements. It is set long enough so that no interference between separate groups of pulses occurs through SBS process. However, long T_i decreases the code length which is available within a given period of transmitting the pump. It has been shown in [1] and [2] that the choice of T_i = 30ns to 100ns makes a practical compromise between these two factors which affect the performance of the coded

discrete-PSP-BOTDA system. Similar results have been reported in the case of RZ coded pulses BOTDA with 1-m spatial resolution [8].

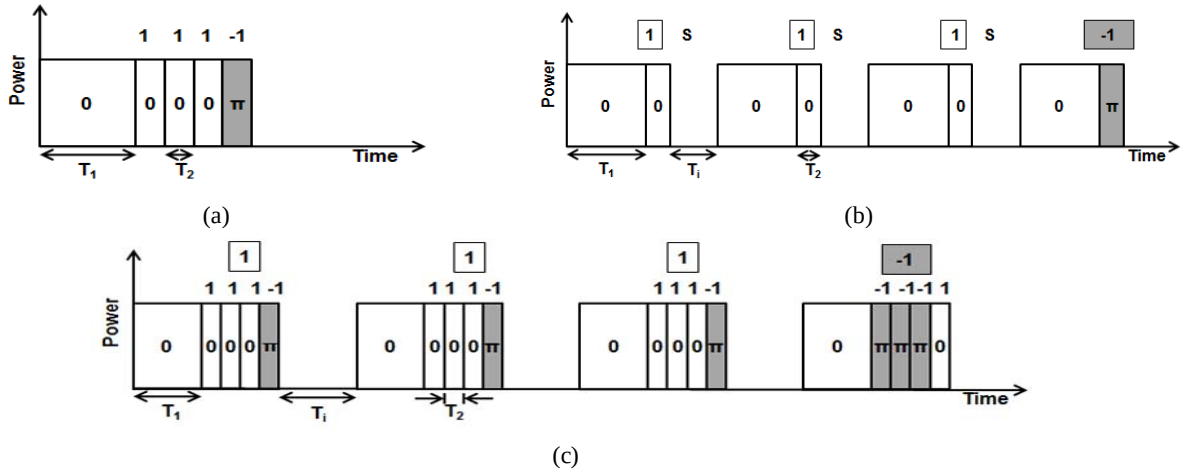

Fig. 7.1. Coded PSP-BOTDA pump configurations in the case of 4 bits (a) coded continuous-PSP-BOTDA (L_{cont}=4 bits), (b) coded discrete-PSP-BOTDA (L_{disc}=4bits) and (c) dual Golay codes PSP-BOTDA (L_{cont}=L_{disc}=4 bits).

7.3 Simulations

7.3.1 Simulation Setup

The SBS process in BOTDA involves the interaction among pulse pump, cw Stokes (probe) and acoustic wave. The configuration of the basic BOTDA system is depicted in Fig. 7.2. The pump with frequency ν_P is injected at the distance z = 0, moving to the +z direction across a test fiber, while a continuous Stokes or called probe with frequency ν_S is injected at the distance of z = L, moving to the direction of –z across the test fiber. The backward SBS wave is generated from the periodical fluctuation of the dielectric constant of the fiber material due to the pressure wave, i.e., acoustic wave excited by the beating between the pump and the probe. Complying with the energy conservation law and the phase matching condition, the probe is amplified when the frequency difference between the pump and the probe coincides with the BFS which is given by [9]

$$\nu_B = \frac{2n\upsilon}{\lambda_p} \tag{7.1}$$

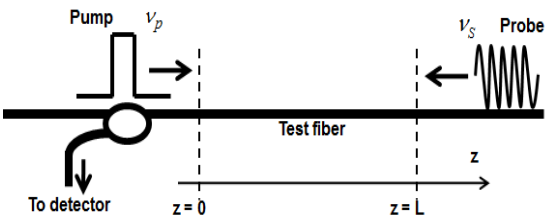

Fig. 7.2. Schematic of BOTDA

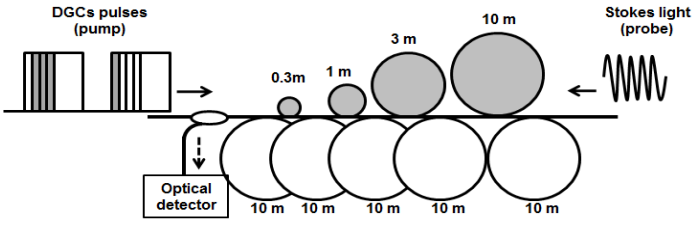

Fig. 7.3. Numerical model for dual Golay codes PSP-BOTDA.

Here n is the refractive index of the fiber, υ is the acoustic velocity and λ_p is the pump wavelength. The amplified probe propagates to the optical coupler and finally is detected at a detector.

The dual Golay codes PSP-BOTDA system resembles the basic BOTDA system except that the pump pulse used in the measurement process is phase coded with the dual Golay codes and the detected signals are processed with the codes. The configuration of the dual Golay codes PSP-BOTDA simulations is shown in Fig. 7.3 where the test fibers are

also shown. The lengths of the test fiber L_f used were 0.3 m, 1 m, 3 m and 10 m. The 10m fibers connected between the test fibers were used as the reference. The difference in the BFS δf between the test fiber and the reference fiber was set to 300 MHz, which simulates a change in 0.6% strain. The optical power of the 1st pulse P_{p1} was set at the same level with that of the 2nd pulses P_{p2}. The values of the parameters used in the simulations are listed in Table 7.1.

Take note that two conditions, Condition A and Condition B were considered in the simulations. Under Condition A, the code length of the continuous pulse codes was fixed at 4 bits and the code length of the discrete pulse codes was varied from 1 to 32 bits. In contrast, under Condition B, the length of the discrete pulse code was fixed at 4 bits and the code length of the continuous pulse codes was varied from 1 to 32 bits.

The physical interactions between the three waves in the fiber optic cable can be modeled as follows: [10]

$$\frac{\partial E_p}{\partial t} + \frac{\partial E_p}{\partial z} = -E_s E_a \tag{7.2a}$$

$$\frac{\partial E_S}{\partial t} - \frac{\partial E_S}{\partial z} = E_p E_a * \tag{7.2b}$$

$$\frac{\partial E_a}{\partial t} + [1 + i\Delta]E_a = E_p {E_S}^* \tag{7.2c}$$

where E_p, E_S and E_a are the normalized pump, Stokes and acoustic fields respectively. Δ is the normalized frequency detuning expressed by $\Delta = (\omega_P - \omega_S) - \omega_B$ where ω_P and ω_S are the frequencies of pump and Stokes wave, respectively, and ω_B is the Brillouin frequency shift.

Table 7.1. Parameters used for the simulations.

Parameter	Symbol	Condition A	Condition B
wavelength	λ	1.55 μm	
fiber refractive index	n	1.5	
strained fiber length	L_f	0.3 m, 1.0 m, 3.0 m, 10 m	
Brillouin frequency shift changes in strained fiber	δf	300 MHz	
1st pulse optical power (pump)	P_{p1}	33 mW	
2nd pulse optical power (pump)	P_{p2}	33 mW	
Stokes power (probe)	P_S	2 mW	
1st pulse width	T_1	30 ns	
2nd pulse width	T_2	1 ns	
interval time	T_i	100 ns	
code length (discrete part)	L_{disc}	1, 2, 4, 8, 16, 32 bits	4 bits (fixed)
code length (continuous part)	L_{cont}	4 bits (fixed)	1, 2, 4, 8, 16, 32 bits

7.3.2 Results and Discussions

A. Simulation Results for Condition A [7]

The Brillouin amplifications for each L_{disc} of Condition A are shown in Fig. 7.4, where the horizontal axis represents the distance and the vertical axis the Brillouin optical signal. It appears that the Brillouin optical power detected at the 0.3 m, 1 m, 3 m and 10 m strained fibers increases with the increment of the discrete pulse code length L_{disc}. At a glance, the rising and the falling edges for each strained length are clearly identified, and no degradation in spatial resolution

can be found for L_{disc}=1 to 32.

Further analysis was performed by investigating the signal power increment and the relative optical signal-to-noise ratio (SNR). These results are depicted in Figs. 7.5 and 7.6, respectively. The signal power increment was evaluated by the ratio of the signal power ΔPs to the power for L_{disc}=1, ΔP0. Take note that the value ΔP0=ΔPs(L_{disc}=1) in Fig. 7.5 corresponded to the sum of two sets of measurements with a 4-bit GCP having two sequences, while ΔPs(L_{disc}≠1) was calculated by one set of measurements with the dual Golay codes of L_{cont} =4 and L_{disc} (≠1) having four sequences; then the number of code sequences used to modulate the transmitting pump waves was the same among the measurements of ΔP0 and ΔPs(L_{disc}≠1)s; thus the measurement time was the same among all measurements with L_{disc} ranging from 1 to 32. Fig. 7.5 shows a linear increment of the relative power with respect to the discrete code length. It is interesting to see that the slope of the relative power increment is near to 1, being almost the same with that in linear system although the PSP-BOTDA system is based on optical nonlinear phenomenon.

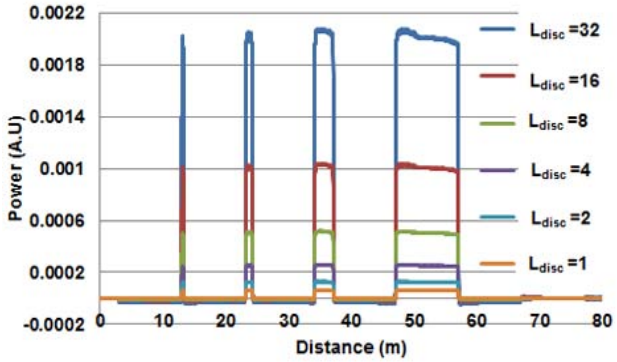

Fig. 7.4. Simulated correlation output of Brillouin amplified signals under Condition A.

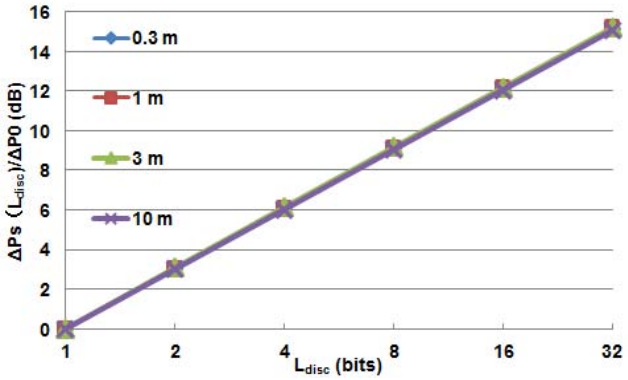

Fig. 7.5. Simulated Brillouin amplified signal power versus code length L_{disc} under Condition A.

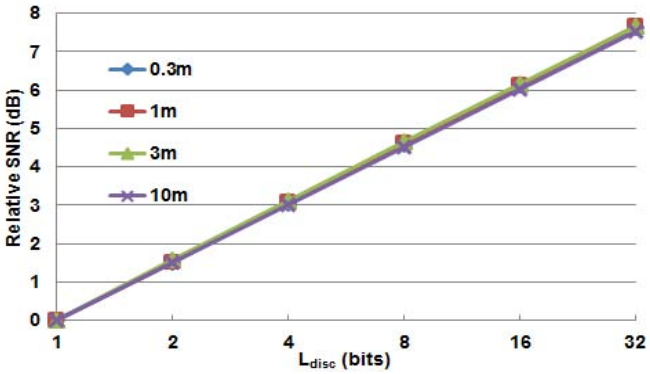

Fig. 7.6. Simulated relative optical SNRs versus code length L_{disc} under Condition A.

However, it should be noted that the noise power also increases during the mutual correlations for the decoding. Assuming that the noise power distribution is Gaussian, the noise in terms of optical power increases in proportion to $\sqrt{L_{disc}}$, for constant L_{cont}. Therefore, at constant L_{cont}, the relative optical SNR can be obtained by dividing the signal power ΔPs(L_{disc})/ ΔP0 by noise power that is proportional to $\sqrt{L_{disc}}$. Thus, the relative optical SNRs calculated are shown in Fig. 7.6. The data in Fig. 7.6 can be well approximated as follows;

$$SNR_{relative} = \sqrt{L_{disc}} \quad (7.3).$$

This improvement in the relative optical SNR is about twice that of intensity-modulation simplex-code BOTDA [8] and

is twice that of intensity-modulation complementary-code BOTDA [11]. The factor 2 comes from the difference in modulation methods: phase shift modulation for the PSP-BOTDA and intensity modulation for the conventional BOTDAs.

The rising edge was also investigated to evaluate the spatial resolution of the system. The results are listed in Table 7.2, which shows the rising edge length of the 3m strained fiber as the representative. The rising edge length was obtained by transforming the time required for the Brillouin signal to rise from 10% to 90% of its final value.

Table 7.2. Rising edge length of 3m strained fiber under Condition A.

L_{disc} (bits)	1	2	4	8	16	32
Rising edge (cm)	8.2	8.2	8.0	8.2	8.2	8.0

The calculated length of around 8.2 cm is a little bit shorter than the theoretical spatial resolution of 10 cm. This is because the evaluation of the rise time only covers about 80% of its total. From Table 7.2, it is concluded that the increment of the discrete code length (L_{disc}) does not deteriorate the spatial resolution of the dual Golay codes PSP-BOTDA system. Thus, it is expected that L_{disc} can be set longer than 32 bits to further improve the optical SNR.

B. Simulation Results for Condition B [7]

The Brillouin amplification results for each L_{cont} under Condition B are shown in Fig. 7.7. As observed in the figure, the Brillouin signal increases with the increment of the code length of L_{cont}. However, the amount of the increment starts to decrease considerably when L_{cont} is set to 16 and 32 bits, especially at the 0.3 m strained region. Furthermore, when L_{cont} is set to 16 and 32 bits, there are noises in the region around the rising and the falling edges. The magnification of the 3m strained region of Fig. 7.7 is shown in Fig. 7.8, where the Brillouin signals for L_{cont}=16 and 32 exhibit overshoots and undershoots that degrade the spatial resolution of the system. The results indicate the appearance of the side lobes of the processed correlations. This is because the total duration of the pulses modulated with the continuous pulse code (16 ns and 32 ns) is larger than the time constant of the acoustic wave τ_a of around 9 ns. Thus, only the first 8 bit pulses strongly interact with the acoustic wave while the rest does not during the measurement. Note that in contrast to the Condition B, the Brillouin signals under Condition A illustrated in Fig. 7.4 showed little degradation in the spatial resolution because $L_{cont}T_2$ was fixed at the value of 4ns that is shorter than τ_a throughout the simulations.

The results of the signal power increment and the relative optical SNRs under Condition B are depicted in Fig. 7.9 and Fig. 7.10, respectively. As in the calculation for Condition A, the value $\Delta P0=\Delta Ps(L_{cont}=1)$ in Fig. 7.9 corresponded to the sum of two sets of measurements with a 4-bit GCP while $\Delta Ps(L_{cont}\neq 1)$ was obtained by one set of measurements with the dual Golay codes of L_{disc}=4 and L_{cont} ($\neq$1); the GCP has two sequences while the dual Golay codes four sequences; thus the measurement time was the same among all measurements with L_{cont} ranging from 1 to 32. In Fig. 7.9, the relative signal power shows a linear increment trend with L_{cont} up to 8 bits. When L_{cont} equals to 16 and 32 bits, the occurrence of positive and negative overshoots causes the increment trend to deviate from its linear form.

The relative optical SNRs were calculated by dividing the relative power increment shown in Fig. 7.9 by the value $\sqrt{L_{cont}}$ since the noise power accumulated by the correlation process is proportional to $\sqrt{L_{cont}}$ under Condition B. It was found from Fig. 7.10 that the relative optical SNRs increase with the increase in L_{cont} up to 8 bits for the 0.3m strained fiber and up to 16 bits for other strained fibers. However, the relative optical SNRs begin to decrease at the longer L_{cont}. This is because the random noise power, processed in the correlations, accumulates with the increase in the code length L_{cont}, while the increase rate of the signal gradually decreases as shown in Fig. 7.9. Take note that the values of $L_{cont}T_2$ for L_{cont} =8 and 16 are 8 ns and 16 ns, which are around τ_a (~9 ns). This implies that when $L_{cont}T_2$ is around

τ_a the relative optical SNR reaches the maximum, which is found from Fig. 7.10 to be less than the value $\sqrt{L_{cont}}$ by about 1dB. It was also confirmed by other simulations that this is also true for narrower pulse widths: T_2 =0.5 ns and 0.25 ns. (See Fig. C.1 of Appendix C).

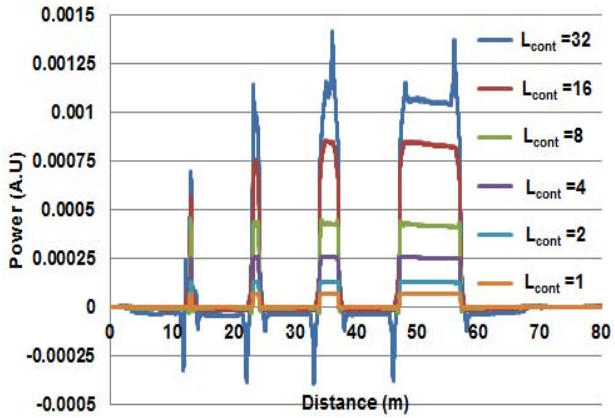

Fig. 7.7. Simulated correlation output of Brillouin amplified signals under Condition B.

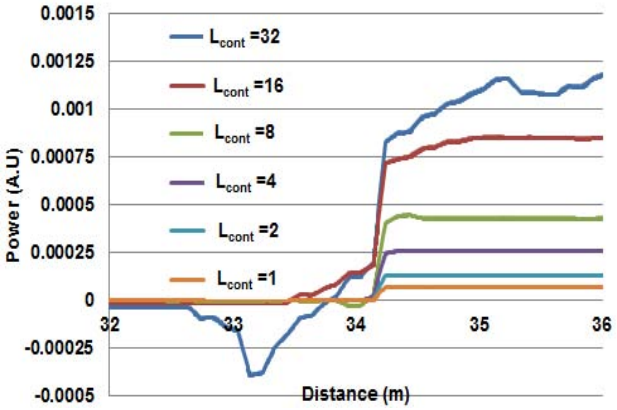

Fig. 7.8. Magnified rising edge region of 3 m strained region of Fig. 7.7.

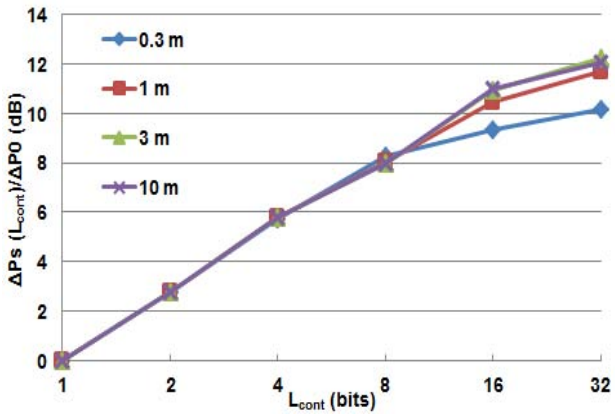

Fig. 7.9. Simulated Brillouin amplified signal power versus code length L_{cont} under Condition B.

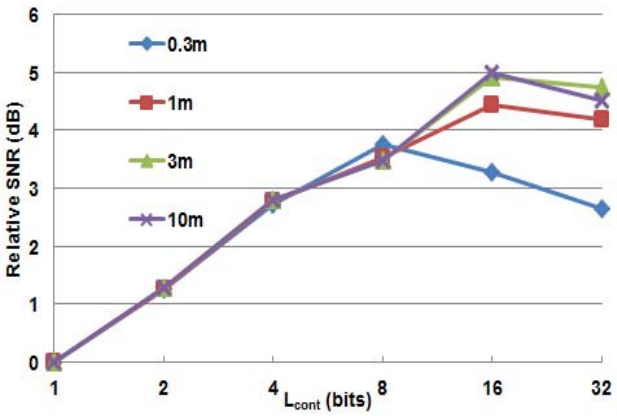

Fig. 7.10. Simulated relative optical SNRs versus code length L_{cont} under Condition B.

Figure 7.10 also shows that the relative optical SNRs for the 0.3m strained fiber drops more steeply than those for other strained fibers in the range of L_{cont} longer than 8 bits. This discrepancy is explained by difference in the crosstalk from the neighboring parts of the fiber. The side-lobes of the correlations explained above caused the crosstalk that made apparent increase in the signal. The crosstalk for the 0.3m strained fiber is less than that for the 1m, 3m, and 10m strained fibers since the range of the neighboring parts of the former fiber is narrower than those of the latter fibers. Thus, it apparently causes the higher relative optical SNRs for the 1 m, 3 m and 10 m strained fibers.

From the discussions above, the relative optical SNR under Condition B can be approximately expressed by

$$SNR_{relative} = \eta\sqrt{L_{cont}} \tag{7.4}$$

where coefficient η $(0 \le \eta \le 1)$ represents the ratio of the optical SNR improvement to the ideal improvement of $\sqrt{L_{cont}}$. The coefficient η also accounts for the acoustic wave attenuation. Consequently, η is about unity when code time $L_{cont}T_2$ is much shorter than τ_a (9ns); η gradually decreases to zero with the increase in $L_{cont}T_2$, as shown in Fig. C.2 of Appendix C. Thus, if one increases L_{cont}, optical $SNR_{relative}$ which is given by the product of η and $\sqrt{L_{cont}}$,

initially rises in proportion to $\sqrt{L_{cont}}$, then takes its maximum and after that gradually decreases. Since η is dependent on the accumulation of the amplitudes of the decreasing acoustic wave, η is a function of code time $L_{cont}T_2$. Numerical simulations show that the relationship between η and $L_{cont}T_2$ are almost the same for T_2=0.25, 0.5 and 1ns, as shown in Fig. C.2. In addition, Fig. C.1 shows that for all T_2 cases, the optical $SNR_{relative}$ takes its maximum when $L_{cont}T_2$ is around the time constant of the acoustic wave τ_a.

The results of further analysis on the rising edge length in the case of the 3m strained fiber are listed in Table 7.3.

Table 7.3. Rising edge length of 3m strained fiber under Condition B.

L_{cont} (bits)	1	2	4	8	16	32
Rising edge (cm)	8.2	8.0	8.2	8.2	61	162

Table 7.3 shows that the length of the rising edge which is estimated from the 10% and 90% response of the Brillouin signal. In Table 7.3, the rising edge lengths for L_{cont}=1 to 8 bits are around 8.2cm, which are the same with that on Condition A. However, it starts to increase at L_{cont} = 16 and 32 bits, as explained above.

From the discussion above, one can conclude that the total duration of the pulses modulated with the continuous pulse code ($L_{cont}T_2$) is limited at the value smaller than τ_a; the numerical results of the rising edge length in Table 7.3 and of the relative optical SNRs in Fig. 7.10 for T_2=1 ns indicate that the effective total duration of the modulated pulses is 8 ns or below.

C. Further Discussion on the SNR and the Brillouin Gain Spectrum (BGS)

It could be concluded from the results shown in Eqs. (7.3) and (7.4) that the optical SNR enhancement (SNRE) for the dual Golay codes PSP-BOTDA is given by

$$SNRE = \eta\sqrt{L_{cont} \cdot L_{disc}} \tag{7.5}$$

Since η accounts for the attenuation of the acoustic wave excited by the 1st pulsed pump for the coded continuous-PSP-BOTDA and we assume that interval time T_i is long enough to avoid interactions among the acoustic waves excited by the 1st pulses, η depends on L_{cont} but does not on L_{disc}. Therefore, if L_{cont} is varied, optical SNRE takes its maximum optical $SNRE_{max}$ when $L_{cont}T_2$ is around the time constant of the acoustic wave as it would for optical $SNR_{relative}$ of Eq. (7.4). Then, considering that $\eta \sim 0.7$ as can be seen from Fig. C.2, optical $SNRE_{max}$ is approximately given by

$$SNRE_{\max} = 0.7\sqrt{L_{cont} \cdot L_{disc}} \tag{7.6}$$

where L_{cont} is given by dividing the time constant of the acoustic wave by duration T_2.

Maximum values of L_{disc} may be limited by the time taken for the pulse light to make a round-trip across the length of the fiber (RTT: round-trip-time). BOTDAs usually inject pulsed pump light into fibers repeatedly to improve the optical SNR with signal averaging techniques. The period of the repetition should be more than the RTT so that the Stokes signal amplified by one pulsed pump should not superimpose on that amplified by the next pulsed pump. When the repetition period is reduced to the RTT, the maximum improvement in optical SNR is obtained via the signal averaging within a given measurement time. Then, the total coded pulse time that is proportional to L_{disc} should not exceed the RTT so that the maximum improvement in optical SNR may not be reduced. This is required in both conventional and proposed coded BOTDAs. However, the proposed coding method can virtually increase the code length by nesting two codes as in a manner described before with just a little increase in the repetition time.

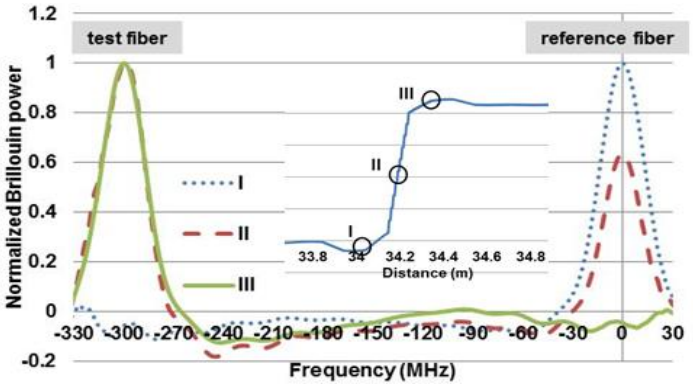

Fig. 7.11. Brillouin gain spectra at the BFS transient range calculated with L_f=3m, L_{cont}=8 and L_{disc}=4. The values of other parameters are as shown in Table I. Inset shows the time domain signal around the transient range.

From the discussion above and Eq. (7.6), it was found that the optical SNR of the dual Golay PSP-BOTDA is approximately $\eta\sqrt{L_{cont}L_{disc}}$ times as large as optical SNR of the PSP-BOTDA with L_{disc}=L_{cont}=1, i.e., single-pulse PSP-BOTDA. Furthermore, PSP-BOTDA has twice optical SNR compared to the intensity modulation BOTDA as explained before. Consequently, the optical SNR enhancement of the dual Golay PSP-BOTDA is approximately $2\eta\sqrt{L_{cont}}$ times that of the conventional high spatial resolution RZ coded BOTDAs. Here, it is noted that one should choose L_{cont} so that $L_{cont}T_2$ is less than the time constant of the acoustic wave τ_a. Then η ranges from 0.7 to 1 as shown in Fig. C.2.

The Brillouin gain spectra (BGS) of the dual Golay codes PSP-BOTDA can be almost the same as that of steady state SBS since the coded continuous- and discrete-PSP-BOTDAs, which are the bases of the dual Golay codes PSP-BOTDA, have approximately the same BGS with the steady state SBS spectrum, as analytically verified in Appendices A and B. The BGS for the dual Golay codes PSP-BOTDA with L_{disc}=4 bits and L_{cont}=8 bits has been also evaluated by numerical simulations based on Eq. (7.2). The simulated fiber had a 3 m section of 300 MHz change in the BFS. Fig. 7.11 shows the BGS calculated at three points I, II, and III in the BFS transition range. It was found that all BGS for the 3m section and for the reference are approximately the same with the steady state BGS having gain widths as narrow as 35MHz, demonstrating that the proposed coding method does not induce distortions in the measured BGS.

7.4 Experiments

7.4.1 Experimental Setup

The experiments on the dual Golay PSP-BOTDA were performed to be compared with the simulations to validate the sensor system's efficiency. The experimental setup of the dual Golay PSP-BOTDA system is shown in Fig. 7.12.

The light from an LD operating at a wavelength of 1550 nm and at power of 6 mW was divided by a 1 x 2 optical coupler (50:50) into one for the pump and the other for the probe. An arbitrary waveform generator (AWG) was used to synthesize the electrical signal which was composed of an electrical 1st pulse and the dual Golay code pulses (2nd pulses). The lightwave for the pump was modulated by a Mach-Zehnder modulator (MZM) with the electrical signal from the AWG. Then, the MZM was biased at the transmission minimum point so that the 2nd optical pulses are phase-coded. A polarization scrambler (PS) was used to hinder the polarization dependence of the Brillouin amplification. The PS used in the experiment modulates the state of polarization (SOP) of light via modulation of birefringence of the fiber inside it. The polarization-induced noise was suppressed at the minimum level by observing that the noise was reduced to less than the white noise at the receiver after averaging 10^3 signal waveforms. The modulated optical signals were amplified

using an erbium-doped fiber amplifier (EDFA1) to set the peak power of the 1st and the 2nd optical pulses to be at 33mW. The widths of the 1st and the 2nd optical pulses are 30 ns and 1ns, respectively. The rise time of the pulsed light is around 0.5 ns. The test fiber cables used in the experiment were the dispersion shift fibers (DSF) with the lengths of 0.3m, 1m, 3m and 10m. Single mode fiber (SMF) cables with the length of 10m were connected between the DSF cables as the references. The difference in BFS between the SMF and the DSF cables is about 300 MHz, which corresponds to about 0.6% strain.

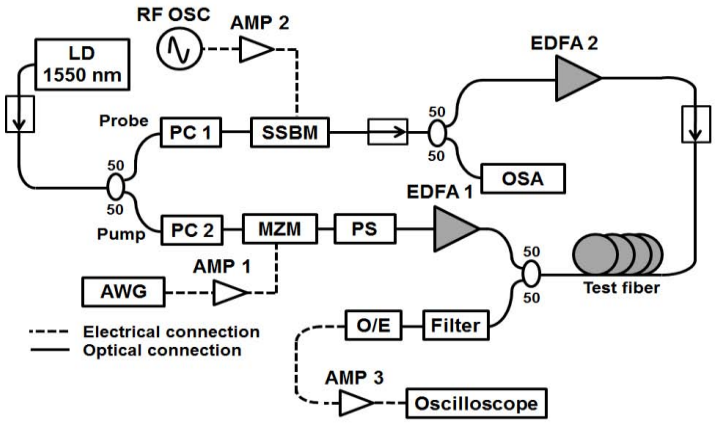

Fig. 7.12. Experimental setup of the dual Golay codes PSP-BOTDA.

As for producing the probe lightwave, the electrical RF signal with a frequency of 10.555 GHz from an RF oscillator (RF OSC) was input to an optical single side-band modulator (SSBM). The SSBM output the Stokes light (probe), whose frequency was downshifted with the amount of 10.555 GHz. EDFA2 was used to amplify the probe light to set the probe power to 2 mW. An optical spectrum analyzer (OSA) was used to monitor the modulated light frequency. The Brillouin amplified signal was converted into an electrical signal and sent to the oscilloscope. The signals were digitized and averaged by the oscilloscope. Then the recorded signals were further processed by a computer for the decoding (mutual correlation calculations).

7.4.2 Results and Discussion

A. Experimental Results for Condition A [7]

The experiments under Condition A were performed for various values of L_{disc} by fixing L_{cont}=4. The experimental results are depicted in Figs. 7.13(a) and 7.13(b). The results in Fig. 7.13 are in good agreement with the simulation shown in Fig. 7.4, although random noise is superimposed on the experimental signals. One can observe that the Brillouin signal peak power is almost the same for all strained regions. Furthermore, as expected, little deterioration can be found in the rising and the falling edges of the signal waveforms even in the case of 32 bits of the discrete pulse code. By using the same approach of calculating the theoretical rising edge length explained in Section 7.3, the experimental spatial resolution was further examined. The rising edge length evaluated at the 3 m strained region was 8.5cm for all values of L_{disc}=1, 2, 4, 8, 16, and 32 bits, being in good agreement with the theoretical value of 10x(0.9 - 0.1) = 8cm.

The optical SNR enhancement (SNRE) measured for L_{disc}=1-32 bits and L_{cont}=4 bits is shown in Fig. 7.14. Notice that the optical SNREs were obtained by using the optical SNR for L_{disc}=L_{cont}=1 bit as a reference. This reference optical SNR corresponded to the optical SNR for the single pulse PSP-BOTDA measured in the same measurement time. The reference optical SNR obtained from the experiment was 4.7 dB. The straight line (SNRE=$\sqrt{L_{disc} * L_{cont}}$ with $L_{cont} = 4$) was also included in Fig. 7.14 for comparisons.

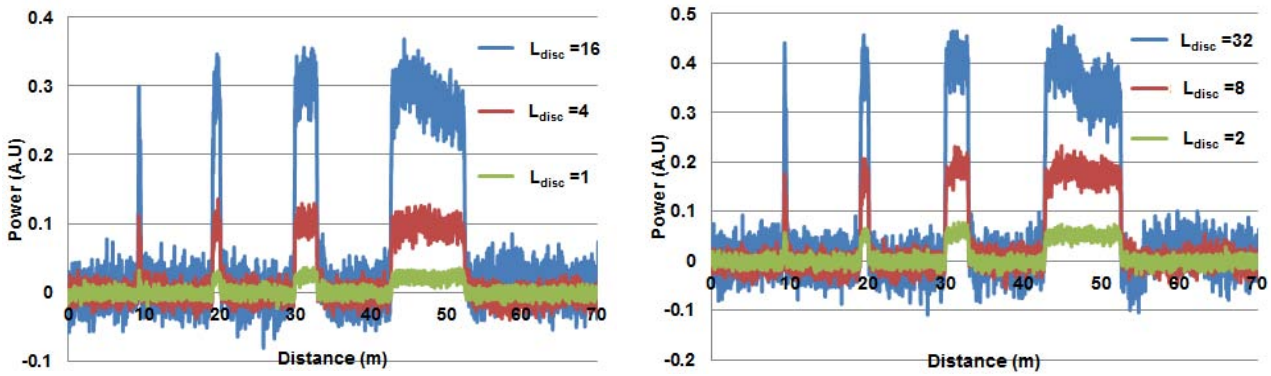

(a) (b)

Fig. 7.13. Measured correlation output of Brillouin amplified signals under Condition A. (a) L_{disc}=1, 4 and 16 (b) L_{disc}=2, 8 and 32.

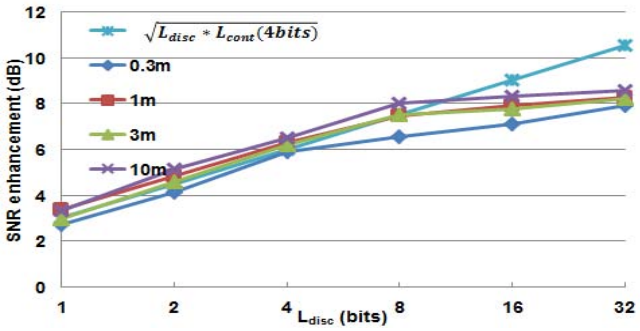

Fig. 7.14. Measured optical SNR enhancement of dual Golay PSP-BOTDA referenced to the single pulse-PSP-BOTDA (optical SNR=4.7 dB).

It was observed that the optical SNRE increases linearly with respect to L_{disc}. When L_{disc}=8, the obtained optical SNRE was as large as about 8dB. In comparison with the SNR obtained with the conventional PSP-BOTDA without coding, this translates into about 40 times faster measurement speed. However, when L_{disc}=8, 16 and 32 bits, the optical SNRE starts to deviate from its linearity. This slightly differs from the simulations shown in Fig. 7.6. This discrepancy was due to the amplification characteristic of the electrical amplifier used to amplify the Golay coded electrical signals from the AWG. The capacitor incorporated in the electrical amplifier cut off the DC level and the low-frequency components of the modulated signals, as has been explained in Chapter 5. This resulted in the inefficient optical modulation by the MZM of the discretely configured coded-pulses of more than 8-bit code. The use of a DC-coupled amplifier or the modifications on the electrical signal configurations would improve the modulation characteristics and increase the optical SNRE in accordance with Eq. (7.3).

B. Experimental Results for Condition B [7]

Figs. 7.15(a) and 7.15(b) show the experimental results under Condition B. It can be found from the figures that the increase in L_{cont} also contributes to the Brillouin power increment of the system. However, as predicted, the increase rate of the Brillouin amplified signal has dropped significantly when L_{cont} = 16 and 32 at the 0.3 m strained region. This is because total time duration of those code length pulses has exceeded the time constant of the acoustic wave τ_a, as explained in Section 7.3. In addition, as predicted from the simulation in Fig. 7.7, the overshoot and undershoot noises can be seen clearly when L_{cont} equals to 16 and 32 bits.

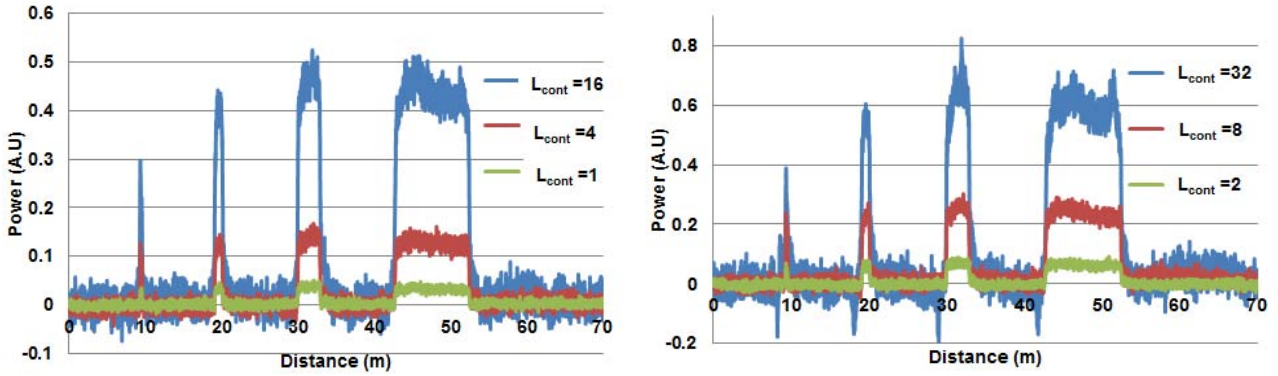

(a) (b)

Fig. 7.15. Measured correlation output of Brillouin amplified signals under Condition B. (a) L_{cont}=1, 4 and 16 (b) L_{cont}=2, 8 and 32.

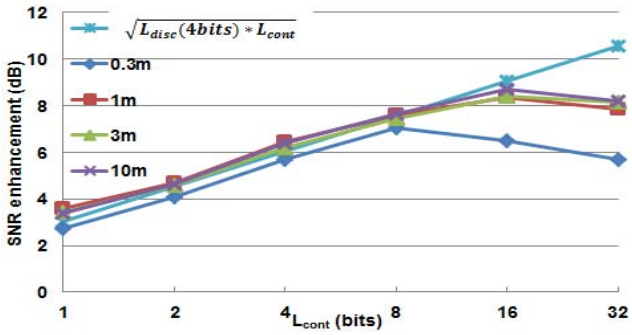

Fig. 7.16. Measured optical SNR enhancement of dual Golay PSP-BOTDA referenced to the single pulse-PSP-BOTDA (optical SNR=4.7 dB).

The optical SNREs for L_{cont}= 1~32 bits and L_{disc} = 4 bits are depicted in Fig. 7.16. The optical SNREs were obtained by using the optical SNR for L_{cont}=L_{disc}=1 bit as a reference, as in the case before. As in Fig. 7.14, the reference optical SNR corresponded to the optical SNR for the single pulse PSP-BOTDA measured in the same measurement time. The reference optical SNR obtained from the experiment was 4.7 dB. The straight line (SNRE=$\sqrt{L_{disc} * L_{cont}}$ with $L_{disc} = 4$) was also included in Fig. 7.16 for comparisons.

The optical SNRE for the strained lengths of 1 m, 3 m, and 10 m increases with L_{cont} up to 16 bits, while it begins to decrease at 16 bits in the case of 0.3 m strained length. It is noticeable that the results in Fig. 7.16 agree well with the simulated relative optical SNR shown in Fig. 7.10 if one takes into account the coding gain with L_{disc}=4bits. For 0.3m test section, when L_{cont}=8, maximum optical SNRE of about 7dB was obtained, while for other test sections, when L_{cont}=16, maximum optical SNRE was about 8dB. As mentioned in Section 7.3, acoustic wave damping explains the reason of the deviation from the straight line of the optical SNRE, i.e., the drop in the optical SNRE for L_{cont} longer than 8 bits. Also, as explained in Section 7.3.2, it should be noted that the further increase in the SNRE for L_{cont}=16 bits case at the 1m, 3m and 10m test sections was caused by the crosstalk. Therefore, it is concluded that the maximum SNRE obtained in this experiment was about 7dB with the use of L_{cont}=8 bits ($L_{cont}T_2$=8ns). In comparison with the SNR obtained with the conventional PSP-BOTDA without coding, this translates into about 25 times faster measurement speed. As we recall from the simulation results (Section 7.3.2 B), the optical SNRE reaches its maxima when $L_{cont}T_2$ is

set around τ_a; i.e. the available code duration for NRZ pulses is limited by τ_a, which in this case is 9ns.

Since the optical SNRE for all test sections increases with L_{cont} up to 8 bits under Condition B, the BGS was measured for dual Golay code of L_{disc}=4 bits and L_{cont}=8 bits case. The BGS measured at the 3m test section and at the reference fiber are shown in Figs. 7.17(a) and 7.17(b). Both spectra measured were fitted well with Lorentzian curves of the bandwidth as narrow as about 30MHz, indicating the BGS obtained by the proposed coding method were approximately the same with the steady state BGS. Therefore, it is confirmed that the use of NRZ coded pulses in the proposed method does not induce distortions in the BGS.

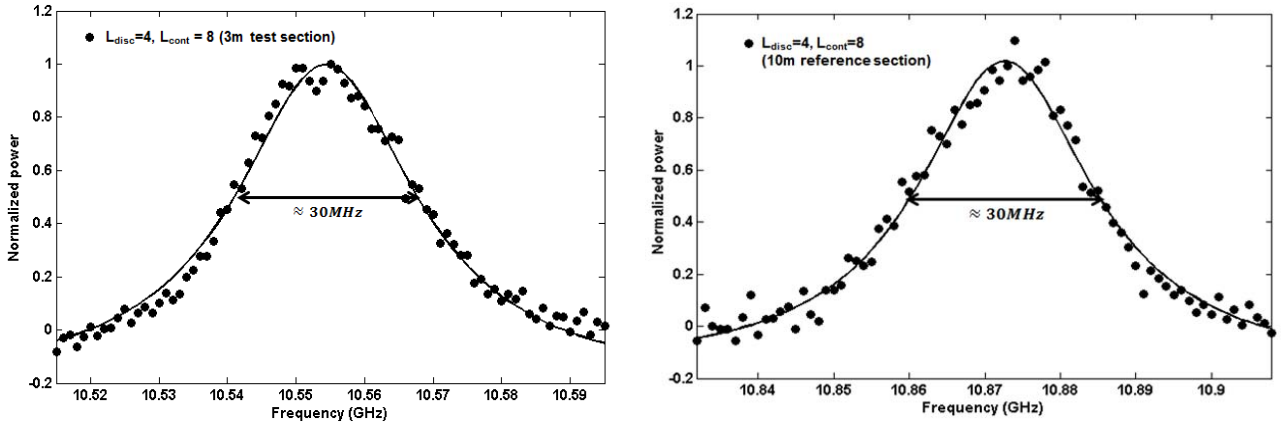

(a) (b)

Fig. 7.17. Measured Brillouin gain spectrum under Condition B with L_{cont}=8bits. (a) 3m test section (b) 10m reference fiber.

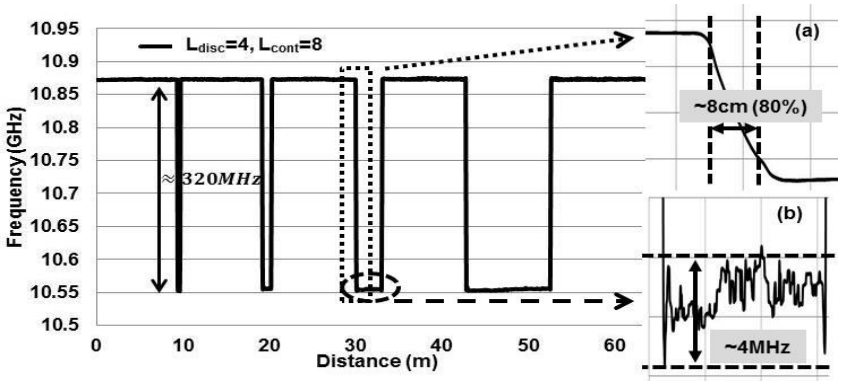

Fig. 7.18. BFS distribution measured under Condition B with L_{cont}=8bits. Insets (a) and (b) show expanded trace of the rising edge and distribution at the 3m section.

The spatial resolution was also evaluated at the rising edge of 3 m strained region. The result showed that the rising edge length was 8.5 cm for L_{cont}=1, 2, 4, and 8 bits. When L_{cont} was set to 16 and 32 bits, the rising edges range over 62cm and 160cm, respectively. It has been confirmed from these experiments that good optical SNRE can be obtained and a high spatial resolution measurement can be achieved on condition that $L_{cont}T_2$ is set less than τ_a. Otherwise, however, not only the optical SNRE but also the spatial resolution deteriorates.

To fully analyze the change in the BFS and verify the spatial resolution, the BFS distribution was also measured. Figure 7.18 shows the BFS distribution measured when L_{cont}=8 and L_{disc}=4, which agreed well with the pseudo-BFS-distribution made by splicing SMFs and DSFs alternatively. The transient BFS is shown in an inset (a) in Fig. 7.18, showing the 80% of the total transient length at 3m test section that is about 8cm. This is in good agreement

with the theoretical spatial resolution (T_2=1ns corresponds to 10cm of spatial resolution). It is also observed from the inset (b) in Fig. 7.18 that the variation in the measured BFS in the 3-m section was estimated at 0.67MHz (standard deviation) that corresponded to the measurement accuracy of $1.3\text{x}10^{-5}$ strain or 0.56°C temperature. Therefore, it is confirmed from the BFS distribution measurement that the high spatial resolution as short as 10cm has been successfully demonstrated.

7.5 Conclusions of Chapter

An algorithm has been presented for synthesizing dual Golay codes for measuring distributed strain and temperature based on phase-shift pulse Brillouin optical time domain analysis (PSP-BOTDA) with high spatial resolution. The proposed dual Golay codes are configured by nesting one Golay complementary pair of sequences (GCP) into the other one. The former is called pair of sequences continuous pulse codes and the latter discrete pulse codes, which are used to generate the pulsed pump with NRZ pulses and RZ pulses, respectively.

Introducing a proper space time between the coded discrete pulses avoids the interference noise through the SBS process. However, the introduction of the space time increases the time slot for one bit, decreasing the code length that is limited by the round-trip-time (RTT). Constructing the coded continuous pulses with the total duration less than the time constant of the acoustic wave τ_a makes it possible to obtain good correlation properties of the Brillouin signals. However, the maximum code length is limited.

The proposed dual Golay codes enable one to use the RZ pulses and NRZ pulses simultaneously and advantageously for coding the pump of the PSP-BOTDA, and to use longer codes than the conventional codes within a given period; let code lengths of the continuous and the discrete pulse codes be L_{cont} and L_{disc}, the code length of each dual Golay code is $L_{cont}L_{disc}$. Then, the optical SNR enhancement, i.e., the coding gain of the proposed method is about $\eta\sqrt{L_{cont}L_{disc}}$, while that of the conventional coded BOTDA based on intensity modulations is $\sqrt{L_{disc}}/2$. Therefore, the optical SNR enhancement of the proposed coding method is $2\eta\sqrt{L_{cont}}$ times as large as that of the conventional coding method. The coefficient $\eta\ (0 \le \eta \le 1)$ represents the efficiency of the optical SNR improvement with the continuous pulse codes and also accounts for the attenuation of the acoustic wave that is excited by the 1st pulsed pump of the PSP-BOTDA. When the product of L_{cont} and the 2nd pulse duration T_2 is longer than τ_a, the quantity η decreases to less than 0.7 and the spatial resolution gets worse than the theoretical one; thus $L_{cont}T_2$ should be less than τ_a; then η ranges from 0.7 to 1.

A new coded PSP-BOTDA system based on the dual Golay codes has been demonstrated by both simulations and experiments. High spatial resolution of 10cm was successfully demonstrated from both simulations and experiments. From the results, it has been clarified that the power of the correlated Brillouin signal has increased with increase in the code length of the new code provided that the total duration of the pulses coded by the continuous pulse codes is less than τ_a. The increase in the Brillouin signal power raises the optical SNR and gives the benefit to BOTDA to attain high spatial resolution. Initial experiments for L_{cont}=4, L_{disc}=8 have demonstrated about 8-dB enhancement in the optical SNR when compared to the single pulse PSP-BOTDA, while for L_{cont}=8, L_{disc}=4, the amount of enhancement achieved was about 7-dB. Finally, it should be noted that the SNIR can be further enhanced by increasing the code length L_{disc} of discrete part, but limited to the round trip time (RTT) of light in fiber. For the continuous part, however, maximum SNIR is achieved when the total code duration $L_{cont}T_2$ is set around the time constant of the acoustic wave amplitude τ_a, in this case $L_{cont}T_{2=}$8ns.

Appendices

In this section, additional notes related to the analytical expressions for the previously introduced coded continuous-PSP-BOTDA and coded discrete-PSP-BOTDA techniques are given. Some numerical analysis on the BGS and the optical SNR for both techniques are also included, which are useful for the purpose of comparing with the numerical results obtained with the dual Golay codes PSP-BOTDA, which have already been discussed above.

Appendix A

In the following, we give the signal for the coded continuous-PSP-BOTDA which is obtained by subtracting the signal ΔP^- measured with a code $\bar{C}$ from the signal ΔP^+ measured with a code C, where $C = \{c_1, c_2, \dots, c_n\}$, $\bar{C} = -C = \{-c_1, -c_2, \dots, -c_n\}$ and $c_k = 1\ or\ -1$, with k=1, 2,…, n. We note here that all parameters of analytical expressions in this Appendix are normalized according to [10].

Let $\Delta E_S(t)$ represent an increment in the Stokes light field produced by SBS after passage of a time t from the time when the pulsed pump enters into a local region along an optical fiber. When $0 \le t \le T_1$, the field $\Delta E_S(t)$ for ΔP^+ and that for ΔP^- are the same. Then, the subtracted signal becomes zero. Therefore we have only to derive the signal $\Delta E_S(t)$ for $t_0 \le t \le t_n$, where $t_k = T_1 + k\tau\ (k = 1,2,\dots,n)$, T_1 is the first pump pulse width and τ is the code element pump pulse width. When $\tau \ll 1$, $t = t_k$, the Stokes light field increment $\Delta E_s(t_k)$ is obtained from Eq. (7.2b) as follows:

$$\Delta E_s(t_k) = \frac{1}{2} c_k E_p E_a^*(t_k)\tau \tag{A.1}$$

The factor 1/2 in Eq. (A.1) comes from the fact that the Stokes light propagates in the direction of –z while the pump light in the opposite.

The acoustic wave field $E_a(t)$ in Eq. (A.1) is obtained from Eq. (7.2c) as follows:

$$E_a(t) = e^{-\Upsilon t}\int_0^t e^{\Upsilon t} E_p(t) E_s^*(t)\,dt \tag{A.2}$$

with $\Upsilon = 1 + i\Delta$ where Δ denotes the normalized frequency detuning. If we express the pulsed pump field as $E_p(t)$=E_p $(0 \le t \le T_1 = t_0)$, $E_p(t)$=$E_p C(t)$ $(t_0 \le t \le t_n)$ and assume $E_S(t)$ is constant, Eq. (A.2) is transformed into

$$E_a(t) = e^{-\Upsilon t} E_p E_s^* (I_1 + I_2(t)) \tag{A.3}$$

with

$$I_1 = \int_0^{T_1} e^{\Upsilon t}\,dt = \frac{e^{\Upsilon T_1} - 1}{\Upsilon} \tag{A.4}$$

and

$$I_2(t) = \int_{t_0}^{t} e^{\Upsilon t} C(t)\,dt \tag{A.5}$$

Here we note that I_1 is due to the acoustic wave excited by the first pulsed pump, while I_2(t) is produced by the sequence of the coded pulsed pump, thus being dependent on the bit pattern of the code.

The Stokes light power increment $\Delta P_s(t_k)$ $(t_0 \le t_k \le t_n)$ is given by

$$\Delta P_s(t_k) = E_s\,\Delta E_s^*(t_k) + c.c. \tag{A.6}$$

where *c.c* denotes complex conjugate. For simplicity, the factor of proportionality in the right side of (A.6) was set to unity. Substituting Eqs. (A.1) and (A.2) into Eq. (A.6), we obtain the Stokes light power increment $\Delta P_s^+(t_k)$ when the

code C is employed as

$$\Delta P_s^+(t_k) = \frac{1}{2} c_k |E_p|^2 |E_s|^2 \tau e^{-\gamma t_k} \{ I_1 + I_2(t_k) \} + c.c. \tag{A.7}$$

On the other hand, when the code $-C(t)$ is used , c_k in Eq. (A.7) and $C(t)$ in $I_2(t)$ are replaced with $-c_k$ and $-C(t)$, thus yielding the Stokes light power increment as:

$$\Delta P_s^-(t_k) = \frac{1}{2} (-c_k) |E_p|^2 |E_s|^2 \tau e^{-\gamma t_k} \{ I_1 - I_2(t_k) \} + c.c. \tag{A.8}$$

Consequently, the differential Stokes light power is given by

$$\begin{aligned} DP_s(t_k) &= \Delta P_s^+(t_k) - \Delta P_s^-(t_k) \\ &= c_k |E_p|^2 |E_s|^2 \tau e^{-\gamma t_k} I_1 + c.c. \end{aligned} \tag{A.9}$$

Here, we find that the subtraction above exactly cancels the bit pattern dependent term $I_2(t_k)$.

In contrast, when the intensity modulation format is employed for coding the pump as in the conventional intensity modulation based BOTDA, codes $(1+C)/2$ and $(1-C)/2$ instead of codes C and $-C$ are used for measuring ΔP_s^+ and ΔP_s^-, respectively. Then, the bit pattern dependent term does not vanish through the subtraction. This is the reason why the coded PSP-BOTDA has better correlation characteristics than the conventional intensity modulation based BOTDAs when the NRZ coded pulses are used.

Substituting Eq. (A.4) into Eq. (A.9) yields the explicit expression of the differential signal of the coded continuous-PSP-BOTDA:

$$\begin{aligned} DP_s(t_k) = &\frac{|E_p|^2 |E_s|^2 \tau}{1+\Delta^2} \\ &\times (2c_k) [\exp(-k\tau) \{ \cos(k\tau\Delta) - \Delta \sin(k\tau\Delta) \} - \exp(-t_k) \{ \cos(t_k\Delta) - \Delta \sin(t_k\Delta) \}] \end{aligned} \tag{A.10}$$

We find from Eq. (A.10) that the spectrum profile of the differential signal is almost the same with that of the steady state, that is equivalent to what is given at the first row of the right side of Eq. (A.10). We also find that the differential signal decreases with the order of the code element c_k in accordance to $\exp(-k\tau)$ where time is normalized by time constant of the acoustic wave. Thus the maximum code length in duration is limited up to about the time constant of the acoustic wave τ_a.

The spectra of the differential signals also have been numerically evaluated based on Eq. (7.4) and shown in Fig. A.1. Then the calculation condition was similar to that provided in Table 7.1. It can be observed that the peak Brillouin power increases linearly with code length up to 8 bits. However, it starts to deviate from its linearity. The reason for this to occur is as what has been explained in sub-section B of Section 7.3.2. While the spectrum width stays around 35MHz in the case of 1 bit to 16 bits, the spectrum width has narrowed to about 30MHz in the case of 32 bits. However, there is little distortion in the spectrum shape.

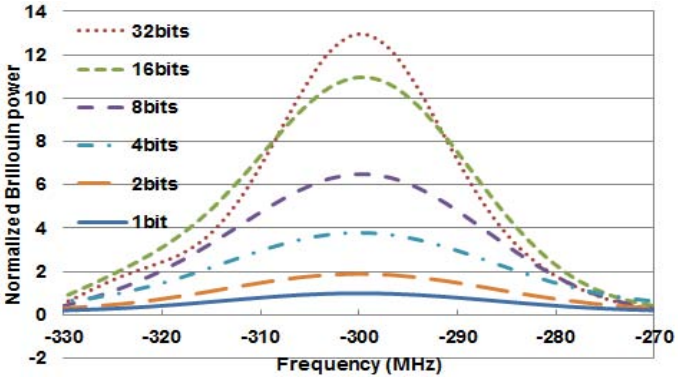

Fig. A.1. Numerical results of BGS at the test section of the fiber for coded continuous-PSP-BOTDA.

Appendix B

In the following, we give the signal for the coded discrete-PSP-BOTDA. As can be seen from Figs. 7.1(a) and 7.1(b), when the code length is one bit, the pump configuration of the coded discrete-PSP-BOTDA is the same with that of the coded continuous-PSP-BOTDA. Therefore, one-bit signal of the coded discrete-PSP-BOTDA is given by Eq. (A.10) with k=1 as follows:

$$DP_s(t_1) = \frac{|E_p|^2 |E_s|^2 \tau}{1+\Delta^2} \times (2c_1)\left[\exp(-\tau)\{\cos(\tau\Delta) - \Delta\sin(\tau\Delta)\} - \exp(-t_1)\{\cos(t_1\Delta) - \Delta\sin(t_1\Delta)\} \right] \quad \text{(B.1)}$$

If we assume typical conditions for measurement with high spatial resolution BOTDA: the one-bit pulse width is far less than the time constant of the acoustic wave τ_a (i.e. $\tau \ll 1$), the first pump pulse width is much greater than τ_a (i.e. t_1=T_1+1 >> 1), and the frequency detuning is within the Brillouin gain bandwidth (i.e. -1 < Δ < 1), then Eq. (B.1) becomes

$$DP_s(t_1) = \frac{2c_1 |E_p|^2 |E_s|^2 \tau}{1+\Delta^2} \quad \text{(B.2)}$$

The factor 2 in Eq. (B.2) comes from two measurements for the subtraction process. Therefore, it is found from Eq. (B.2) with eliminating the factor 2 that the Brillouin gain spectrum of the coded discrete-PSP-BOTDA for one bit is identical to that in the steady state in terms of both magnitude and bandwidth.

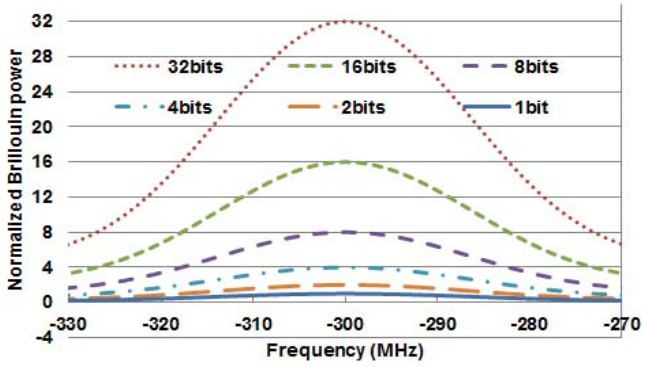

Fig. B.1. Numerical results of BGS at the test section of the fiber for coded discrete-PSP-BOTDA.

If we configure the pulsed pump of the coded discrete- PSP-BOTDA as shown in Fig. 7.1(b) with separation T_i much longer than τ_a, each pulsed pump for one bit does not interfere with the others. Then, the bit patterning effects are

reduced and the Brillouin signal for the *k*-th bit is given by the right side of (B.2) with replacing c_1 by c_k.

The spectra of the differential signals are evaluated numerically as in a manner of Appendix A, and are illustrated in Fig. B.1. The Brillouin power for each code length is normalized to the peak Brillouin power for 1-bit code. It is observed that the power increases linearly with the increase in the code length. Also, as expected, the shape of the spectra was not distorted and their widths were found to stay about 35MHz; as narrow as the value for the steady state SBS.

Appendix C

In the following, we give the relative optical $SNR_{relative}$ and the coefficient η in Eq. (7.4), which are numerically evaluated based on Eq. (7.2) for various T_2 of 0.25, 0.5 and 1ns. The numerical calculations were performed based on Condition B of Table I except that the code lengths L_{cont} were set up to 64 bits for T_2 = 0.5ns and up to 128 bits for T_2 = 0.25ns. Fig. C.1 shows optical $SNR_{relative}$ as a function of code time $L_{cont}T_2$ for the 0.3m section. It can be seen from Fig. C.1 that for all T_2 cases, optical $SNR_{relative}$ takes maxima when $L_{cont}T_2$ is around τ_a of 9ns.

Fig. C.2 shows coefficient η that is obtained by dividing optical $SNR_{relative}$ shown in Fig. C.1 by $\sqrt{L_{cont}}$ according to its definition given by Eq. (7.4). We found from the figure that code time dependence of η is almost the same for different pulse durations of T_2=0.25, 0.5 and 1ns. We also found that when optical $SNR_{relative}$ is maximum, that is when $L_{cont}T_2$=8ns or 9ns (time constant of the acoustic wave τ_a) according to Fig. C.1, η takes the value of about 0.8 or 0.7 even for different T_2 values.

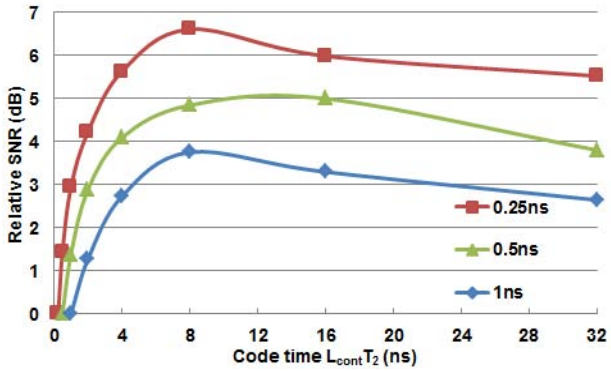

Fig. C.1. Relative optical SNR vs code time $L_{cont}T_2$ for different T_2.

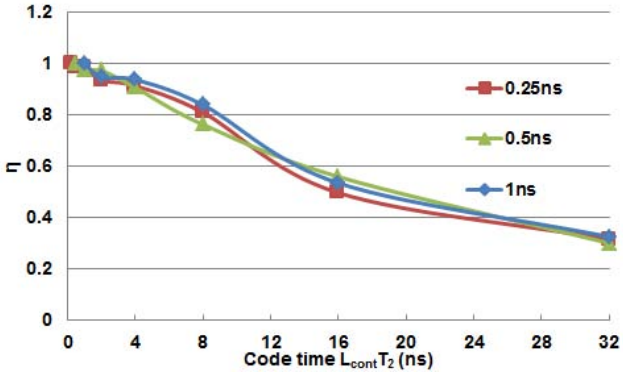

Fig. C.2. Coefficient η vs code time $L_{cont}T_2$ for different T_2.

References

[1] R. Muroi, T. Horiguchi, Y. Miyamoto, Y. Sato, A. Tachibana and A. Takakura, "PSP-BOTDA based on Golay code", IEICE Trans. Commun. (in Japanese), vol. J91-B, no. 11, pp. 1493-1501, November 2008.

[2] T. Sasaki, T. Horiguchi, **M. S. D. Zan** and D. Uchiyama, "Coded pulse interval dependence of the characteristics in discretely coded PSP-BOTDA", The IEICE Trans. Commun. (in Japanese), vol. J94-B no. 11, pp. 1481-1489, Nov. 2011.

[3] **M. S. D. B. Zan**, T. Horiguchi, "A new electrical signal configuration for modulating pump light of coded discrete-phase shift pulse-BOTDA," Proc. of the IEEE 3rd Int. Conf. on Photonics (ICP 2012), vol., no., pp.294,298, Oct. 2012.

[4] D. Uchiyama, T. Horiguchi, H. Ando, Y. Okumoto, T. Sasaki and Y. Sawai, "Signal to noise improvement ratio for coded PSP-BOTDA", Technical report of IEICE. OFT 109 (377) (in Japanese), pp. 33-38, Jan. 2010.

[5] **M. S. D. B. Zan**, T. Tsumuraya and T. Horiguchi, "The use of Walsh functions in modulating pump light of high-spatial resolution BOTDA with NRZ pulses" 22nd International. Conf. on Optical Fiber Sensors (OFS-22) 2012, pp. 84219J-1 -

84219J-4, Oct. 2012.

[6] **M. S. D. B. Zan**, T. Tsumuraya and T. Horiguchi, "The use of Walsh code in modulating the pump light of high spatial resolution phase-shift-pulse Brillouin optical time domain analysis with non-return-to-zero pulses", J. Meas. Sci. Technol., vol. 24, no. 9 (094025), pp. 1-13, Jul. 2013.

[7] **M. S. D. B. Zan** and T. Horiguchi, "A dual Golay complementary pair of sequences for improving the performance of phase-shift pulse BOTDA fiber sensor", J. Lightw. Technol. vol. 30, no. 21, pp. 3338-3356, Nov. 2012.

[8] M. A. Soto, G. Bolognini and F. Di. Pasquale, "Analysis of pulse modulation format in coded BOTDA sensors", Opt. Exp., vol. 18, no. 14, pp. 14878-14892, Jul. 2010.

[9] R. W. Boyd, Nonlinear Optics, 3rd ed. New York: Academic 2008.

[10] V. Lecoeuche, D. J. Webb, C. N. Pannell and D. A. Jackson, "Transient response in high-resolution Brillouin-based distributed sensing using probe pulses shorter than the acoustic relaxation time", Opt. Lett., vol. 25, no. 3, pp. 156-158, Feb. 2000.

[11] H. Liang, W. Li, N. Linze, L. Chen and X. Bao, "High-resolution DPP-BOTDA over 50 km LEAF using return-to-zero coded pulses", Opt. Lett., vol. 35, no. 10, pp. 1503-1505, May 2010.

Chapter 8: Combined Walsh and Golay Codes PSP-BOTDA

8.1 Introduction to Chapter

It has been shown previously in Chapter 7 that the combination of RZ and NRZ pulses in coding the pump light of PSP-BOTDA with dual Golay codes has contributed to the achievement of higher optical SNR than that of the previously introduced coded continuous- and coded discrete-PSP-BOTDAs and obviously higher than that of the conventional PSP-BOTDA [1]. However, in terms of spatial resolution, it was found from Chapter 7 that the available code duration for Golay coded NRZ pulses case in the dual Golay codes PSP-BOTDA is still limited by the time constant of the acoustic wave τ_a. This is because the assignment of Golay coded NRZ pulses of code duration longer than τ_a in the dual Golay codes PSP-BOTDA have induced distortion in the measured Brillouin signals, which consequently caused the degradation in the spatial resolution. Nonetheless, we recall from Chapter 6 that the use of Walsh coded NRZ-pulses in the coded continuous-PSP-BOTDA has overcome this issue [2, 3].

Therefore, based on the issue and findings presented in Chapter 6 and Chapter 7, the author proposes in this chapter the combination use of different codes, namely Golay codes and Walsh codes in modulating the pump light of PSP-BOTDA. The analysis of combining Golay codes and Walsh codes in modulating the pump light of the PSP-BOTDA is discussed. In the simulation and experimental analysis, it was found that assigning Walsh codes as the NRZ pulses has given better spatial resolution than that of the Golay codes of the same pulse formation [4-6]. Also, as predicted, simultaneous use of RZ- and NRZ pulses formats in the pump light of PSP-BOTDA has contributed to the achievement of higher optical SNR than that of using only one kind of pulse formation. In this chapter, both combinations of i) Walsh codes (NRZ) + Golay codes (RZ) and ii) Walsh codes (RZ) + Golay codes (NRZ) are examined to analyze their impact to the efficiency of the PSP-BOTDA.

8.2 Pump Light Configurations

An example of a pump light modulated with the combined Golay and Walsh codes is illustrated in Fig. 8.1.

In Fig. 8.1, a 4-bit Walsh code was assigned as the NRZ pulses while a 4-bit Golay code the RZ pulses. The elements of the Walsh code were then multiplied with each element of Golay code. This multiplication yields 16 pulses coded by the combination of the two codes. It should be noted here that as the Golay codes are generated from a pair of codes and the Walsh codes are based on an $M \times M$ Hadamard matrices, the number of generated code patterns will be $2 \times M \times 2$. The first factor 2 denotes the two patterns of Golay codes, while the other factor 2 indicates the use of inverted codes for the measurement in the coded PSP-BOTDA system [1-9].

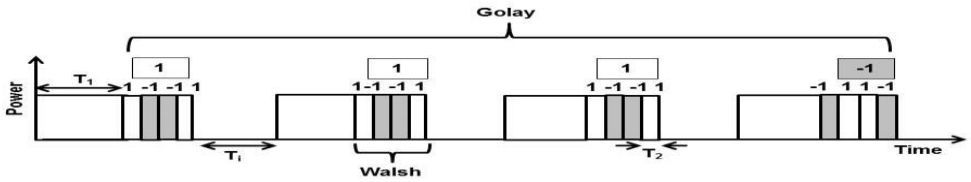

Fig. 8.1. Pump light configuration of combined Walsh and Golay codes. A 4-bit Walsh code was assigned as the NRZ pulses while a 4-bit Golay code the RZ pulses.

8.3 Simulations

8.3.1 Simulation Setup

The simulation setup of the combined Walsh and Golay codes is shown in Fig. 8.2. An example of pump light coded

with the combined Walsh and Golay codes is also shown in Fig. 8.2 where a 2-bit Golay code was assigned to RZ pulses while a 4-bit Walsh code to NRZ pulses. In this case, the multiplication yields eight pulses coded by the combination of the two codes.

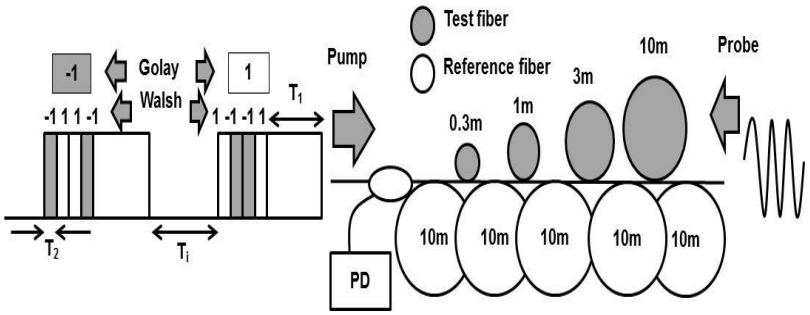

Fig. 8.2. Numerical model for combined Walsh and Golay codes PSP-BOTDA.

The durations of the 1st pulse T_1, 2nd pulse T_2 and interval T_i were 30ns, 1ns and 100ns, respectively. The optical powers for the pump and probe were respectively set to 60mW and 2mW. The artifact fiber consisted of four different lengths of test fiber; 0.3m, 1m, 3m and 10m. Reference fiber of length 10m each was spliced alternately, as shown in Fig. 8.2. The BFS difference between the test and reference fibers was 300MHz, which is equivalent to a change of 0.6% in strain. The value of the Brillouin gain spectrum width ($\Delta\nu_B$) used in the simulation was 35MHz, which translates into 9ns of τ_a. The simulations were divided into two cases; (A) assignment of Walsh codes to NRZ pulses and Golay codes to RZ pulses and (B) assignment of Walsh codes to RZ pulses and Golay codes to NRZ pulses.

8.3.2 Results and Discussions

A. Assignment of Walsh Codes to NRZ Pulses and Golay Codes to RZ Pulses Case [4]

In this simulations, the lengths of Walsh coded NRZ pulses (L_{Walsh}) were set to 1, 2, 4, 8, and 16 bits. For every L_{Walsh} case, the lengths of Golay coded RZ pulses (L_{Golay}) were set to 1, 2, 4, 8, 16 and 32 bits. Assuming that frequency difference between the pump and probe is tuned to the test fiber BFS, the simulation results for various L_{Golay} and L_{Walsh}=16bits are illustrated in Fig. 8.3.

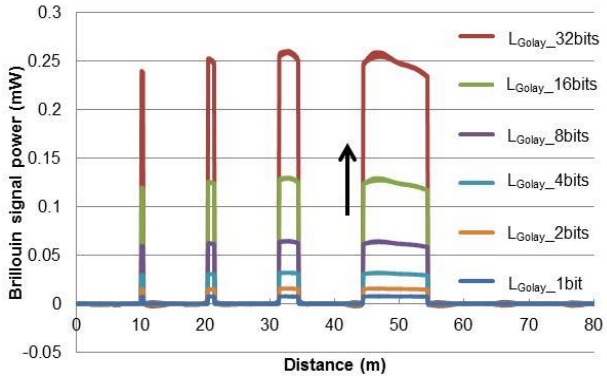

Fig. 8.3. Simulation results showing the Brillouin signals increase with L_{Golay} (RZ) for a fixed 16-bit L_{Walsh} (NRZ).

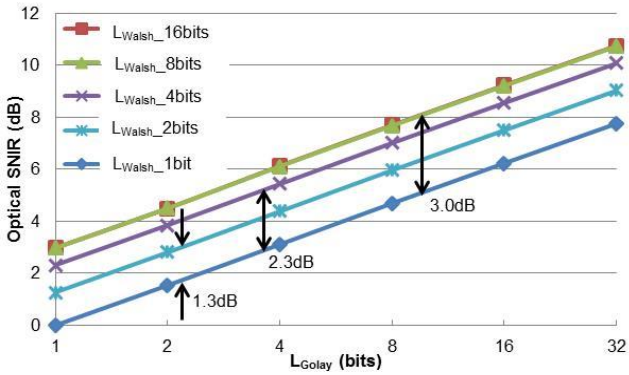

Fig. 8.4. Optical SNIR simulated at 1m test section versus L_{Golay} (RZ) for five L_{Walsh} (NRZ) cases.

It is observed from Fig. 8.3 that the Brillouin signal increases almost linearly with the increase in L_{Golay}. Furthermore, we can see that the Brillouin signals rose and fell very sharply even though the Walsh coded NRZ pulses of duration longer than τ_a was used in the simulation [4]. Compared to the correlation calculations for dual Golay codes system,

decoding process via Hadamard transform for Walsh codes produces more correct decoded Brillouin signal, due to the robustness of Hadamard transform calculations against the variation in the received signal amplitudes [2, 3]. This result is in contrast to that obtained by dual Golay codes PSP-BOTDA [1], where for L_{Golay}=16 of NRZ pulses, the rising and falling edges significantly increased, resulting in fatal degradation of the spatial resolution. For verification, we analyzed the spatial resolution at 3m test section by transforming the rise time of the Brillouin signal from 10% to 90% of its final value into rising edge length of about 8cm.

We then analyzed the optical signal-to-noise improvement ratio (SNIR) of the decoded Brillouin signals, being shown in Fig. 8.4. For a fixed L_{Walsh} case, the optical SNIR increases linearly by about 1.5dB at every doubling L_{Golay}. This result confirms that the use of coded RZ pulses contributes to the linear increase in the optical SNIR. Figure 8.4 also shows the increase in the optical SNIR with the increase in the length of Walsh coded NRZ pulses. When L_{Walsh} was set to 2, 4 and 8 bits, the optical SNIR increased to approximately 1.3dB, 2.3dB and 3.0dB, respectively, which is however, a nonlinear increment. Furthermore, the optical SNIR showed little increase when L_{Walsh}=16bits. This nonlinear increase is caused by the decrease in the Brillouin signal with ascending Walsh code sequence. To further analyze the contribution of Walsh coded NRZ pulses to the optical SNIR, we continued the simulations to calculate the optical SNIRs in the case of L_{Walsh}=1~32 (NRZ) at a fixed L_{Golay}=4 (RZ). The optical SNIRs calculated at 1m test section is shown in Fig. 8.5, showing that the optical SNIR has started to decrease when L_{Walsh}=16 and 32 bits. Therefore, from this simulation, we found that the maximum optical SNIR was obtained when the duration ($L_{Walsh}T_2$) of Walsh codes was around 8ns, near to τ_a.

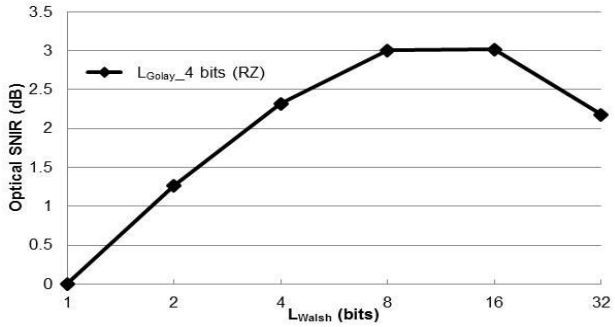

Fig. 8.5. Optical SNIR simulated at 1m test section versus L_{Walsh} (NRZ) for a fixed L_{Golay}=4bits (RZ).

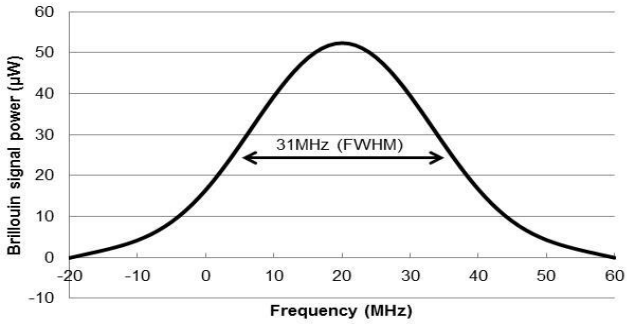

Fig. 8.6. Simulated Brillouin gain spectrum in the case of 4 bits for both L_{Walsh} and L_{Golay}.

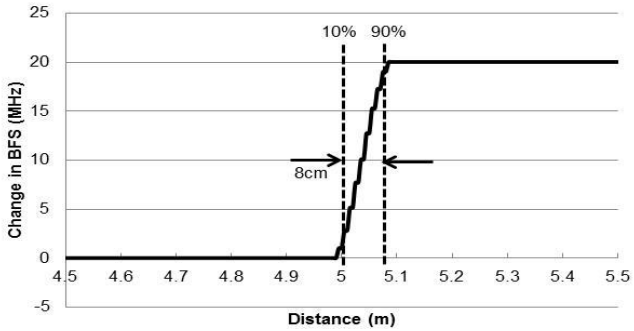

Fig. 8.7. Simulated BFS distribution around the boundary between the test and reference fibers.

Another simulation was performed for the case of small BFS difference between test and reference fibers. In this simulation, a test fiber of length 3m was spliced between two reference fibers of length 5m each. The BFS difference

was 20MHz. L_{Walsh} and L_{Golay} were both set to 4 bits. Figure 8.6 shows the BGS obtained from the simulation. From Fig. 8.6, the spectrum width obtained was 31MHz, which is almost the same with that of steady-state gain spectrum. We also confirmed that there was no distortion in the spectrum shape, confirming that the proposed coding method does not induce distortion in the BGS measured. The BFS distribution was then analyzed, being shown in Fig. 8.7. We found that the frequency variation from the true 20MHz BFS difference was as small as 0.07MHz, which might be regarded as numerical error and could be ignored. By evaluating the 80% of the total rising edge length, it was also confirmed from Fig. 8.7 that 8cm of rising edge length has been obtained, confirming a good agreement with the theoretical spatial resolution of 10cm.

B. Assignment of Walsh Codes to RZ Pulses and Golay Codes to NRZ Pulses Case [4]

In these simulations, L_{Walsh} (RZ) was set to 4 bits while L_{Golay} (NRZ) was set to 1, 2, 4, 8, 16 and 32 bits. The decoded Brillouin signals are illustrated in Fig. 8.8, showing the distortion of the Brillouin signal in the case of L_{Golay} = 16 and 32 bits. The decrease in the traced Brillouin signals in the order of Golay coded NRZ pulses has caused the appearance of significant side-lobes after the Golay codes correlation calculations [4]. The side-lobes can be clearly observed at the magnified rising edge region of 3m test section shown in Fig. 8.9.

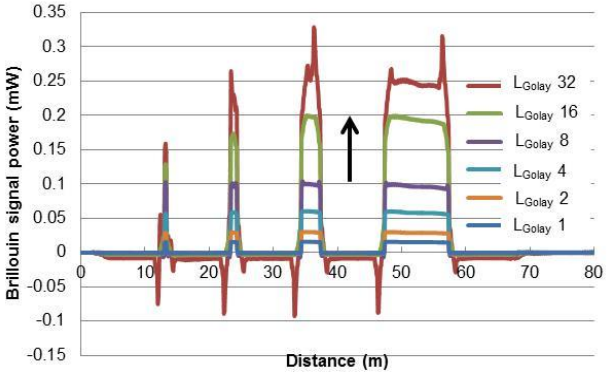

Fig. 8.8. Simulation results showing the Brillouin signals increase with L_{Golay} (NRZ) for a fixed 4-bit L_{Walsh} (RZ).

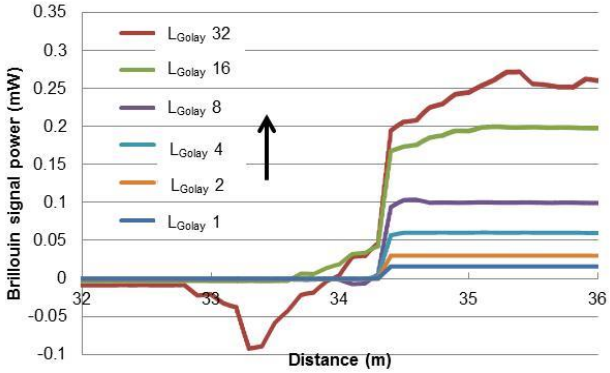

Fig. 8.9. Magnified rising edge region at 3m test section.

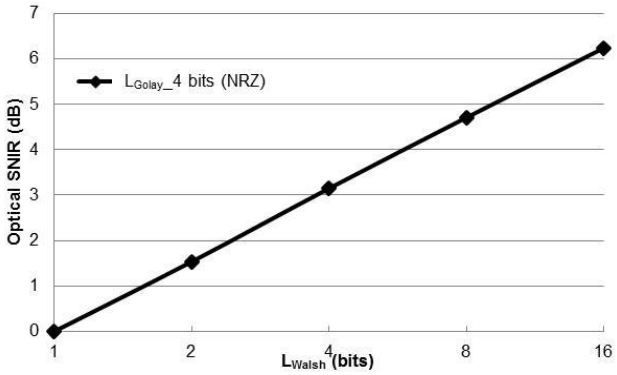

Fig. 8.10. Optical SNIR simulated at 1m test section versus L_{Walsh} (RZ) for a fixed L_{Golay}=4bits (NRZ).

We then calculated the rising edge length at 3m test section, obtaining the values of around 60cm and 160cm for 16 and 32 bits cases, respectively. The decoded Brillouin signals shown in Fig. 8.8 are quite similar to the previously proposed dual Golay codes PSP-BOTDA system [1]. Thus, it is confirmed that compared to Walsh coded NRZ pulses explained in sub-section A of Section 8.3.2, the Golay coded NRZ pulses with code duration longer than the time

constant of the acoustic wave τ_a has fatally distorted the Brillouin signal.

Another simulation was performed to examine the effect of the increase in the code length of Walsh coded RZ pulses to the optical SNIR by assuming white noise. In this analysis, L_{Golay} (NRZ) was fixed at 4 bits at all times while L_{Walsh} (RZ) was set to 1, 2, 4, 8 and 16 bits. The optical SNIR result simulated at 1m test section is shown in Fig. 8.10, indicating the optical SNIR increased linearly with L_{Walsh}. This result is identical to that shown in Fig. 8.4, showing that the optical SNIR also increases linearly with the increase in length of Golay coded RZ pulses. Therefore, it is confirmed that both Golay and Walsh codes contribute to the optical SNR improvement in accordance with $\sqrt{L}$ when the codes are assigned to RZ pulses.

8.4 Experiments

8.4.1 Experimental Setup

The arrangement of the fiber used in the experiments was similar to the simulation setup of Fig. 8.2. The experimental setup for combined Walsh and Golay codes PSP-BOTDA is almost the same with other coded PSP-BOTDAs (coded continuous-PSP-BOTDA, coded discrete-PSP-BOTDA and dual Golay codes PSP-BOTDA), except that the pump is modulated with the combined Walsh and Golay codes. The experimental setup for the combined Walsh and Golay codes is illustrated in Fig. 8.11.

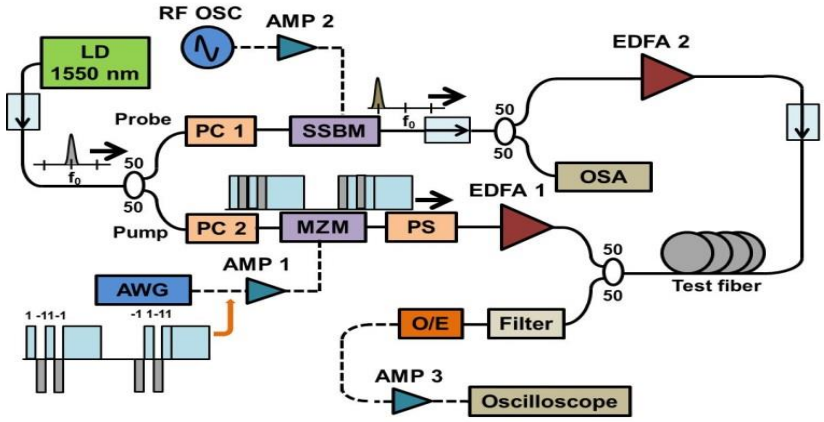

Fig. 8.11. Experimental setup for combined Walsh and Golay codes PSP-BOTDA.

The pump and probe powers and durations T_1, T_2 and T_i were set to be the same with those of simulations. Furthermore, as has been discussed and proposed in Chapter 5, to avoid electrical signal distortion for long pulse train due to the use of AC-coupled amplifier, the 1st pulse signal to drive an electro-optic modulator was alternately set to positive and negative amplitudes [7].

8.4.2 Results and Discussion

A. Assignment of Walsh Codes to NRZ Pulses and Golay Codes to RZ Pulses Case [5, 6]

Preliminary experiments were performed to analyze the relationship between the optical SNIR with the increase in the Golay coded RZ pulses. In the experiments, L_{Walsh} was fixed at 4 bits at all times while L_{Golay} was set to 2 and 4 bits. The measured Brillouin signals for both L_{Golay} cases are shown in Fig. 8.12.

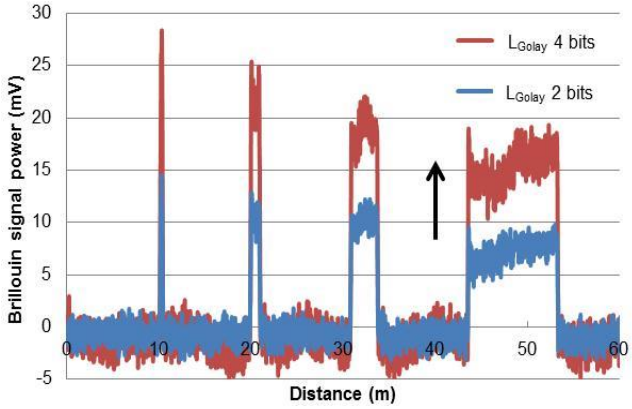

Fig. 8.12. Measured Brillouin signals for L_{Golay}=2 and 4 bits cases at fixed L_{Walsh}=4 bits.

As observed from Fig. 8.12, when L_{Golay} was increased from 2 to 4 bits, the measured Brillouin signal increased almost twice [5]. The absolute optical SNR measured at 1m test section for L_{Golay}=2bits case was about 11.4dB. We then analyzed the optical SNIR at the 1m test section for L_{Golay}=4 bits, obtaining an improvement of 1.8dB. Based on the evaluation method explained in Section 8.3.2, the achievement of 10cm spatial resolution measurement by measuring the 80% of rising edge length at all test sections for both 2 and 4 bits L_{Golay} cases was confirmed, which agrees well with the simulation result and the theoretical value.

A more detailed analysis was performed to examine the effect of the code length of Walsh coded NRZ-pulses to the optical SNR [6]. In the experiments, the code length of Golay coded RZ pulses was fixed at 4 bits while the code length of Walsh coded NRZ pulses was set to 1, 2, 4, 8 and 16 bits. The decoded Brillouin signals for all L_{Walsh} cases are illustrated in Fig. 8.13, showing that the Brillouin signal for all L_{Walsh} cases produces sharp rise and fall at the transition area between the test and reference fibers. The rising edge length measured between 10% and 90% of final peak power at the 3m test section was approximately 8cm, which was transformed from the rise time. This result is in good agreement with that of simulations discussed in sub-section A of section 8.3.2. Take note that even for $L_{Walsh}T_2$=16ns that was longer than the acoustic wave time constant τ_a of 9ns, the spatial resolution of around 10cm has been achieved. In contrast, under the same condition of coded NRZ pulse duration of 16ns, the previous dual Golay codes PSP-BOTDA had poorer performance in the spatial resolution [1]. Therefore, it has been confirmed that the high spatial resolution measurement with the combined Walsh and Golay codes has been demonstrated.

It was also observed from Fig. 8.13 that at fixed L_{Golay} (4 bits), as L_{Walsh} increased, the Brillouin signal decreased accordingly. However, the random noise also decreased more rapidly with the increase in L_{Walsh}. Thus, as a representative, the optical SNIR at the 1m test section was measured, being shown in Fig. 8.14. The maximum optical SNIR of approximately 3dB was obtained when L_{Walsh}=8 bits. Furthermore, we also analyzed the optical SNIR obtained by the proposed system compared to the conventional PSP-BOTDA without coding. The absolute optical SNR for L_{Walsh}=8 bits case was about 21.9dB, while for the conventional PSP-BOTDA the optical SNR of about 16.2dB was obtained under the same measurement time; thus, compared to the conventional PSP-BOTDA, we obtained the optical SNIR of 5.7dB, in good agreement with the calculation of 6.0dB.

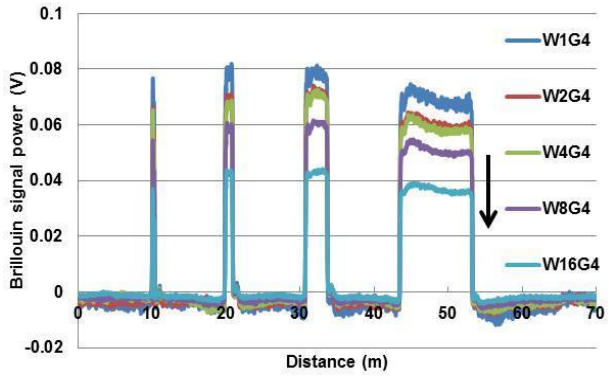

Fig. 8.13. Experimental results showing the Brillouin signals for various L_{Walsh} (NRZ) cases and L_{Golay} (RZ) = 4.

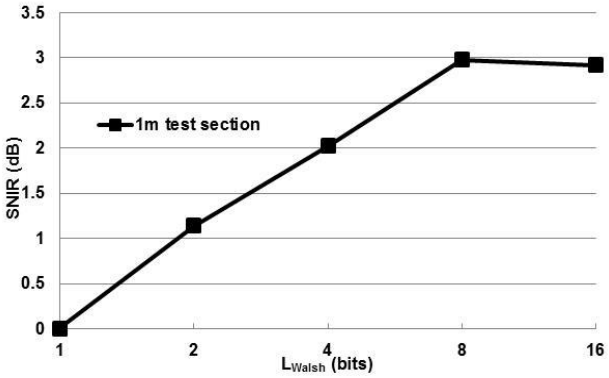

Fig. 8.14. Optical SNIR (dB) measured at the 1m test section.

B. *Assignment of Walsh Codes to RZ Pulses and Golay Codes to NRZ Pulses Case*

The contribution of the code length of Walsh coded NRZ pulses to the Brillouin signals and the optical SNIR are discussed. Since the use of Golay coded NRZ pulses of code length longer than the acoustic wave time τ_a has caused the degradation in the spatial resolution [1-3, 8], in this analysis, L_{Golay} was fixed at fixed at 4 bits while L_{Walsh} was set to 1, 2, 4, 8 and 16 bits. The measured Brillouin signals for all L_{Walsh} cases are illustrated in Fig. 8.15, showing that at all L_{Walsh} cases, the Brillouin signal power is almost same. This result is in contrast to that for Walsh coded NRZ pulses discussed in the sub-section A of section 8.4.2.

However, it is interesting to observe that even though the Brillouin signal power does not increase, the random noise decreased rapidly with the increase in L_{Walsh}. Therefore, the optical SNIRs were further analyzed; the results measured at all test sections are being shown in Fig. 8.16. It was observed in Fig. 8.16 that the optical SNIR increased almost linearly with L_{Walsh}, which agrees well with that simulation results shown in Fig. 8.10. Furthermore, we should recall that the configuration of the electrical signal for this experiment is based on that proposed in Chapter 5. It appears that the employment of the proposed signal configuration has also contributed to the linear increment of the SNIR. This strong evidence suggests that the electrical signal configuration proposed in Chapter 5 is also applicable to the combined codes system. As can be seen from Fig. 8.16, the maximum optical SNIR of approximately 6dB was obtained when L_{Walsh}=16 bits. The absolute optical SNR was also evaluated in order to compare the result with that obtained by the conventional PSP-BOTDA without coding. The absolute optical SNR for L_{Walsh}=16 bits case evaluated at the 1m test section was about 24.4dB, while for the conventional PSP-BOTDA the optical SNR of about 15.6dB was obtained under the same measurement time, indicating the achievement of maximum optical SNIR of approximately 8.8dB. In comparison with the SNR obtained with the conventional PSP-BOTDA without coding, this translates into about 60 times faster measurement speed.

Take note that the assignment of Golay codes as RZ pulses also contributes to the linear increase of optical SNIR, as being discussed based on the simulation results in Fig. 8.4 and the experimental results in sub-section A of section 8.4.2. Thus, it has been verified that both Golay- and Walsh coded RZ pulses contributes to the linear increase of optical SNIR.

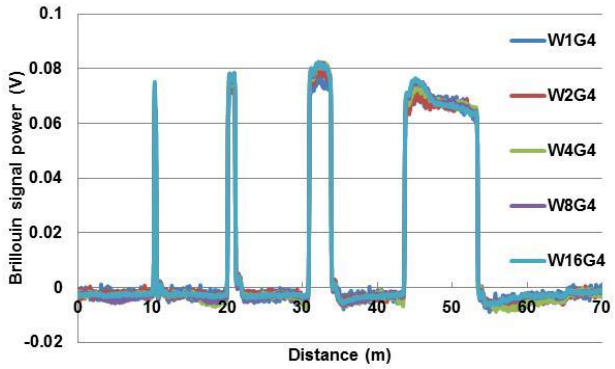

Fig. 8.15. Measured Brillouin signals for various L_{Walsh} (RZ) cases and L_{Golay} (NRZ) = 4.

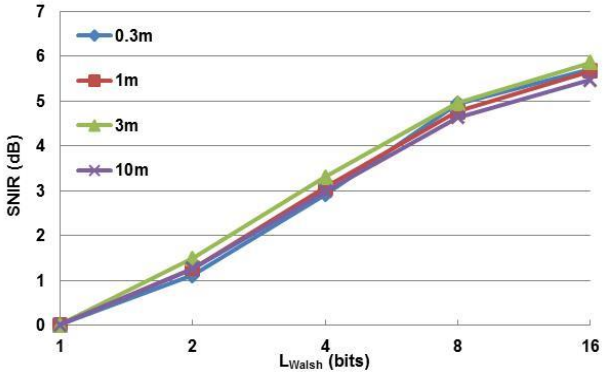

Fig. 8.16. Optical SNIR (dB) measured at all test sections.

8.5 Conclusions of Chapter

The proposal of combining two different codes in modulating the pump light of PSP-BOTDA fiber sensor for distributed strain measurement was reported. From the simulation and experimental results, it was confirmed that the assignment of Walsh codes to NRZ pulses has kept the spatial resolution high even for code length of longer than the time constant of the acoustic wave τ_a case. Even though the Brillouin signal measured by the code sequences exponentially decays, the decoding process via Hadamard transform for Walsh coded NRZ pulses in the proposed system still produces more accurate decoded signals than that via Golay codes correlation calculations. From the rising edge length result obtained with the combined codes, we achieved the spatial resolution of 10cm.

It was also found that the combination of Golay and Walsh codes has contributed higher optical SNIR than that of using only one kind of code in coded continuous- and coded discrete-PSP-BOTDAs. In the analysis, for both Golay and Walsh codes cases, it was found that the use of coded RZ pulses increases the optical SNIR by $\sqrt{L}$. For NRZ pulses, however, the improvement became slow with increasing L and finally dropped from the maximum for long code length. This is due to the decrease of Brillouin signal induced by the acoustic wave decay. It was observed that the optical SNIR reached its maximum when the code length of the NRZ pulses was 8ns, confirming that code duration of the NRZ pulses is limited by the time constant of the acoustic wave τ_a.

References

[1] **M. S. D. B. Zan** and T. Horiguchi, "A dual Golay complementary pair of sequences for improving the performance of phase-shift pulse BOTDA fiber sensor", J. Lightw. Technol. vol. 30, no. 21, pp. 3338-3356, Nov. 2012.

[2] **M. S. D. B. Zan**, T. Tsumuraya and T. Horiguchi, "The use of Walsh functions in modulating pump light of high-spatial resolution BOTDA with NRZ pulses" Proc. of the 22nd Int. Conf. on Optical Fiber Sensors (OFS-22) 2012, China, pp. 84219J-1 - 84219J-4, Oct. 2012.

[3] **M. S. D. B. Zan**, T. Tsumuraya and T. Horiguchi, "The use of Walsh code in modulating the pump light of high spatial resolution phase-shift-pulse Brillouin optical time domain analysis with non-return-to-zero pulses", J. Meas. Sci. Technol., vol. 24, no. 9, 094025, Jul. 2013.

[4] **M. S. D. B. Zan** and T. Horiguchi, "Analysis on the Employment of Combined Codes in Modulating the Pump Light of Phase Shift Pulse Brillouin Optical Time Domain Analysis (PSP-BOTDA)", Proc. of 51st Meeting on Lightwave Sensing Technol., LST51-17, pp. 115-120, Jun. 2013.

[5] **M. S. D. B. Zan**, K. Yokoyama and T. Horiguchi, "Combination of Walsh and Golay codes in modulating the pump light of

phase-shift pulse BOTDA sensor", Proc. of the IEEE 4th Int. Conf. on Photonics (ICP 2013) 2013, No. 46 D2-AM2-A, Oct. 28-30, 2013, Malacca, Malaysia.

[6] **M. S. D. B. Zan** and T. Horiguchi, "Experiments on the employment of combined Walsh and Golay codes in modulating the pump light of PSP-BOTDA system" Proc. of the 2013 IEICE Soc. Conf., B-13-38, Sept. 2013.

[7] **M. S. D. B. Zan** and T. Horiguchi, "A new electrical signal configuration for modulating pump light of coded discrete-phase shift pulse-BOTDA", Proc. of the IEEE 3rd Int. Conf. on Photonics (ICP 2012) 2012, Malaysia, pp. 294-298, Oct. 2012.

[8] D. Uchiyama, T. Horiguchi, H. Ando, Y. Okumoto, T. Sasaki and Y. Sawai, "Signal to noise improvement ratio for coded PSP-BOTDA", Technical report of IEICE. OFT 109 (377) (in Japanese), pp. 33-38, Jan. 2010.

[9] R. Muroi, T. Horiguchi, Y. Miyamoto, Y. Sato, A. Tachibana and A. Takakura, "PSP-BOTDA based on Golay code", IEICE Trans. Commun. (in Japanese), vol. J91-B, no. 11, pp. 1493-1501, November 2008.

Chapter 9: Dual Walsh Codes PSP-BOTDA

9.1 Introduction to Chapter

It has been shown numerically and experimentally in the Chapter 6 and Chapter 8 that the assignment of Walsh codes to the NRZ pulses in the coded PSP-BOTDA system does not degrade the spatial resolution of the Brillouin signal, even though the total duration of the code length used exceeds the time constant of the acoustic wave τ_a [1-4]. Furthermore, it was found that for coded continuous-PSP-BOTDA employing Golay complementary pair (GCP) (Chapter 6) and dual Golay codes PSP-BOTDA (Chapter 7) cases, the use of code duration of longer than τ_a for the NRZ coded pulses have caused the degradation in the spatial resolution. The employment of Walsh codes described in Chapter 6 has overcome this issue.

Since the employment of Walsh codes has shown great advantage especially in terms of high spatial resolution, in this chapter, the author proposes another new technique of employing dual Walsh codes in the coded PSP-BOTDA. Similar to the dual Golay codes described in Chapter 7, NRZ and RZ pulses formations were employed in this new technique, except that rather than using two GCPs, two Walsh codes are assigned to the respective NRZ and RZ pulses. Simulation analyses were performed and the results obtained were also compared with that obtained by the dual Golay codes to identify their performance.

9.2 Pump Light Configurations

Figure 9.1 illustrates an example of a pump light of PSP-BOTDA that is composed of the 1st pulses and the dual Walsh coded 2nd pulses. The pump light configuration shown in Fig. 9.1 was generated from two Walsh codes having the same code length of 4 bits and the same bit elements (1, -1, 1, -1). The process of generating the dual Walsh codes is exactly the same with that of generating dual Golay codes or combined Walsh and Golay codes. Since Walsh codes are generated based on a Hadamard matrix, the process of combining an $M \times M$ Hadamard matrix with another $N \times N$ Hadamard matrix will generate dual Walsh codes that have $M \times N \times 2$ number of code patterns. As has been explained in the previous chapters, the factor 2 denotes the needs of using codes' inversion for the measurement in the coded PSP-BOTDA. The code length of the generated dual Walsh codes is $M \times N$.

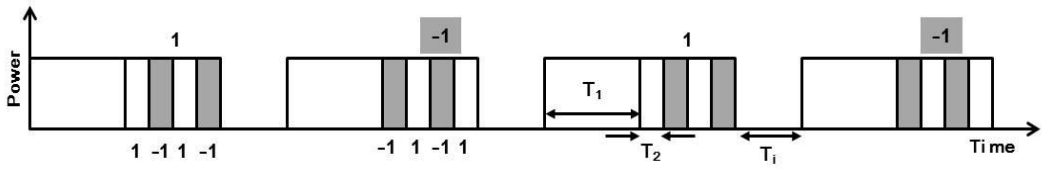

Fig. 9.1. A configuration showing the combined two Walsh codes (dual Walsh codes) in a single pump light of PSP-BOTDA. The Walsh codes used in the configuration were both set to 4 bits.

9.3 Simulations

9.3.1 Simulation Setup

The numerical model for the dual Walsh codes PSP-BOTDA is depicted in Fig. 9.2. Generally, the model is almost the same with the model for dual Walsh codes or combined Walsh and Golay codes systems, which is based on the model introduced by Lecoeuche et al. [5]. The code length for the discrete part, L_{disc} was set at 4 bits throughout the simulations, while the code length for the continuous part, L_{cont} was set to 1, 2, 4, 8 and 16 bits. Four test fibers of 0.3m, 1m, 3m and 10m in length were set in the simulations. Between the test sections, reference fibers of 10m in length were

set. The BFS of the test fibers was set to 300MHz lower than that of the reference fibers, which was approximately 0.6% strain.

9.3.2 Results and Discussions

A. Coded Pulse Duration T_2 = 2ns Case

In this simulation analysis, the durations T_1, T_2 and T_i were respectively set to 30ns, 2ns and 100ns. The pulse duration T_2 of 2ns translates into 20cm of spatial resolution. The pump and probe powers were set to 60mW and 2mW, respectively. Tuning the frequency difference of the two lights to match with the BFS of the test fibers, we obtained the simulated Brillouin signals for L_{cont}=1, 2, 4, 8 and 16 bits at fixed L_{disc}=4 bits as illustrated in Fig. 9.2, indicating that the signals rise and fall sharply at all test sections, even for L_{cont}=16 bits ($L_{cont}T_2$=32 ns) case. Thus, we obtained the spatial resolution of 16cm by transforming the 10%~90% (80% of total time) of rise/fall time of the signal at the transition area into distance value, proving that the results agree well with the theoretical one. In addition, as expected, at fixed L_{disc}, we observed the decrease in the average of processed Brillouin signal with the increase in the L_{cont}, which was due to the fact that the acoustic wave excited by the 1st pulse for SBS generation experiences exponential decrease with time.

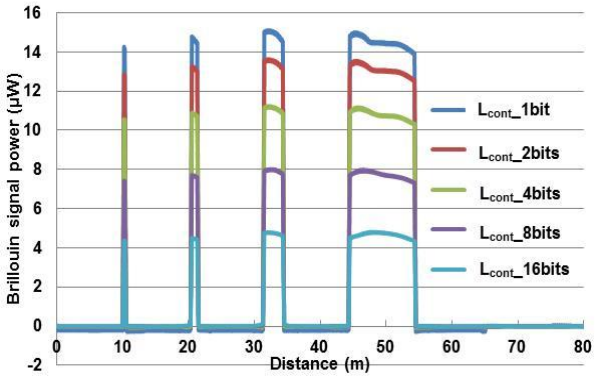

Fig. 9.2. Simulated Brillouin signals for dual Walsh codes with various L_{cont} cases at fixed L_{disc} = 4 bits.

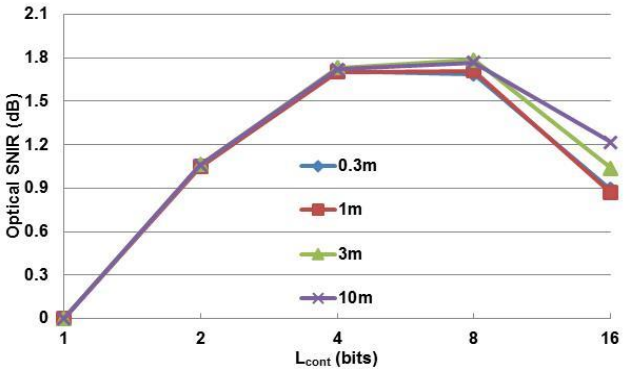

Fig. 9.3. Calculated optical SNIR at all test sections for dual Walsh codes case.

Considering the inclusion of random noise and the same measurement times for all L_{cont} cases, we then calculated the optical SNIRs (dB) of the simulated signals, being depicted in Fig. 9.3. The optical SNIRs plotted in Fig. 9.3 were calculated at all test sections, showing that the optical SNIRs reached their maximum value of around 1.7dB for L_{cont} = 8 and 16 bits cases.

B. Coded Pulse Duration T_2 = 1ns Case

In this simulation, the coded pulse duration, T_2 was set to 1ns, which translates into 10cm of spatial resolution. Figure 9.4 plots the calculated Brillouin signal for L_{disc}=4 bits and L_{cont}=1, 2, 4, 8 and 16 bits cases, when the frequency difference between the pump and probe was tuned to the BFS of the test fibers. It was observed from Fig. 9.4 that the transitions of the Brillouin signals at all test sections were very sharp, even in the case of L_{cont}=16 bits (16 ns) that is much longer than the time constant of the acoustic wave τ_a (9ns). Calculating the rise time between 10% and 90% of the Brillouin signals, 8cm of rising edge length was obtained at all test sections for all L_{cont} cases. As explained in Chapter 6, it should be noted that since the acoustic wave excited by the 1st pulse (T_1) exponentially decays, one can see from Fig. 9.4 that as L_{cont} increased, the average Brillouin signal processed decreased accordingly.

On the other hand, in the case of dual Golay codes, as depicted in Fig. 9.5, the side-lobes that appeared at all test sections for L_{cont}=16 and 32 bits cases have caused the increase in the rising and falling edge lengths [4]. Applying the

same evaluation method to analyze the spatial resolution, for L_{cont} of 16 and 32 bits, the rising edge lengths obtained were 50cm and 130cm, respectively. Therefore, by comparing the simulation results illustrated in Figs. 9.4 and 9.5, it has been confirmed that compared to dual Golay codes, one can obtained more accurate Brillouin signal recovery with the use of dual Walsh codes.

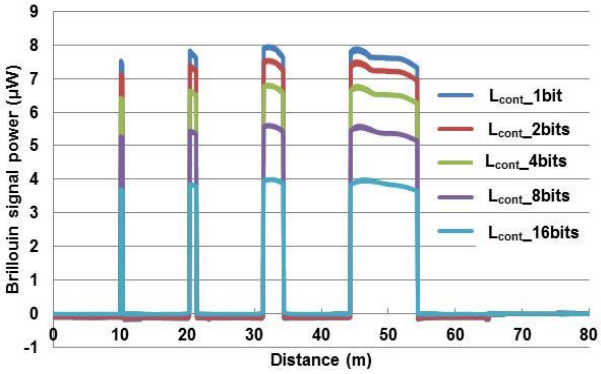

Fig. 9.4. Simulated Brillouin signals for dual Walsh codes with various L_{cont} cases at fixed L_{disc} = 4 bits.

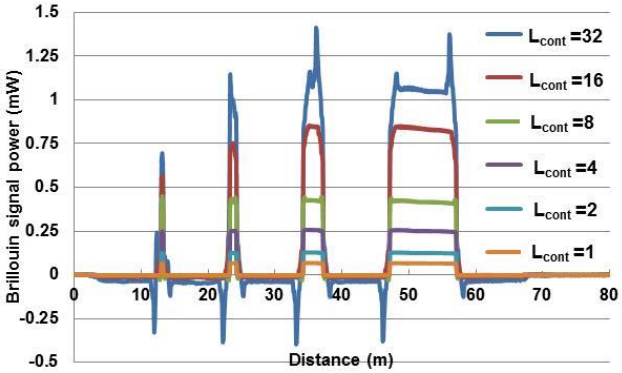

Fig. 9.5. Simulated Brillouin signals for dual Golay codes with various L_{cont} case at fixed L_{disc} = 4 bits.

Then, the optical SNIRs of the simulated Brillouin signals employing dual Walsh codes were also analyzed and compared with that of dual Golay codes, being depicted in Figs. 9.6 and 9.7, respectively. In the case of dual Walsh codes, it is clearly observed from Fig. 9.6 that the maximum optical SNIR was obtained when L_{cont} = 8 and 16 bits.

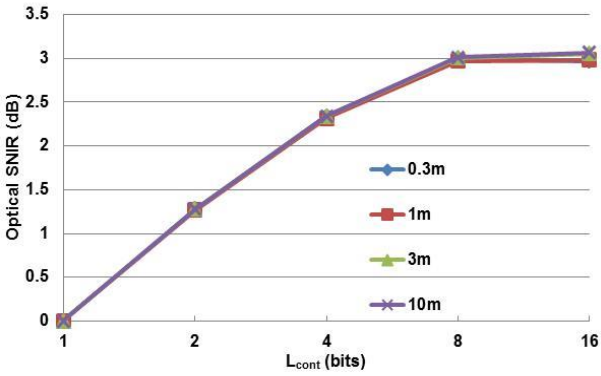

Fig. 9.6. Calculated optical SNIR at all test sections for dual Walsh codes case.

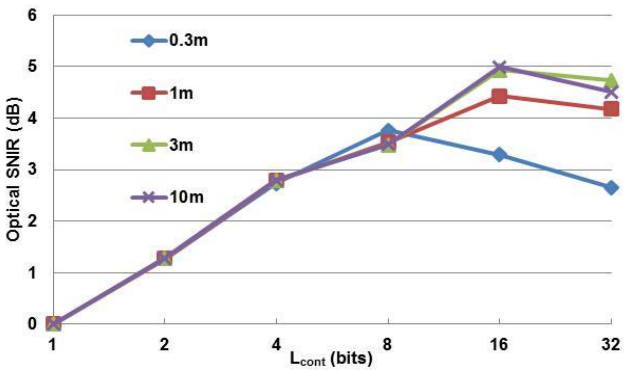

Fig. 9.7. Calculated optical SNIR at all test sections for dual Golay codes case.

In contrast, in the case of dual Golay codes of Fig. 9.7, by accounting the scattered optical SNIRs for L_{cont}=16 and 32 bits at all four test sections, it was considered that the maximum optical SNIR was obtained when L_{cont} = 8 bits. Even though the optical SNIRs further increased for longer L_{cont} (16 and 32 bits) for the test fibers other than the 0.3m fiber, these optical SNIRs were merely caused by the crosstalk for different test length [1, 4]. As the amount of crosstalk contribution varied with the length of the individual test fiber, the amount of the optical SNIR also varied; causing the scattered optical SNIR results for L_{cont} of longer than 8 bits cases, as can be seen from Fig. 9.7. Also, the slightly higher optical SNIR for dual Golay codes than that for dual Walsh codes can be explained by the crosstalk to the intrinsic signal after the auto-correlation calculations for decoding the dual Golay codes, indicating that the optical SNIRs obtained by employing dual Walsh codes would give more sensible results.

9.4 Experiments

9.4.1 Experimental Setup

Preliminary experiment on dual Walsh codes were performed with the parameter was set to be the same with that of the simulations. However, in this preliminary experiment, we only analyzed the impact of L_{disc} on the Brillouin signals. In this case, L_{cont} was fixed to 4 bits throughout the experiments, while L_{disc} was set to 1, 2 and 4 bits. The coded pulse duration T_2 was set to 1ns, which theoretically translates into 10cm of spatial resolution. In addition, the configuration of the electrical signal was made based on the configuration proposed in Chapter 5. In details, the amplitudes of the 1st pulses were set to positive and negative values alternately, so that amplified electrical signals with uniform amplitude can be generated (see Chapter 5). To perform a fair analysis, the measurement for all L_{disc} cases was performed under the same measurement time. The measurement with conventional PSP-BOTDA without coding was also performed and its optical SNR was analyzed. Thus, based on the SNR result, the improvement in the SNR (SNIR) contributed by L_{disc} can also be examined. With the increase in L_{disc}, it is apparent beforehand that an increase in the SNR would be a desirable outcome.

9.4.2 Results and Discussion

We begin the discussion with the analysis on the decoded Brillouin signals, being illustrated in Fig. 9.8.

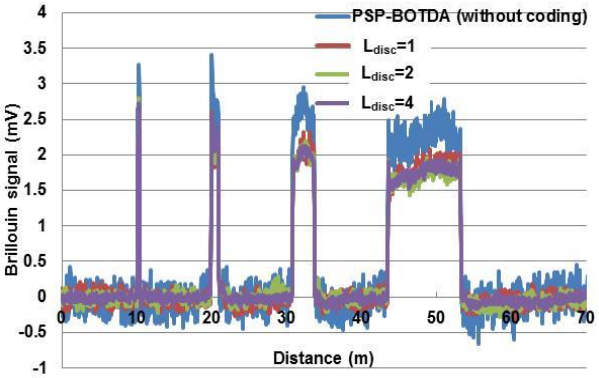

Fig. 9.8. Decoded Brillouin signals for dual Walsh codes with various L_{disc} at fixed L_{cont} (=4 bits).

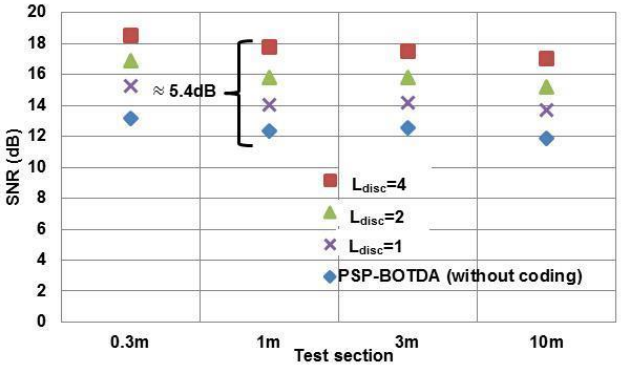

Fig. 9.9. Measured optical SNIR for various L_{disc} at fixed L_{cont} (=4bits).

As clearly observed from Fig. 9.8, under the same measurement conditions, the measured Brillouin signal is almost same for all L_{disc} cases. However, it is also seen that the random noise decreased with L_{disc}. In addition, for all L_{disc} cases, we found little distortion at the rising and falling edges at all test sections, except for random noise. As a representative, we calculated the 80% of rising edge length at 10m test section and obtained 8cm of rising edge length for all L_{disc} cases. Therefore, this result suggests that the spatial resolution of 10cm can be obtained for any L_{disc} case.

We then performed the analysis on the SNR, being depicted in Fig. 9.9. It was found that from the PSP-BOTDA without coding case to L_{disc}=1 case (L_{cont} fixed at 4 bits) that, at 0.3m test section, the SNR increased from 13.1dB to 15.2dB; about 2dB of SNR improvement. Furthermore, for L_{disc}=2 and 4 bits cases, the SNR further increased significantly up to respectively 17dB and 18.5dB; a linear increase in the SNIR. For all test sections, the total SNIR was between 5.0 dB ~ 5.4dB, which is in good agreement with the theoretical SNIR. Even though the experiments were performed only for three L_{disc} cases, we have experimentally verified the effectiveness of pump light coding with dual Walsh codes in improving the SNR of the Brillouin signal. We should also take note that the electrical signal configuration that based on the analysis in Chapter 5 has also contributed to this linear SNIR increment. Furthermore, it

is suggested that there is a tendency for the SNR to further increase with the use of longer L_{disc}. As future works, the analysis on the effect of L_{cont} to the measured signals should be performed in order to further analyze the effectiveness of the proposed code system.

9.5 Conclusions of Chapter

9.5.1 Comparison with dual Golay codes (Simulations)

We have performed the simulations of PSP-BOTDA employing dual Walsh codes and compared the results with that obtained with dual Golay codes. For clearer understanding on the comparison between the dual Walsh codes and dual Golay codes, the simulation results for both techniques are concluded in Table 9.1. As has also been explained in Chapter 6, the robustness of Hadamard transform against the variations in the received signal amplitudes during the decoding process for dual Walsh codes has contributed to the achievement of high spatial resolution measurement, even for $L_{cont}T_2$ > time constant of the acoustic wave τ_a cases [1]. In contrast, for dual Golay codes PSP-BOTDA, the appearance of side-lobes has caused the increase in the rising and falling edge lengths when the dual Golay codes of $L_{cont}T_2$ longer than τ_a were used [4]. For code sequence beyond τ_a, the Brillouin interaction became weak and this consequently distorted the Brillouin signal after the correlation.

Table 9.1. Comparison between dual Walsh codes- and dual Golay codes PSP-BOTDAs (requirements of total code duration $L_{cont}T_2$)

	dual Walsh codes	dual Golay codes
Spatial resolution=10cm or 20cm	$L_{cont}T_2$ up to 16 ns or more	$L_{cont}T_2 \leq$ 9ns (time constant of the acoustic wave)
Maximum optical SNIR	$L_{cont}T_2$ = 8 and 16ns cases	$L_{cont}T_2$ = 8ns

In terms of the optical SNIR, for dual Walsh codes case, the maximum optical SNIR was obtained when $L_{cont}T_2$ is set to around τ_a and $2\tau_a$, while for dual Golay codes the optical SNIR reached its maximum value when $L_{cont}T_2$ was set around τ_a. Based on these findings, one might conclude that both dual Walsh- and dual Golay codes would exhibit the same measurement performance. However, if one takes into account the spatial resolution results obtained by these two techniques, the dual Walsh codes would provide better tolerance of setting the total duration of the coded NRZ pulses ($L_{cont}T_2$) than Golay code to achieve the best optical SNIR and simultaneously maintain high spatial resolution. This is especially beneficial in the practical applications when one tries to measure strain along a fiber having varied Brillouin gain bandwidth. Therefore, it can be concluded in this chapter that the employment of dual Walsh codes in coding the pump light of the PSP-BOTDA offers better measurement performance than that of the dual Golay codes PSP-BOTDA.

9.5.2 The Impact of L_{disc} on Brillouin Signals (Preliminary Experiment)

We have performed preliminary experiment on dual Walsh codes to study the impact of L_{disc} to the measured Brillouin signals. For all L_{disc} cases, it was found that the measured Brillouin signal is almost at the same level, but with decreased in random noise amplitude in inverse proportion to L_{disc}. Furthermore, it was found that the SNIR increased linearly with the increase in L_{disc}, which is consistent with the theoretical SNIR increment. Under the same measurement time, the SNR obtained with the conventional PSP-BOTDA without coding was about 13.1dB, while for L_{disc}= 4 bits (L_{cont} fixed at 4 bits), the SNR was about 18.5dB. This gives the total SNIR of about 5.4dB, which agrees well with the theoretical SNIR (6dB). We concluded from the experimental results that the increment of L_{disc} in dual Walsh coded PSP-BOTDA has contributed to the linear increase in the SNIR. However, we should note that the employment of new design in the electrical signal, which is based on the proposal explained in Chapter 5, also plays an important role in realizing such a good SNIR result. In addition, we also conclude that even though only three cases of L_{disc} were studied,

the use longer L_{disc} would also contribute to the linear increment in SNIR; as future works, this analysis should be performed. Also, in the future, the experimental analysis on the impact of L_{cont} on the Brillouin signals should be conducted in order to gain a deeper understanding of the dual Walsh codes employment in PSP-BOTDA technique.

References

[1] **M. S. D. B. Zan**, T. Tsumuraya and T. Horiguchi, "The use of Walsh code in modulating the pump light of high spatial resolution phase-shift-pulse Brillouin optical time domain analysis with non-return-to-zero pulses", J. Meas. Sci. Technol., vol. 24, no. 9 (094025), pp. 1-13, Jul. 2013.

[2] **M. S. D. B. Zan** and T. Horiguchi, "Analysis on the Employment of Combined Codes in Modulating the Pump Light of Phase Shift Pulse Brillouin Optical Time Domain Analysis (PSP-BOTDA)", Proc. of 51st Meeting on Lightw. Sensing Technol., LST51-17, pp. 115-120, Jun. 2013.

[3] **M. S. D. B. Zan**, K. Yokoyama and T. Horiguchi, "Combination of Walsh and Golay codes in modulating the pump light of phase-shift pulse BOTDA sensor", Proc. of the IEEE 4th Int. Conf. on Photonics (ICP 2013) 2013, No. 46 D2-AM2-A, Oct. 28-30, 2013, Malacca Malaysia.

[4] **M. S. D. B. Zan** and T. Horiguchi, "A dual Golay complementary pair of sequences for improving the performance of phase-shift pulse BOTDA fiber sensor", J. Lightw. Technol. vol. 30, no. 21, pp. 3338-3356, Nov. 2012.

[5] V. Lecoeuche, D. J. Webb, C. N. Pannell and D. A. Jackson, "Transient response in high-resolution Brillouin-based distributed sensing using probe pulses shorter than the acoustic relaxation time", Opt. Lett., vol. 25, no. 3, pp. 156-158, Feb. 2000.

Chapter 10: Analytical Study on the Measurement Performance of BOTDA Employing Proposed Coding Techniques

10.1 Introduction to Chapter

In this chapter, the measurement performance of BOTDA by employing the proposed coding techniques is numerically analyzed.

The BFS measurement in BOTDA is performed by estimating the peak frequency of the BGS measured at multiple frequencies. The measurement error can be classified into two; the error due to random noise and the systematic error of the measurement system. For the former, the error depends on the SNR, while for the latter the error is caused by the nonlinear effects in fiber.

At the beginning of this section, the SNR measured at the peak frequency and its relationship with the error in the BFS will be explained.

In addition, within the range of first-order approximation, the intensity of the BOTDA signal increases with the increase in the pump and probe powers. However, the maximum power of the pump light that can be injected into the fiber is limited by nonlinear effects occurring in the fiber. Thus, in the next section, the main factors of nonlinear effects such as self-phase modulation, modulation instability and the Raman scattering will be explained.

Furthermore, the systematic error of the measurement system occurs when the transfer of the pump power to the probe during the Brillouin amplification process cannot be neglected; it is called pump depletion. Therefore, in the next sections, the dependence of pump depletion on the probe power and the relationship between the probe power and the error in BFS is described.

At the end of this chapter, based on the study results, the measurement performance of the conventional BOTDA without coding and BOTDA employing proposed coding techniques will be explained.

10.2 Relationship Between SNR and the Error in BFS Measurement

SNR is of important factor in determining the measurement accuracy of the BFS. In the early study of BOTDA, the relationship between BFS error ν_{Be} and SNR is given as follows [1].

$$\nu_{Be} = \Delta\nu_B / \sqrt{2}\,(SNR_e)^{\frac{1}{4}} \tag{10.1}$$

It should be noted that SNR_e in Eq. (10.1) is the SNR for electrical signal. Since the SNR used in this thesis is for optical signal, SNR $= \sqrt{SNR_e}$. Equation (10.1) is derived by assuming that the BFS should be regarded as the frequency at which the Brillouin signal becomes maximum although random noise is superimposed on the signal. Equation (10.1) describes the importance of the SNR in determining the accuracy of BFS in BOTDA, and also the degradation of BFS measurement accuracy due to the increase in the Brillouin gain bandwidth $\Delta\nu_B$. However, in the recent BOTDA studies, the BFS is determined by approximating the suitable function to the data of the BGS measured at multiple frequencies. Therefore, based on the actual calculation procedure, the relationship between the BFS error and SNR was studied. The numerical calculation was performed according to the following assumptions.

i) The BGS is Lorentzian having gain bandwidth $\Delta\nu_B$ of 35MHz.

ii) The frequency analyzed is ranged within the FWHM of the BGS with 2MHz step.

iii) The spectral shape is approximated by a quadratic polynomial.

iv) The peak frequency obtained from the equation is regarded as the BFS.

v) The probability distribution of noise is Gaussian.

vi) The standard deviation of the BFS obtained is defined as the measurement error.

The result of the numerical calculation is depicted in Fig. 10.1. It should be noted here that the SNR is defined for the optical signal. It was found from Fig. 10.1 that the BFS error decreased significantly for the SNR of 8dB and larger. For SNR less than 8dB the error increased steeply. Along with the increase in the random noise, the BFS approximate expression has become very close to the linear equation, causing huge error in the BFS for SNR of lower than 8dB. When SNR = 8dB, the BFS error determined from standard deviation was approximately 1MHz. Therefore, it is concluded that the SNR of 10dB is satisfactory in order to realize a BFS measurement with error of below 1MHz.

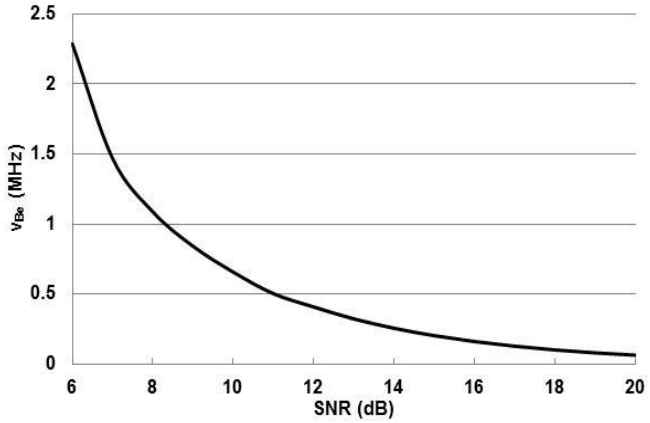

Fig. 10.1. The relationship between the optical SNR and the error in BFS measurement.

10.3 Maximum Pump Power and Its Relationship with Nonlinear Effects

The maximum pump power that can be used in the BOTDA is mainly limited by the self-phase modulation, modulation instability and stimulated Raman scattering (SRS) [2].

The pump light frequency is shifted by self-phase modulation effect when Gaussian-like pulse of high peak power is used [3]. Since the amount of the frequency shift is inversely proportional to the pulse width, the effect of self-phase modulation becomes dominant especially when performing high spatial resolution measurement. For instance, for a pump of width 65ns and peak power 23dBm propagating through a 25km length of fiber, the frequency shift was about ±10MHz. Furthermore, the increase in Brillouin gain bandwidth of 25MHz was also observed in experiments [4]. However, since the frequency shift also depends on the shape of the pump pulse, it was found that the effect of self-phase modulation is less susceptible when using pump pulse that is close to square wave [2], [4].

Modulation instability (MI) occurs in the wavelength region of anomalous dispersion of the optical fiber [3]. In the case of standard SMF, 1.3μm wavelength gives zero dispersion while longer wavelength gives anomalous dispersion. Therefore, MI effect can easily occur when injecting an LD light of wavelength 1.5μm into a standard SMF. In fact, the effect of MI when injecting a pump light of pulse width 20ns and peak power of higher than 24dBm into a standard SMF of length 11.8km has been reported [5].

In addition, the effect of forward SRS also gives a significant limit to the pump power. The threshold of the pump power is however much higher than that for MI effect [3]. Thus, it is understood that in the wavelength region of anomalous dispersion where MI effect becomes dominant, the SRS could be ignored. Nevertheless, if one uses dispersion-shift fiber (DSF) in the wavelength region for normal dispersion, SRS effect would play a role in limiting the pump power.

From the above explanations, it can be concluded that the maximum optical pump power available for measurement differs depending on the pump pulse shape and the fiber type. Based on the previous experimental findings explained above, the use of pump pulse of maximum power 20dBm was considered a safe choice to analyze the performance of BOTDA.

10.4 Pump Depletion Effects and Its Impact on Probe Power Limitation

It is known that the maximum probe power is limited by pump depletion effect [6], [7]. When pump light propagates along a fiber, it experiences power loss due to the Brillouin amplification. The effect of pump depletion can be expressed as the transmittance *D* of the pump light, which is given as

$$D(\delta\nu) = exp\left[-\frac{g}{A} S_B(\delta\nu) P_{cw}^i \frac{\{1-exp(-\alpha L)\}}{\alpha}\right] \tag{10.2}$$

where

$$S_B(\delta\nu) = \frac{\left(\frac{\Delta\nu_B}{2}\right)^2}{\delta\nu^2 + \left(\frac{\Delta\nu_B}{2}\right)^2} \tag{10.3}$$

and

$$\delta\nu = \Delta\nu - \nu_B \tag{10.4}.$$

It can be seen from Eq. (10.2) that *D* becomes minimum when the frequency difference $\Delta\nu$ between the pump and the probe coincides with the BFS ν_B, while it approaches to unity when $\Delta\nu$ moves away from ν_B. In Eq. (10.2), g is the Brillouin gain coefficient, *A* is the fiber effective cross-section, P_{cw}^i is the probe input power, α is the fiber loss coefficient, *L* is the fiber length and $\Delta\nu_B$ is the Brillouin gain bandwidth measured as full width at half maximum value (FWHM).

Therefore, the BGS measured from pump light intensity having such a frequency characteristic would be distorted compared to the original spectrum, which would produce the error in the BFS. The error ν_{Be} is greatest when measuring the end of a fiber having a uniform BFS value. In this worst condition, let us assume that the change in the BFS at the fiber end is δ_B. Then, the distorted spectrum measured at the fiber end due to the pump depletion can be described as

$$I(\delta\nu) = D(\delta\nu + \delta_B)\left\{exp\left[\frac{g}{A} S_B(\delta\nu) P_P^i exp(-\alpha L) \frac{\left(c/n\right)\tau}{2}\right] - 1\right\} \tag{10.5},$$

where $\delta\nu$ is the detuning amount of frequency difference between the pump and the probe at the fiber end, P_P^i is the pump input power, *c* is the speed of light in vacuum, *n* is the fiber refractive index and τ is the pump pulse width. Since τ is very narrow, Eq. (10.5) can be approximated as

$$I(\delta\nu) = J(\delta\nu)\frac{g}{A} P_P^i exp(-\alpha L)\frac{\left(c/n\right)\tau}{2} \tag{10.6},$$

where

$$J(\delta\nu) = D(\delta\nu + \delta_B) S_B(\delta\nu) \tag{10.7}.$$

Therefore, $\delta\nu$ that maximizes Eq. (10.7) gives the measurement error ν_{Be} of the BFS of the fiber end [7].

In calculating the measurement error ν_{Be}, the Brillouin gain coefficient was set to the typical value of $g =$

$1.12\text{x}10^{-11}$ m/W. In addition, the effective cross-section for standard SMF was assumed to be $A = 90\mu m^2$. The numerical calculation results are depicted in Fig. 10.2. From Fig. 10.2 (a), for fiber length L = 1km, the measurement error in the BFS for both α =0.2 dB/km and 0.3 dB/km cases is almost same. In addition, for probe input power of P_{cw}^{i}=0dBm, the maximum $\nu_{Be}/\Delta\nu_B$ was approximately 0.02. If we use $\Delta\nu_B$=35MHz, this translates into ν_{Be}= 0.7MHz that is lower than 1MHz (1MHz corresponds to $2\text{x}10^{-5}$ in strain and 1°C in temperature). From Fig. 10.2 (b), for fiber length L = 10km, the measurement error in the BFS for α =0.2 dB/km case is slightly higher than that for α =0.3 dB/km case. However, when the probe input power was set to P_{cw}^{i}= -10dBm, ν_{Be} for both cases is lower than 1MHz.

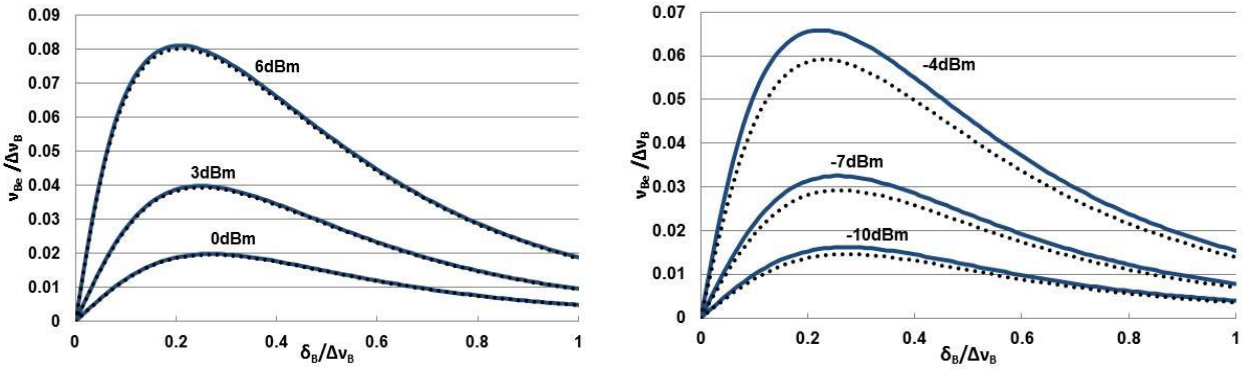

(a) (b)

Fig. 10.2. Relationship between frequency error ν_{Be} and BFS difference δ_B. (a) L=1km, (b) L=10km. The power in dBm unit shown in the graph is the probe input power. The solid line and dotted line represent the result for α =0.2 dB/km and 0.3 dB/km cases, respectively.

10.5 Numerical Results of the SNR for BOTDA and Discussions

When we use a photo diode (PD) for direct detection, the signal-to-noise ratio SNR_{PD} can be described as follows

$$SNR_{PD} = \frac{i_s}{\sqrt{\left(2ei_{cw} + \frac{4FkT}{R}\right)B}} \tag{10.8},$$

where i_s is the photocurrent from the increase amount in BOTDA optical signal power detected by PD and i_{cw} is the photocurrent from the probe power detected by the PD. Since the Brillouin amplification rate is very small, we assume that $i_s << i_{cw}$. Furthermore, e=$1.60\text{x}10^{-19}$ C is the electron charge, k=$1.38\text{x}10^{-23}$ J/K is the Boltzmann coefficient, T=300K is the room temperature given in Kelvin unit and R=50 Ω is the load resistance. The bandwidth of receiver B is given by $B = 1/\tau$ Hz where τ is pump pulse width. The noise figure of amplifier F was set to F=3. The photocurrents i_s and i_{cw} are proportional to the optical signal power, which can be described as follows.

$$\begin{aligned} i_s &= S\Delta P_{cw} \\ i_{cw} &= SP_{cw} \end{aligned} \tag{10.9},$$

where S is the sensitivity coefficient of PD, which is about 1.12 (A/W) for 1550nm wavelength case. Furthermore, ΔP_{cw} is the increase amount of probe power detected by PD due to Brillouin amplification while P_{cw} is the probe power detected by PD.

In this BOTDA model, we consider the utilization of optical circulator as a directional coupler to channel the BOTDA signal to the PD. In this case, if we can neglect the pass loss, the Brillouin amplified signal ΔP_{cw} at far end of the fiber, i.e. at the probe side, which is detected by the PD at the pump side can be described as

$$\Delta P_{cw} = \left[exp\left(\frac{g}{A} P_P^i e^{-\alpha L} \frac{\left(c/n\right)\tau}{2} \right) - 1 \right] P_{cw}^i e^{-\alpha L} \quad (10.10).$$

Similarly, we can describe P_{cw} detected by the PD as

$$P_{cw} = P_{cw}^i e^{-\alpha L} \quad (10.11).$$

Based on the above discussion, we calculated the SNR for coded PSP-BOTDA. In the calculation, we set $\alpha = 0.3\text{dB/km}$. Then, we calculated the SNR for spatial resolution Δz = 10cm (τ=1ns) and 2cm (τ=0.2ns) for fiber length L=1km and 10km cases. In the calculation, it is assumed that τ=0.2ns is the minimum pulse duration that can be set for obtaining the highest spatial resolution, in order to avoid the signals overlap in the frequency region between the Rayleigh scattered light and the amplified probe light.

For Δz = 10cm, L=1km case, the relationship between the SNR and measurement time is illustrated in Fig. 10.3. It should be noted that the x-axis in Fig. 10.3 shows only the total time required for measuring BOTDA signal at a given frequency value. Therefore, in the actual measurement, this measurement time must be multiplied with the number of the steps of the frequency sweep. Take note that the same consideration is also applied when describing the relationship between the SNR and the measurement time illustrated in Figs. 10.4, 10.5 and 10.6. For sweeping 100MHz of frequency range with frequency step of 2MHz, the number of steps would be 51.

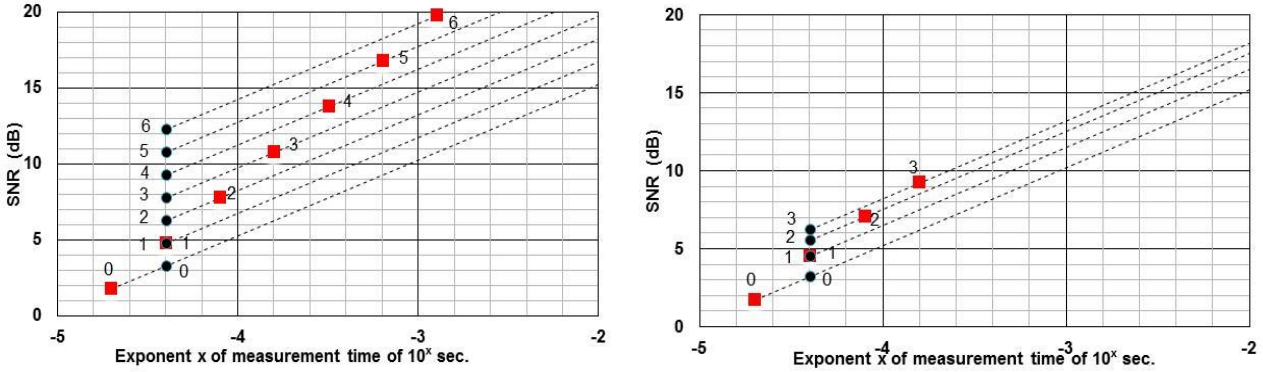

(a) (b)

Fig. 10.3. The relationship between the SNR and the measurement time for coded PSP-BOTDA case. L=1 km, Δz=10 cm. (a) coded discrete-PSP-BOTDA (●Golay, ■Walsh), (b) coded continuous-PSP-BOTDA (●Golay, ■Walsh).

In Fig. 10.3, the ● and ■ signs show the SNR results for coded discrete-PSP-BOTDA employing Golay code and Walsh code, respectively. The numbers assigned next to ● and ■ signs indicate the index numbers of code length of power of 2. In Fig. 10.3 (a) for coded discrete-PSP-BOTDA, the code time for 1 bit includes pre-pump pulse duration of 30ns, 1 bit pulse duration of 1ns and bit interval duration of 100ns, which give the total duration of 131ns. Furthermore, for fiber of length L=1km, the RTT of light to travel the fiber is 10μs. Therefore, it is explicitly understood that the maximum code bit for coded discrete-PSP-BOTDA technique is 10μs/131ns≒76 bits.

Fig. 10.3 (a) illustrates the results for code lengths of 2^0, 2^1, 2^2, 2^3, 2^4, 2^5 and 2^6 which comply with the above condition. Furthermore, in calculating the measurement time, it is assumed that the measurement time it takes for a single codeword corresponds to the fiber RTT (10μs), and the decoding process time can be neglected. For Golay codes case, regardless to the code length, the total measurement time is 10μs x 2 x 2=40μs. The first factor 2 represents the complementary codes A and B, while the second factor 2 represents the two measurements by a code and its inversion.

On the other hand, for Walsh codes, the number of code patterns increases with the code length. Thus, the total measurement time for this case is 10μs x (code length) x 2. As a result, for code length of 2^1, the total measurement time for both Walsh and Golay codes is same. For longer code length, however the total measurement time for Walsh codes increases. As discussed above, to achieve the BFS measurement error of below 1MHz, 10dB SNR is required. Therefore, from Fig. 10.3 (a), for Golay codes case, the minimum required code length is 2^5 (32 bits); the total measurement time is 40μs (10μs x 2 x 2). On the other hand, for Walsh codes case, the required code length is 2^3 (8 bits). In this case, the total measurement time is 160μs (10μs x 8 x 2). Based on the above findings, in term of SNR analysis, it was found that the measurement time for Golay codes is much faster than that for Walsh codes. However, if one considers signal addition process to further improve the achievable SNR with Walsh codes, the result could be interpreted differently. In Fig. 10.3, the dashed lines indicate the SNR results when implementing signal addition process. From Fig. 10.3, for the same code length, if one includes signal addition process for Walsh codes, the relationship between the SNR and the measurement time for both Golay and Walsh codes cases would be same. For example, in the case of 2^3 bits of Walsh code, and measurement time of longer than 160μs, we can see no difference in the SNR characteristic. Furthermore, we should recall that as revealed in the previous chapter, in contrast to Golay codes, even if there are variations in the magnitude of the signal strength corresponding to the code elements, a good decoded signal can still be obtained by using Walsh codes.

From the above discussion, we can make a conclusion that Golay code is preferable when one considers fast measurement time as a priority. However, if variations in the signal amplitudes are anticipated in the measurement, Walsh codes would offer a better solution.

Furthermore, we can see that even without the use of combined codes techniques, the desired minimum SNR with error in BFS measurement of lower than 1MHz has already been achieved by only using coded discrete-PSP-BOTDA technique.

Next, we discuss the result shown in Fig. 10.3 (b). Figure 10.3 (b) illustrates the relationship between the SNR and the measurement time for coded continuous-PSP-BOTDA technique. It has been explained in previous chapters that the available code duration for this case is limited by the time constant of the acoustic wave τ_a of 9ns. For 1ns of code pulse duration, the available code lengths are 2^0, 2^1, 2^2 and 2^3. It is observed that the improvement in the SNR in Fig. 10.3 (b) is lower than that shown in Fig. 10.3 (a). This is because the amplitude of the excited acoustic wave for Brillouin amplification process exponentially decays. Because of the factors of short available code length and the decay of acoustic wave amplitude, the improvement in the SNR would be small compared to the ideal case, which finally leads to the fail in reaching 10dB SNR. We can see from Fig. 10.3 (b) that the SNR of 10dB can be achieved when signal addition process is introduced. However, the measurement time increases to 230μs, which is much longer than that for coded discrete-PSP-BOTDA employing Golay code.

Figure 10.4 illustrates the relationship between the SNR and measurement time over 1km fiber when the spatial resolution Δz of 2cm is required. Figures 10.4 (a) and (b) show the results for coded discrete- and coded continuous-PSP-BOTDAs, respectively. In the case of coded discrete-PSP-BOTDA, we can see from Fig. 10.4 (a) that for both Walsh and Golay codes, the maximum code length that can be used is 2^6, which is similar to that for $\Delta z = 10\text{cm}$ case. However, when Δz was set to 2cm, i.e. the pulse width was narrowed to 0.2ns, the SNR dropped accordingly. This is because narrowing the pulse width resulted in the reduced signal power and the use of wide bandwidth receiver leads to the increase in noise. As a result, the use of discrete coding alone cannot achieve 10dB SNR

without increasing the numbers of signal addition; this requires measurement time of 1.7ms.

For the coded continuous-PSP-BOTDA case, as the pulse width is narrowed to 0.2ns (2cm of spatial resolution), the maximum code length that can be used increases to 2^5, as observed in Fig. 10.4 (b). However, as expected, since this code length is still shorter than that for the discrete coding and furthermore the acoustic wave decay causes the decrease in measured Brillouin signal, the use of continuous coding alone cannot meet the requirement of 10dB SNR. Although the signal addition process could increase the SNR, the total measurement time would increase up to 10ms.

Based on the above discussion, if one intends to improve the spatial resolution up to 2cm for L=1km, the proposed dually coded systems (dual Golay and dual Walsh codes) or combined codes in this thesis would perhaps provide a more effective solution. We analyzed the relationship between the SNR and the measurement time for the proposed code systems, being illustrated in Fig. 10.4 (c). The combinations of continuous and discrete codings by using Walsh and Golay codes are listed as follows.

1) discrete coding: Golay code (●) + continuous coding: Golay code (●)
2) discrete coding: Golay code (●) + continuous coding: Walsh code (◆)
3) discrete coding: Walsh code (■) + continuous coding: Golay code (●)
4) discrete coding: Walsh code (■) + continuous coding: Walsh code (▲)

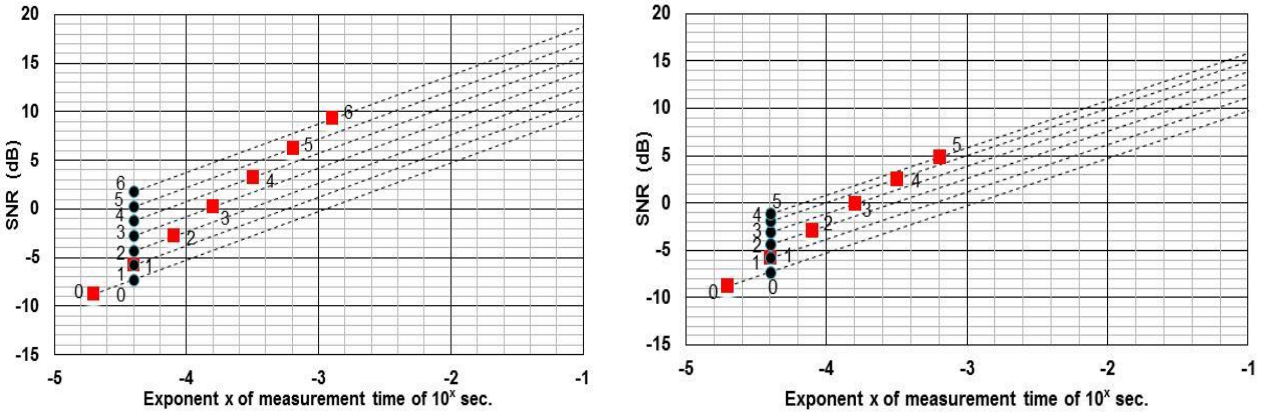

(a) (b)

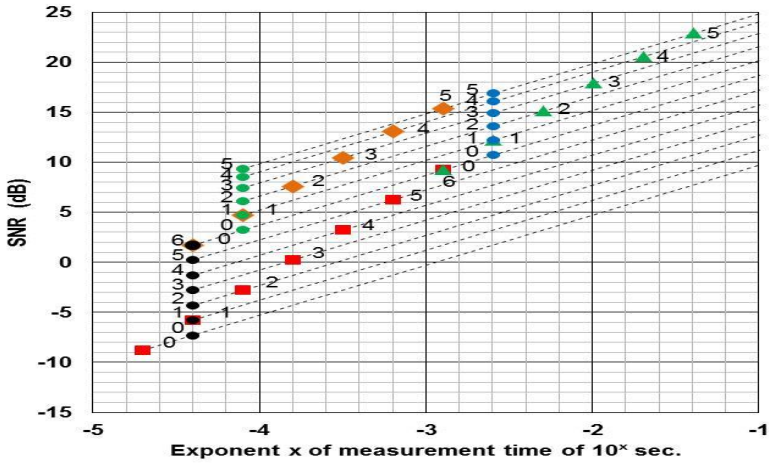

(c)

Fig. 10.4. Relationship between the SNR and the measurement time for coded PSP-BOTDA case. L=1 km, Δz =2 cm. (a) coded discrete-PSP-BOTDA, (b) coded continuous-PSP-BOTDA, (c) combined code systems.

Note that the sign in parentheses represents the code name and its type of modulation. From Fig. 10.4 (c), for combination no. 1) (discrete coding: Golay code (●) + continuous coding: Golay code (●)), i.e. dual Golay codes, when the discrete code length is 2^6 and the continuous code length is 2^5, with the inclusion of signal addition process, the SNR of 10dB was achieved in a very short time of about 100μs. Furthermore, for combination no. 2) (discrete coding: Golay code (●) + continuous coding: Walsh code (◆)), when Golay code of length 2^6 and the Walsh code of length 2^3 are combined, the SNR of about 11dB was achieved in 320μs of measurement time. If we compare this measurement time with that of results in Figs. 10.4 (a) and (b) that consider signal addition process, the proposed combined codes would provide more than 5 times faster measurement speed. For combined code systems of 3) (discrete coding: Walsh code (■) + continuous coding: Golay code (●)), when Walsh code of length 2^6 and Golay code of length 2^1 were used, the total measurement time was 2.5ms. The combination no. 4) (discrete coding: Walsh code (■) + continuous coding: Walsh code (▲)) also gave the same measurement time of 2.5ms when the combination of Walsh code (discrete coding) of length 2^6 and Walsh code (continuous coding) of length 2^1 was used. This measurement time is however much slower than that of combinations no. 1) and 2), and a little bit slower than even that of the use of the single code with the signal addition shown in Fig. 10.4 (a).

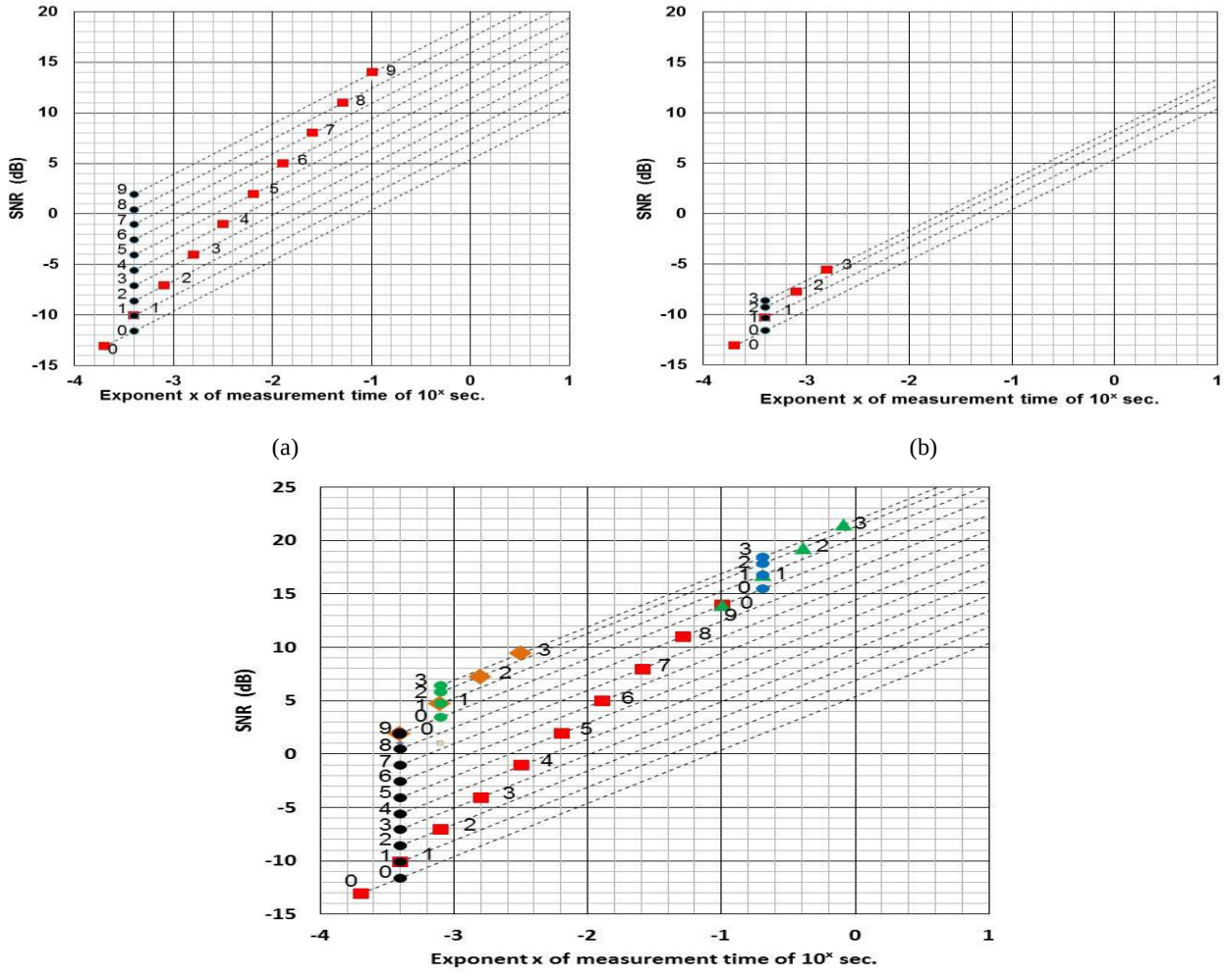

Fig. 10.5. Relationship between the SNR and the measurement time for coded PSP-BOTDA case. L=10 km, Δz =10cm. (a) coded discrete-PSP-BOTDA, (b) coded continuous-PSP-BOTDA, (c) combined code systems.

We then performed the same analysis but for the fiber length of L=10km. As has been explained before, to avoid the pump depletion effect, for L=10km, the probe power was set to -10dBm. For the spatial resolution of $\Delta z = 10\text{cm}$ case, the relationship between the SNR and measurement time of coded discrete-PSP-BOTDA employing Golay code or Walsh code is depicted in Fig. 10.5 (a). The sign ● represents Golay codes while ■ indicates the employment of Walsh codes. As the fiber length L is increased to 10km, the maximum code length for both Walsh and Golay codes is 2^9 = 512 bits. In the case of Golay codes, with the inclusion of signal additional process, the 10dB of SNR was achieved in 16ms of measurement time. On the other hand, for Walsh codes of length 2^8=256 bits, 12 dB of SNR was achieved in approximately 50ms of measurement time. In comparison with the measurement time of L=1km case of Fig. 10.3 (a) (40μs and 160μs respectively for Golay code and Walsh code), the measurement time of Fig. 10.5 (a) will be 30 times to 40 times longer.

Next, we discuss the numerical result when employing Golay code or Walsh code in coded continuous-PSP-BOTDA, being depicted in Fig. 10.5 (b). Due to the decay of acoustic wave amplitude, the maximum available code length for both codes is 2^3 = 8 bits. As a result, even with the additional implementation of signal addition process for achieving the 10dB of SNR, the measurement time would take longer than 2 seconds.

From the above analysis, again, we expect that the employment of dually coded systems or combined codes would provide better solution. The relationship between the SNR and the measurement time for the proposed codes systems is illustrated in Fig. 10.5 (c). Similar to Fig. 10.4 (c), the combination of Walsh and Golay codes and their code modulation type are given as follows.

1) discrete coding: Golay code (●) + continuous coding: Golay code (●)
2) discrete coding: Golay code (●) + continuous coding: Walsh code (◆)
3) discrete coding: Walsh code (■) + continuous coding: Golay code (●)
4) discrete coding: Walsh code (■) + continuous coding: Walsh code (▲)

From the result of Fig. 10.5 (c), the combinations no. 1) and 2) give faster measurement speed in order to obtain the 10dB SNR. With the inclusion of signal addition process, combinations no. 1) and no. 2) required the same measurement time of 4ms in order to achieve the SNR = 10dB; 4 times faster than that of employing Golay codes in coded discrete-PSP-BOTDA (see Fig. 10.5 (a)).

We then performed calculations to examine the relationship between the SNR and the measurement time for L=10km, but for the pulse duration narrowed to 0.2ns (spatial resolution Δz =2cm). The results for coded discrete-, coded continuous- and combined codes-PSP-BOTDA are illustrated in Figs. 10.6 (a), (b) and (c), respectively.

We begin with the analysis on the results shown in Fig. 10.6 (a). When we employ either Golay code or Walsh code, the maximum code length that can be used in the coded discrete-PSP-BOTDA is 2^9=512 bits. However, as we narrowed the pulse width from 1ns to 0.2ns, the increase in the bandwidth of the receiver also has caused the decrease in the SNR. As a result, it is necessary for both codes to include signal addition process in the measurement in order to realize 10dB of SNR, which leads to the increase in the measurement time to 2 seconds.

Next, from the result of Fig. 10.6 (b), it is obvious to see that since the maximum code length that can be used for either Golay code or Walsh codes is 2^5=32bits, the 10dB SNR cannot be achieved with the use of continuous coding alone.

We then discuss the result of Fig. 10.6 (c), which illustrates the relationship between SNR and measurement time when measured with dually coded system and combined codes system. The combinations of the codes and their code

modulation type are listed as follows.

1) discrete coding: Golay code (●) + continuous coding: Golay code (●)
2) discrete coding: Golay code (●) + continuous coding: Walsh code (◆)
3) discrete coding: Walsh code (■) + continuous coding: Golay code (●)
4) discrete coding: Walsh code (■) + continuous coding: Walsh code (▲)

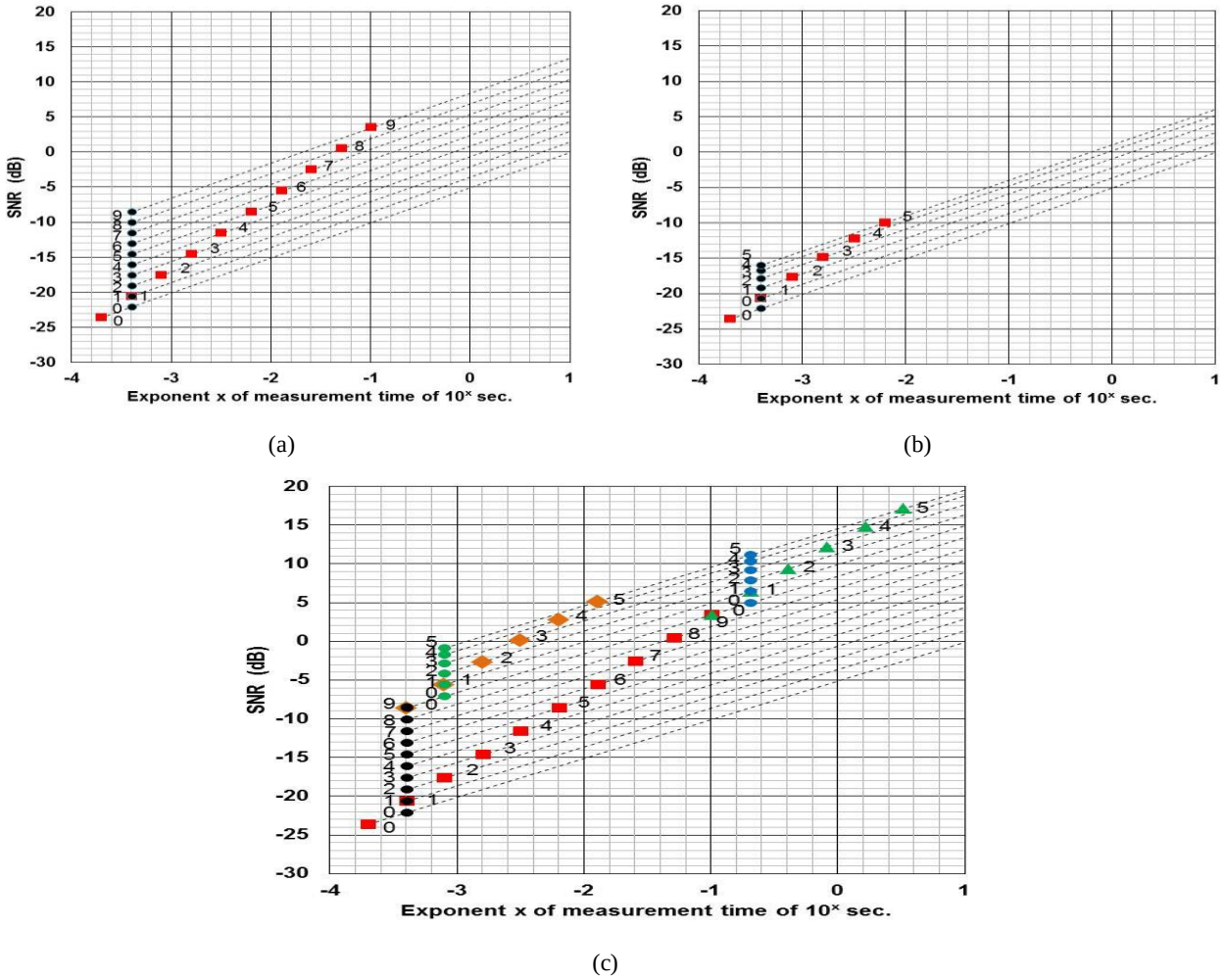

Fig. 10.6. Relationship between the SNR and the measurement time for coded PSP-BOTDA case. L=10 km, Δz =2cm. (a) coded discrete-PSP-BOTDA, (b) coded continuous-PSP-BOTDA, (c) combined code systems.

For combinations no. 1) and 2) with the combined use of signal addition, the SNR=10dB was achieved in 130ms. Thus, if we compare this result with that of discrete coding employing only Golay code or Walsh code (see Fig. 10.6 (a)), the combinations no. 1) and 2) provide 16 times faster measurement speed.

For combination no. 3), it took longer than that for no. 1) and 2), which is about 200ms. However, this measurement speed is 10 times faster than that of Fig. 10.6 (a). We should also note that the measurement of the combination no. 3) did not include the signal addition process.

Finally for combination no. 4), the SNR of 10dB was achieved with the use of signal addition process. Compared to the case of no. 3), it took 500ms to complete the measurement, and is about 4 times faster than that for the result of Fig. 10.6 (a).

From the above discussions, it was found that when Walsh code is assigned to the discrete coding, the measurement

time tends to increase with the code length. This is because in order to obtain higher SNR, longer Walsh code must be used, which resulted in the increase in the number of code patterns. This obviously leads to a longer measurement time. In contrast, for Golay code, regardless to the code length, only a pair of codes is used in the measurement. Therefore, if one aims to measure strain with fast measurement speed, combination no. 1) would be the best option.

On the other hand, as discussed in Chapter 6, when we have no information about the fiber type, there is a case where the total duration of continuously coded pulses happens to be twice longer than the time constant of the acoustic wave amplitude τ_a. If this is the case for Golay code, it will cause the distortion in the decoded signal, which leads to the degradation of spatial resolution. Then, the employment of Walsh code would provide a better solution. In addition, compared to the discrete coding employing Walsh code, it was found that the maximum allowable Walsh code length for continuous coding is usually much shorter. In other words, the measurement time of the continuous Walsh coding would not be a problem for almost cases.

Let us give an example of a fiber of length 500m. In the case of discrete coding, regardless to the pulse width τ, the maximum code length is 32 bits. On the other hand, if we set τ=0.2ns, in order to obtain spatial resolution that corresponds to the pulse width, the maximum allowable code length for continuous coding is also 32bits. For L of longer than 500m, however, the allowable code length increases for discrete coding, but remains unchanged for continuous coding. Consequently, the code length of the discrete coding can be often set longer than that of the continuous coding.

Furthermore, when using the 32 bits of Walsh code for the continuous coding, compared to that before code employment, the increase in the SNR is 15dB. In most cases of the continuous coding system, the SNR of 10dB cannot be achieved with the SNR improvement of 15dB (See Figs. 10.3 (b), 10.4 (b), 10.5 (b) and 10.6 (b)). Therefore, the implementation of signal addition process could be required additionally. Then, it takes the same time for both Walsh code and Golay code to reach the 10dB SNR.

Based on the above discussion, when there is variation in τ_a along the fiber, the use of Walsh code in continuous coding would be preferable in order to obtain decoded signal with no degradation in spatial resolution. On the other hand, for discrete coding, in terms of fast measurement speed, Golay code would offer a more effective selection. Therefore, it can be concluded that combination no. 2) provides a good tradeoff between the spatial resolution and measurement time. Since combination no. 3) is the opposite combination of no. 2), little merit of this combination can be found.

For combination no. 4), the measurement time would become a problem. In this study, since the goal is to perform the measurement of BFS with error of below 1MHz, the minimum required SNR of 10dB achievement was assumed. If we further want to perform a more accurate BFS measurement (much lower than 1MHz), however, the use of dual Walsh codes only would hardly obtain the required corresponding SNR. Thus, the signal addition process should be implemented additionally. In that case, as explained before, since there is no difference in the measurement time between Walsh code and Golay codes, combination no. 4) would be preferable for further obtaining smaller error in the BFS measurement with better spatial resolution.

10.6 Conclusions of Chapter

In this chapter, the measurement performance that can be achieved by BOTDA with the employment of proposed coding systems has been numerically presented.

First, the required SNR for achieving small error in BFS measurement was presented. In details, the simulations

were performed so that the method to estimate the BFS should be as similar as possible with that of the actual measurement. Based on the results, in order to achieve BFS measurement error of below 1MHz, the required optical SNR was found to be about 10dB.

Next, the allowable maximum power of pump pulse and probe was discussed. For the pump case, the maximum optical power that can be used for the measurement is limited by the nonlinear effects in fiber: self-phase modulation effect, modulation instability (MI), Raman scattering etc. It was explained that the maximum allowable pump power that can be used without the influence of the nonlinear effects above was around 100mW. Therefore, in the simulations, the pump power was set to 20dBm (100mW).

For probe case, the maximum allowable power is influenced by the pump depletion effect. In this case, the probe input power depends on the fiber length L. Thus, the relationship between the BFS error and the probe power input was studied for two different fiber lengths, L=1km and L=10km. For L=1km case, in order to obtain BFS error of below 1MHz, the probe power was found to be less than 0dBm, while for L=10km case, the probe power should be less than -10dBm. These power settings were used to analyze the performance of the BOTDA employing code systems.

Based on the above considerations, the SNR of the conventional coded PSP-BOTDA (coded discrete- and coded continuous-PSP-BOTDAs) and the coded PSP-BOTDA employing code systems proposed in this thesis were analyzed and compared. In the simulations, fiber length L was set to 1km and 10km. In each fiber length case, the measurement with the spatial resolution Δz of 10cm and 2cm was considered. In this thesis, the employment of Walsh code and Golay code was proposed. The combinations of these codes that produce the dually coded system (dual Golay codes and dual Walsh codes) and the combined codes system are listed as follows.

1) discrete coding: Golay code + continuous coding: Golay code
2) discrete coding: Golay code + continuous coding: Walsh code
3) discrete coding: Walsh code + continuous coding: Golay code
4) discrete coding: Walsh code + continuous coding: Walsh code

From the simulation results, it can be concluded that

i) Combination no. 1) provides the fastest measurement speed.
ii) If the variation in the BGS along the test fiber is anticipated in the measurement, the combination no. 2) would provide the best solution to obtain the good tradeoff between the spatial resolution and measurement time.
iii) Compared to other combinations, combination no. 3) has little merit.
iv) If BFS measurement error of much lower than 1MHz is required, the combination no. 4) would be appropriate.

References

[1] T. Horiguchi, T. Kurashima, and M. Tateda, "Nondestructive measurement of optical-fiber tensile strain distribution based on Brillouin spectroscopy", IEICE Trans. B-I, vol. J.73-B-I, no. 2, pp. 144-152, Feb. 1990.

[2] H. Izumita, Y. Koyamada, S. Furukawa, and I. Sankawa, "The performance limit of coherent OTDR enhanced with optical fibre amplifiers due to optical nonlinear phenomena", J. Lightwave Technol., vol. 12, no. 7, pp. 1230-1238, 1994.

[3] G. Agrawal, "Nonlinear Optics", fourth ed. Academic Press, (2008).

[4] V. Lecoueche, D. J. Webb, C. N. Pannel, and D. A. Jackson, "25 km Brillouin based single-ended distributed fibre sensor for threshold detection of temperature or strain", Optics Communications, vol.168, pp.95-102, Sept. 1999.

[5] D. Alasia, M. G. Herraez, L. Abrardi, S. M. Loppez, and L. Thevenaz, "Detrimental effect of modulation instability on distributed optical fibre sensors using stimulated Brillouin scattering", 17th OFS (2005), in Proceedings of SPIE 5855, pp.

587-590.

[6] T. Horiguchi and M. Tateda, “BOTDA - Nondestructive measurement of single-mode optical fiber attenuation characteristics using Brillouin interaction: Theory”, J. Lightwave Technol., vol.7, no.8, pp.1170-1176, Aug. 1989.

[7] T. Kurashima, T. Horiguchi and M. Tateda, “Distributed optical fiber sensor using Brillouin scattering”, IEICE Trans. C-II, vol. J.74-C-II, no. 5, pp. 467-476, May 1991.

Chapter 11: Conclusions and Future Works

11.1 Conclusions of Each Chapter

The conclusions described in this chapter cover the topics discussed from Chapter 4 to Chapter 9, as these chapters are the main contributions to this thesis.

11.1.1 Chapter 4

The author has proposed in Chapter 4 new coding system called combined codes system which includes dual Golay codes, combined Walsh and Golay codes and dual Walsh codes for modulating the pump light of the PSP-BOTDA. It has been discussed theoretically that this new concept can contribute to the achievement of higher signal-to-noise ratio (SNR) compared to that of using only one kind of code (coded continuous- and coded discrete-PSP-BOTDAs), and obviously higher than that of the conventional single pulse PSP-BOTDA.

11.1.2 Chapter 5

It has been discussed in Chapter 5 that the employment of Golay complementary pair (GCP) in the coded discrete-PSP-BOTDA system can contribute to the improvement in the signal-to-noise ratio (SNR) with the code length on the condition that coded pulses with uniform optical power must be used to realize such improvement in SNR. However, when an AC-coupled amplifier is used to amplify the coded electrical signals which are input to an electro-optic modulator, the waveform of the optical pulses modulated are distorted. This distortion has resulted in the degradation of the correlation characteristic of the coded BOTDA signal. Experiments for bit duration T_2 of 1ns have shown that the relative SNR increases almost linearly for code length up to 8 bits; however in the case of 16 and 32 bits, the relative SNR decreases and deviate from its linear form.

To improve the relative SNR, the author has introduced a new electrical signal configuration for the input signal of the AC-coupled electrical amplifier. The author has modified the Golay coded electrical signal by alternately setting the amplitude of the 1st pulse to positive and negative values. As a result, the amplitude of the amplified signal becomes uniform at all pulse groups and the shift of the mean voltage of the pulse signal is reduced. The analysis of the measured relative signal-to-noise ratio (SNR) shows that the relative optical SNR in dB increases linearly with respect to the increase in the Golay code length as expected from the theory.

11.1.3 Chapter 6

Modulating the pump light of the conventional BOTDA with non-return-to-zero (NRZ) formatted code system to realize sub-meter spatial resolution measurement has induced distortion in the Brillouin signal due to the variety of Brillouin gain caused by the preceding coded pulses, when coded pulse duration is around or less than the time constant of the acoustic wave amplitude τ_a. However, the author has shown that this problem can be overcome by introducing NRZ formatted coding system which includes Walsh codes and bipolar Golay codes in coded continuous-phase-shift pulse BOTDA (PSP-BOTDA). This is because in contrast to the conventional BOTDA that is based on the intensity modulation, PSP-BOTDA can remove the Brillouin gain variation due to the sequence of the coded pulses and utilizes the only Brillouin gain that is induced by pre-pump pulse.

By comparing the processed Brillouin signals with that obtained by using Golay codes, it was found that the use of Walsh codes decodes the Brillouin signal without degrading the spatial resolution even when the total code pulse duration becomes two times as long as τ_a at least. It was also found that for the Golay coded PSP-BOTDA, in contrast, the use of the coded pulses whose total duration exceeds τ_a increasingly degrades the spatial resolution. This

advantage of the Walsh code over the Golay code comes from the fact that the decoding the Brillouin signals via Hadamard transform is robust not only against variations in launched coded-pulse amplitudes but also against those in response signals. The spatial resolution of 20cm and 10cm was successfully attained by using NRZ formatted code system having pulse durations of 2ns and 1ns, respectively.

In terms of the Brillouin gain spectrum (BGS), it was found from the simulation and experimental results that the BGS measured by using Walsh coded PSP-BOTDA has become narrower than the steady-state gain spectrum. This narrowing is favourable to measure the BFS accurately. Furthermore, it was also found that the use of Walsh codes has contributed to the achievement of higher BFS measurement accuracy than that of using conventional PSP-BOTDA technique.

The author has also shown that the experimental SNIR dependence on the code length for Walsh codes agrees well with that calculated by analytical and numerical methods. For both Walsh and Golay codes, the maximum SNIR can be achieved only for total code duration of around τ_a; so the author has verified by experiments that 8-bit Walsh and Golay codes having 1ns pulse each enable the optical signal-to-noise improvement ratio (SNIR) of about 3dB. Even though the maximum SNIR for Golay codes measured is slightly higher than that for Walsh codes, this difference is merely caused by the crosstalk to the intrinsic signal after the auto-correlation calculations for decoding the Golay codes. Furthermore, this crosstalk contribution varies for different fiber length. Therefore, from these findings it is confirmed that the employment of Walsh codes in the coded continuous-PSP-BOTDA offers a more intrinsic SNIR compared to that of Golay codes.

It is also confirmed that even when the total coded pulse duration becomes two times as long as τ_a at least, the spatial resolution of the Walsh coded PSP-BOTDA maintains high spatial resolution and almost the same SNIR with the maximum SNIR that is obtained when the total coded pulse duration is around τ_a.

Based on the findings described above, it is concluded that the Walsh coded PSP-BOTDA offers better solution than the Golay coded PSP-BOTDA. This is because the former maintains high spatial resolution even if the acoustic wave time constant τ_a of fibers used, which is inversely proportional to the Brillouin gain bandwidth, varies and happens to be less than the total coded pulse duration designed. In contrast, for the latter, the spatial resolution is significantly degraded.

11.1.4 Chapter 7

An algorithm has been presented for synthesizing dual Golay codes for measuring distributed strain and temperature based on PSP-BOTDA technique with a high spatial resolution. The proposed dual Golay codes are configured by nesting one Golay complementary pair of sequences (GCP) into the other one. The former is called pair of sequences continuous pulse codes and the latter discrete pulse codes, which are used to generate the pulsed pump with NRZ-pulses and RZ-pulses, respectively.

The proposed dual Golay codes enable one to use the RZ-pulses and NRZ-pulses simultaneously and advantageously for coding the pump of the PSP-BOTDA, and to use longer codes than the conventional codes within a given period; let code lengths of the continuous and the discrete pulse codes be L_{cont} and L_{disc}, the code length of each dual Golay code in the dual Golay code is $L_{cont}L_{disc}$. Then, the SNR enhancement, i.e., the coding gain of the proposed method is about $\eta\sqrt{L_{cont}L_{disc}}$, while that of the conventional coded BOTDA based on intensity modulations is $\sqrt{L_{disc}}/2$. Therefore, the SNR enhancement of the proposed coding method is $2\eta\sqrt{L_{cont}}$ times as large as that of the conventional coding method. The coefficient η $(0 \leq \eta \leq 1)$ represents the efficiency of the SNR improvement with

the continuous pulse codes and also accounts for the attenuation of the acoustic wave that is excited by the 1st pulsed pump of the PSP-BOTDA. When the product of L_{cont} and the 2nd pulse duration T_2 is longer than the time constant of the acoustic wave τ_a, the quantity η decreases to less than 0.7 and the spatial resolution gets worse than the theoretical one; thus $L_{cont}T_2$ should be chosen to be less than τ_a; then η ranges from 0.7 to 1.

A new coded PSP-BOTDA system based on the DGC has been demonstrated by both simulations and experiments. High spatial resolution of 10 cm was successfully demonstrated from both simulations and experiments. Furthermore, it has been clarified that the power of the correlated Brillouin signal has increased with increase in the code length of the new code provided that the total duration of the pulses coded by the continuous pulse codes is less than τ_a. The increase in the Brillouin signal power raises the signal-to-noise ratio and is to BOTDA's benefit to attain high spatial resolution. Initial experiments for L_{cont}=4, L_{disc}=8 have demonstrated about 8-dB enhancement in the optical signal-to-noise ratios when compared to the single pulse PSP-BOTDA, while for L_{cont}=8, L_{disc}=4, the amount of enhancement achieved was about 7-dB. Finally, it should be noted that the SNIR can be further enhanced by increasing the code length L_{disc} of discrete part, but limited to the round trip time (RTT) of light in fiber. For the continuous part, however, maximum SNIR is achieved when the total code duration $L_{cont}T_2$ is set around τ_a, in this case $L_{cont}T_2$=8ns.

11.1.5 Chapter 8

The proposal of combining two different codes in modulating the pump light of PSP-BOTDA fiber sensor for distributed strain measurement was reported. From the simulation and experimental results, it was confirmed that the assignment of Walsh codes to NRZ pulses has kept the spatial resolution high even for code length of longer than the time constant of the acoustic wave case. Even though the Brillouin signal measured by the code sequences exponentially decays, the decoding process via Hadamard transform for Walsh coded NRZ pulses in the proposed system still produces more accurate decoded signals than that via Golay codes correlation calculations. From the rising edge length of the increase in the amplified probe signal obtained with the combined codes, we concluded that we achieved the spatial resolution of 10cm.

It was also found that the combination of Golay and Walsh codes has contributed higher SNIR than that of using only one kind of code in coded continuous- and coded discrete-PSP-BOTDAs. In the analysis, for both Golay and Walsh codes cases, it was found that the use of coded RZ pulses increases the SNIR by $\sqrt{L}$. For NRZ pulses, however, the improvement became slow and dropped for long code length. This is due to the decrease of Brillouin signal induced by the acoustic wave decay. It was observed that the SNIR reached its maximum when the code length of the NRZ pulses was 8ns, confirming that code duration of the NRZ pulses is limited by the time constant of the acoustic wave τ_a.

11.1.6 Chapter 9

The analysis on the employment of dual Walsh codes in the PSP-BOTDA for strain measurement has been discussed. The process of generating the dual Walsh codes is almost similar to that for generating the dual Golay codes. Therefore, in Chapter 9, the simulation results for dual Walsh codes have been compared with the results of dual Golay codes PSP-BOTDA (Chapter 7). It has been found from the simulations that the robustness of Hadamard transform against the variations in the received signals during the decoding process for dual Walsh codes has contributed to the achievement of high spatial resolution measurement, even for $L_{cont}T_2$ of longer than the time constant of the acoustic wave τ_a cases. In contrast, for dual Golay codes PSP-BOTDA, the appearance of side-lobes has caused the increase in the rising and falling edge lengths when the dual Golay codes of $L_{cont}T_2$ longer than τ_a were used. For code sequence beyond τ_a, the Brillouin interaction became weak and this consequently distorted the Brillouin signal after the correlation.

As for the SNIR, for dual Walsh codes case, the maximum SNIR was obtained when $L_{cont}T_2$ is set in the range of τ_a to $2\tau_a$, while for dual Golay codes the SNIR reached its maximum value when $L_{cont}T_2$ was set to around τ_a. The maximum SNIR (when $L_{cont}T_2$=8ns) for dual Golay codes is slightly higher than that for the dual Walsh codes. This slight difference is however caused by the contribution of the crosstalk to the Brillouin signals during the mutual correlation calculations for dual Golay codes. Otherwise, if no crosstalk exists, the SNIR both codes are same. However, if one takes into account the spatial resolution results obtained by these two techniques, as has been discussed above, the dual Walsh codes would provide better tolerance of setting the total duration of the coded NRZ pulses ($L_{cont}T_2$) than Golay code to achieve the best SNIR and to simultaneously maintain high spatial resolution. This is especially beneficial in the practical applications when one tries to measure strain along a fiber having varied Brillouin gain bandwidth. Therefore, it can be concluded in that the employment of dual Walsh codes in coding the pump light of the PSP-BOTDA offers better measurement performance than that of the dual Golay codes PSP-BOTDA.

11.1.7 Chapter 10

The analytical study on the measurement performance of BOTDA with the employment of proposed coding systems has been presented. The parameters such as the BFS measurement error, SNR and the limit in the pump and probe powers must be first analyzed upon simulating the performance of the BOTDA.

First, it has been found in the study that in order to achieve BFS error of below 1MHz in the BOTDA technique, the required optical SNR was about 10dB.

In the case of the pump power, the maximum input power that can be used is limited by the nonlinear effects in fiber such as self-phase modulation, modulation instability (MI), Raman scattering etc. Based on the experimental results from the previous reports, it is concluded that the use of pump input power of 100mW was considered tolerable to be used to examine the performance of the BOTDA.

In the case of probe, the effect of pump depletion plays a role in limiting the maximum probe power that can be used in the measurement. In the analytical study, the relationship between the BFS error and the probe input power was studied for two different fiber lengths, L=1km and L=10km. For L=1km case, in order to obtain BFS error of below 1MHz, the probe power was found to be less than 0dBm, while for L=10km case, the probe power less than -10dBm.

The parameters obtained above were used in the simulations to study the relationship between the SNR and the measurement time of PSP-BOTDA employing the proposed coding systems. In the simulations, fiber length L was set to 1km and 10km. In each fiber length case, the spatial resolution Δz of 10cm and 2cm was assumed. In this thesis, the employment of Walsh code and Golay code was proposed.

From the simulation results, it is concluded the dual Golay codes PSP-BOTDA provides the fastest measurement speed. Next, if the variation in the BGS along the test fiber is anticipated in the measurement, the combination of Golay code (RZ) and Walsh code (NRZ) would provide the best solution since we can obtain a good tradeoff between the spatial resolution and measurement time. The opposite combination of Golay code (NRZ) and Walsh code (RZ) has found little merit. Finally, if the BFS measurement error of much lower than 1MHz is required, the employment of dual Walsh codes PSP-BOTDA would be appropriate.

11.2 Overall Conclusions on the Performance of Combined Codes Systems

It can be concluded from the experimental results of Chapter 5 that the new electrical signal configuration proposed in the coded discrete-PSP-BOTDA has solved the problem of signal distortion especially for long RZ pulses of code length 8 bits and longer. This new concept has also been implemented in the combined RZ- and NRZ coded pulses

employing Walsh and Golay codes of Chapter 8 and dual Walsh codes of Chapter 9, showing identical experimental results with that of Chapter 5. Thus, the author suggests that the new concept can be generally applied to both coded discrete-PSP-BOTDA (RZ pulses) and combined codes PSP-BOTDA techniques (dual Golay codes, dual Walsh codes and combined Walsh- and Golay codes).

Based on the analysis explained from Chapter 7 to Chapter 10, the author has summarized the findings obtained from the proposed coding technique into the Fig. 11.1.

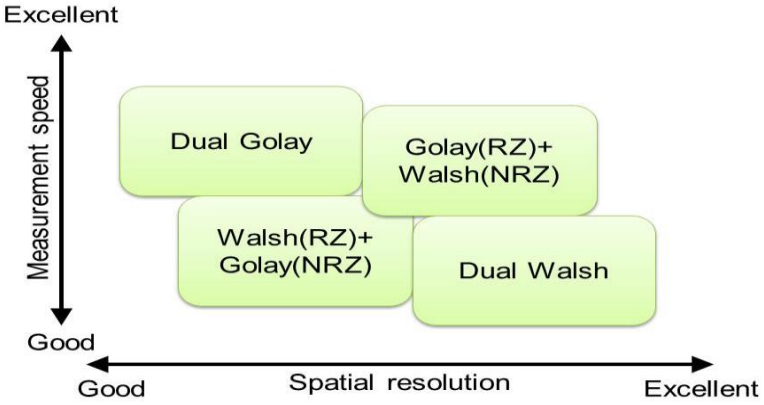

Fig. 11.1. Summary of performance of dual Golay codes-PSP-BOTDA, dual Walsh codes-PSP-BOTDA and the two kinds of combined codes-PSP-BOTDAs in terms of measurement speed and spatial resolution.

From Fig. 11.1, in terms of measurement speed, it is seen that the dual Golay codes provide the fastest measurement speed. This is because the Golay code uses only two codewords and thus the total measurement time is same for any dual Golay code length. In contrast, for dual Walsh code, the total measurement time increases with the increase in the code length since the number of the codewords of the Walsh code is identical to the code length. Thus, the dual Walsh codes PSP-BOTDA gives the slowest measurement time. For the combination of Golay (RZ) + Walsh (NRZ), as explained in Chapter 8 and Chapter 10, the maximum code length is limited by time constant of the acoustic wave τ_a ; in this case, the maximum duration of the $L_{cont}T_2$ for obtaining the highest SNR is 8ns. Then, the SNR can only be further improved by increasing Golay code length, which will not cause the increase in the measurement time. For the opposite combination (Golay (NRZ) + Walsh (RZ)), the Golay code length is also limited to 8ns. In order to further improve the SNR, Walsh code length should be further increased. However, this will result in the increase in measurement time.

In terms of spatial resolution, it is concluded that the dual Walsh codes PSP-BOTDA offers the best spatial resolution measurement, because of the robustness of Hadamard transform against the variation in the signal amplitude. In contrast, the use of dual Golay codes PSP-BOTDA would cause the degradation in the spatial resolution of the measured signal, if the code duration of the NRZ pulses modulated with the Golay code significantly exceeds τ_a. Furthermore, in the actual measurement, another factor that can induce distortion in the measured Brillouin signal is the gain depletion of EDFA. Soto et al have previously reported the decrease in the amplified-coded pump pulse down to 60% of its initial power due to the gain saturation of the EDFA when placed after the MZM, especially for amplifying pump light coded with relatively long RZ pulses [1]. To avoid this effect, they have proposed in the same report to place the EDFA before the MZM, so that a uniform peak pulse power can be generated. Based on the above finding and discussion, if the power of the optically amplified RZ pulses is uniform, the combination of Golay (RZ) + Walsh (NRZ) can provide better spatial resolution measurement than that of the opposite combination of Golay (NRZ) + Walsh (RZ).

From the summary in Fig. 11.1, the author suggests that each coding system proposed in this thesis has its own merits and demerits, which could be judged according to the measurement conditions. For a fast speed measurement with high SNR, dual Golay codes would be the best option. The combination of NRZ pulses modulated with Walsh code and RZ pulses with Golay code would produce a good tradeoff between the spatial resolution and the measurement time. Besides, if one seeks for a high spatial resolution measurement, the dual Walsh codes could be suggested for the best coding system.

Finally, from Chapter 6 through Chapter 9, the simulations and experiments were performed over fiber cable of distance about 70m. In this case, the expected applications are for health monitoring system of bridge of distance around 35m (considering a round trip fiber of distance 70m) and for crack detection system for small size aircraft. More detailed measurements over long range fiber of a few to ten kilometers should be performed in order to realize long-range measurement system.

11.3 Proposed Future Works

Some of future works that can be considered for further enhancements/verifications of the coded PSP-BOTDA techniques discussed in this dissertation are listed as below:

i) Long distance measurement: The main subject discussed in this dissertation is focused on the effect of coding system to the PSP-BOTDA measurement. Therefore, the simulations and the experimental results reported were obtained over a fiber optic cable of distance about 70m. For more detailed analysis on the measurement efficiency, the employment of coded PSP-BOTDA for long distance measurement should be performed.

ii) Compared to Golay codes, a large number of code patterns for long Walsh codes may impose more overhead of signal processing on the coded PSP-BOTDA. Therefore, it is important in the future to perform a comprehensive analysis of the advantages and disadvantages of the kind of codes when designing a practical BOTDA system.

iii) The author would like to propose to simultaneously use Brillouin gain and Brillouin loss measurement in the combined codes system: In this thesis, only Brillouin gain component was utilized in both simulations and experiments. When using only gain component, the energy transfer occurs only from the light of higher frequency to the lower one, in this case, from pump to probe. Since the Brillouin signal is hugely contributed by the interaction between the 1st pulse and the acoustic wave induced by the 1st pulse, the use of especially long RZ pulses (L_{disc}) may induce error and distortion in the decoded Brillouin signal as the small Brillouin signals contributed by the coded pulses are hidden by the relatively large former Brillouin signal. By alternately modulating the 1st pulses with the frequencies for generating Brillouin gain and Brillouin loss, mutual energy transfer would occur between the pump and the probe, which would result in a balanced increase and decrease of Brillouin signals.

References

[1] M. A. Soto, G. Bolognini, F. Di Pasquale and L. Thevenaz, "Long-range Brillouin optical time-domain analysis sensor employing pulse coding techniques", J. Meas. Sci. Technol., vol. 21, no. 9 (094024), pp. 1-7, Jul. 2010.

Research Publications

Refereed Journal Articles:

[1] **Mohd Saiful Dzulkefly Bin Zan** and Tsuneo Horiguchi, "A dual Golay complementary pair of sequences for improving the performance of phase-shift pulse BOTDA fiber sensor", J. Lightwave Technol., Vol. 30, No. 21, pp. 3338-3356, Nov. 2012.

[2] **Mohd Saiful Dzulkefly Bin Zan**, Tatsuya Tsumuraya and Tsuneo Horiguchi, "The use of Walsh code in modulating the pump light of high spatial resolution phase-shift-pulse Brillouin optical time domain analysis with non-return-to-zero pulses", J. Meas. Sci. Technol., Vol. 24, 094025 (13pp), July 2013.

Refereed International Conference Articles:

[1] **Mohd Saiful Dzulkefly Bin Zan**, Tsuneo Horiguchi, Takashi Sasaki and Daisuke Uchiyama, "Phase shift pulse Brillouin optical time domain analysis (PSP-BOTDA) employing dual Golay codes", International Conference on Computer and Communication Engineering (ICCCE 2010), 3B, 217, pp. 1-6, May 11-12, 2010, Kuala Lumpur, Malaysia.

[2] **Mohd Saiful Dzulkefly Bin Zan** and Tsuneo Horiguchi, "A new electrical signal configuration for modulating pump light of coded discrete-phase shift pulse-BOTDA", 3rd International Conference on Photonics (ICP 2012), L-D2-PM1, pp. 294-298, Oct. 1-3, 2012, Penang, Malaysia.

[3] **Mohd Saiful Dzulkefly Bin Zan**, Tatsuya Tsumuraya and Tsuneo Horiguchi, "The use of Walsh functions in modulating pump light of high-spatial-resolution BOTDA with NRZ pulses", 22nd International Conference on Optical Fiber Sensors (OFS-22), Proc. of SPIE, Vol. 8421, 84219U_1-U_4, Oct. 15-19, 2012, Beijing, China.

[4] **Mohd Saiful Dzulkefly Bin Zan**, Kosuke Yokoyama and Tsuneo Horiguchi, "Combination of Walsh and Golay codes in modulating the pump light of phase-shift pulse BOTDA sensor", 4th International Conference on Photonics (ICP 2013), No. 46 D2-AM2-A, Oct. 28-30, 2013, Malacca, Malaysia.

Domestic Conference Articles:

[1] **Mohd Saiful Dzulkefly Bin Zan**, Toshio Kurashima and Tsuneo Horiguchi, "Code time dependence of the signal to noise ratio in the continuously coded PSP-BOTDA system", Optics & Photonics Japan 2011 (OPJ 2011), 30pB6, Nov. 28-30, 2011, Osaka.

[2] **Mohd Saiful Dzulkefly Bin Zan**, Tatsuya Tsumuraya and Tsuneo Horiguchi, "The employment of Walsh functions in the coded PSP-BOTDA", Proceedings of the 2012 IEICE General Conference, B-13-11, Mar. 20-23, 2012, Okayama.

[3] **Mohd Saiful Dzulkefly Bin Zan** and Tsuneo Horiguchi, "The effects of AC-coupled electrical amplifier in amplifying Golay formatted electrical signal for producing pump light of coded discrete PSP-BOTDA fiber sensor", Proceedings of the 2012 IEICE Society Conference, B-13-13, Sept. 11-14, 2012, Toyama.

[4] **Mohd Saiful Dzulkefly Bin Zan** and Tsuneo Horiguchi, "Comparing the analysis of employing Walsh codes and Golay codes in the coded continuous-PSP-BOTDA", Proceedings of the 2013 IEICE General Conference, B-13-20, Mar. 19-22, 2013, Gifu.

[5] **Mohd Saiful Dzulkefly Bin Zan** and Tsuneo Horiguchi, "Analysis on the employment of combined codes in

modulating the pump light of phase shift pulse Brillouin optical time domain analysis (PSP-BOTDA)", Proceedings of the 51st Meeting on Lightwave Sensing Technology (LST-51), LST51-17, pp. 115-120, June 4-5, 2013, Tokyo.

[6] **Mohd Saiful Dzulkefly Bin Zan** and Tsuneo Horiguchi, "Experiments on the employment of combined Walsh and Golay codes in modulating the pump light of PSP-BOTDA system", Proceedings of the 2013 IEICE Society Conference, B-13-38, Sept. 17-20, 2013, Fukuoka.

Acknowledgements

Firstly, I would like to express my deepest appreciation and thanks to my supervisor Professor Dr. Tsuneo Horiguchi. He has been a great mentor and teacher for me. His patience guidance and enthusiastic encouragement on my research have been priceless. I will never forget the precious time that I have spent in his laboratory, learning so many things from him.

I would also like to thank my co-supervisor Professor Dr. Norio Kashima, the reviewers of my thesis Professor Dr. Atsushi Saitoh from the Department of Communications Engineering of Shibaura Institute of Technology, Professor Dr. Yoshikazu Koike from the Department of Electronic Engineering of Shibaura Institute of Technology and Professor Dr. Yahei Koyamada from the Department of Media and Telecommunications Engineering of Ibaraki University, for their precious comments and suggestions on my dissertation.

Furthermore, I would especially like to thank the postgraduate and undergraduate students of Communication and Measurement Laboratory of Shibaura Institute of Technology for helping me with the experiments and data collection.

I would also like to express my gratitude to the National University of Malaysia (Universiti Kebangsaan Malaysia UKM) and to the Department of Higher Education of Malaysia (Ministry of Education Malaysia) for providing me the funds for my PhD study.

Finally I would like to give special thanks to my beloved and supportive wife Mulhizah Binti Ismail, my children Suri Mardhiyani and Muqry Ramadhani.